Microwave-Assisted Synthesis, Characterisation, and Evaluation of Biological Activities of Pyridine-Functionalised (Benz)imidazolium Salts.

Mah Wee Li

A thesis submitted for the degree of Doctor of Philosophy at

Monash University

Faculty of Science

2021

COPYRIGHT NOTICE

ABSTRACT

Imidazolium salt, derived from the parent imidazole, serves as a highly versatile scaffold in medicinal chemistry, where desired functionality can be introduced into the structure readily. Despite the fact that imidazolium salts have a poorer hydrogen bonding ability compared to their parent imidazoles, the cationic imidazolium cores allow the compound to interact with biological systems electrostatically. In this thesis, a series of *N*-alkyl-substituted pyridine-functionalised (benz)imidazolium salts were synthesised and characterised using both conventional heating method and microwave irradiation. The imidazolium salts and their benzimidazolium analogues were synthesised and compared their biological activities to evaluate how the extended π-conjugation in benzimidazolium salts affect the biological properties. Five different alkyl chains (hexyl, heptyl, octyl, nonyl, decyl) were selected to study the influence of increasing carbon number on the biological properties, which include antimicrobial property and cell cytotoxicity. All synthesised compounds were tested against a list of microorganisms that constitutes of eight Gram-positive and four Gram-negative bacterial species, and three yeast species. Besides, the synthesised (benz)imidazolium salts were tested for their *in vitro* cell cytotoxicity against four selected cancerous cell lines.

Chapter 1 provides a brief introduction of imidazolium salts and the medicinal applications of existing imidazolium salts. The examples of bioactive imidazolium salts were detailed and discussed. In addition, their applications as the precursors to ionic liquids and *N*-heterocyclic carbenes were also discussed. A brief history and background of metal *N*-heterocyclic carbene complexes were also discussed and their medicinal applications were detailed.

Chapter 2 focuses on the synthesis and characterisation of a series of *N*-alkyl-substituted pyridine-functionalised (benz)imidazolium salts. The synthesised (benz)imidazolium salts bear a pyridine-containing backbone, which can be prepared through the reduction of 2-benzoylpyridine, followed by halogenation. Subsequent reaction with *N*-alkyl-substituted (benz)imidazole derivatives gives the desired (benz)imidazolium salts with different *R* group at the *N*-wingtip (*R* = hexyl, heptyl, octyl, nonyl, decyl). Silver *N*-heterocyclic carbene complexes of the lead compound (**Im-71g**) was also synthesised and characterised. Attempt to crystallise the silver NHC

complex was unsuccessful and the crystal of silver NHC complex was not obtained, however, the crystal of its precursor **Im-76g-PF_6** was isolated. All synthesised compounds were characterised with ^{1}H- and ^{13}C-NMR, as well as mass spectrometry. The crystalline product was analysed using X ray diffraction (XRD). Besides, the Lipinski's Rule of Five was used as the reference for *in-silico* study. This computational study revealed that all synthesised compounds did not violate the rules and are deemed to be orally active.

Chapter 3 highlights on the antimicrobial screening and the evaluation of the antimicrobial profiles of the synthesised compounds. The synthesised compounds were tested against the selected pathogenic microorganism strains, which constitutes of eight Gram-positive and four Gram-negative bacteria, and three yeast species. From this study, it was noticed that the increasing alkyl chain length of the *R* group yielded improved antimicrobial properties, from hexyl to decyl, with lowest MIC value from 500 µg/mL to 7.81 µg/mL, respectively. Growth curves of *B. cereus* ATCC 14579 and *E. coli* ATCC 25922 cultured in the presence of the lead (benz)imidazolium salts, **Im-71g** and **Bz-71g** were plotted and they showed that the compounds started killing the bacteria the moment the bacteria were in contact with the compounds. Further test using intracellular component leakage test confirmed that the leakage took placed in the early phase of incubation.

Chapter 4 discusses the cell cytotoxicity profiles of the synthesised (benz)imidazolium salts against four selected cancerous cell lines. The half maximal inhibitory concentrations (IC_{50}) were determined and compared to the reference cisplatin reading. Similarly, the increasing alkyl chain length at the *N*-wingtip showed enhancement in the anticancer properties, from hexyl to decyl, with lowest IC_{50} value from 3.30 to 0.71 µM, respectively. The selectivity indices were determined for all synthesised (benz)imidazolium salts against two non-cancerous cell lines. There was no selectivity due to the rapid growth of non-cancerous cell lines where the compounds could not differentiate the cancerous and non-cancerous cell lines. Besides, intracellular ROS assay was conducted, and the results showed decrement in the ROS level in HCT-116 cell line. This observation stated that the mode of action of the synthesised (benz)imidazolium salts was not through oxidative stress elevation. This result was in agreeable to other literature reports where imidazolium salts in nature possess antioxidant properties.

In short, a series of *N*-alkyl-substituted (benz)imidazolium salts were synthesised and characterised with various spectroscopic techniques. This study revealed that the *R* group and the extended π-conjugation of benzimidazole had an influence on the biological properties. While the mode of action of imidazolium salts are not known, the moderate biological properties discovered from this study had shown the potential of (benz)imidazolium salts as candidate in drug developments in the future.

DECLARATION

This thesis contains no materials which has been accepted for the award of any other degree or diploma at any university or equivalent institution and that, to the best of my knowledge and belief, this thesis contains no material previously published or written by another person, except where due reference is made in the text of the thesis.

Print Name : Mah Wee Li

Date : 15th September 2021

RESEARCH OUTPUT

<u>Poster Presentation #1</u>

Facile Synthesis of Bioactive Pyridine-Functionalised Imidazolium Salts

Bioheterocycles 2019: 18th International Conference on Heterocycles in Bioinorganic Chemistry, 17th – 20th June (Ghent, Belgium)

<u>Poster Presentation #2</u>

Facile Synthesis of Bioactive Pyridine-Functionalised Imidazolium Salts

ACS on Campus, 3rd October (University of Malaya, Malaysia)

<u>3-Minute-Thesis Presentation #1</u>

Fighting Cancer with Coinage Metals

Three Minute Thesis (3MT®) 2019 Campus Finals, 30th May (Monash University Malaysia, Malaysia)

ACKNOWLEDGEMENTS

Firstly, I would like to express my utmost gratitude towards my research supervisor, Dr. Cheow Yuen Lin, for his patience and guidance throughout my Ph.D candidature. I'm grateful and indebted to him for the continuous supports and encouragements extended to me. I would also like to take this opportunity to thank my co-supervisors, Dr. Yeong Keng Yoon and A/Prof. Lee Sui Mae for the constructive feedback, especially on the biological application parts.

Millions thanks to the Ministry of Higher Education (MoHE) Malaysia for the financial support *via* Fundamental Research Grant Scheme (FRGS) (FRGS/1/2018/STG03/MUSM/02/1), Tropical Medicine and Biology (TMB) Multidisciplinary Platform *via* TMB seed grant, and Monash University Malaysia, School of Science *via* the research grant. Also, millions thanks to Monash University Malaysia for awarding me with the Merit Scholarship.

Besides, many thanks to the collaborators, who include Dr. Lee Wai Leng, A/Prof. Kumaran Narayanan, and Dr. Michelle Yap Khai Khun from Monash University Malaysia, and A/Prof. Tan Kong Wai from University of Malaya for providing resources and spending valuable time on this project. Not to be forgotten, the Ph.D administrators Dr. Tan Wooi Boon, Ms. Sujatha Nanoo, Ms. Emily Ng, and Ms. Juanita Rajamanickam for the administrative supports. Besides, many thanks to the amazing technical supports from the laboratory technical staffs, who include Mr. Syamil Razak, Mr. Syafiq Ashari and Mr. Jegan Ramasamy. Additionally, I would also like to thank the external technical supports from A/Prof. Anton Dolzhenko, Dr. Felicia Lim, and Ms. Jia Hui from NMR Monash University Malaysia Infrastructure Platform, and Dr. Tan Yee Seng from Research Centre for Crystalline Materials School of Science and Technology, Sunway University Malaysia.

Furthermore, I wish to express my sincere thanks to my candidature review panel members, A/Prof. Adeline Ting Su Yien, Dr. Pushpamalar Janarthanan, and Dr. Irene Ling for the research input during my candidature. Deepest gratitude to my supportive senior from the lab, Dr. Choo Kar Bee, for the unconditionally patience and guidance. Moreover, those who had taught me things and given me the moral supports, who include Dr. Hikari Oh Kan Fu, Dr. Yew Peng Nian, Dr. Yaw Chong Wey, Dr. Wong Kak Ming, Dr. Eng Shu Kee, Dr. Khoo Xin Hui, Dr. Steven Aw Yong Kit, Dr. Ong

Kuan Shion, Dr. Amy Teh, Dr. Patric Chua Tze Chien, Dr. Andrew Osahor, Dr. Krystle Santiago, Dr. Yeo Eng Hwa, Dr. Athena Ng Xin Hui, Dr. Tan Hui Li, Dr. Ooi Teng Sin, Allan Ng Wee Ren, Ding Zhen Shern, Yap Ling Sze, Chin Jia May, Calvin Goh Bok Sun, Gan Peck Teng, Tan Karl Vern, Wong Yin Cheng, Clerance Cheong Su Yee, Yong Yanning, Yean Ru Ann, Tammy Tan Xing Mei, Su Kar Yan, Loh Sze Le, Khor Zong Chin, Gan I-Ning, Chin Kar Wei, Caleb Cheah, Ho Jia Min, Teoh Shun Qi, and Tan Xiu Jun, I'm grateful that this Ph.D candidature had granted me the opportunity to have met all of you. I sincerely wish all of you the best!

Further, I would also like to thank the 5th Monash Science Symposium 2018 committee members. It was an honour to co-chair the event alongside with Dr. Krystle Santiago. Additionally, I sincerely thank Monash University Postgraduate Association 2019 for electing me as the co-activity manager with Yap Ling Sze. It was also my pleasure to be part of the American Chemical Society Monash University Malaysia International Student Chapter 2018 and 2019, as the School of Science Representative and Vice President, respectively. Also, many thanks to Monash University Australia for awarding me the award entitled Faculty of Science Award for Outstanding Contributions by a Graduate Research Student to the life of the Faculty/School Community.

In addition, I would like to extend my sincere thanks to all my friends for all the moral supports. Herein, I would like to thank all of you, especially Clement Chin Fung Ling, Chong Yee Aun, Loh Zhi Pei, Wong Yin Wee, Cheong Hoi Yee, Cheow Hee Keong, Wong Kah Chun, Lim Sip Yee, Chan Fu Mun, Low Vi Vien, Choi Zu Er, Cloe Yap, Lim Shan Jin, Tan Hsin Yen, Liew Kah Hsing, Chia Juin Yee, and Garry Law Kim Wee.

Finally, my heartfelt gratitude meant to be extended to my family, especially my parents for their unconditional loves and supports throughout the pursuit of my doctoral degree. None of this could have happened without my parents. The faith they have in me had been the reasons and energy I needed to face all the obstacles and the challenging paths. This dissertation stands as a testament to their love, their patience, their supports, and their encouragements extended to me.

TABLE OF CONTENT

LIST OF TABLES

LIST OF FIGURES

LIST OF SCHEMES

ABBREVIATIONS

AMP	Antimicrobial peptide
APD	Action potential deduction
ATCC	American Type Culture Collection
BMD	Broth microdilution
CHL	Chloramphenicol
CLSI	Clinical Laboratory Standards Institute
CHX	Cycloheximide
DCF	2’,7’-dichlorofluorescein
DCFDA	2’,7’-dichlorodihydrofluorescein diacetate
DHEA	Dehydroepiandrosterone
DLC	Delocalised lipophilic cation
DMSO	Dimethyl Sulfoxide
DNA	Deoxyribose nucleic acid
DPPH	2,2-diphenyl-1-picrylhydrazyl
DMEM	Dulbecco’s Modified Eagle Medium
DMEM-F12	Dulbecco’s Modified Eagle Medium-F12
EDTA	Ethylenediamine tetraacetic acid
ESI	Electronspray ionisation
FBS	Foetal bovine serum
FRAP	Ferric reducing antioxidant power
FT-IR	Fourier-transform infrared
GC	Gas chromatography
GSH	Glutathione (reduced form)
GSSG	Glutathione (oxidised form)
HPLC	High performance liquid chromatography
IL	Ionic liquid
IMR	Institute of Medical Research
MBC	Minimum bactericidal concentration
MHA	Muller-Hinton agar

MHB	Muller-Hinton broth
MIC	Minimum inhibitory concentration
MRSA	Methicillin-resistant *Staphylococcus aureus*
MS	Mass spectrometry
MSSA	Methicillin-sensitive *Staphylococcus aureus*
MTT	3-(4,5-dimethylthiazol-2-yl)-2,5-diphenyltetrazolium bromide
MW	Microwave irradiation
NHC	*N*-heterocyclic carbene
NMR	Nuclear magnetic resonance
PBS	Phosphate-buffered saline
Ro5	Lipinski's Rule of Five
ROS	Reactive oxygen species
RPMI	Roswell Park Memorial Institute
RNA	Ribose nucleic acid
SEM	Scanning electron microscopy
SI	Selectivity index
t-bu	*tert*-butyl
TEA	Triethylamine
TEAI	Tetraehtylammonium iodide
TLC	Thin layer chromatography
TPP	Triphenylphosphonium
UV	Ultraviolet
VRE	Vancomycin-resistant *Enterococcus* spp.
VT-NMR	Various temperature-nuclear magnetic resonance

CHAPTER 1 INTRODUCTION AND LITERATURE REVIEW

1.1 Overview of bioactive heterocycles

Heterocycles, or heterocyclic compounds, are cyclic compounds that consist of more than one different element situated within the ring structures. Heterocycles are widely distributed in nature, where most of them are greatly associated with our life (Gupta *et al* 2013). For instance, the genetic materials such as DNA and RNA are composed of heterocyclic bases namely pyrimidines and purines. Like cyclic hydrocarbon species, heterocycles are generally classified into heterocycloalkanes, heterocycloalkenes, and heteroaromatic systems, further subdivided based on the type of heteroatom, in which the heterocycle is not limited to, can contain several heteroatoms (Pozharskii *et al* 2011). Pyrimidine, pyrazine, pyrazole, and imidazole are examples of heterocycles with more than one identical or different heteroatoms within the ring structure **(Figure 1)**.

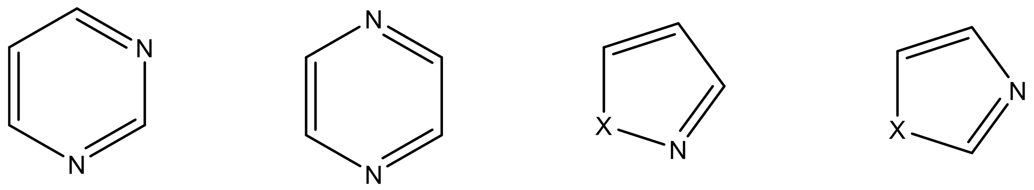

Pyrimidine

Pyrazine

Pyrazole (X = NH)
Isoxazole (X = O)
Isothiazole (X = S)

Imidazole (X = NH)
Oxazole (X = O)
Thiazole (X = S)

Figure 1. Heterocycles with more than one identical or different heteroatoms within the ring structure.

Heterocycles also play an important role in pharmaceutical and agricultural sciences. Several heterocycles such as amrinone used in the treatment of congestive heart failure, and paraquat which is used as a total herbicide, exhibit remarkable biological properties when bearing no or small substituent(s), which proves that the heterocyclic ring is part of the pharmacophore **(Figure 2)** (Angelucci & Bolle 1974; Yamatsu *et al* 1974). To date, more than 70 % of pharmaceutical drugs and agrochemicals constitute at least one heterocycle (Lamberth & Dinges 2012). Some of the biggest commercial products in the market today, such as the blood cholesterol reducer atorvastatin and the broad-spectrum fungicide azoxystrobin fall under the category of bioactive heterocycles **(Figure 3)** (Thrash *et al* 2007; Wynne *et al* 1980). In addition, heterocycles are an easily accessible scaffold that allows structural modification and formulation to produce more potent compounds. Simple aliphatic heterocycles such as *gem*-diethyl-substituted barbituric acid barbital used as a sleeping aid also demonstrate excellence biological properties **(Figure 4)** (Van der Burg *et al* 1970).

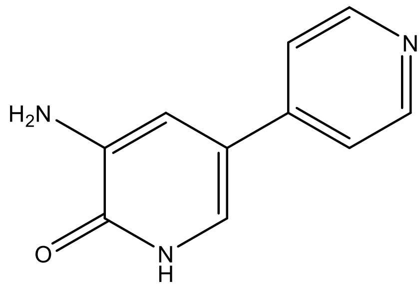

Amrinone

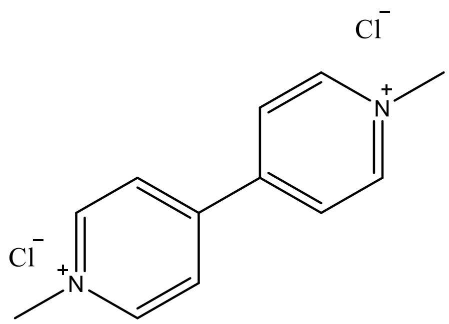

Paraquat

Figure 2. Amrinone (left) and paraquat (right) are the examples of highly active bipyridyl derivatives bearing small substituents.

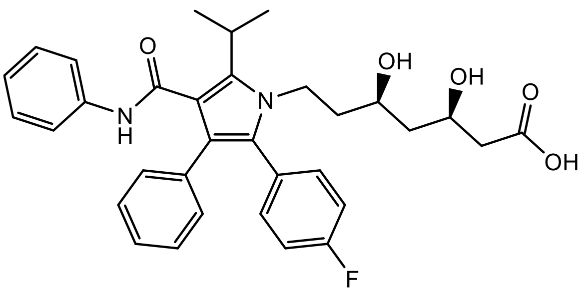

Atorvastatin

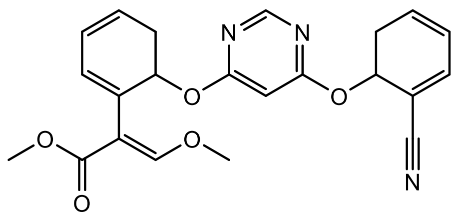

Azoxystrobin

Figure 3. Atorvastatin (left) and azoxystrobin (right) are two of the currently most successful pharmaceutical drugs and agrochemicals in the market.

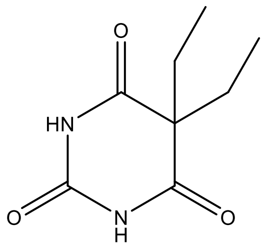

Barbital

Figure 4. Chemical structure of barbital, which is used as a sleeping aid.

1.2 Imidazole and imidazolium salts

Imidazole is a five-membered heterocycle species which consists of two nitrogen atoms within the ring structure, with a carbon atom situated in between. Imidazole was first prepared in 1858 by a scientist named Debus, using glyoxal and ammonia, and glyoxaline was the original name to indicate its source **(Scheme 1)** (Debus & Liebigs 1858). Later, as it falls under the azole family, which the term "azole" is used to describe five-membered polyheteroatomic ring systems, and the presence of an imino group within the ring structure, the name imidazole was given and more commonly used in the modern literature (Hantzsch 1888). While the chemical structure of imidazole appears to be almost symmetrical, the two nitrogen atoms in the heterocyclic ring exhibit different properties, where the nitrogen that is bound to a hydrogen (N_1H) is like that in a pyrrole ring, whereas the other nitrogen (N_3) is much like the nitrogen found in a pyridine (**Figure 5**). Imidazoles bearing a free imino hydrogen are expected to exhibit tautomeric character, however, the removal of this hydrogen or the addition of a proton to the pyridine nitrogen leads to the formation of ions, which results in the loss of possibility for tautomerism **(Scheme 2)**. Moreover, the electron-rich heterocycle could not only readily accept or donate hydrogen, but also able to form weak interactions, which enables the derivatives to easily interact with target enzymes and receptors in biological systems, thereby exhibiting wide range of biological properties (Zhang *et al* 2014). Furthermore, imidazole is amphoteric in nature, where the properties can be easily tuned by the addition or removal of proton, allowing the imidazole to act both as a base and acid, with pK_a values of 14.50 and 7.01, respectively (**Scheme 2**).

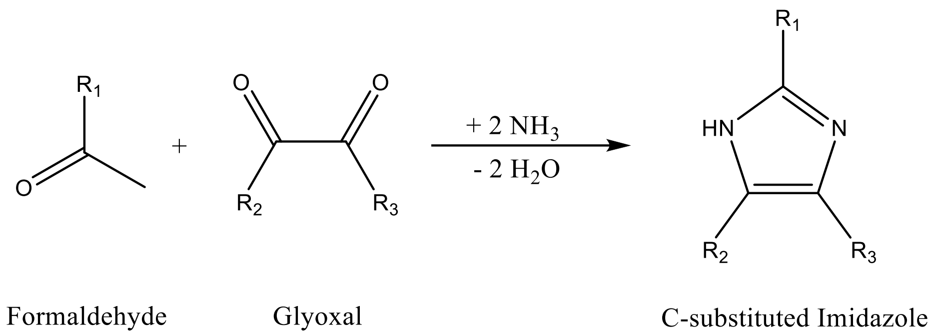

Scheme 1. Synthesis route to obtain C-substituted imidazole using glyoxal and ammonia by Debus.

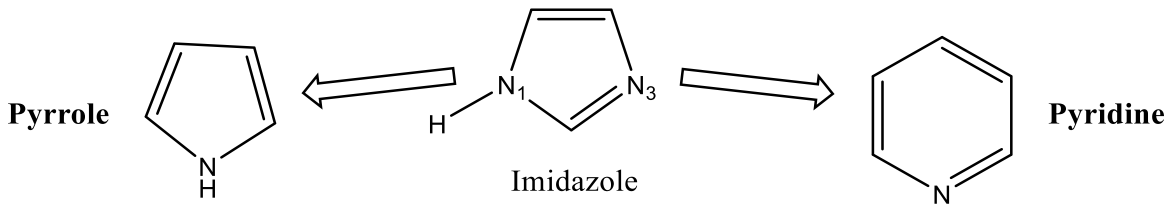

Figure 5. Illustration of the chemical properties of the nitrogen atoms in imidazole.

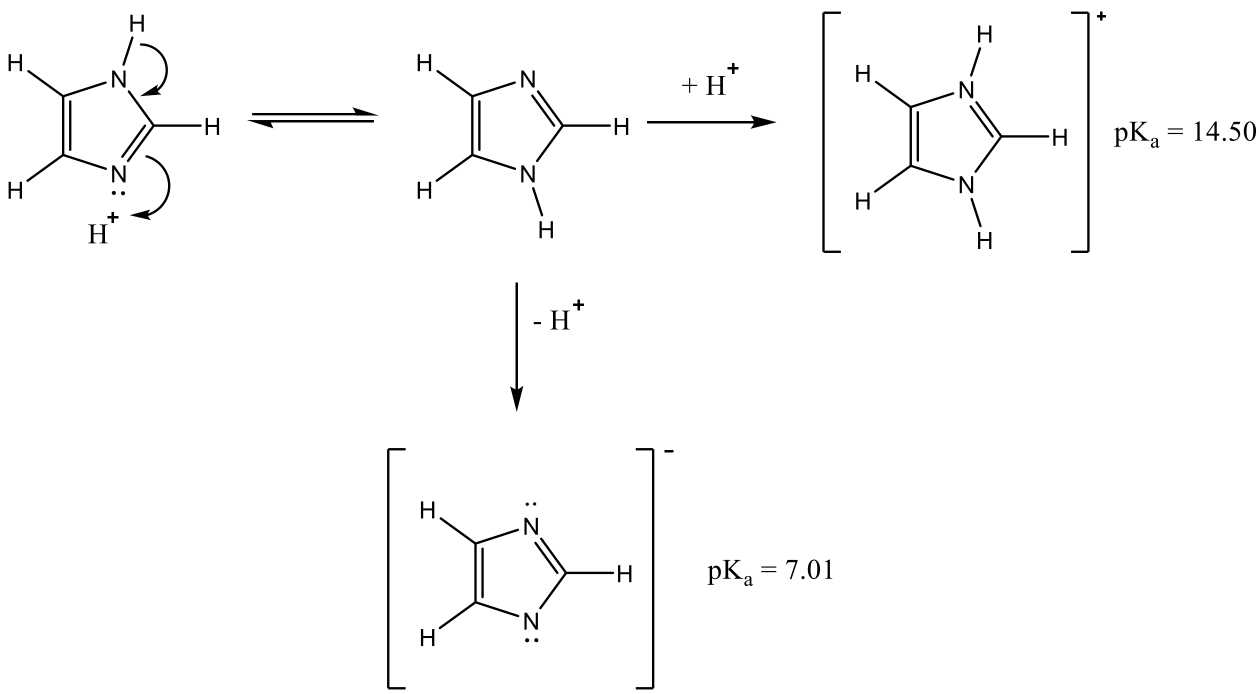

Scheme 2. Tautomeric imidazole losing its tautomerism after gaining a proton at the pyridine nitrogen or losing a proton from the imino nitrogen.

The discovery of imidazole has initiated the rapid development of imidazole-based compounds due to their various possible applications in pharmaceutical and agricultural sciences, artificial materials, supramolecular chemistry, and catalysis (Zhang *et al* 2014). Imidazole with multiple binding sites can coordinate with inorganic metal ions or interact with organic molecules to produce supramolecular drugs, which can possibly exert double biological action mechanisms to combat against drug resistances (Zhou *et al* 2010; Zhou *et al* 2009). In fact, enormous number of drugs in the market are imidazole-based, where these drugs are applied in various therapeutic treatments such as anticancer (dacarbazine and azathioprine), antifungal (clotrimazole and miconazole), antiparasitic (metronidazole and benznidazole), antihistaminic (cimetidine and thioperamide), antineuropathic (nafimidone and fipamezole), and antihypertensive (losartan and eprosartan) **(Figure 6)** (Ashley 2010; Burnier & Wuerzner 2011; Mishra & Ganguly 2012; Steinman *et al* 2012). This has proven the great developmental value in research of developing imidazole-based drugs.

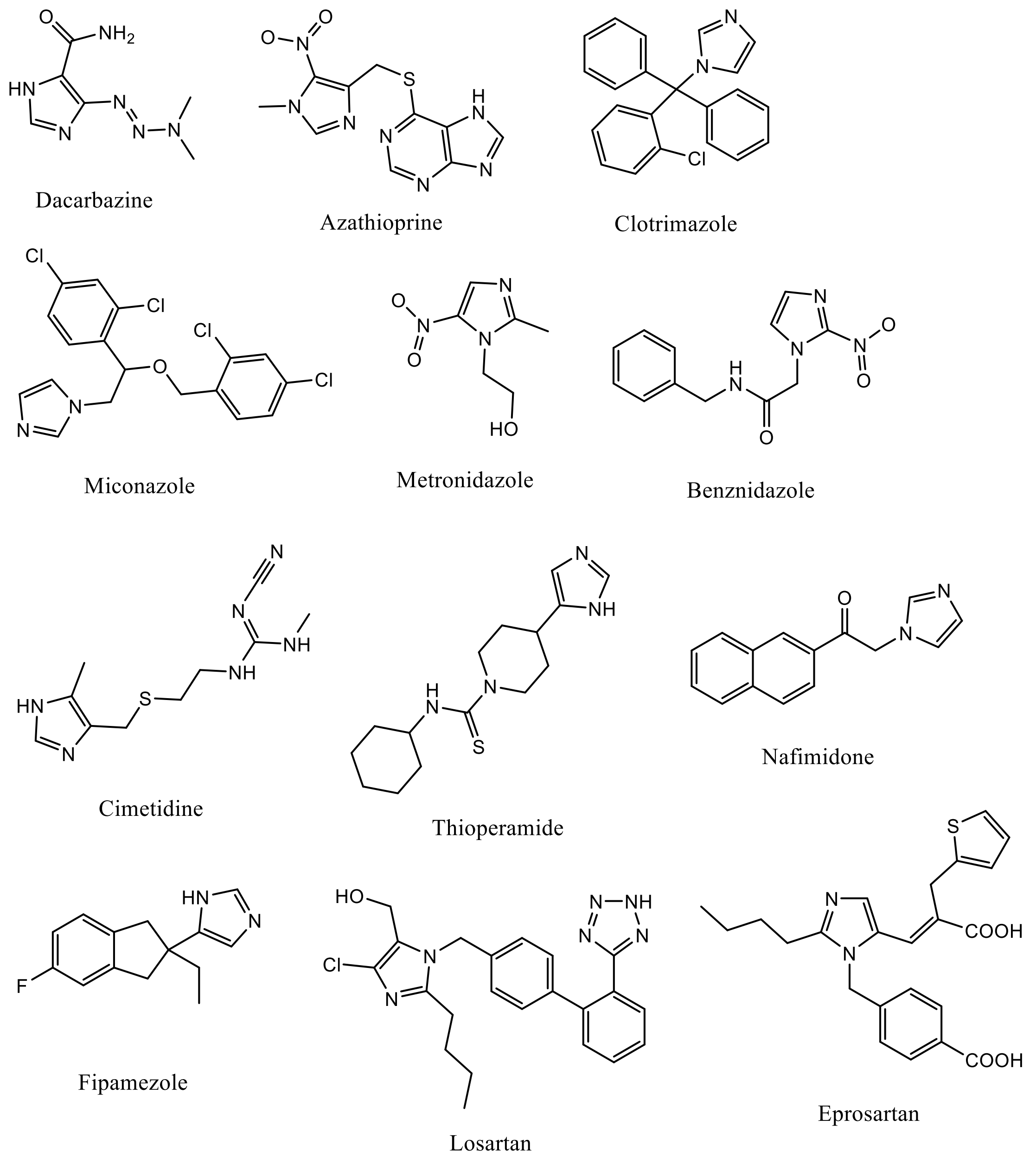

Figure 6. Common imidazole-based drugs in the market.

Imidazolium salts, derived from the parent imidazole, belong to the azolium salts family. Like imidazole, imidazolium salt serves as a highly versatile scaffold in medicinal chemistry, where desired functionality can be introduced into the structure readily. Despite the fact that imidazolium salts have a poorer hydrogen bonding ability compared to their parent imidazoles, the cationic imidazolium cores allow the compound to interact with biological systems electrostatically (Riduan & Zhang 2013). Furthermore, imidazolium salts are also famous for their application as ionic liquids

(ILs). With the astonishing chemical stability, ILs are often used as electrolytes and green solvents in the past decades (Zhang & Chan 2010). More recently, their potential application in biological processes is also being explored. In addition, imidazolium salts are also well-known as pro-ligands to produce *N*-heterocyclic carbenes (NHCs), which have even more applications in catalysis, coordination chemistry, supramolecular chemistry et cetera, due to their high stability and enhanced chemical properties (Marion *et al* 2007).

1.2.1 Synthesis of imidazolium salts

There are several ways to prepare imidazolium salts, where most popular options being direct nucleophilic substitution at the nitrogen atoms of imidazole, or by multicomponent reactions yielding *N,N'*-substituted heterocycles. Direct nucleophilic substitution can be further divided into two types: symmetrical and asymmetrical substitution at the *N*-wingtip of imidazole **(Scheme 3)** (Glushkov *et al* 2012; Li *et al* 2014; Pernak *et al* 2004). Meanwhile, the multicomponent reactions often adopt a simple one-pot synthesis method with glyoxal, amine and formaldehyde in presence of acid **(Scheme 4)** (Hans *et al* 2015; Herrmann 2002)

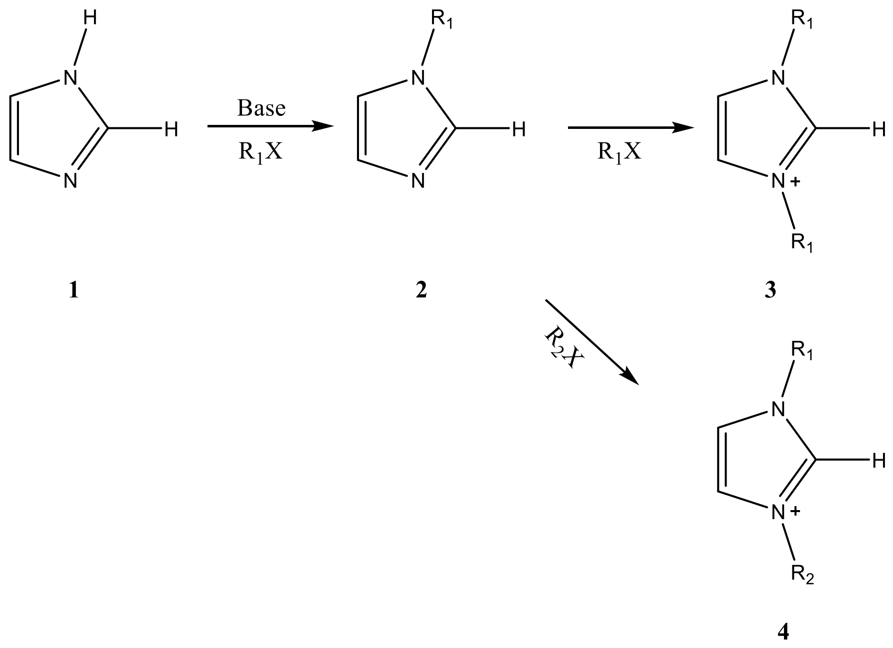

Scheme 3. General synthesis route of imidazolium salts *via* symmetrical **(3)** and asymmetrical **(4)** nucleophilic substitution.

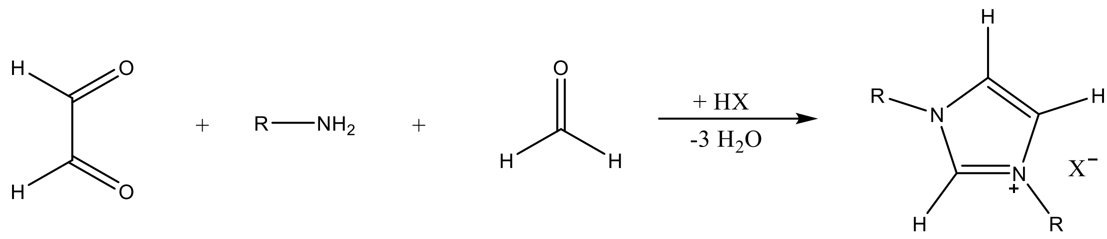

Scheme 4. General synthesis route of imidazolium salts *via* the multicomponent reactions using glyoxal **(5)**, amine **(6)** and formaldehyde **(7)** in presence of acid.

Besides, such readily synthesised compounds also have another astounding feature, which is the flexibility to design and introduce desired functionalities into the chemical system, thus altering the chemical and physical properties, or even enhancing the biological properties. For instance, the functional group of sotalol, an antiarrhythmic agent, was introduced into an imidazolium core by Lis and co-workers, yielding imidazolium derivative of sotalol to overcome the diminishing of myocardial function in patients with ventricular arrhythmia caused by sotalol **(Figure 7)** (Lis *et al* 1987). Out of all the derivatives, compound **8** displayed best antiarrhythmic properties, where 1.6 µM of compound **8** was able to cause a 20 % increase (+) and decrease (-) in action potential duration at 95 % repolarisation (APD_{95}), while sotalol was only able to show similar effect at 14.4 µM.

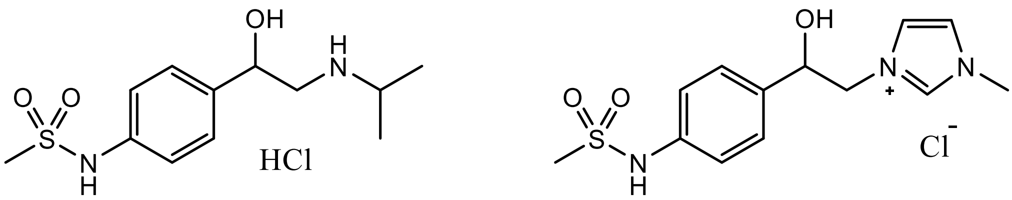

Sotalol **8**

Figure 7. Chemical structures of sotalol and compound **8.**

1.2.2 Industrial applications of imidazolium salts

In the recent development, ionic liquids (ILs) have become the emerging subject in industries to seek a replacement for the conventional organic solvents due to their low vapour pressure and their low melting points properties. While imidazolium based ILs may meet some of the ideal requirements as solvent option such as high solute selectivity, inertness to materials, non-flammability and low carrier selectivity, the cost and toxicity of ILs remained as important issues to be addressed (Mallakpour & Dinari 2012). The first imidazolium based IL was discovered by John Wilkes's group in early 1980s, where 1-alkyl-3-methylimidazolium chloride aluminium chloride ionic liquids ($[C_nC_1im]Cl\text{-}AlCl_3$, where $n = 1 – 4$) were introduced and $[C_2C_1im]^+$ showed the best transport properties **(Figure 8)** (Wilkes *et al* 1982). Over the past decades, a group of scientists developed a series of imidazolium based ILs and used them to synthesise a series of antiviral nucleoside drugs namely stavudine, brivudine and trifluridine (Kumar & Malhotra 2008). From their experiment, they found that the replacement of dimethylacetamide with the synthesised ILs **9 – 11** to synthesise stavudine reduced the reaction time from 30 minutes to as low as 5 minutes with yield increased from 81 % to up to 93 % **(Figure 9) (Scheme 5) (Table 1)**.

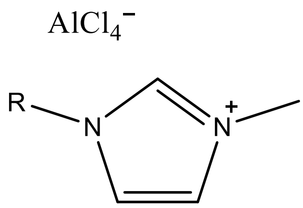

R = methyl, ethyl, propyl, butyl

Figure 8. Chemical structure of 1-alkyl-3-methylimidazolium chloride aluminium chloride ionic liquids.

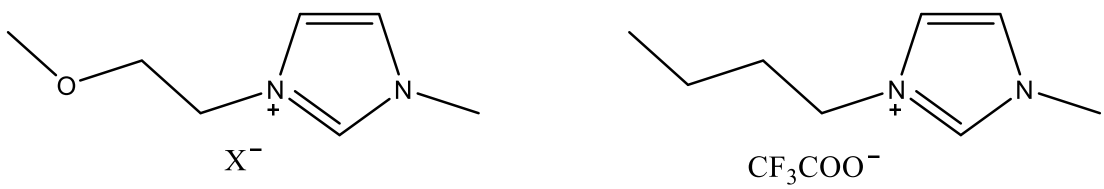

9, X = $CH_3SO_3^-$
10, X = CF_3COO^-

11

Figure 9. Chemical structures of the ILs used as the reaction medium for the synthesis of antiviral nucleoside drugs.

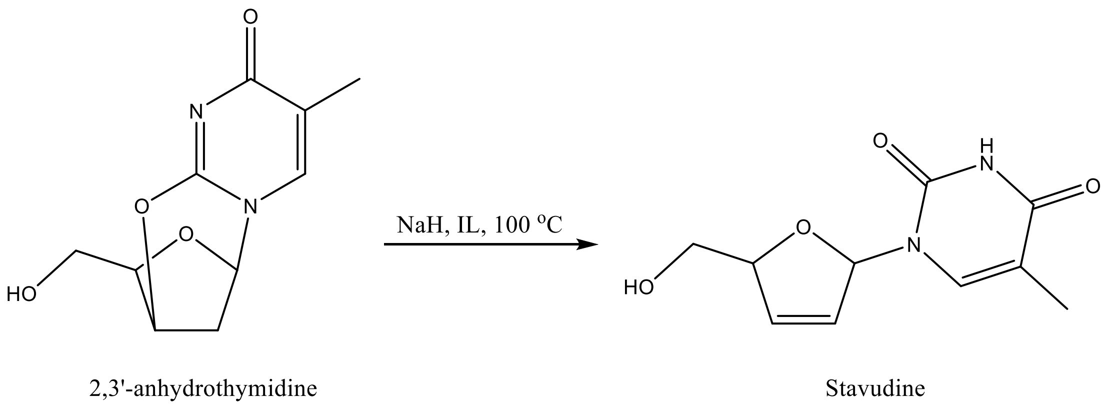

Scheme 5. Synthesis of stavudine *via* elimination of reaction on 2,3'-anhydrothymidine.

Table 1. Reaction conditions and yield of stavudine.

Solvent	Duration (min)	Yield (%)
Dimethylacetamide	30	81
9	10	89
10	5	93
11	10	91

Besides, 1-butyl-3-methylimidazolium ionic liquid was adopted as the solvent to conduct dimerisation of simple olefines and it was found to have improvements in catalytic activity, selectivity, and recyclability of the ILs and catalysts (Wasserscheid & Welton 2008). In addition, the report also showed that the propene dimers produced in ILs can be readily transformed into ethers or alkanes to produce high octane number additives for gasoline (Chauvin *et al* 1995). This non-protic liquid and its free of coordinating species also circumvented the issue faced by most of the organometallic catalytic systems which are highly sensitive to protons or bases, where the solvating media must be carefully chosen.

Despite most attempts in ILs has been focusing on the solvation capability for chemical synthesis and polymerisation, ILs have also been used in exploration of their potential in separation science such as being used as the stationary phase in HPLC and GC (Reid *et al* 2008; Wang *et al* 2006). Furthermore, ILs have also found to be portraying an excellent role as mobile phase additives in chromatography. Many pharmaceutical research facilities have interest in most basic compounds due to their potential therapeutic properties, however, the amino group in the compounds often interact with the residual silanols on the packing materials during isolation and purification, resulting in asymmetric peaks, low efficiencies, and irreproducible retention (Nawrocki 1997; Vervoort *et al* 1992). To overcome this problem, triethylamine (TEA) is commonly used as additive to suppress the silanols activity, thus enhancing the separation and resolution of the chromatogram. Over the past decades, IL **12** was found to display much more superior suppressive properties to TEA where the elution efficiencies were greater and higher plate numbers were achieved at same concentration (Ruiz-Angel *et al* 2006). Moreover, **12** also has neglectable influence on the retention factors while TEA decreases them due to the dual nature of ILs where both the constituting anion and cation partake in the retention mechanism (Berthod *et al* 2005).

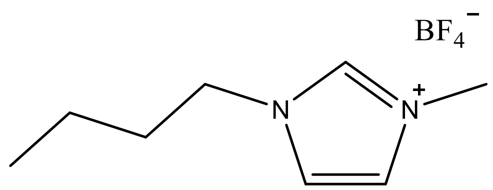

12

Figure 10. Chemical structure of IL **12**.

1.2.3 Potentials of imidazolium salts in medicinal applications

Aside from its well-known applications as ionic liquids, imidazolium salts also gain uniformly increasing popularity in medicinal chemistry. With the alarming news on the emergence of drug resistance and undesirable side effects of the existing drugs, imidazolium salts may be a potential scaffold as it fulfils the new molecular parameters introduced on drug discovery, which includes heteroatomicity, aromaticity, and structural diversity (Demberelnyamba *et al* 2004). Owing to the unique features of imidazolium salts, increasing numbers of novel imidazolium derivatives have been reported with their numerous biological properties explored, which include antimicrobial, antifungal, antitumour, antioxidant, antihelminthic, antiparasitic, and antiviral properties.

1.2.3.1 Antimicrobial and antifungal properties of imidazolium salts

Antimicrobial imidazolium salts have drawn much attention lately due to their ability in reinforcing ionic affinity, water solubility, membrane permeability, and preventing bacterial motion, thus improving the antimicrobial efficacy (Qian *et al* 2017). Transformation of imidazole into imidazolium would result in antimicrobial compounds with broadened spectrum, which can potentially combat against tough microorganisms with multiple drug resistance. The first reported antimicrobial imidazolium salts were a series of 1-alkyl-3-methylimidazolium halides (**13a – f**) and 1-alkyl-3-hydroxyethylimidazolium chlorides (**14a – b**) that exhibited low minimum inhibitory concentration (MIC) ranging from 4 – 500 µg/mL. Based on the study, it was explained that most imidazolium salts act through interacting with bacterial cytoplasmic membrane and subsequently disrupting the permeability of the cell membrane (Demberelnyamba *et al* 2004). Besides, the same group also showed that the introduction of long alkyl chain, and the hydroxyethyl and methyl groups in different positions within the imidazolium structure affected the antimicrobial properties mostly. It was suggested that the compounds behave similarly to quaternary ammonium compounds, where the longer alkyl chain length attributes to better surfactant properties, resulting in better antimicrobial properties.

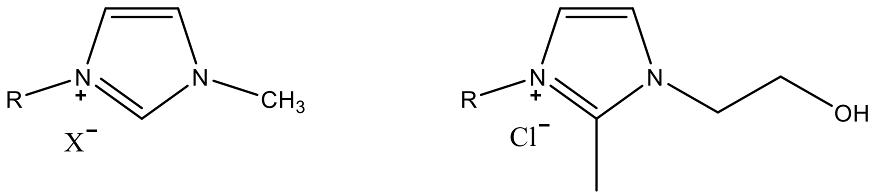

13a, *R* = C_8H_{17}, X = Cl
13b, *R* = $C_{10}H_{21}$, X = Cl
13c, *R* = $C_{12}H_{25}$, X = Cl
13d, *R* = $C_{14}H_{29}$, X = Cl
13e, *R* = $C_{14}H_{29}$, X = Br
13f, *R* = $C_{16}H_{33}$, X = Cl

14a, *R* = $C_{14}H_{29}$
14b, *R* = $C_{16}H_{33}$

Figure 11. Chemical structures of **13a – f** and **14a – b**.

Pushing beyond the traditional design, Morzycki and his co-workers (2019) worked on a new class of imidazolium salts which bear steroid functionality (Hryniewicka *et al*

2019). The idea behind fusing two bioactive compounds into one hybrid molecules aims to develop a new class of compound that can exert a broader spectrum of biological applications, which is also a common practice in medicinal chemistry. The first two steroids that were adopted in the compound design were lithocholic acid **(15)** and 3-oxo-23,24-dinorchol-4-en-22-al **(16)**, yielding **17a – d** and **18a – d** respectively. Based on the study, all the tested steroid-derived imidazolium salts showed great antimicrobial efficacy against the chosen bacteria and fungi with MIC values from 0.25 to 64 µg/mL. Comparing between the two series, **17a – d** generally displayed better antimicrobial properties against *S. aureus*, *B. cereus*, and *C. albicans*, however, less effective in antimicrobial properties against *E. coli* than **18a – d**. Moreover, the very same study also demonstrated that the antimicrobial properties are enhanced when the number of carbon atoms in the alkyl substituent increases. Encouraged from the results, the group employed dehydropiandrosterone (DHEA, **19**) as the steroid option in their compound design (Hryniewicka *et al* 2021). A total of 11 compounds were synthesised **(20a – k)**, bearing the alkyl substituent ranging from -CH_3 to -$C_{16}H_{23}$, and one with aromatic substituent. The antimicrobial properties evaluation demonstrated promising antimicrobial properties against the selected microorganisms with MIC values ranging from 0.25 to 64 µg/mL. While some antibiotics might cause drug-induced hemolytic anemia and thrombocytopenia, hemocompatibility has become one of the important criteria for successful *in vivo* administration as antibiotics. Based on the study, compound **20a – k** demonstrated low hemolytic activity at the MIC values. However, the data suggested that the longer the alkyl chain length, the hemolytic activity becomes worsen.

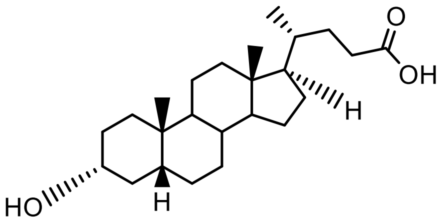

15

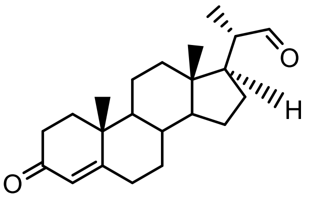

16

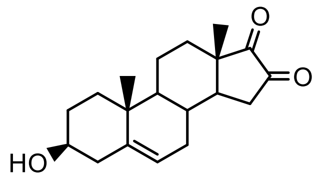

19

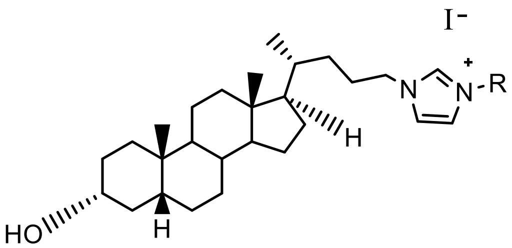

17a, $R = CH_3$
17b, $R = C_2H_5$
17c, $R = C_5H_{11}$
17d, $R = C_6H_{13}$

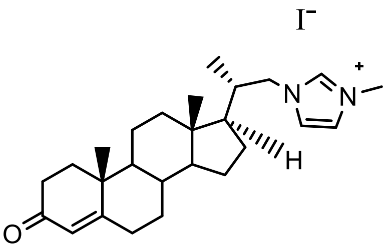

18a, $R = CH_3$
18b, $R = C_2H_5$
18c, $R = C_5H_{11}$
18d, $R = C_6H_{13}$

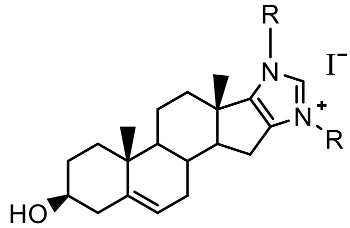

20a, $R = CH_3$
20b, $R = C_3H_7$
20c, $R = C_4H_9$
20d, $R = C_6H_{13}$
20e, $R = C_7H_{15}$
20f, $R = C_8H_{17}$
20g, $R = C_9H_{19}$
20h, $R = C_{10}H_{21}$
20i, $R = C_{12}H_{25}$
20j, $R = C_{16}H_{33}$
20k, $R = CH_2Ph$

Figure 12. Chemical structures of steroid-derived imidazolium salts.

Antimicrobial peptides (AMPs), a type of heterogenous antibiotic molecules produced by most multicellular organisms such as animals and plants, were also utilised to produce imidazolium-AMP conjugates (**21a** – **b** and **22a** – **b**) that were found to be effective against the chosen microorganisms with MIC values ranging from 0.25 to 5 µM (Reinhardt *et al* 2014). From the study, it was found that the bioactive cathelicidin AMP, LL-37 peptides **(21a – b)**, can penetrate better into *B. subtilis*, which constitute

a more compact peptidoglycan layered cell wall, compared to the other cathelicidin AMP, sC18 (**22a** – **b**). The peptide sC18 used in this study was a synthetic short C-terminal fragment of the cationic antimicrobial peptide of LL-37 that binds to lipopolysaccharides. Furthermore, the synthesised compounds produced best antimicrobial properties against the acid-fast bacterium, *Mycolicibacterium phlei*. This was claimed as unexpected phenomenon as *M. phlei* is rather tough towards antibiotic treatment due to their complex myolic acid layered cell wall. Meanwhile, a different group of scientists developed biocompatible imidazolium salt-derived hydrogels which bear antimicrobial properties (Liang *et al* 2019). A total of 6 hydrogels were developed, where 4 were based on vinyl imidazolium bromide (**23a – d**) and 2 were based on *N*-(3,6-dioxaoctane) imidazolium bromide and *N*-butylimidazolium itaconate (**24a – b**). Such hydrogels were found to be effective against selected multidrug-resistant microorganisms with MIC values ranging from 2 – 256 µg/mL, thus allowing potential application as biomaterials to prevent bacterial infections in clinical settings.

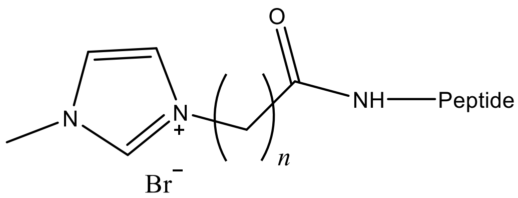

21a, *n* = 4, Peptide = LL-37
21b, *n* = 15, Peptide = LL-37
22a, *n* = 4, Peptide = sC18
22b, *n* = 15, Peptide = sC18

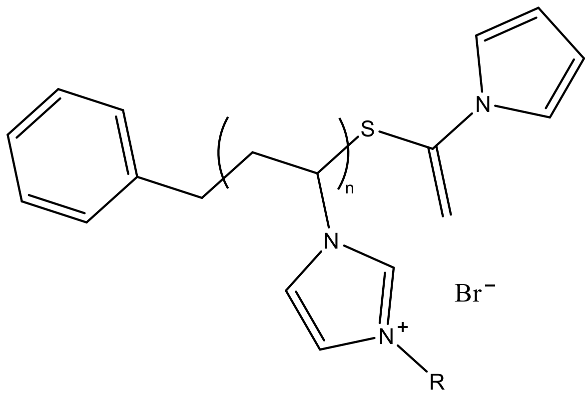

23a, *R* = C_2H_5
23b, *R* = C_4H_9
23c, *R* = C_6H_{13}
23d, *R* = $C_{10}H_{21}$

Figure 13. Chemical structures of AMP-containing imidazolium salts and imidazolium salt-derived hydrogel.

1.2.3.2 Anticancer properties of imidazolium salts

The structural versatility has positioned imidazolium salts as one of the targets of strategic advancement in drug development. Hitherto, lots of compounds that exhibited excellent anticancer properties could not proceed into the animal trials due to the high toxicity possessed by the compounds. With the versatility, imidazolium salts can carry organic moiety that masks the toxicity, while inducing highly cytotoxic properties. In the early 21st century, Cui and co-workers isolated the naturally occurring imidazolium salts, **24** and **25**, from the root extract of *Lepidium meyenii* and their cytotoxic profiles were evaluated against several cancer cell lines. While **24** was only moderately cytotoxic to the ovarian carcinoma FDIGROV with IC_{50} of 7.39 µg/mL, **25** was more aggressive against the tested cancer cell lines, which include human bladder carcinoma UMUC3, human pancreatic adenocarcinoma PACA2, human breast carcinoma MDA231, as well as FDIGROV cell lines with IC_{50} of 6.46, 1.38, 1.66 and 5.26 µg/mL respectively (Cui *et al* 2003).

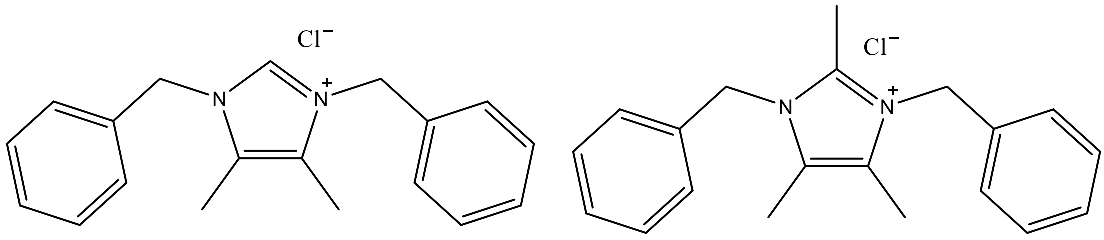

24 **25**

Figure 14. Chemical structure of **24** and **25** isolated from *Lepidium meyenii*.

Inspired by the cytotoxic profiles of **24** and **25**, Yang and co-workers adopted the chemical structures of **24** and **25** as the scaffold and developed a series of hybrid imidazolium salts with various functional groups within one single compound. A total of 21 compounds (**26a – u**) were synthesised and their anticancer properties were evaluated against myeloid leukaemia HL-60 and K562, epidermoid carcinoma A431, ovarian carcinoma SKOV-3, gastric carcinoma MKN-28, liver carcinoma SMMC-7721, laryngeal carcinoma Hep-2, and lung carcinoma GLC-15. Remarkably, amongst the synthesised compounds, some were extremely cytotoxic to the HL-60 and A431 cell lines with IC_{50} values as low as 1.1 µM (Yang *et al* 2009). Like the antimicrobial profile, the anticancer properties are greatly associated with the lipophilicity of the compounds, where increasing the lipophilicity can greatly enhance the cytotoxic properties. Besides, the study also revealed that compounds bearing *tert*-butyl group at position 1 or 3 were almost inactive against the tested cell lines, while compounds bearing a bulkier functional group at such position were more active, followed by compounds bearing aromatic moiety at position 1 or 3 being the most active. These findings escalated the extended study on hybrid imidazolium salts, where the same group of researchers conducted structure-activity relationship on (dihydro)benzofuran imidazolium salts. Another 15 compounds (**27a – o**) were synthesised and their cytotoxic properties were evaluated against MCF7 and HL-60 cell lines (Liu & Gust 2013; Wang *et al* 2013). Despite the cytotoxic profiles were not as promising as **26a – u**, **27a – o** were considered relatively potent, given that the IC_{50} values were as low as 5.78 µM against the tested cell lines.

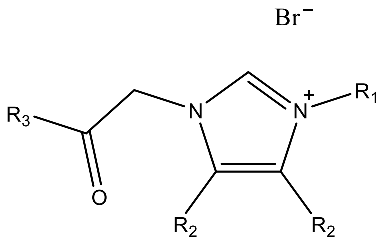

26a - u

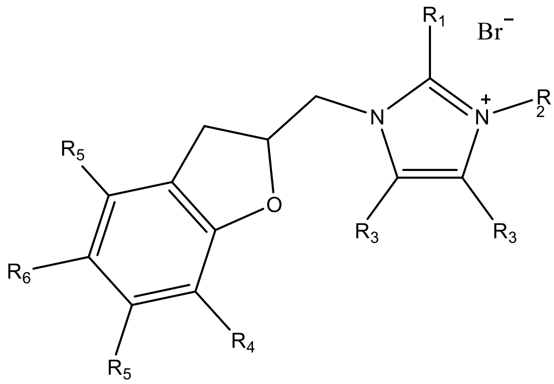

27a - o

	26			**27**					
	R1	*R2*	*R3*	*R1*	*R2*	*R3*	*R4*	*R5*	*R6*
a	*t*-C_4H_9	H	C_6H_5	H	naphthylacyl	H	H	H	H
b	*t*-C_4H_9	H	$C_6H_4(OCH_3)$-4	H	naphthylacyl	H	H	H	Cl
c	$C_6H_2(CH_3)_3$-2,4,6	H	*t*-C_4H_9	H	4-methoxyphenacyl	H	H	H	Cl
d	adamantyl	H	C_6H_5	H	4-bromophenacyl	CH_3	H	H	Cl
e	adamantyl	H	$C_6H_4(OCH_3)$-4	H	4-methoxyphenacyl	CH_3	H	H	Cl
f	adamantyl	H	2-naphthyl	H	naphthylacyl	H	H	CH_3	H
g	$C_2H_4C_6H_2(OCH_3)_2$-3,4	H	$C_6H_4(OCH_3)$-4	H	4-bromophenacyl	H	H	CH_3	H
h	$C_2H_4C_6H_2(OCH_3)_2$-3,4	H	2-naphthyl	H	2-bromobenzyl	H	H	CH_3	H
i	$C_6H_2(CH_3)_3$-2,4,6	H	C_6H_5	H	4-methoxyphenacyl	H	H	CH_3	H
j	$C_6H_2(CH_3)_3$-2,4,6	H	$C_6H_4(OCH_3)$-4	H	benzyl	H	H	H	H
k	$C_6H_4(CH_2COCH_3)$-4	H	C_6H_5	CH_3	benzyl	H	H	H	H
l	$C_6H_4(CH_2COCH_3)$-4	H	$C_6H_4(OCH_3)$-4	C_2H_5	benzyl	H	H	H	H
m	$C_6H_4(NO_2)$-4	H	$C_6H_4(OCH_3)$-4	C_2H_5	2-bromobenzyl	H	H	H	H
n	$C_6H_2(CH_3)_3$-2,4,6	H	2-naphthyl	C_2H_5	butyl	C_6H_5	H	H	H
o	$C_6H_3(i\text{-}C_3H_7)_2$-2,6	H	$C_6H_4(OCH_3)$-4	H	benzyl	H	H	H	H
p	$C_6H_3(i\text{-}C_3H_7)_2$-2,6	H	2-naphthyl						
q	$C_6H_2(CH_3)_3$-2,4,6	H	$C_6H_3(3\text{-}CH_2OCH_2\text{-}4)$						
r	$C_6H_3(i\text{-}C_3H_7)_2$-2,6	H	$C_6H_3(3\text{-}CH_2OCH_2\text{-}4)$						
s	$C_6H_2(CH_3)_3$-2,4,6	CH_3	2-naphthyl						
t	$C_6H_2(CH_3)_3$-2,4,6	H	$C_6H_4(Br)$-4						
u	$C_6H_3(i\text{-}C_3H_7)_2$-2,6	H	$C_6H_4(Br)$-4						

Figure 15. Chemical structures of **26a – u** and **27a – o.**

Utilising the delocalised lipophilic cations (DLC) such as triphenylphosphonium (TPP) salts' ability to kill cancer cells through accumulation in and disruption of mitochondria, Stromyer's group designed a new imidazolium salt bearing TPP (**28**) and the cytotoxicity was evaluated *in vitro* and *in vivo* against bladder cancer. Based on the study, **28** was able to produce GI_{50} (the concentration where 50 % of maximal inhibition of cell proliferation is observed) value ranging from 200 to 250 µM over a period of one hour (Stromyer *et al* 2020). Compound **28** was found to inhibit bladder cancer through induction of apoptosis and appeared to behave like mitochondrial toxin. Similar efficacy was observed when the compound was administered into a mouse model intravesically. On the other hand, Haque and co-workers designed a series of (benz)imidazolium salts (**29** and **30a – c**) suitable to be used as ligands for synthesis of *N*-heterocyclic carbene complexes (Haque *et al* 2013; Haque *et al* 2013). The ligands were evaluated their cytotoxic profiles against the K562 cell lines and the IC_{50} values were as low as 8.9 µM. Besides, the study also revealed that the longer the alkyl chain length substituted, the better the anticancer activities induced by the compounds.

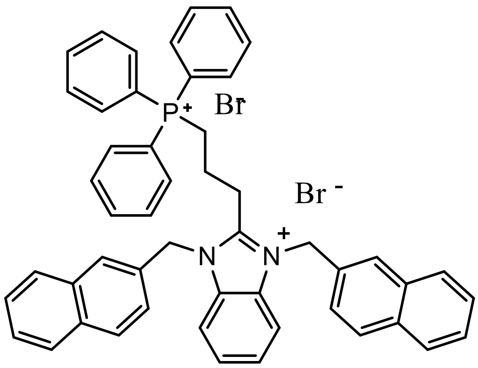

28

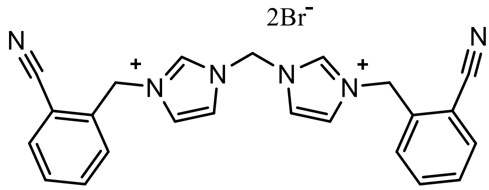

29

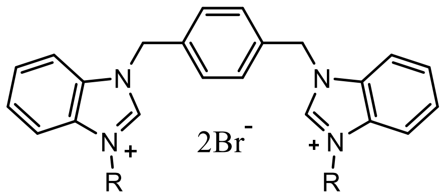

30a, *R* = C_8H_{17}
30b, *R* = C_9H_{19}
30c, *R* = $C_{10}H_{21}$

Figure 16. Chemical structures of TPP-bearing imidazolium salts and alkyl-substituted imidazolium salts.

1.2.3.3 Antioxidant properties of imidazolium salts

While imidazolium salts have been well studied for their antimicrobial and anticancer properties, the antioxidant properties of imidazolium salts remain in the infancy stage in research. Based on a research conducted by Zhuo and co-workers, compound **31** and **32** demonstrated reducing power that could reduce the glutathione (GSSG – oxidised form) into glutathione (GSH – reduced form), which increased the GSH/GSSG ratio dramatically to 7.4-fold of the control. It was found that **31** reduced GSSG through neutralisation of oxidative stress imposed by the exogenous H_2O_2 on the cells (Zhang *et al* 2009). Meanwhile, Haque's group also tested their compounds (**30a – c**, **Figure 16**) on their antioxidant properties, and it was found that **30a** was able to reduce 17.91 % of DPPH, while the standard reference for DPPH assay, gallic acid, was able to reduce the DPPH by 77.68 % at 400 µM (Haque *et al* 2013). Recently, Sharhan and co-workers synthesised a series of imidazolium salts and evaluated their antioxidant properties. A total of 16 compounds (**33a – p**) were synthesised and the IC_{50} for DPPH assay was found to be as low as 43 ± 2 µM. However, those compounds with lower IC_{50} values do not possess similar antioxidant properties in terms of FRAP assay. Unexpectedly, those that displayed high IC_{50} values for DPPH assay demonstrated high reducing power in FRAP assay, where **33h** and **33l** showed value of 211 µg FE/mL. The poor correlation of the two assays suggested that the analysis of antioxidant properties was only limited to DPPH assay (Sharhan *et al* 2018).

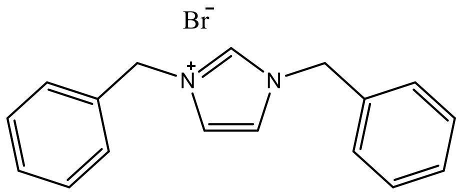

31

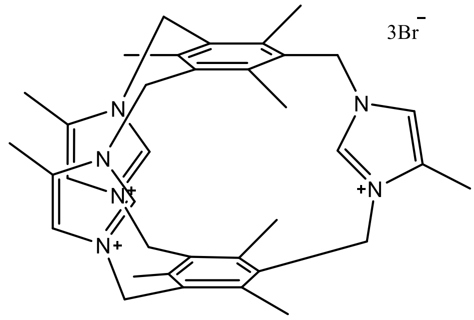

32

Figure 17. Chemical structures of compound **31** and **32**.

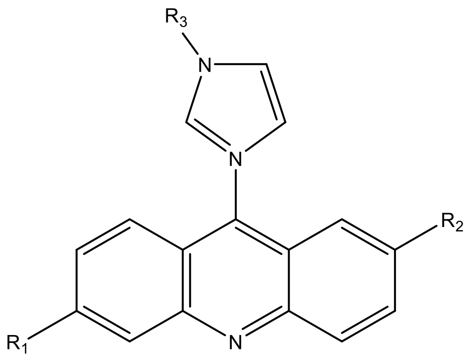

33a, R_1 = H, R_2 = OCH_3, R_3 = C_6H_{13}
33b, R_1 = H, R_2 = OCH_3, R_3 = CH_3
33c, R_1 = H, R_2 = OCH_3, R_3 = C_4H_9
33d, R_1 = Cl, R_2 = OCH_3, R_3 = CH_3
33e, R_1 = Cl, R_2 = OCH_3, R_3 = C_2H_5
33f, R_1 = Cl, R_2 = OCH_3, R_3 = C_4H_9
33g, R_1 = Cl, R_2 = OCH_3, R_3 = C_8H_{17}
33h, R_1 = H, R_2 = H, R_3 = *p*Me-Bn
33i, R_1 = H, R_2 = H, R_3 = *p*Br-Bn
33j, R_1 = H, R_2 = H, R_3 = *o*Br-Bn
33k, R_1 = H, R_2 = H, R_3 = *p*NO_2-Bn
33l, R_1 = H, R_2 = H, R_3 = $BzCH_2$
33m, R_1 = H, R_2 = H, R_3 = *p*Br-$BzCH_2$
33n, R_1 = Cl, R_2 = OCH_3, R_3 = Bn
33o, R_1 = Cl, R_2 = OCH_3, R_3 = $BnCH_2$
33p, R_1 = Cl, R_2 = OCH_3, R_3 = *p*Br-$BzCH_2$

Figure 18. Chemical structures of **33a – p**.

1.2.4 *N*-heterocyclic carbene – Synthesis and applications

A carbene molecule is a neutral compound containing a divalent carbon atom with six-valence shell. The incomplete electron octet of carbene carbon results in structural instability of free carbene, rendering it being used only as reactive species in organic transformation reactions such as cyclopropanation in the olden days (Hopkinson *et al* 2014). In late 1980s, carbenes were isolated and stabilised through substituent migration from silicon or phosphorous core to carbene carbon atom (Igau *et al* 1988). Later, first successful isolation of free carbene was reported and characterised as *N*-heterocyclic carbene (NHC) (Arduengo III *et al* 1991). This momentous breakthrough has turned NHCs pivotal in developments of new class of compounds to be used in wide range of industrial capacities, including catalysis and medical research.

NHCs are heterocyclic species containing a carbene carbon with divalent electron shell derived from persistent carbenes and at least one nitrogen atom situated within the ring structures (de Frémont *et al* 2009). Despite having a six valent electron shell, the carbene carbon remains stable as it is stabilised electronically by the adjacent nitrogen atoms through the π-electron donating and σ-electron withdrawing effect, creating a push-and-pull mechanism, granting NHCs the remarkably enhanced structural stability **(Figure 19)** (Hopkinson *et al* 2014).

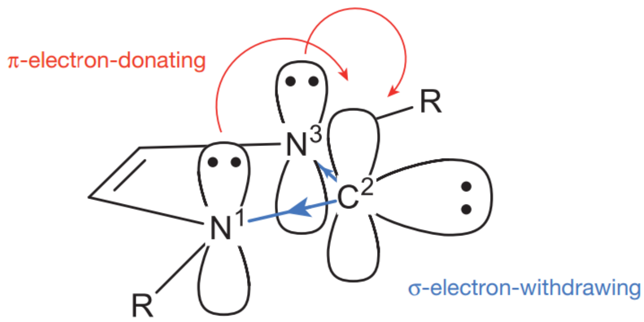

Figure 19. The π-electron donating and σ-withdrawing effect in a ground-state electronic structure of NHC, stabilises the six valent electrons carbene structure (Hopkinson *et al* 2014).

There are numerous classes of NHCs that have been discovered over the past three decades. The most extensively studied classes of NHCs are mainly derived from the five-membered ring moieties known as imidazolylidenes **(Figure 20)**. The formulation of NHCs originated from a mere laboratory curiosity and have evolved into a powerful tool used in variety of applications due to their structural diversity. NHCs can easily undergo modification by introducing a functional moiety at various positions on the NHC core (Johnson *et al* 2017). Besides, most NHCs are relatively stable to air and moisture, thus having a longer storage life as compared to phosphine ligands. As such, the preparation of NHCs are generally more favourable as the reactions can be conducted under ambient conditions. Generally, different substituted imidazolylidenes can be either prepared from deprotonation of imidazolium salts with the use of strong base such as sodium hydride, or by reductive desulphurisation of imidazoline-2-thiones **(Scheme 6)** (Bornemann *et al* 2020). In this study, the deprotonation of imidazolium salts with the use of base pathway was adopted for all synthesis of NHCs.

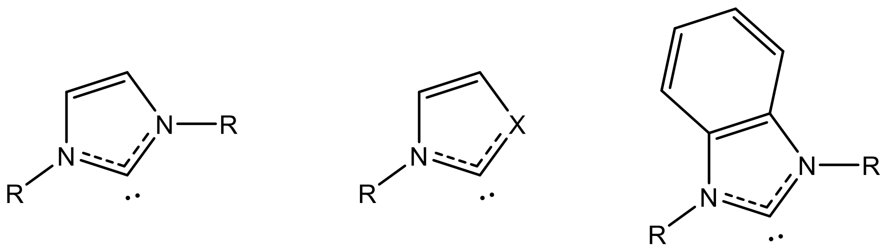

34a **34b** **34c**

Figure 20. Chemical structures of most studied NHC scaffolds: imidazolylidene **(34a)**, triazolylidene **(34b)** and benzimidazolylidene **(34c)**.

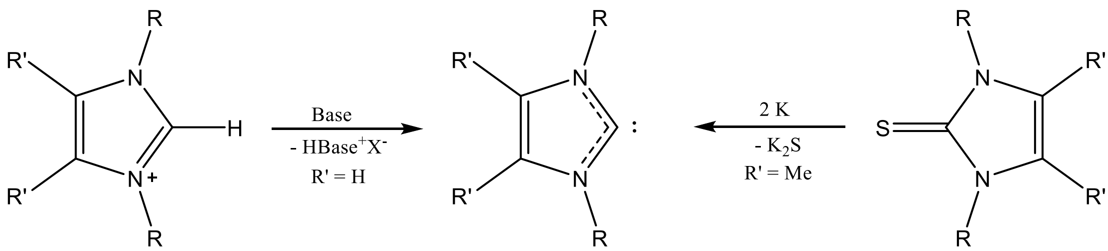

35 **36** **37**

Scheme 6. General synthesis route of imidazolylidenes, **36**.

1.2.4.1 Emergence of metal NHC complexes

N-heterocyclic carbenes are often involved in coordination to transition metals. The first metal NHCs were reported back in 1968, where Wanzlick and Ofele, independently, produced mercury(II) and chromium(0) NHCs respectively (Öfele 1968; Wanzlick & Schönherr 1968). The strong σ-donor capabilities and the ability to partake in π-backbonding have allowed NHC ligands to coordinate wide range of metal ions with either low or high oxidation number, forming stable metal NHC complexes (Johnson *et al* 2017; Rubio-Pérez *et al* 2013; Samantaray *et al* 2006; Zhuang *et al* 2013). Moreover, NHCs have the ability to displace 2-e^- donor ligands such as amines and ethers in metal coordination, rendering NHCs to bind more strongly to a metal centre as compared to traditionally used phosphine ligands, making the metal-NHC complexes more active in oxidative addition reactions (Baratta *et al* 2000; Perry *et al* 2003). The strong bonding between the NHCs and metals impedes the rate of dissociation, overcoming the common issues in most modern catalysts that are prone to rapid decomposition in catalysing reactions (Correa *et al* 2011).

1.2.4.2 Current application of metal NHC complexes

Metal NHC complexes emerged as one of the most powerful synthetic tools in catalysis chemistry over the past decades. For instance, Grubbs' second-generation catalyst derived from ruthenium NHC has replaced its phosphine-based catalyst in olefin metathesis **(Figure 21)** (Grubbs 2004). The employment of NHCs has proven to produce better catalytic activities and the better structural stability has make NHCs more favourable candidates in catalysis than phosphine (Derat & Maestri 2013). Furthermore, recognised with the Nobel Prize in Chemistry, Mizoroki-Heck reaction is one of the most significant coupling reactions that unravels the mystery to carbon-carbon bond formation (Astruc 2011; Jagtap 2017). Despite the fact that palladium phosphine was initially used as the catalyst, the discovery of palladium NHC replaces the phosphine-palladium system due to the requirement of excess phosphine to compensate the ligand loss from the P-C bond cleavage that reduces the catalyst efficiency (Herrmann *et al* 1999; Sabounchei *et al* 2015).

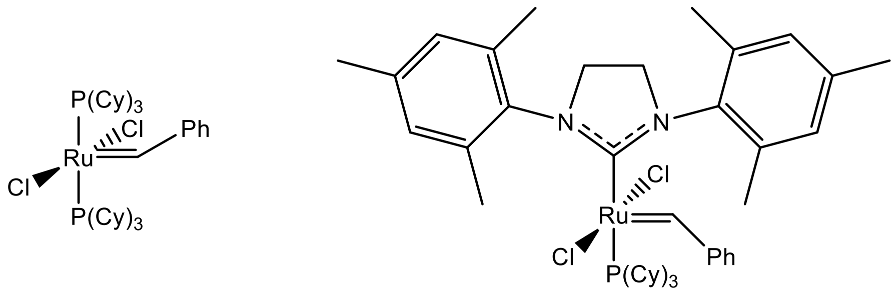

38 **39**

Figure 21. Chemical structure of Grubbs catalyst; first generation **(38)** and second generation **(39)**.

Metal NHCs have also gained popularity in the realm of medicinal chemistry over the years. A wide range of transition metals including silver, gold, palladium, platinum, rhodium and ruthenium have become favourite choices of metal for bioactivity evaluations. Besides, the structural versatility allows NHCs to carry desired functionality, whilst bearing a bioactive metal centre and masking the toxicity of the metal, which make them useful in drug designs (Johnson *et al* 2017; Storr *et al* 2006). In addition, the remarkable stability of metal NHCs prevents them from dissociation before reaching the biomolecular target, which in turn enhances the efficacy of the immunoresponses (Reedijk 2008). Moreover, the nitrogenous moiety of the NHC core provides a new centre for hydrogen bonding, which could influence the binding of the compound to the biomolecular target (Hendricks *et al* 1936; Ramos-Lima *et al* 2010). These features have driven the interest of metal NHCs to a lesser-known function in biological applications, from their renowned capabilities as industrial catalysts.

The very first bioactive metal NHCs were reported back in year 1996, where rhodium(I) NHC **(40)** and ruthenium(II) NHC **(41)** were synthesised and biologically evaluated in the study **(Figure 22)**. Both **40** and **41** were active against *Enterococcus faecalis* and *Staphylococcus aureus* at minimum inhibitory concentration (MIC) value as low as 5.00 µg/mL, while **41** was also found to be effective against *Escherichia coli* and *Pseudomonas aeruginosa* at 1.00 g/mL **(Table 2)** (Çetinkaya *et al* 1996). Despite the antimicrobial activities were not as potent as the commercially used ampicillin, this discovery sparks the potential in metal NHCs as drug candidates. In this research, silver was chosen as the metal of interest.

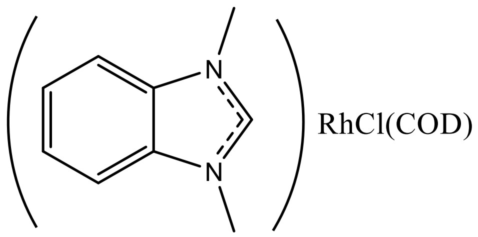

40

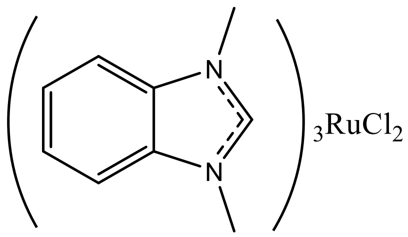

41

Figure 22. Chemical structures of rhodium(I) NHC **(40)** and ruthenium(II) NHC **(41)** complexes.

Table 2. Minimum inhibitory concentration (µg/mL) of **40** and **41** with ampicillin as control.

Compound	Minimum inhibitory concentration (µg/mL)			
	E. faecalis ATCC 29212	*S. aureus* ATCC 29213	*E. coli* ATCC 25922	*P. aeruginosa* ATCC 27853
Ampicillin	0.78	0.39	3.12	> 75.00
40	5.00	5.00	> 1000.00	> 1000.00
41	6.25	6.25	1000.00	1000.00

1.2.4.3 Silver NHC complexes in medicinal chemistry

Despite majority of the bioactivity evaluations have been focused on platinum- and gold NHC complexes, the bioactive model of silver-NHC complexes are well documented too (Hindi *et al* 2009; Johnson *et al* 2017; Oehninger *et al* 2013). Silver was commonly used as antiseptics for several medical conditions before revelation of the respective causative agents and was the third metal known to be used after gold and copper (Alexander 2009). Later in the 19th century, silver nitrate was used to treat ulcers and burns by promoting crust formation on the wound surface and removing the granulation tissues, thus allowing wound healing through epithelisation (Klasen 2000). However, use of silver-based drugs were dampened due to the side effects such as rare pigmentation of the skin and eyes caused by prolonged exposure, and accidental discovery of penicillin during the World War II (Drake & Hazelwood 2005). The amazingly effective penicillin against pathogenic bacteria has led to excessive usage of penicillin in fighting bacterial infections, creating unwanted resistant strains of common bacteria such as *Staphylococcus aureus*, *Neisseria gonorrhoeae*, *Escherichia* *coli*, and *Pseudomonas aeruginosa* in the 20th century (Alanis 2005). Silver-based drugs such as silver sulfadiazine was then "resurrected" to treat several bacterial infections caused by burn and has become the first line defence against wound infections in burn wards **(Figure 23)** (Fox 1968).

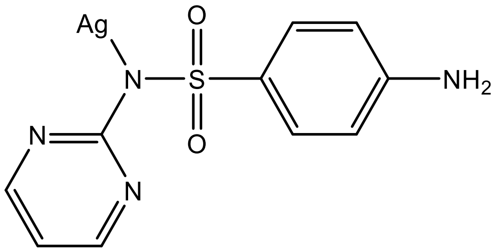

42

Figure 23. Chemical structure of silver sulfadiazine.

Although the mechanism of how silver-based compounds act has not been fully elucidated yet, it is suggested that most silver-based drugs involve the release of Ag^+ ions that enter the target cell membranes to disrupt the cellular functions by inactivating the viral enzymes through reacting with the thiol groups, or by interacting with DNA helix, which results in pyrimidine dimerisation and prevents DNA replication (Matsumura *et al* 2003). Despite of having great activity observed in silver-based drugs, the expeditious release of Ag^+ ions causes the drugs to be less effective over a short period of time (Liu & Gust 2013). Even though antimicrobial pharmaceuticals such as silver sulfadiazine, are effective in inhibiting the growth of bacteria, these drugs tend to lose their effectiveness over time due to development of resistance. This results in a need to search for alternative compounds that release Ag^+ ions much slower. Hence, strong coordinating ligands such as NHCs can be employed to prevail the abovementioned limitations, developing new class of drugs that are more long-lasting.

In 2004, first antimicrobial silver NHC complexes were reported to be effective *in vitro* against *E. coli*, *S. aureus*, and *P. aeruginosa* at MIC value of 281 mg/mL, which both complex **43** and **44** were at least 10 folds more potent than the traditionally used silver nitrate **(Figure 24)** (Melaiye *et al* 2004). This finding has quickly led to its dinuclear analogue **45**, encapsulated in Tecophilic polyurethanes, and it was found to demonstrate enhanced effectiveness than silver sulfadiazine and silver nitrate **(Figure 24)** (Melaiye *et al* 2005). The same group then moved on to further investigations on xanthine-functionalised silver NHCs **46** and **47** and these complexes demonstrated potent activities against the tested microorganisms with MIC values ranging from 1 to 8 µg/mL **(Figure 24)** (Knapp *et al* 2010). Later, *in vivo* study showed that with **46** nebulised into lungs of mice infected with *P. aeruginosa,* 83 % of infected mice survived the infection three days after the inoculation (Panzner *et al* 2009).

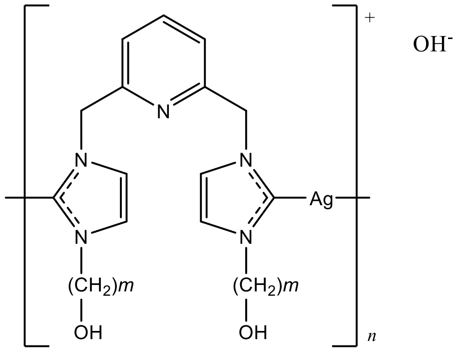

43, m = 2
44, m = 3

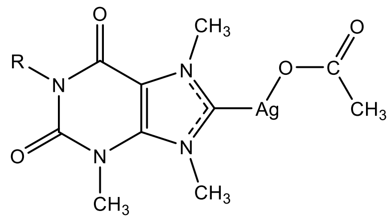

46, R = $-CH_3$
47, R = $-CH_2CH_2OH$

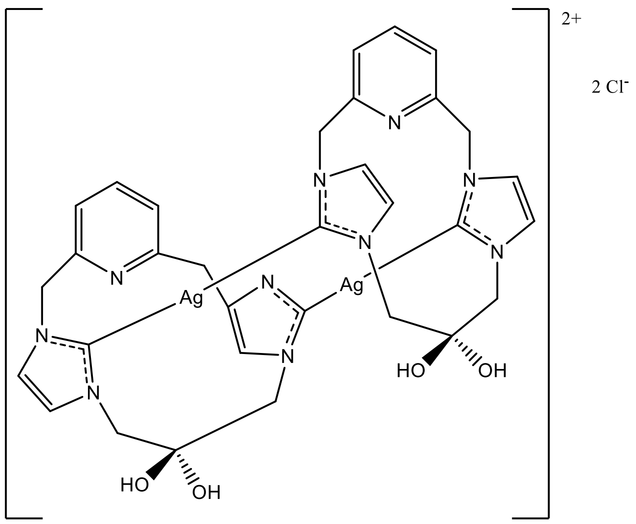

45

Figure 24. Chemical structures of Ag(I) NHC complexes by Young's group (Knapp *et al* 2010; Melaiye *et al* 2004; Melaiye *et al* 2005).

The profound success of **43** inspired the development of series of novel silver NHC complexes by other group of researchers. A pyrimidine-functionalised silver NHC complex **48** was reported to have much lower MIC values as compared to a list of commercially available antibiotics **(Figure 25) (Table 3)**. According to the study, **48** permeabilising the cell wall by binding to the receptor on the bacterial peptidoglycan layer, hence inhibiting the bacterial cell division (Roymahapatra *et al* 2012).

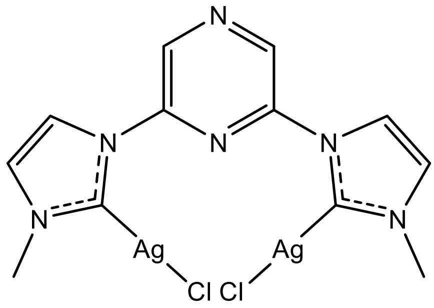

48

Figure 25. Chemical structure of pyrimidine-functionalised silver(I) NHC complex **48**.

Table 3. Determination of MIC value (µg/mL) of compound **25** comparing to commercially available antibiotics.

Compound	Minimum inhibitory concentration (µg/mL)	
	E. coli (Clinical isolate)	*S. aureus* (Clincial isolate)
Streptomycin	128	64
Ampicillin	64	32
Vancomycin	64	32 - 64
Ciprofloxacin	128	32
Chloramphenicol	16 - 32	64 - 128
48	8	4

Besides its acclaimed debut in antimicrobial properties, numerous reports have shown that silver NHCs demonstrated anticancer properties too. Young's group has synthesised a class of silver NHC derived from 4,5-dimethylimidazolium salts, **49** – **51**, where all three complexes show promising half maximal inhibitory concentration (IC_{50}) with the exception that **49** was reported to be 2 times more cytotoxic than cisplatin against breast carcinoma MB157 **(Figure 26)** (Medvetz *et al* 2008). An *in vitro* study was also conducted by the same group to support the finding where **49** eliminated the ovarian carcinoma OVCAR-3 tumour without causing damage to the major organs of the infected mice.

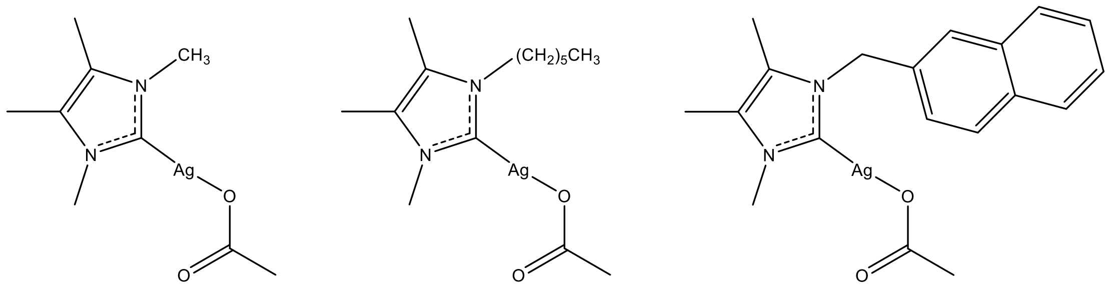

49 **50** **51**

Figure 26. Chemical structures of silver NHC complexes prepared by Young's group.

Aside from Young's group, Haque and coworkers have contributed in synthesis of a library of mono- and dinuclear silver NHCs and the anticancer properties were evaluated. Silver NHC complex **52** portrayed deadly cytotoxic properties against colon carcinoma HCT-116 with IC_{50} value of 0.31 µM, while **53** and **54** showed much weaker inhibition on the cellular proliferation with IC_{50} value of 15.1 and 1.99 µM respectively (Atif *et al* 2020). Based on the observations, HCT-116 cells treated with **52** lost their pseudopodial-shaped extensions and viability wherein cellular debris remained in the growth medium. Both **52 – 54** were found to induce caspase-independent apoptotic cellular death *via* mitochondrial apoptosis-inducing factor and deposit silver ions in cytosol to disrupt the cellular functionality while interacting with rate-limiting enzymes and proteins that are essential in cellular metabolic pathways. A tetra-NHC species **55** was designed and evaluated against HCT 116 cells alongside with fluorouracil (5-FU) (Fatima *et al* 2017). Interestingly, **55** shows better anticancer activities against HCT-116 cells with IC_{50} value of 6.61 ± 0.50 µM than 5-FU. Further investigation shows that **55** has the tendency to promote wound closure by inhibiting metastatic activity of HCT-116, where with concentration of 2.5 and 5 µg/mL, 15.37 ± 3.43 % and 32.9 ± 5.62 % wound closure activity was recorded after 6 hours, 5.54 ± 1.07 % and 6.24 ± 3.76 % after 12 hours of treatment. The similar group has also synthesised nitrile-functionalised silver NHC complexes **56** and **57** which have shown to possess anticancer properties with IC_{50} values as low as 4.1 and 3.7 µM against breast cancer cell line MCF-7 (Hussaini *et al* 2018). The study was conducted alongside with tamoxifen, a drug that is commonly used to treat early-stage breast cancer, with IC_{50} value of 11.2 µM. This finding has attributed to the potential of silver NHC complexes as the novel drugs for cancer treatments.

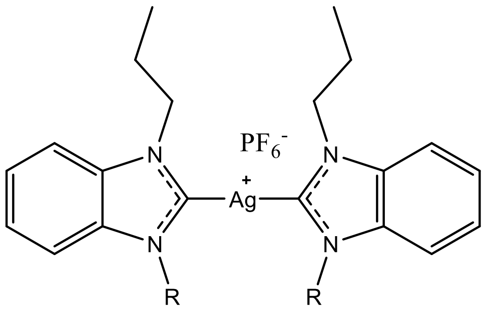

52, *R* = *n*-propyl
53, *R* = *n*-heptyl
54, *R* = benzyl

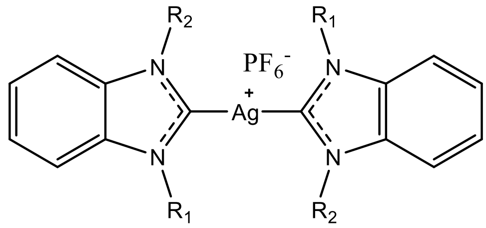

56, R_1 = cyanobutyl, R_2 = cyanopentyl
57, R_1 = R_2 = cyanopentyl

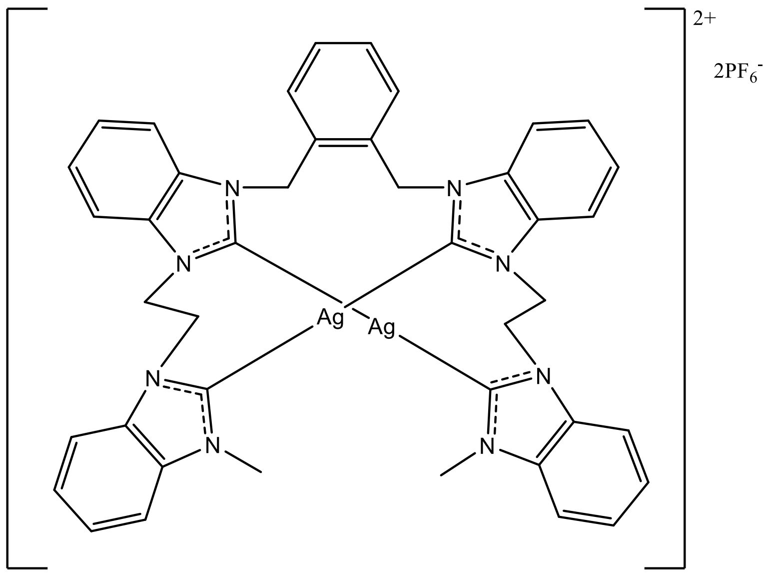

55, *R* = *n*-decyl

Figure 27. Chemical structures of silver NHC complexes prepared by Haque's group.

Other notable silver NHC complexes include sulfonated silver NHC complexes **58** – **62** developed by Yaşar's group. These complexes were tested against pancreatic carcinoma HeLa cells, colorectal adenocarcinoma HT-29, and murine fibroblast L929 alongside with cisplatin, and were found to be more effective than cisplatin with IC_{50} values ranging from 5.99 – 61.6 µM (Yaşar *et al* 2018). In addition, Roland's group worked on silver NHC complexes **63** and **64** derived from imidazoline-based ligands bearing steric *R*-group such as diisopropylphenyl and trimethylphenyl (Eloy *et al* 2012). Complexes **63** and **64** were tremendously more cytotoxic than cisplatin against various cell lines, including HCT-116, HCT-15, MCF-7, MCF-7R, HL-60, HL-60R, MRCS and EPC cells, with IC_{50} value ranging from 28 ± 1 to 3295 ± 55 nM. Besides, **63** and

64 were found having ability to induce apoptosis in HL-60 cells through release of mitochondrial materials into the cytoplasm as soon as 24 hours after treatment with negligible effect on necrosis.

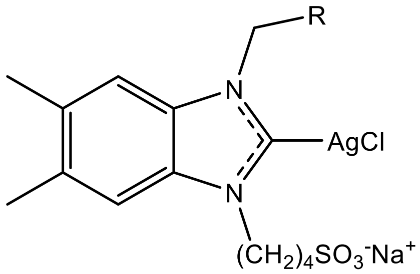

58, *R* = $C_6H_4CH_3$
59, *R* = $C_6(CH_3)_6$

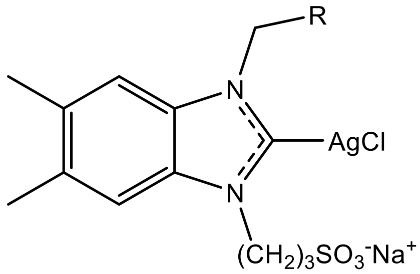

60, *R* = $CH_2C_4H_8NO$
61, *R* = $C_6H_5C_4H_9$
62, *R* = $C_6H_4(CH_3)_2$

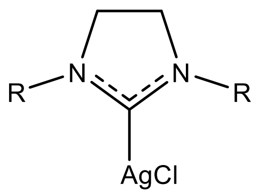

63, *R* = SIPr
64, *R* = SIMe

Figure 28. Chemical structures of silver NHC complexes synthesised by Yaşar's and Roland's group.

1.3 Microwave-assisted organic synthesis

Since the first attempt of microwave-assisted organic synthesis using a domestic microwave oven by Gedye and Giguere, independently, in 1986, microwave-assisted organic synthesis has embarked a new wave of interest in synthetic chemistry (Gedye *et al* 1986; Gedye *et al* 1988; Giguere *et al* 1986). Being situated between infrared radiation and radio frequencies, microwave region lies within the wavelength range from 0.1 – 1 m in air, corresponding to a frequency range of 0.3 – 3 GHz (Berk 2018). Generally, the heat is generated by the electric component of microwave electromagnetic field through dipolar polarisation, where molecules with dipole moment, once being irradiated with electromagnetic field, rotate and align to the applied electric field. As the electric field oscillates, the molecules tend to orientate themselves, aligning to the direction of electric field, resulting in a constant rotation of molecules. As fast as the molecules try to align themselves to the field, the molecules will never accurately align to the field, leading to a phase difference between the field and molecules, where energy is lost in form of heat through intermolecular friction and dielectric loss (Nüchter *et al* 2004).

Microwaves have been applied in various industries, including the textile and sterilisation industries. Today, microwave irradiation has been widely used in various organic synthesis, including acylation, alkylation, condensation, elimination, and coupling reactions that involve catalytic activation such as C-C or C-N activation (Keglevich *et al* 2013). The main feature of microwave irradiation is that it significantly reduces the reaction time from days to minutes, while increasing the yield and preventing decomposition of reactants (Hosseini *et al* 2007; Safari *et al* 2007). The traditional heating techniques with the use of oil or sand baths are rather slower compared to microwave irradiation, as the wall of reaction vessel absorbs the energy first before the heat is passed to the reaction mixture *via* convection. This could also cause the formation of temperature gradient within the reaction, resulting in formation of multiple products from side reactions and overheating of the reaction which can unnecessarily decompose the reagents or products (Lidström *et al* 2001). In contrast, microwave irradiation runs on dielectric heating where the microwave energy radiates through the wall of vessel, causing the molecules to vibrate, thereby generating the heat from the molecules.

Gedye's group presented the first microwave-assisted Diels-Alder reaction, where anthracene was reacted with dimethyl fumarate in a significant reduced reaction time from 4 hours to 10 minutes **(Scheme 7)** (Gedye *et al* 1986). Not long after, Gedye's group performed a small experiment to investigate the types of molecules that absorb the microwave energy. Based on this study, it was found that polar compounds such as acids, esters, alkyl halides, primary alcohols and amines, and carbonyl compounds absorbed significant amounts of microwave energy readily, where compounds with boiling points of less than 100 °C achieved their boiling point within a minute. On the other hand, the less polar ether, tertiary amine, and bulkier alcohol absorbed the microwave energy poorly, while the nonpolar carbon tetrachloride and hydrocarbon solvents did not absorb any of the microwave energy (Gedye *et al* 1988). Meanwhile, Giguere's group presented a list of reactions with dramatic reductions in reaction time in microwave using the Diels-Alder reaction, ene reaction, and Claisen condensation (Giguere *et al* 1986).

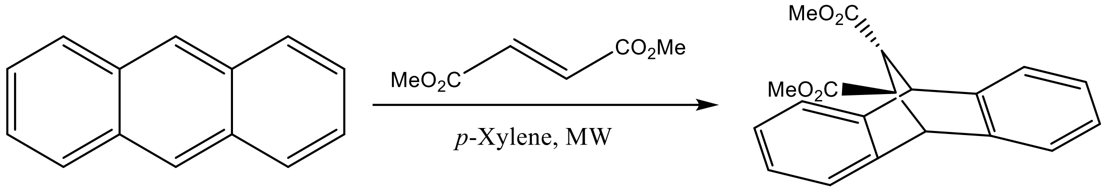

Anthracene

Scheme 7. Diels-Alder reaction of anthracene with dimethyl fumarate *via* microwave irradiation (MW).

Perillo's group presented the results of microwave-assisted synthesis of *N*-alkylisatins **66** by *N*-alkylation of isatin **(65)** with desired alkyl and benzyl halides **(Scheme 8)** (Shmidt *et al* 2008). A comparison study between microwave-assisted synthesis and conventional heating revealed that reactions that require one to four hours using conventional heating were reduced to two to seven minutes when the reactions were carried out using microwave irradiation. Besides, the products yielded from microwave-assisted synthesis were higher than those of conventional heating method. For instance, microwave-assisted reaction of isatin and equimolar amount of bromoallylbenzene led to 24 % increase in yield production and reaction was completed in two minutes instead of four hours with the use of conventional heating method.

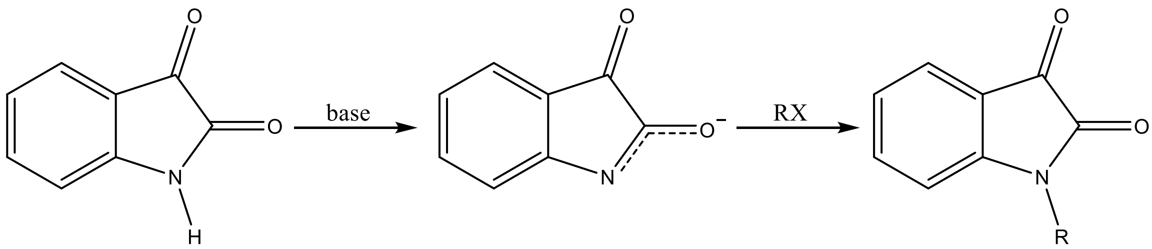

65 **65⁻** **66**

Scheme 8. Synthetic route for *N*-substituted isatins **65**.

Pyridine-functionalised isoniazid, prescribed in combination with other drugs such as ethambutol, rifampin, streptomycin or pyrazinamide, is often used to treat latent tuberculosis. However, the emergence of drug-resistance in bacteria requires development of new derivatives, many of which bear pyrazole moieties that possess strong antimicrobial activity, while serving a vital role in the biological system (Castagnolo *et al* 2008; Castagnolo *et al* 2009). However, such development could be time and energy consuming, given that each of the conventional synthesis requires hours to days to optimise and achieve the desired products. Hence, a rapid protocol such as microwave-assisted *N*-alkylation becomes a handy tool to combat the issue. Muthusubramanian's group presented the rapid synthesis of arylthiol/cyclohexylthio-substituted pyrazoles using microwave irradiation **(Scheme 9)** (Manikannan *et al* 2010). The cyclisation of ω-arylthio-substituted acetophenoneazine **67** was achieved at 150 °C for 30 – 60 seconds to afford almost quantitative conversion of reactants.

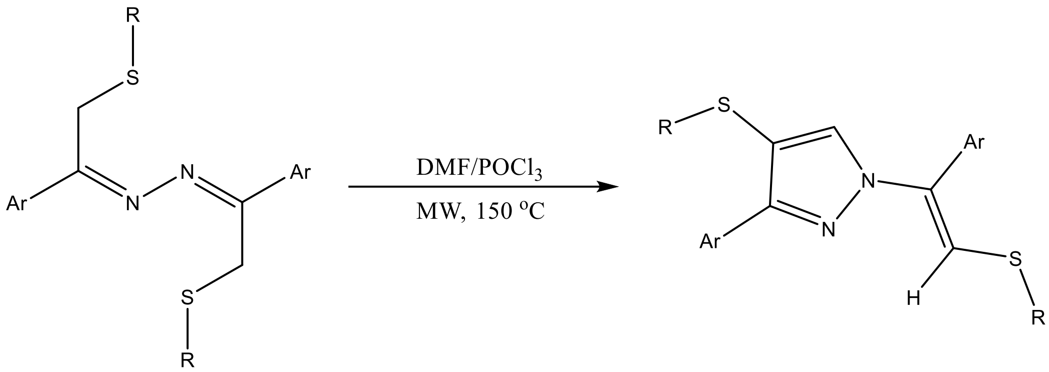

67 **68**

Scheme 9. Synthetic route for ω-arylthio-substituted acetophenoneazine.

Besides its role in discovery of novel antibiotics, microwave irradiation has also been useful in the search for non-steroidal anti-inflammatory agents. Belongs to the heterocycle family, imidazole possesses both anti-inflammatory and antifungal properties (Garella *et al* 2013). Tripathy's group has demonstrated the schematic route to prepare new analgesic and anti-inflammatory compounds derived from variously substituted imidazole **70 (Scheme 10)** (Tripathy *et al* 2010). The cyclisation of benzil **69** with aldehyde and imine was achieved in eight minutes using microwave irradiation, affording acceptable yields of 60 – 70 %.

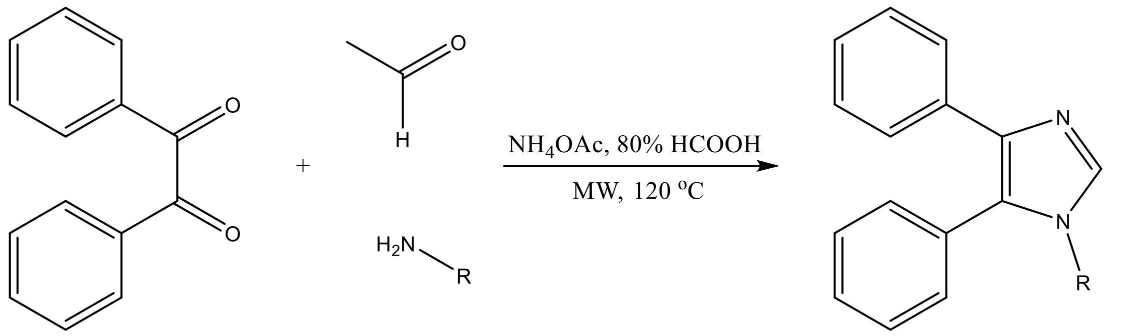

69 **70**

Scheme 10. Synthetic route for 1,4,5-substituted imidazole **70**.

1.4 Research objectives

Previously, our lab reported the synthesis and characterisation of a series of bioactive pyridine-functionalised alkyl-substituted imidazolium salts, **71a** – **c**, which possess moderate antimicrobial properties with MIC values as low as 1.25 mM and MBC values as low as 2.50 mM. However, **71a – c** were not cytotoxic to the tested human carcinoma cell lines (H103, HCT116, and MCF7) at the highest tested concentration (40 µM) (Choo *et al* 2018; Choo *et al* 2019). This could be due to the short alkyl chain (*N*-methyl) or the steric hindrance induced by the phenyl ring and branched alkyl chain (*tert*-butyl) in **71a** – **c**.

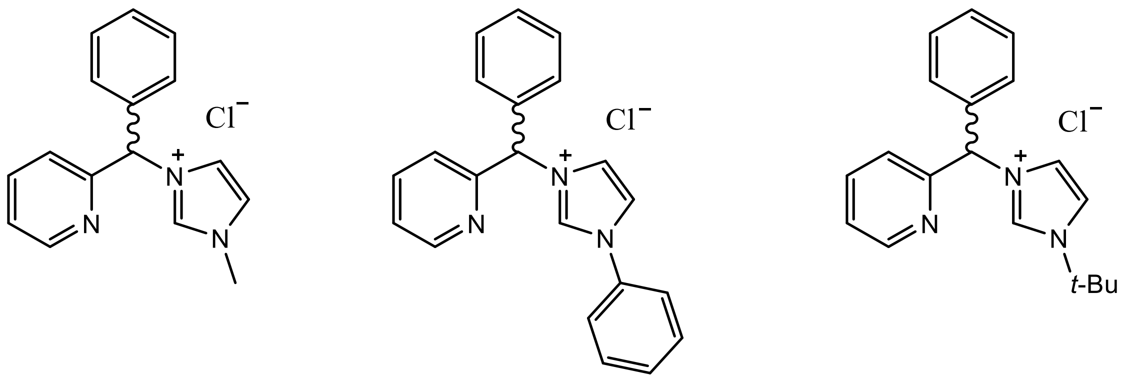

71a **71b** **71c**

Figure 29. Pyridine-functionalised imidazolium salts synthesised and reported by our lab.

In this study, a series of pyridine-functionalised (benz)imidazolium salts were synthesised and characterised. With the biological potential of imidazolium salts, as supported by all the published studies, it is hypothesised that the compounds of interest in this study shall display similar or enhanced biological properties. Besides that, the influence of alkyl chain length in their biological properties were investigated. As literature implies, the increased lipophilicity of the compound facilitates the penetration of the lipid membrane of the biomolecular target, inhibiting the binding sites of enzymes, leading to disturbance of the cellular respiration and protein synthesis, thereby inhibiting the cellular growth (Choo *et al* 2019). Moreover, the effect of extended π-conjugation in benzimidazolium core on the biological activities were also evaluated. Furthermore, microwave-assisted *N*-alkylation were performed to prepare the *N*-substituted imidazole and their corresponding imidazolium salts to demonstrate a greener synthetic route. Finally, the antimicrobial and anticancer properties of the synthesised complexes were evaluated against several microorganism strains and cell lines. Therefore, the objectives of this study are summarised as follow:

i. To synthesise and characterise a series of *N*-alkyl-substituted (benz)imidazole and their corresponding (benz)imidazolium salts *via* the conventional heating method and microwave-assisted *N*-alkylation **(Chapter 2)**.
ii. To evaluate the antimicrobial properties of all synthesised compounds against selected microorganism strains, which include Gram-positive and Gram-negative bacteria, and yeast **(Chapter 3)**.
iii. To evaluate the cell cytotoxicity of all synthesised compounds against selected human carcinoma cell lines **(Chapter 4)**.

In this thesis, the objectives will be deliberated and discussed in detailed in sequential order, from **Chapter 2** to **Chapter 4** correspondingly.

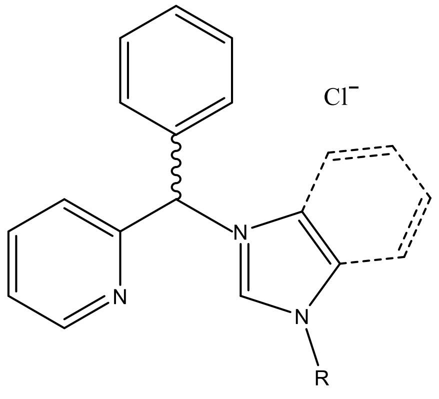

R = hexyl, heptyl, octyl, nonyl, decyl

General representation of chemical structures of compounds synthesised in this thesis.

CHAPTER 2 SYNTHESIS AND CHARACTERISATION OF *N*-ALKYL-SUBSTITUTED (BENZ)IMIDAZOLE AND THEIR CORRESPONDING SALTS *via* CONVENTIONAL HEATING AND MICROWAVE-ASSISTED *N*-ALKYLATION

2.1 Introduction

As mentioned in subchapter **1.4**, our lab has previously synthesised and characterised a series of pyridine-functionalised alkyl-substituted imidazolium salts with moderate antimicrobial properties with MIC value as low as 1.25 mM, and no cytotoxic properties were observed. The pyridinyl ligand and the imidazole derivatives were synthesised separately as per literature methods with slight modifications **(Scheme 11)** (Chiang *et al* 2010; Kim & Kang 2014).

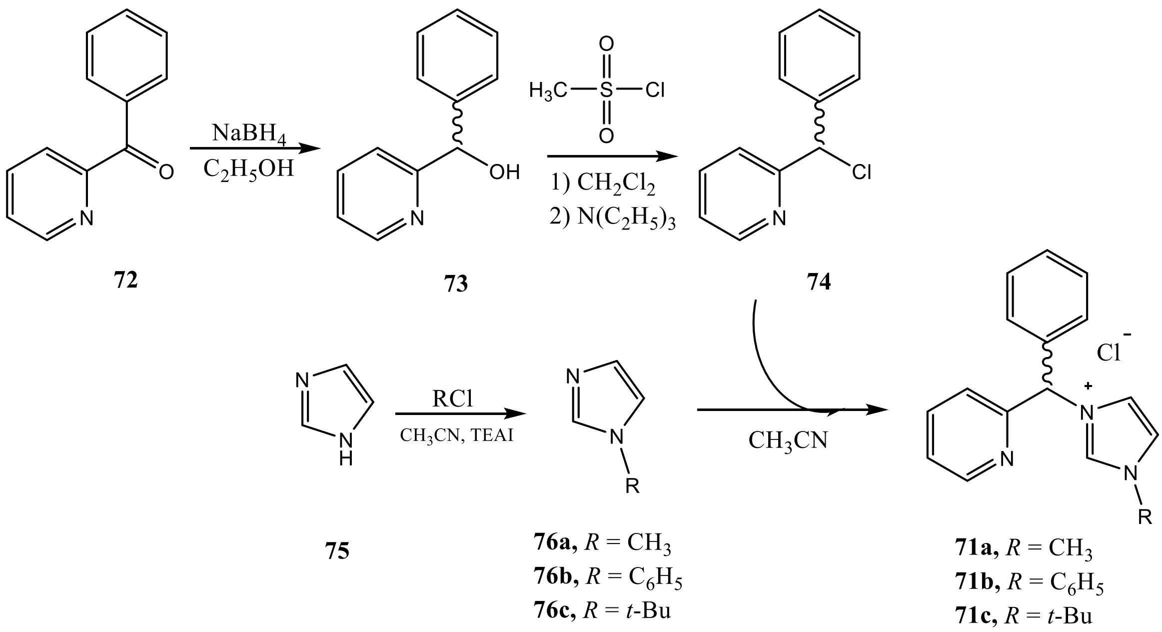

Scheme 11. General synthesis route of pyridine-functionalised alkyl-substituted imidazolium salts by our lab.

Based on our previous study, it was shown that the antimicrobial profiles of imidazolium salts **71a – c** corresponded to several reported studies, where simply tuning the imidazolium core by introducing an additional functional group would yield an enhance antimicrobial profile (Borowiecki *et al* 2013; Demberelnyamba *et al* 2004; Gravel & Schmitzer 2017; Mumtaz *et al* 2016). However, the antimicrobial profiles of

71a – c were not comparable to several reported imidazolium salts where the antimicrobial properties were shown to be with MIC values in µM range (Riduan & Zhang 2013). Since the biological properties are greatly influenced by the *N*-substituted *R* group, it was suggested that the weak antimicrobial profiles of **71a – c** were most likely due to the lack of binding affinity in the side chain. Furthermore, **71a – c** were not cytotoxic to the chosen human carcinoma at the highest tested concentration (40 µM). As previously suggested, the *R* group plays a fairly important role on the biological profiles. To prove our hypotheses and claims, alkyl chains with different number of carbons were used to substitute the *R* group to evaluate how the elongated alkyl chain length would affect the biological properties. Besides, benzimidazole will also be studied in this research to see the influence of the extended π-conjugation in benzimidazole on the biological properties.

In this chapter, the synthesis and characterisation of *N*-alkyl-substituted (benz)imidazolium salts were discussed. Similar to **71a – c**, the newly synthesised salts, **71d – h** possessed a five-membered imidazole ring (additional extended π-conjugation for benzimidazole derivatives), a pyridinyl functional group, a chiral backbone bearing a phenyl group, and chloride as the anion **(Figure 30)**. The synthesis of **71d – h** adopted the method shown in **Scheme 11** with further modification to improve the results. Finally, microwave irradiation was utilised in the synthesis to develop a greener synthesis route, where lesser energy and time are being used. Characterisation and identification of all synthesised compounds were done using several spectroscopic techniques, including proton (^{1}H) and carbon (^{13}C) NMR, FT-IR and mass spectrometry. While in a racemic drug, it is known that each enantiomer possesses its own pharmacological activities where that can be null, similar, different, or opposite (Nguyen *et al* 2006). However, the chirality of the synthesised compounds was not resolved and the effect of chirality on the biological activities was not evaluated.

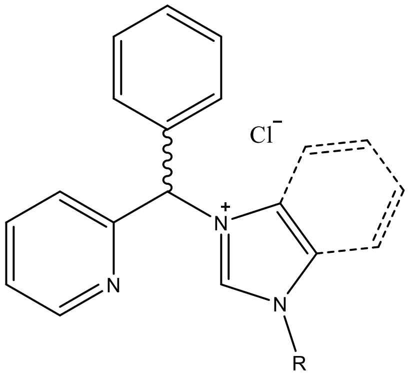

Im-71d, *R* = C_6H_{13}
Im-71e, *R* = C_7H_{15}
Im-71f, *R* = C_8H_{17}
Im-71g, *R* = C_9H_{19}
Im-71h, *R* = $C_{10}H_{21}$

Bz-71d, *R* = C_6H_{13}
Bz-71e, *R* = C_7H_{15}
Bz-71f, *R* = C_8H_{17}
Bz-71g, *R* = C_9H_{19}
Bz-71h, *R* = $C_{10}H_{21}$

Figure 30. General representation chemical structure of (benz)imidazolium salts synthesised in this study (Im = imidazolium core; Bz = benzimidazolium core).

2.2 Results and Discussion

2.2.1 Synthesis of alkyl-substituted (benz)imidazolium salts *via* conventional heating

As shown in **Scheme 11**, the pyridinyl ligand was synthesised through reduction of commercially available 2-benzoylpyridine **(72)** using sodium borohydride into phenyl(pyridin-2-yl)methanol **(73)**, followed by halogenation using methanesulphonyl chloride to yield 2-[chloro(phenyl)]methyl]pyridine **(74)**. On the other hand, (benz)imidazole derivatives were synthesised through reacting (benz)imidazole **(Im-75** or **Bz-75)** with their respective alkyl bromide (C_6 to C_{10}) to yield **76d – h (Figure 31)**. Upon obtaining the (benz)imidazole **76d – h**, compound **74** was added as the second alkylating agent to yield (benz)imidazolium salt **71d – h**.

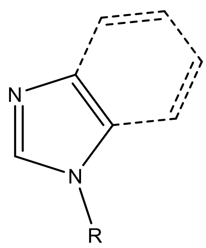

Im-76d, *R* = C_6H_{13}
Im-76e, *R* = C_7H_{15}
Im-76f, *R* = C_8H_{17}
Im-76g, *R* = C_9H_{19}
Im-76h, *R* = $C_{10}H_{21}$

Bz-76d, *R* = C_6H_{13}
Bz-76e, *R* = C_7H_{15}
Bz-76f, *R* = C_8H_{17}
Bz-76g, *R* = C_9H_{19}
Bz-76h, *R* = $C_{10}H_{21}$

Figure 31. General representation chemical structure of (benz)imidazole synthesised in this study (Im = imidazole core; Bz = benzimidazole core).

Compound **73** was prepared and isolated as pale green oil, further crystallised into clear white crystal *via* slow evaporation method, where result was in agreement as per literature method (Kim & Kang 2014). The physical appearance and retention factor (R_f = 0.65) on a TLC were used as reference to confirm the formation of **73**. Further identification was performed using FT-IR where the O-H stretch was observed at wavenumber 2990 to 3090 cm^{-1}. Upon obtaining the pure **73** crystal, subsequent halogenation was performed using methanesulphonyl chloride in the presence of triethylamine as per stated in the literature (Chiang *et al* 2010). The alcohol moiety of **73** allows it to attack the sulphur centre of methanesulphonyl chloride, removing its chloride and forming a weakly stable intermediate mesyl-**73** complex **(Scheme 12)**. The triethylamine then removes the proton from the intermediate complex to prevent the reversion of the reaction (Bruice 2014). Due to the good leaving nature of mesyl group, the free chloride released from the methanesulphonyl chloride backside attacks the carbon centre, displacing the methyl group through S_N2 mechanism and forming **74** as red oil (Lee *et al* 1996). The red oil was then subjected to column chromatography (hexane/ethyl acetate, 80:20 v/v) to yield yellow oil. The physical appearance and the retention factor (R_f = 0.80) on a TLC were used as reference to confirm the formation of **74**. Further identification was performed using FT-IR where the O-H stretch was no longer observable, confirming the presence of **74**. Compound **74** must be prepared fresh prior to be used as the alkylating agent as the chloro- is highly reactive.

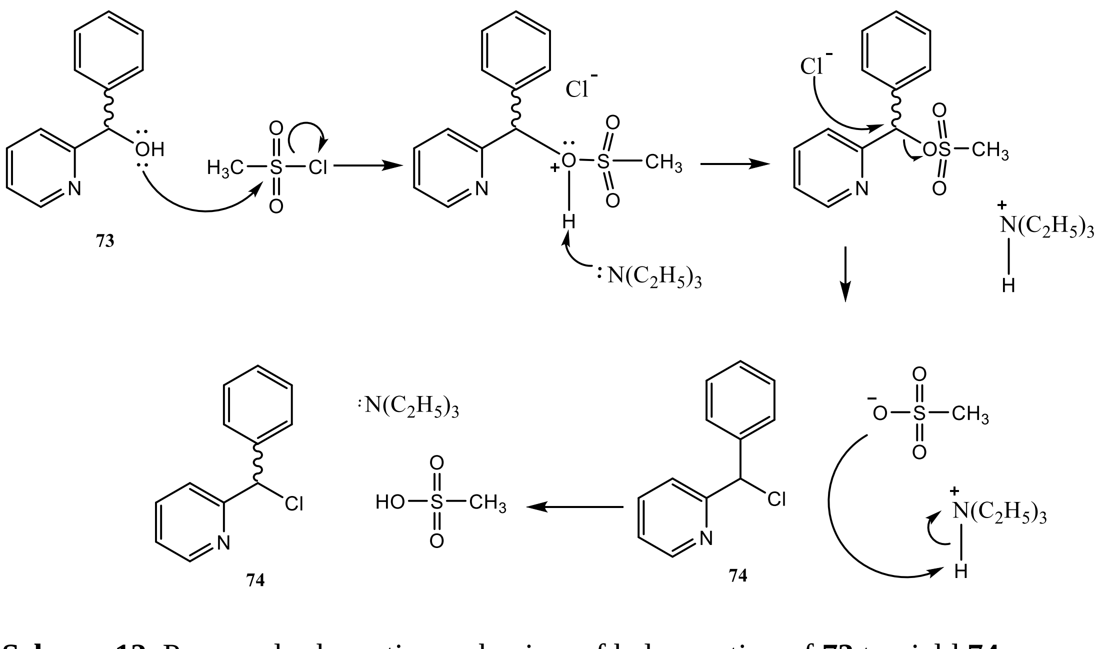

Scheme 12. Proposed schematic mechanism of halogenation of **73** to yield **74**.

2.2.1.1 Synthesis of 1-alkyl-substituted (benz)imidazole, 76d – h

The (benz)imidazole derivatives were synthesised in similar analogous fashion, where (benz)imidazole, potassium carbonate, tetraethylammonium iodide (TEAI), and alkyl bromide were used **(Scheme 13)**. The (benz)imidazole was first stirred in acetonitrile in the presence of potassium carbonate for one hour to deprotonate the pyrrolyl hydrogen of the (benz)imidazole. The respective alkyl bromide was then added into the reaction mixture and heated to reflux temperature for five to seven consecutive days to yield the crude *N*-alkyl-substituted (benz)imidazole derivatives. Pure fraction of **76d – h** was isolated as yellow oil from liquid-liquid extraction to remove the acidic by-products, followed by column chromatography (chloroform/ethanol, 95:5 v/v). TEAI serves as a phase transfer catalyst to assist the bond formation between the pyrrolyl nitrogen of the imidazole and alkyl chain (Starks *et al* 1994). In addition, TLC was used to monitor the progress of the reaction. As the imidazole derivatives **Im-76d – h** were not UV active, a subsequent iodine stain method was used to monitor the progress of the reaction.

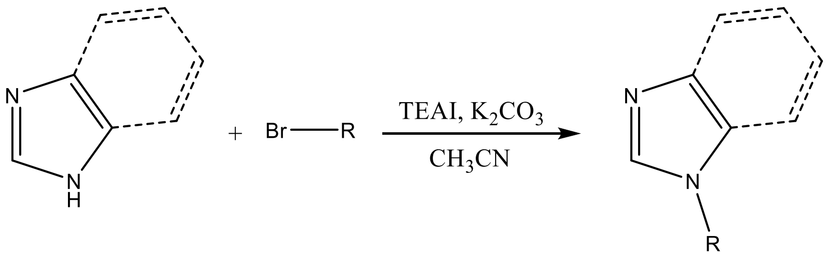

75

76d, $R = C_6H_{13}$
76e, $R = C_7H_{15}$
76f, $R = C_8H_{17}$
76g, $R = C_9H_{19}$
76h, $R = C_{10}H_{21}$

Scheme 13. General synthesis route of (benz)imidazole derivatives.

The formation of product was confirmed with ^{1}H- and ^{13}C-NMR, and mass spectrometry. Based on the ^{1}H-NMR, all imidazole derivatives **Im-76d – h** showed similar trend, with the only difference of two additional protons in the upfield region (approximately δ 1.00 – 1.50 ppm) for each increment in the methylene protons of the alkyl chain. The chemical shift of methyl peak can also be seen at approximately δ 0.87 ppm, followed by a quintet ($CH_2C\mathit{H}_2CH_2$) and a triplet ($CH_2C\mathit{H}_2N$) at approximately δ 1.75 and 3.90 ppm, respectively. The characteristics imidazolium proton peak (NC*H*N) was also observed at approximately δ 7.43 ppm, deducing that all imidazole derivatives were successfully synthesised and characterised. Similarly, the benzimidazole derivatives **Bz-76d – h** were also displaying same NMR spectra as those of **Im-76d – h**. The four additional protons from the extended π-conjugated benzene ring in benzimidazole can be observed at the aromatic region, approximately δ 7.20 – 7.90 ppm. Besides, the number of carbons in the ^{13}C-NMR spectrum corresponded to the respective (benz)imidazole derivatives, further confirming the chemical structure of the synthesised compounds. Moreover, the molecular ion peak $[M+H]^+$ for each derivatives was analysed using a triple quadrupole mass spectrometer and the data are summarised in **Table 4**. Based on the table, it could be noticed that the experimental *m/z* ratio of benzimidazole derivatives appeared to be [M] instead of $[M+H]^+$. This is supported by the theory that the electronic withdrawing power of the extended π-conjugation in benzimidazole weakens the bond between the C-H bond of the benzimidazole proton, causing it to be more susceptible to cleavage in exposure to ionisation during the ESI-MS (Abiramasundari *et al* 2015; Breslow 2019; Chai *et al* 2016; Di Marco *et al* 2016). A separate study also revealed the possibility of loss of hydrogen atom upon protonation in the mass spectrometer chamber, further supporting the above observation (Sioud *et al* 2014).

Table 4. The *m/z* of **Im-76d – h** and **Bz-76d – h**.

Compound	Molecular weight	*m/z*: $[M+H]^+$	
		Calculated	Experimental
Im-76d	152.24	153.14	152.90
Im-76e	166.27	167.15	166.90
Im-76f	180.30	181.17	181.00
Im-76g	194.32	195.19	195.00
Im-76h	208.35	209.20	209.00
Bz-76d	202.30	203.15	202.47
Bz-76e	216.33	217.17	216.79
Bz-76f	230.36	231.19	230.48
Bz-76g	244.38	245.19	244.47
Bz-76h	258.41	259.21	258.49

**see appendices for the spectra*

2.2.1.2 Synthesis of 1-alkyl-substituted (benz)imidazolium salt, 71d – h

The 1-alkyl-substituted (benz)imidazolium salt **71d – h** were synthesised in an analogous fashion, where the respective (benz)imidazole derivatives **76d – h** were reacted with **74**. The reaction mixtures were heated at reflux for two to four days and yielded reddish brown oil (imidazolium salts) and pinkish hygroscopic solid (benzimidazolium salts) upon three successive precipitation from chloroform and diethyl ether. In several cases where impurities were shown on TLC, the products were subjected to column chromatography (chloroform/ethanol, 95:5 v/v) to remove the impurities.

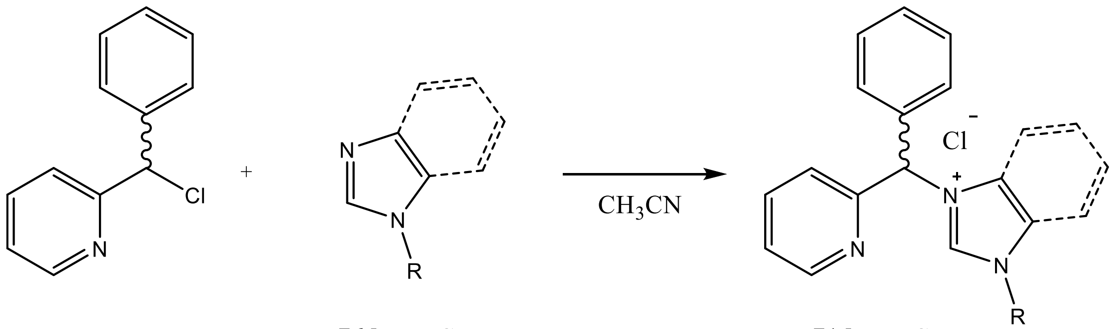

74

76d, $R = C_6H_{13}$
76e, $R = C_7H_{15}$
76f, $R = C_8H_{17}$
76g, $R = C_9H_{19}$
76h, $R = C_{10}H_{21}$

71d, $R = C_6H_{13}$
71e, $R = C_7H_{15}$
71f, $R = C_8H_{17}$
71g, $R = C_9H_{19}$
71h, $R = C_{10}H_{21}$

Scheme 14. General synthesis route of (benz)imidazolium salts.

The downfield shift of characteristic imidazolium proton peak (NC*H*N) on ^{1}H-NMR to approximately 10.30 ppm signified the successful alkylation at the pyridinyl nitrogen of the imidazole ring. Such phenomenon was observed due to the delocalized positive charge within the heterocycle, thus deshielding the NCHN proton (Weader 2020). Similarly, the respective alkyl chain can be observed at the aliphatic region where the number of carbons and hydrogens are in agreement to the respective chemical structure. The proton on the chiral centre of the compound has a downfield shift that appeared in the aromatic region on the ^{1}H-NMR spectrum and was indistinguishable from other aromatic protons. However, this finding is consistent with those reported in the literatures (Chiang *et al* 2010; Choo *et al* 2018; Choo *et al* 2019). Meanwhile, based on the aliphatic region of the ^{1}H-NMR spectra of most (benz)imidazolium salts (**Im-71e – h**, **Bz-71d – e** and **Bz-71g – h**), it was noticed that the number of integrated protons at the aliphatic region was two times to the expected ratio to the aromatic region. For instance, the NCH_2C peak of **Im-71e** appeared to be split triplets at approximately δ 4.50 ppm **(Figure 32)**. It was suspected that such phenomenon could be most likely due to the NMR time scale effect, where the compounds relaxed in the solvent, slowing the overall molecular motion, resulting in the freely rotating alkyl chain to be captured by the NMR twice (Huggins *et al* 2020). One of the compounds was subjected to various temperature-NMR (VT-NMR) with temperatures ranged from 25 – 55 °C, however, the split triplets at approximately δ 4.50 ppm did not show any significant coalescence even at 55 °C (see **Figure A3.21**). Nevertheless, the number of carbons integrated corresponded to their respective compounds, and the molecular ion peak $[M\text{-}Cl]^+$ for each derivatives was analysed and summarised in **Table 5**.

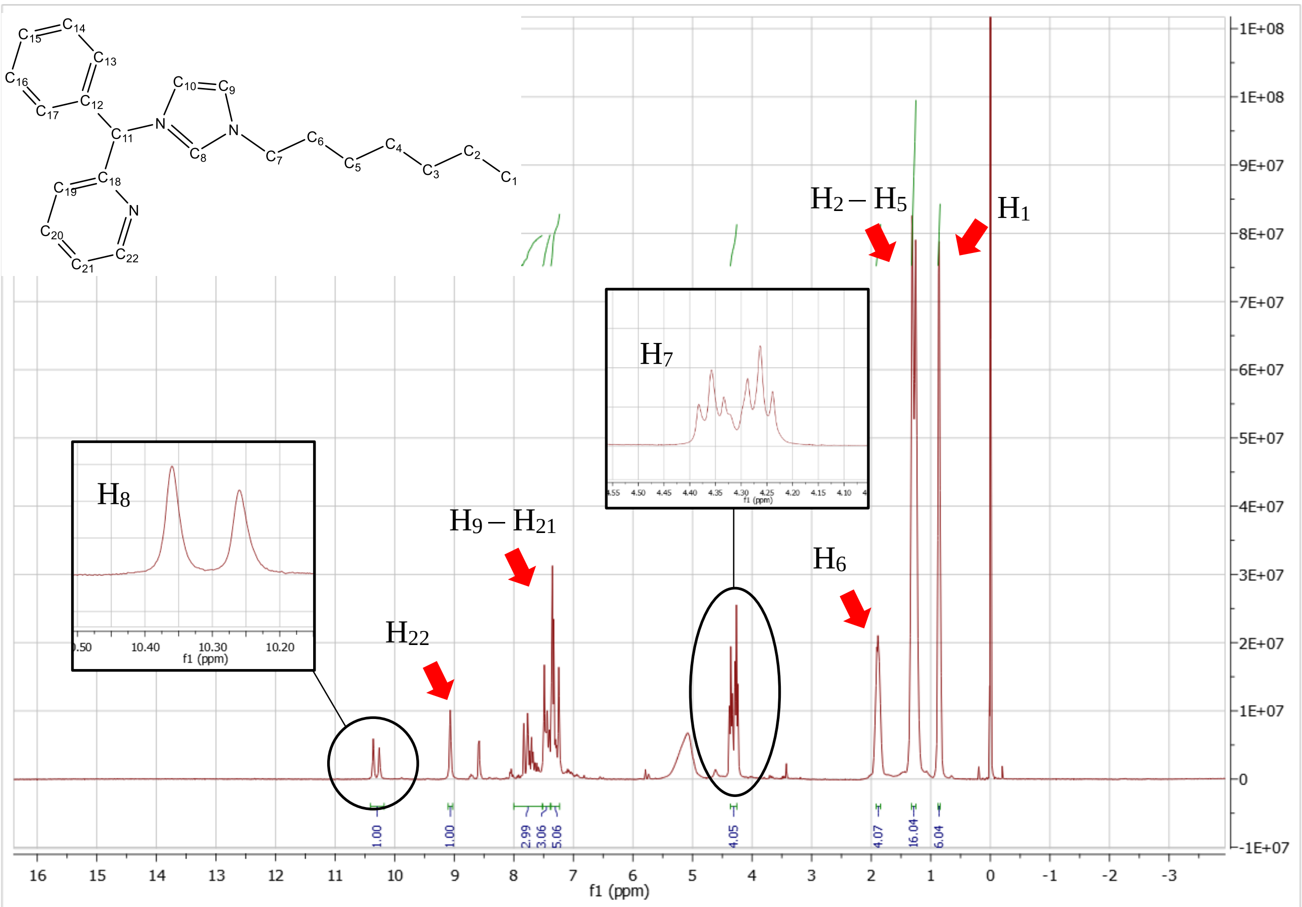

Figure 32. ^{1}H-NMR spectrum for compound **Im-71e.**

Table 5. The *m/z* of **Im-71d – h** and **Bz-71d – h**.

Compound	Molecular weight	*m/z*: [M-Cl]$^+$	
		Calculated	Experimental
Im-71d	355.91	320.21	319.93
Im-71e	369.94	334.23	333.93
Im-71f	383.96	348.24	348.10
Im-71g	397.99	362.26	361.71
Im-71h	412.02	376.28	375.98
Bz-71d	405.97	370.23	369.72
Bz-71e	420.00	384.24	383.77
Bz-71f	434.02	398.26	397.92
Bz-71g	448.05	412.28	411.73
Bz-71h	462.08	426.29	425.88

**see appendices for the spectra*

2.2.1.3 Synthesis of [1-nonyl-3-[phenyl(pyridin-2-yl)methyl]-1H-imidazol-3-ium]silver bromide, Im-77g

Our lab has previously reported the synthesis of nickel, palladium, and platinum NHC complexes. While nickel is different, palladium and platinum NHC complexes were synthesised *via* transmetallation, which involved an intermediate formation of silver NHC complex **(Im-77a) (Scheme 15)**. In this study, we intended to isolate the intermediate silver NHC complex. Expectedly, the highly light sensitive nature of the silver NHC intermediate hindered the isolation. In addition, the metal-NHC bond bears significant resemblance to simple metal-carbon bond in terms of bond length and polarisation, which causes the alkyl complexes to undergo decomposition reactions, namely reductive elimination (Boehme & Frenking 1998; Frenking *et al* 2005). Several attempts to optimise the synthesis of the designated silver NHC complex were performed and summarised in **Table 6**. However, regardless of the reaction conditions and parameters, the product was always extracted in oil form, and decomposed overtime during the subsequent workup steps.

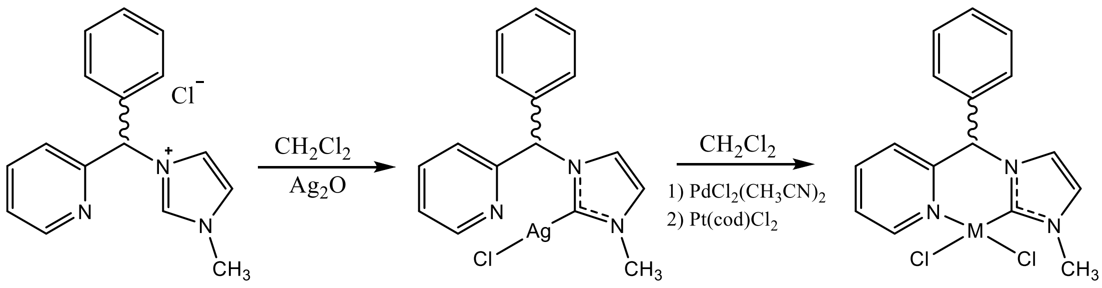

Im-71a **Im-77**a **Pt-Im-78a** **Pd-Im-78a**

Scheme 15. Synthesis route of platinum and palladium NHC complexes *via* transmetallation.

Table 6. List of synthesis conditions and parameters to obtain Ag NHC complexes.

Entry	Reactant (A)	Ag source (B)	Ratio (A:B)	Solvent	Temp. (°C)	Duration	Remarks
1	**Im-71a (Cl^-)**	Ag_2O	2 : 1	CH_2Cl_2	25	12 hours	No
2	**Im-71a (Cl^-)**	Ag_2O	1 : 1	CH_2Cl_2	25	12 hours	No
3	**Im-71a (Cl^-)**	Ag_2O	1 : 2	CH_2Cl_2	25	12 hours	No
4	**Im-71a (Cl^-)**	Ag_2O	1 : 2	CH_2Cl_2	25	12 hours	No
5	**Im-71a (Cl^-)**	Ag_2O	2 : 1	CH_3OH	25	12 hours	No
6	**Im-71a (Cl^-)**	Ag_2O	1 : 2	CH_3OH	25	12 hours	No
7	**Im-71a (Cl^-)**	$AgCH_3COO$	1 : 2	CH_2Cl_2	25	72 hours	No
8	**Im-71a (Cl^-)**	$AgNO_3/Ag_2O$	1 : 2 : 1	CH_3OH	25	12 hours	No
9	**Im-71a (PF_6^-)**	Ag_2O	2 : 1	CH_2Cl_2	25	12 hours	No*
10	**Im-71g (Br^-)**	Ag_2O	2 : 1	CH_2Cl_2	25	12 hours	Yes

The "Remarks" column stating "Yes" indicates successful crystallisation, while "No" indicates unsuccessful attempt.

**Crystallisation took place and the crystal suitable for X-ray diffraction was analysed, but the structure was Im-77a-PF_6*

As counterion is one of the factors contributing to the formation of halogeno complexes, where the relative stabilities of halogeno complexes are $I^- > Br^- > Cl^-$, chloride ion as the ancillary ligand is generally less stable (Garrison & Youngs 2005). Hence, bromide was opted as the alternative ancillary ligand to reduce the reactivity of the complex. Before subjecting the salt to complexation, the anion was exchanged between chloride into bromide ion. **Im-71g-Br** was selected for the complexation due to its highest antimicrobial profile, which will be discussed in **Chapter 3**, and the generally higher molecular weight of the nonyl *R* group than a methyl *R* group should possess better chances in crystallisation in the later stage. To prevent chemical decomposition, the synthesised silver NHC complex **Im-77g-Br** was immediately characterised with NMR spectroscopy. Based on the ^{1}H-NMR spectrum, the disappearance of downfield imidazolium proton peak (approximately 10.30 ppm) signified the formation of bond between silver and the carbene carbon where the proton at C_2 position had been displaced. This observation was in agreement to those reports that demonstrated the synthesis of silver mono-NHC in a similar fashion (Gök *et al* 2014; Slimani *et al* 2020). Besides, the ^{13}C-NMR spectrum also showed that three carbon signals were not observable on the spectrum, where two of them, namely C_{14} and C_{20}, are quaternary carbons which do not bear a hydrogen atom. The third missing carbon signal could be C_2, due to the lack of Ag(I)-^{13}C coupling caused by the labile nature in chiral silver complexes (Garner *et al* 2015; Williams *et al* 2010). Such phenomenon was also observed in several studies on chiral silver(I) NHC complexes (Bonnet *et al* 2003; Hu *et al* 2003).

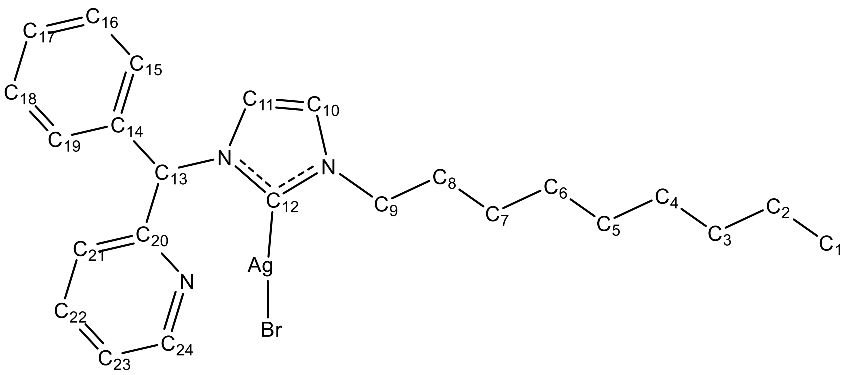

Figure 33. Chemical structure of silver NHC complex **Im-77g-Br**.

Meanwhile, attempt to crystallise silver NHC complex **Im-77a-PF$_6$** was also performed. It was intended to synthesise a bisimidazolium silver NHC using hexafluorophosphate as crystallising anion due to its capability to coordinate multiple hydrogen bonds (Grepioni *et al* 1998). Unexpectedly, the crystal obtained from the mother liquor of **Im-77a-PF$_6$** was found to be its precursor **Im-71a-PF$_6$**, despite that the ^{1}H-NMR spectrum showed disappearance of imidazolium proton peak at the carbene carbon, indicating the formation of carbene. The molecular structure of the compound is shown in **Figure 35** and the selected bond lengths and bond angles are compiled as shown in **Table 7**. The reason behind the regaining of proton by the carbene, forming the imidazolium salt remained unclear. However, it was hypothesised that one of the possible reason could be due to the attraction of hydrogen from the solvent (methanol) (Liebman & Greenberg 1989; Ramnial 2006).

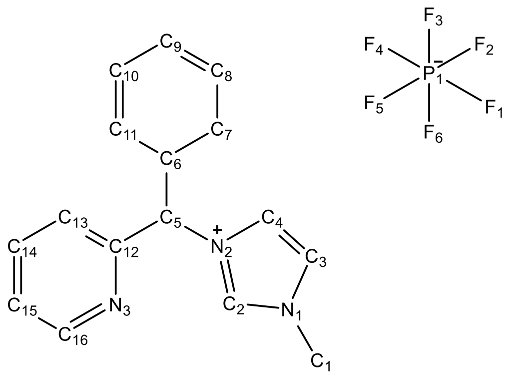

Figure 34. Chemical structure of **Im-71a-PF$_6$**, obtained from crystallisation.

Table 7. Selected bond lengths (Å) and angles (°) for **Im-71a-PF$_6$**.

Bond length (Å)	N(1)-C(1)	1.470(3)	N(1)-C(2)	1.325(4)
	N(1)-C(3)	1.380(3)	N(2)-C(2)	1.337(3)
	N(2)-C(4)	1.382(3)	N(2)-C(5)	1.478(3)
	C(3)-C(4)	1.343(3)	C(5)-C(6)	1.524(3)
	C(5)-C(12)	1.521(3)	C(6)-C(7)	1.389(3)
	C(7)-C(8)	1.390(4)	C(8)-C(9)	1.388(4)
	C(9)-C(10)	1.378(3)	C(10)-C(11)	1.393(3)
	C(11)-C(6)	1.392(3)	C(12)-N(3)	1.387(4)
	N(3)-C(16)	1.394(3)	C(16)-C(15)	1.377(4)
	C(15)-C(14)	1.388(4)	C(14)-C(13)	1.337(3)
	C(13)-C(12)	1.337(3)		
Bond angle (°)	N(1)-C(2)-N(2)	108.64(2)	N(2)-C(5)-C(12)	109.96(2)
	C(5)-C(12)-N(3)	119.49(2)	C(12)-N(3)-C(16)	117.98(2)

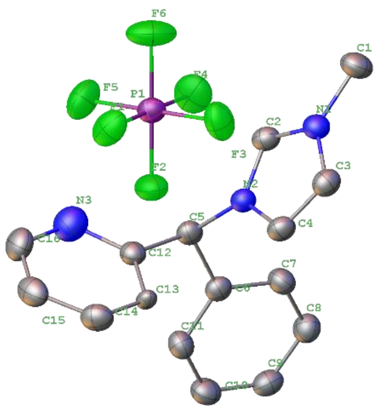

Figure 35. Molecular structure of **Im-71a-PF$_6$** with thermal ellipsoids at 50 % probability. Hydrogen atoms are omitted for clarity.

Table 8. Crystallographic data of **Im-71a-PF$_6$**.

Formula	$C_{16}H_{16}N_3PF_6$
Formula weight	395.29
Crystal system	Triclinic
Space group	*P*-1
Temperature (K)	100
a, *b*, *c* (Å)	8.5368(19), 10.2143(3), 10.9118(3)
α, β, γ (°)	65.377(2), 85.113(2), 80.762(2)
V (Å^3)	853.56(4)
Z	2
Radiation type	Cuκα
μ (mm^{-1})	2.07
Crystal size (mm)	0.10 × 0.06 × 0.04
No. of measured, independent and observed [$I \geq 2u(I)$] reflections	20346, 3046, 2744
R_{int}	0.037
R_1	0.044
wR_2	0.130
$\Delta\rho_{max}$, $\Delta\rho_{min}$ (e Å^{-3})	0.78, - 0.72

The **Im-71a-PF$_6$** crystallises in the triclinic space group *P*-1 and in asymmetric manner as shown in **Figure 35**. The presence of hexafluorophosphate anion in the lattice balances the overall charge of the compound. The structural parameters within the cation are in agreement to those reported previously in other salts. The internal ring angle of imidazolium ring, N(1)-C(2)-N(2), has a bond angle of 108.64(2), which shows similar angle to those reported literatures for the bond angle between the NCN (Haque *et al* 2015; Haziz *et al* 2016; Iqbal *et al* 2013; Selvarajoo *et al* 2017). The carbenium-nitrogen distances between N(1)-C(2)-N(2) were 1.325(4) and 1.337(3) Ǻ, which are similar to those reported distances of 1.325(3) and 1.337(3) Ǻ (Shih *et al* 2009).

2.2.2 Synthesis of alkyl-substituted (benz)imidazole and (benz)imidazolium salts *via* microwave irradiation

2.2.2.1 Optimisation of reaction condition

Like conventional heating method, the ratio between the reactants remained unchanged. The amount of each reactants used per synthesis was reduced due to the small capacity of the vial to be inserted into dedicated microwave synthesiser. Before the parameters and conditions were decided for the synthesis, optimisations of reaction conditions were performed using imidazole **(75)** and 1-bromohexane to identify the best reaction parameter combinations **(Scheme 16)**. Based on **Table 9a**, reaction was found to be unsuccessful when tetraethylammonium iodide (TEAI) was absent. Despite having reaction carried forward with the use of triethylamine, the use of potassium carbonate is more favoured as the reaction only produces water and carbon dioxide as by-products. Thus, Entry 2 was selected to screen for the reaction duration, ranging from 30 minutes to 180 minutes (**Table 9b**). The reaction was found to be completed at 180 minutes, with the yield of 86.3 %, as there was no significant increment in % yield at 210 minutes. From the results, it showed that the use of microwave irradiation has shortened the reaction duration from 5 – 7 days to 3 hours and increased the % yield for about 20 % as shown in **Table 10**. Similarly, the reaction parameters for synthesis of (benz)imidazolium salts derivatives using microwave irradiation were first optimised using **Im-76a** and **74** to identify the best reaction duration **(Scheme 18)**. The reaction was found to be completed at 60 minutes, with a yield of 79.9 %. From the results, it showed that the use of microwave irradiation has shortened the reaction duration from 2 – 4 days to 1 hour and increased the yield % for about 20 to 30 % as shown in **Table**

12. All the synthesised (benz)imidazole and (benz)imidazolium salts were confirmed with [1]H-NMR.

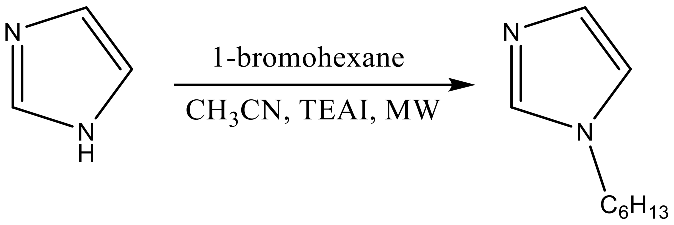

Im-75 **Im-76d**

Scheme 16. Synthesis pathway of **Im-76d** using microwave irradiation.

Table 9a. Screening reaction conditions for alkylation of imidazole **75** with 1-bromohexane.

Entry	Base	Catalyst	Solvent	Yield (%)*
1	K_2CO_3	-	CH_3CN	-
2	K_2CO_3	TEAI	CH_3CN	31.1
3	K_2CO_3	TEAI	CH_2Cl_3	-
4	K_2CO_3	TEAI	$CHCl_3$	-
5	K_2CO_3	TEAI	H_2O	-
6	NaOH	TEAI	CH_3CN	-
7	KOH	TEAI	CH_3CN	-
8	Triethylamine	TEAI	CH_3CN	25.6

* *Yield (%) refer to isolated yield.*

Table 9b. Screening reaction duration for alkylation of imidazole with 1-bromohexane.

Entry	Time/min	Temperature/°C	Yield (%)
9	30	150	31.1
10	45	150	44.4
11	60	150	62.7
12	120	150	71.9
13	180	150	86.3
14	210	150	85.5

* *Yield (%) refer to isolated yield.*

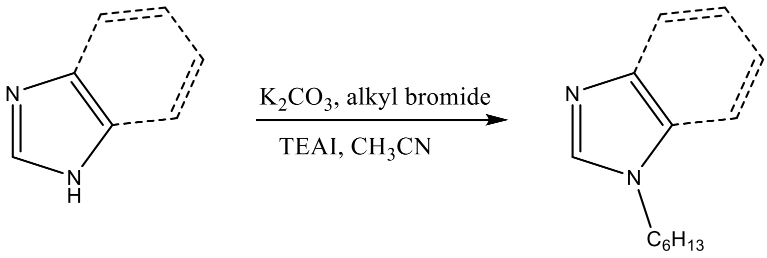

75

76d, R = C_6H_{13}
76e, *R* = C_7H_{15}
76f, *R* = C_8H_{17}
76g, *R* = C_9H_{19}
76h, *R* = $C_{10}H_{211}$

Scheme 17. Synthesis pathway of (benz)imidazole using microwave irradiation.

Table 10. Comparison of reaction yields for (benz)imidazole *N*-alkylation under microwave irradiation (3 hours) and conventional heating (120 hours).

Compound	Yield (%)	
	Conventional heating	Microwave irradiation
Im-76d	67.7	86.3
Im-76e	56.4	88.0
Im-76f	62.3	82.1
Im-76g	47.7	83.1
Im-76h	68.0	84.8
Bz-76d	54.2	76.3
Bz-76e	60.5	81.4
Bz-76f	50.2	60.9
Bz-76g	54.8	77.1
Bz-76h	56.8	68.8

** Yield (%) refer to isolated yield.*

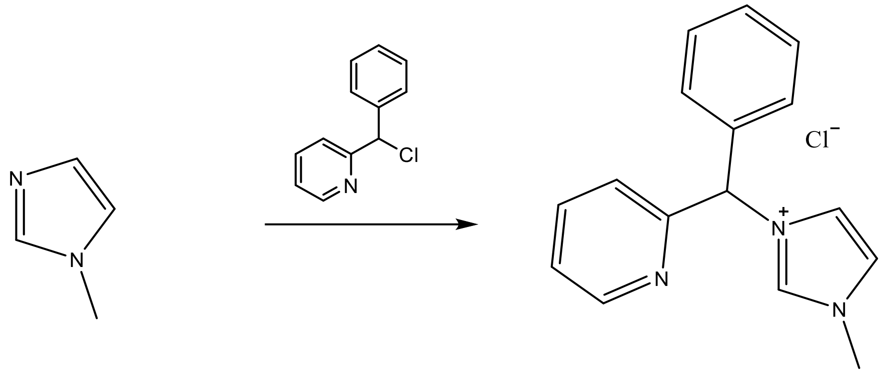

Im-76a **Im-71a**

Scheme 18. Synthesis pathway of **Im-71a** using microwave irradiation.

Table 11. Screening of reaction duration for *N*-alkylation of 1-methylimidazole.

Entry	Time/min	Temperature/°C	Yield (%)
1	15	150	-
2	30	150	10.5
3	60	150	79.1
4	90	150	79.9

** Yield (%) refer to isolated yield.*

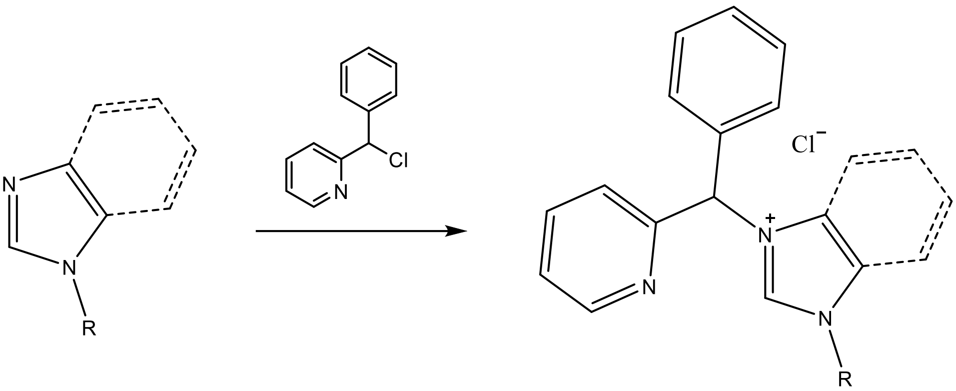

76d, $R = C_6H_{13}$
76e, $R = C_7H_{15}$
76f, $R = C_8H_{17}$
76g, $R = C_9H_{19}$
76h, $R = C_{10}H_{21}$

71d, $R = C_6H_{13}$
71e, $R = C_7H_{15}$
71f, $R = C_8H_{17}$
71g, $R = C_9H_{19}$
71h, $R = C_{10}H_{21}$

Scheme 19. Synthesis pathway of **71** using microwave irradiation.

Table 12. Comparison of reaction yields for imidazolium salts under microwave irradiation (60 minutes) and conventional heating (48 hours).

Compound	Yield (%)	
	Conventional heating	Microwave irradiation
Im-71a	49.1	79.1
Im-71d	53.6	71.1
Im-71e	49.9	79.4
Im-71f	50.2	83.7
Im-71g	36.6	80.8
Im-71h	46.1	82.4
Bz-71d	46.5	86.4
Bz-71e	34.1	88.7
Bz-71f	40.1	89.6
Bz-71g	63.4	91.3
Bz-71h	52.0	87.6

** Yield (%) refer to isolated yield.*

2.2.3 Lipinski's Rule of Five Analysis

The Lipinski's Rule of Five (Ro5) was formulated by Lipinski and his coworkers in the 1990s, which suggests that having calculated properties and descriptors similar to oral drugs may increase the likelihood of a compound being orally active (Shultz 2018). Based on this "drugability" guidelines, a compound that violates the Ro5, such as having more than five hydrogen bond donors, 10 hydrogen bond acceptors, molecular weight is greater than 500, and the calculated Log P (CLog P) is greater than five, is more likely to have poor absorption or permeation (Benet et al 2016). A CLog P value is defined as the logarithm of its partition coefficient between *n*-octanol and water, which demonstrates the compound's hydrophilicity. A CLog P value of greater than five indicates that the compound may be too lipophilic, thus having weaker aqueous solubility and compromising its bioavailability. The compound may also be sequestered by body fatty tissue, resulting in difficulty in excretion. This leads to accumulation of such compound, which may impact the systemic toxicity of the substance. Furthermore, compounds with much lower CLog P values have better penetration through certain barriers, such as central nervous system drugs with CLog P value of approximately 2, and orally absorbed drugs with CLog P value around 1.5 (Greenberg 1980; Hansch *et al* 1987). For compounds **Im-71d – h** and **Bz-71d – h**, *in silico* predictions were performed to study if the compounds conform to the Lipinski's Ro5 using the

Chemicalise software and summarised in **Table 12**. Based on **Table 13**, the molecular structures of all synthesised compounds (**Im-71d – h** and **Bz-71d – h**) did not show any violation to the Lipinski's Ro5. With no hydrogen bond donor and one hydrogen bond acceptor, molecular weight being less than 500 Da, and CLog P value lower than five, **Im-71d – h** and **Bz-71d – h** conformed to the Ro5 and are presumed to be orally active.

Table 13. Chemical information of compounds **Im-71d – h** and **Bz-71d – h**.

Compound	Formula	H-bond donor	H-bond acceptor	Exact mass (Da)	CLog P	Ro5
Im-71d	$C_{21}H_{26}N_3Cl$	0	1	355.1815	1.268	Yes
Im-71e	$C_{22}H_{28}N_3Cl$	0	1	369.1972	1.712	Yes
Im-71f	$C_{23}H_{30}N_3Cl$	0	1	383.2128	2.157	Yes
Im-71g	$C_{24}H_{32}N_3Cl$	0	1	397.2285	2.602	Yes
Im-71h	$C_{25}H_{34}N_3Cl$	0	1	411.2441	3.046	Yes
Bz-71d	$C_{25}H_{28}N_3Cl$	0	1	405.1972	2.316	Yes
Bz-71e	$C_{26}H_{30}N_3Cl$	0	1	419.2128	2.761	Yes
Bz-71f	$C_{27}H_{32}N_3Cl$	0	1	433.2285	3.205	Yes
Bz-71g	$C_{28}H_{34}N_3Cl$	0	1	447.2441	3.650	Yes
Bz-71h	$C_{29}H_{36}N_3Cl$	0	1	461.2598	4.094	Yes

2.3 Conclusion

In this chapter, a series of *N*-alkyl-substituted (benz)imidazole derivatives and their respective pyridine-functionalised (benz)imidazolium salts were successfully synthesised. The chemical structures and identities of the synthesised compounds were confirmed by using analytical spectroscopic techniques, which include ^{1}H- and ^{13}C-NMR, FT-IR, and mass spectrometry. The silver NHC complex for **Im-71g-Br** was also synthesised and characterised. The attempt to crystallise the silver NHC complex was unsuccessful, and its imidazolium salt **Im-71a-PF$_6$** crystallised *via* unexplainable regaining of imidazolium proton. In addition, a greener synthesis protocols which involved microwave irradiation for both (benz)imidazole derivatives and their respective salts were also developed. It was found that the reaction durations were shortened significantly from 5 – 7 days to 3 hours, and from 2 – 4 days to 1 hour. The yield percentage of each derivative was increased about 20 – 30 % as compared to the yield isolated from the conventional heating method. Furthermore, *in silico* study showed that the synthesised compounds **Im-71d – h** and **Bz-71d – h** conformed to Lipinski's Ro5, which make them potential drug candidates for medicinal applications.

2.4 Experimental

2.4.1 General procedures

All the commercially available chemicals and solvents were used without prior drying or purification. Synthesis of **73** and **74** were conducted as per literature method with slight modifications (Chiang *et al* 2010; Kim & Kang 2014). The synthesis of alkyl-suibstituted (benz)imidazoles was performed in analogous fashion with the respective alkyl bromide (hexyl, heptyl, octyl, nonyl, decyl). The synthesised alkyl-substituted (benz)imidazoles were then reacted with **74** to yield the respective alkyl-substitued (benz)imidazolium salts. Reactions involving light sensitive compounds were conducted with aluminium foil-wrapped glass apparatuses. The solvent system used for all TLC was similar to the solvent system used in the respective column chromatography. Mass spectra were recorded on Waters Xevo TQ-XS Triple Quadrupole Mass Spectrometer. ^{1}H- and ^{13}C-NMR spectroscopy were performed on a Bruker Avance 300 NMR Spectrometer. The number of protons (n) for a given resonance was indicated by n H. Coupling constants were reported as a J value in Hz. ^{1}H-NMR spectra were reported as δ in units of parts per million (ppm) downfield from $SiMe_4$ (δ = 0.00). ^{13}C-NMR spectra were reported as δ in units of parts per million (ppm) relative to the signal of chloroform-*d* (δ = 77.16 ppm, triplet) and DMSO-d_6 (δ = 39.52 ppm, septet). All chemical shifts reported were referenced to the chemical shifts of their respective residual solvent resonances. Unless stated otherwise, all NMR experiments were carried out at 300 K. The VT-NMR analysis was performed by Faculty of Science, University of Malaya. The single crystal X-ray diffraction analysis was performed by Research Centre for Crystalline Materials at Sunway University, Malaysia. The Lipinski's Rule of Five analysis was conducted using Chemicalise software. The microwave-assisted *N*-alkylation was performed using Anton Paar Monowave 450.

2.4.2 Synthesis of *N*-alkyl-substituted imidazole

2.4.2.1 Synthesis of 1-hexylimidazole, [Im-76d]

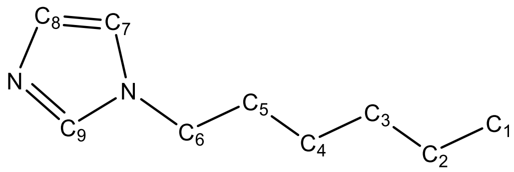

To a solution of imidazole **Im-75** (0.34 g, 5.0 mmol) in acetonitrile (20 mL), potassium carbonate (1.38 g, 10.0 mmol) and tetraethylammonium iodide (0.13 g, 0.5 mmol) were added and the mixture was stirred for 1 hour at room temperature. Subsequently, 1-bromohexane (0.76 g, 5.0 mmol) was added into the solution and the mixture was stirred for 5 days under reflux condition. Water (30 mL) was added to the mixture and the water phase was extracted three times with ethyl acetate (50 mL). The organic phase was washed with a saturated solution of sodium chloride and dried over anhydrous magnesium sulphate. Ethyl acetate was removed *in vacuo* and the reaction mixture was subjected to column chromatography (chloroform: ethanol = 95:5). The pure product was obtained as yellow liquid (0.22 g, 1.4 mmol, 29.1 %). **^{1}H-NMR** (300 MHz, $CDCl_3$): δ = 0.85 – 0.89 (*t*, 3 H, H1, $^3J_{H,H}$ = 6.9 Hz), 1.27 – 1.31 (*m*, 6 H, H2 – H4), 1.69 – 1.79 (*quin*, 2 H, H5, $^3J_{H,H}$ = 6.9 Hz), 3.87 – 3.92 (*t*, 2 H, H6, $^3J_{H,H}$ = 6.9 Hz), 6.89 (*s*, 1 H, aromatic), 7.01 (*s*, 1 H, aromatic) and 7.43 (*s*, 1 H, H 9) ppm. **^{13}C-NMR** (300 MHz, $CDCl_3$): δ = 13.92 (C1), 22.37 (C2), 25.84 (C3), 30.28 (C4), 31.07 (C5), 47.13 (C6), 118.99 and 128.91 (aromatic), 136.95 (C9) ppm. MS (ESI) *m/z*: $[M+H]^+$ calcd. for $C_9H_{16}N_2$ 153.14, found 152.90.

2.4.2.2 Synthesis of 1-heptylimidazole, [Im-76e]

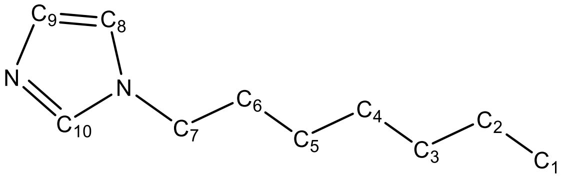

To a solution of imidazole **Im-75** (0.34 g, 5.0 mmol) in acetonitrile (20 mL), potassium carbonate (1.38 g, 10.0 mmol) and tetraethylammonium iodide (0.13 g, 0.5 mmol) were added and the mixture was stirred for 1 hour at room temperature. Subsequently, 1-bromoheptane (0.83 g, 5.0 mmol) was added into the solution and the mixture was stirred for 5 days under reflux condition. Water (30 mL) was added to the mixture and the water phase was extracted three times with ethyl acetate (50 mL). The organic phase was washed with a saturated solution of sodium chloride and dried over anhydrous magnesium sulphate. Ethyl acetate was removed *in vacuo* and the reaction mixture was subjected to column chromatography (chloroform: ethanol = 95:5). The pure product was obtained as yellow liquid (0.47 g, 2.8 mmol, 56.4 %). **^{1}H-NMR** (300 MHz, $CDCl_3$): δ = 0.81 – 0.97 (*t*, 3 H, H1, $^{3}J_{H,H}$ = 6.9 Hz), 1.14 – 1.40 (*m*, 8 H, H2 – H5), 1.64 – 1.85 (*quin*, 2 H, H6, $^{3}J_{H,H}$ = 6.9 Hz), 3.83 – 3.96 (*t*, 2 H, H7, $^{3}J_{H,H}$ = 6.9 Hz), 6.89 (*s*, 1 H, aromatic), 7.02 (*s*, 1 H, aromatic) and 7.43 (*s*, 1 H, H 10) ppm. **^{13}C-NMR** (300 MHz, $CDCl_3$): δ = 14.02 (C1), 22.53 (C2), 26.47 (C3), 28.72 (C4), 31.09 (C5), 31.63 (C6), 46.94 (C7), 118.80 and 129.19 (aromatic), 137.02 (C10) ppm. MS (ESI) *m/z*: $[M+H]^+$ calcd. for $C_{10}H_{18}N_2$ 167.15, found 166.90.

2.4.2.3 Synthesis of 1-octylimidazole, [Im-76f]

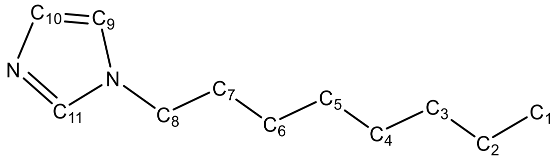

To a solution of imidazole **Im-75** (0.34 g, 5.0 mmol) in acetonitrile (20 mL), potassium carbonate (1.38 g, 10.0 mmol) and tetraethylammonium iodide (0.13 g, 0.5 mmol) were added and the mixture was stirred for 1 hour at room temperature. Subsequently, 1-bromooctane (0.90 g, 5.0 mmol) was added into the solution and the mixture was stirred for 5 days under reflux condition. Water (30 mL) was added to the mixture and the water phase was extracted three times with ethyl acetate (50 mL). The organic phase was washed with a saturated solution of sodium chloride and dried over anhydrous magnesium sulphate. Ethyl acetate was removed *in vacuo* and the reaction mixture was subjected to column chromatography (chloroform: ethanol = 95:5). The pure product was obtained as yellow liquid. **^{1}H-NMR** (300 MHz, $CDCl_3$): δ = 0.76 – 0.99 (*t*, 3 H, H1, $^{3}J_{H,H}$ = 6.9 Hz), 1.12 – 1.39 (*m*, 10 H, H2 – H6), 1.59 – 1.84 (*quin*, 2 H, H7, $^{3}J_{H,H}$ = 6.9 Hz), 3.85 – 3.89 (*t*, 2 H, H8, $^{3}J_{H,H}$ = 6.9 Hz), 6.88 (*s*, 1 H, aromatic), 6.98 (*s*, 1 H, aromatic) and 7.43 (*s*, 1 H, H 11) ppm. **^{13}C-NMR** (300 MHz, $CDCl_3$): δ = 14.06 (C1), 22.61 (C2), 26.53 (C3), 29.04 (C4), 29.10 (C5), 31.10 (C6), 31.73 (C7), 46.94 (C8), 118.77 and 129.22 (aromatic), 137.01 (C11) ppm. MS (ESI) *m/z*: $[M+H]^+$ calcd. for $C_{11}H_{20}N_2$ 181.17, found 181.00.

2.4.2.4 Synthesis of 1-nonylimidazole, [Im-76g]

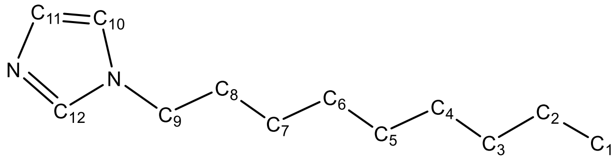

To a solution of imidazole **Im-75** (0.34 g, 5.0 mmol) in acetonitrile (20 mL), potassium carbonate (1.38 g, 10.0 mmol) and tetraethylammonium iodide (0.13 g, 0.5 mmol) were added and the mixture was stirred for 1 hour at room temperature. Subsequently, 1-bromononane (0.97 g, 5.0 mmol) was added into the solution and the mixture was stirred for 5 days under reflux condition. Water (30 mL) was added to the mixture and the water phase was extracted three times with ethyl acetate (50 mL). The organic phase was washed with a saturated solution of sodium chloride and dried over anhydrous magnesium sulphate. Ethyl acetate was removed *in vacuo* and the reaction mixture was subjected to column chromatography (chloroform: ethanol = 95:5). The pure product was obtained as yellow liquid (0.22 g, 1.4 mmol, 29.1 %). **^{1}H-NMR** (300 MHz, $CDCl_3$): δ = 0.84 – 0.88 (*t*, 3 H, H1, $^{3}J_{H,H}$ = 6.9 Hz), 1.12 – 1.41 (*m*, 12 H, H2 – H7), 1.66 – 1.76 (*quin*, 2 H, H8, $^{3}J_{H,H}$ = 6.9 Hz), 3.78 – 3.97 (*t*, 2 H, H9, $^{3}J_{H,H}$ = 6.9 Hz), 6.86 (*s*, 1 H, aromatic), 6.98 (*s*, 1 H, aromatic) and 7.44 (*s*, 1 H, H 12) ppm. **^{13}C-NMR** (300 MHz, $CDCl_3$): δ = 14.08 (C1), 22.64 (C2), 26.53 (C3), 29.07 (C4), 29.18 (C5), 29.39 (C6), 31.09 (C7), 31.82 (C8), 47.00 (C9), 118.77 and 129.25 (aromatic), 137.03 (C12) ppm. MS (ESI) *m/z*: $[M+H]^+$ calcd. for $C_{12}H_{22}N_2$ 195.33, found 195.00.

2.4.2.5 Synthesis of 1-decylimidazole, [Im-76h]

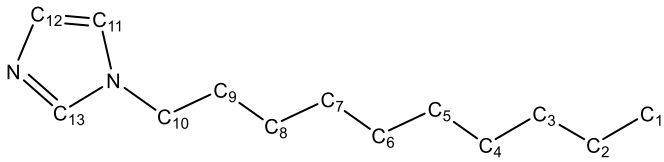

To a solution of imidazole **Im-75** (0.34 g, 5.0 mmol) in acetonitrile (20 mL), potassium carbonate (1.38 g, 10.0 mmol) and tetraethylammonium iodide (0.13 g, 0.5 mmol) were added and the mixture was stirred for 1 hour at room temperature. Subsequently, 1-bromodecane (1.11 g, 5.0 mmol) was added into the solution and the mixture was stirred for 5 days under reflux condition. Water (30 mL) was added to the mixture and the water phase was extracted three times with ethyl acetate (50 mL). The organic phase was washed with a saturated solution of sodium chloride and dried over anhydrous magnesium sulphate. Ethyl acetate was removed *in vacuo* and the reaction mixture was subjected to column chromatography (chloroform: ethanol = 95:5). The pure product was obtained as yellow liquid (0.70 g, 3.4 mmol, 68.0 %). **^{1}H-NMR** (300 MHz, $CDCl_3$): δ = 0.82 – 0.92 (*t*, 3 H, H1, $^{3}J_{H,H}$ = 6.7 Hz), 1.20 – 1.36 (*m*, 14 H, H2 – H8), 1.70 – 1.83 (*quin*, 2 H, H9, $^{3}J_{H,H}$ = 6.7 Hz), 3.87 – 3.96 (*t*, 2 H, H10, $^{3}J_{H,H}$ = 6.9 Hz), 6.90 (*s*, 1 H, aromatic), 7.05 (*s*, 1 H, aromatic) and 7.46 (*s*, 1 H, H 13) ppm. **^{13}C-NMR** (100 MHz, $CDCl_3$): δ = 14.09 (C1), 22.66 (C2), 26.56 (C3), 29.07 (C4), 29.26 (C5), 29.43 (C6), 29.48 (C7), 31.09 (C8), 31.86 (C9), 47.08 (C10), 118.78 and 129.29 (aromatic), 137.05 (C13) ppm. MS (ESI) *m/z*: $[M+H]^+$ calcd. for $C_{13}H_{24}N_2$ 209.20, found 209.00.

2.4.3 Synthesis of *N*-alkyl-substituted benzimidazole

2.4.3.1 Synthesis of 1-hexylbenzimidazole, [Bz-76d]

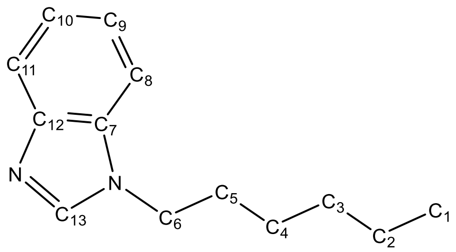

To a solution of benzimidazole **Bz-75** (1.19 g, 10.0 mmol) in acetonitrile (30 mL), potassium carbonate (2.00 g, 14.5 mmol) and tetraethylammonium iodide (0.26 g, 1.0 mmol) were added and the mixture was stirred for 1 hour at room temperature. Subsequently, 1-bromohexane (1.65 g, 10.0 mmol) was added into the solution and the mixture was stirred for 7 days under reflux condition. Water (100 mL) was added to the mixture and the water phase was extracted three times with ethyl acetate (100 mL). The organic phase was washed with a saturated solution of sodium chloride and dried over anhydrous magnesium sulphate. Ethyl acetate was removed *in vacuo* and the reaction mixture was subjected to column chromatography (chloroform: ethanol = 95:5). The pure product was obtained as yellow liquid (1.10 g, 5.4 mmol, 54.2 %). **^{1}H-NMR** (300 MHz, $CDCl_3$): δ = 0.81 – 0.92 (*t*, 3 H, H1, $^3J_{H,H}$ = 6.8 Hz), 1.21 – 1.41 (*m*, 6 H, H2 – H4), 1.78 – 1.95 (*quin*, 2 H, H5, $^3J_{H,H}$ = 7.2 Hz), 4.09 – 4.20 (*t*, 2 H, H10, $^3J_{H,H}$ = 7.2 Hz), 7.22 – 7.34 (*m*, 2 H, aromatic), 7.35 – 7.43 (*m*, 1 H, aromatic), 7.77 – 7.85 (*m*, 1 H, aromatic) and 7.88 (*s*, 1 H, H 13) ppm. **^{13}C-NMR** (100 MHz, $CDCl_3$): δ = 13.94 (C1), 22.46 (C2), 26.56 (C3), 26.48 (C4), 29.77 (C5), 45.12 (C6), 109.67, 120.35, 122.01, 122.78, 133.82, 142.98 (aromatic), 143.84 (C13) ppm. MS (ESI) *m/z*: $[M+H]^+$ calcd. for $C_{13}H_{19}N_2$ 203.15, found 202.47.

2.4.3.2 Synthesis of 1-heptylbenzimidazole, [Bz-76e]

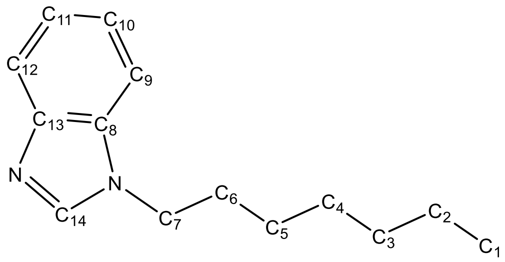

To a solution of benzimidazole **Bz-75** (1.19 g, 10.0 mmol) in acetonitrile (30 mL), potassium carbonate (2.00 g, 14.5 mmol) and tetraethylammonium iodide (0.26 g, 1.0 mmol) were added and the mixture was stirred for 1 hour at room temperature. Subsequently, 1-bromoheptane (1.79 g, 10.0 mmol) was added into the solution and the mixture was stirred for 7 days under reflux condition. Water (100 mL) was added to the mixture and the water phase was extracted three times with ethyl acetate (100 mL). The organic phase was washed with a saturated solution of sodium chloride and dried over anhydrous magnesium sulphate. Ethyl acetate was removed *in vacuo* and the reaction mixture was subjected to column chromatography (chloroform: ethanol = 95:5). The pure product was obtained as yellow liquid (1.31 g, 6.1 mmol, 60.5 %). **^{1}H-NMR** (300 MHz, $CDCl_3$): δ = 0.82 – 0.93 (*t*, 3 H, H1, $^{3}J_{H,H}$ = 6.7 Hz), 1.18 – 1.40 (*m*, 8 H, H2 – H5), 1.81 – 1.88 (*quin*, 2 H, H6, $^{3}J_{H,H}$ = 6.7 Hz), 4.11 – 4.22 (*t*, 2 H, H10, $^{3}J_{H,H}$ = 7.1 Hz), 7.23 – 7.35 (*m*, 1 H, aromatic), 7.36 – 7.44 (*m*, 1 H, aromatic), 7.77 – 7.85 (*m*, 1 H, aromatic) and 7.89 (*s*, 1 H, H 14) ppm. **^{13}C-NMR** (100 MHz, $CDCl_3$): δ = 14.00 (C1), 22.53 (C2), 26.79 (C3), 28.76 (C4), 29.83 (C5), 31.61 (C6), 45.14 (C7), 109.67, 120.36, 122.03, 122.79, 133.83 and 142.92 (aromatic), 143.84 (C14) ppm. MS (ESI) *m/z*: $[M+H]^+$ calcd. for $C_{14}H_{21}N_2$ 217.17, found 216.79.

2.4.3.3 Synthesis of 1-octylbenzimidazole, [Bz-76f]

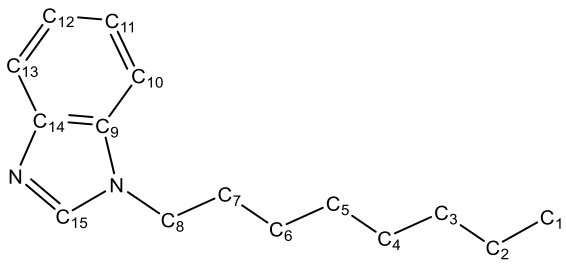

To a solution of benzimidazole **Bz-75** (1.19 g, 10.0 mmol) in acetonitrile (30 mL), potassium carbonate (2.00 g, 14.5 mmol) and tetraethylammonium iodide (0.26 g, 1.0 mmol) were added and the mixture was stirred for 1 hour at room temperature. Subsequently, 1-bromoheptane (1.93 g, 10.0 mmol) was added into the solution and the mixture was stirred for 7 days under reflux condition. Water (100 mL) was added to the mixture and the water phase was extracted three times with ethyl acetate (100 mL). The organic phase was washed with a saturated solution of sodium chloride and dried over anhydrous magnesium sulphate. Ethyl acetate was removed *in vacuo* and the reaction mixture was subjected to column chromatography (chloroform: ethanol = 95:5). The pure product was obtained as yellow liquid (1.16 g, 5.0 mmol, 50.2 %). **^{1}H-NMR** (300 MHz, $CDCl_3$): δ = 0.81 – 0.94 (*t*, 3 H, H1, $^3J_{H,H}$ = 6.7 Hz), 1.15 – 1.42 (*m*, 10 H, H2 – H6), 1.78 – 1.97 (*quin*, 2 H, H7, $^3J_{H,H}$ = 7.0 Hz), 4.09 – 4.21 (*t*, 2 H, H8, $^3J_{H,H}$ = 6.9 Hz), 7.22 – 7.34 (*m*, 1 H, aromatic), 7.35 – 7.44 (*m*, 1 H, aromatic) 7.76 – 7.84 (*m*, 1 H, aromatic) and 7.88 (*s*, 1 H, H 15) ppm. **^{13}C-NMR** (100 MHz, $CDCl_3$): δ = 14.05 (C1), 22.58 (C2), 26.81 (C3), 29.06 (C4), 29.07 (C5), 29.80 (C6), 31.71 (C7), 45.12 (C8), 109.67, 120.35, 121.99, 122.77, 133.81 and 142.92 (aromatic), 143.84 (C15) ppm. MS (ESI) *m/z*: $[M+H]^+$ calcd. for $C_{15}H_{13}N_2$ 231.19, found 230.48.

2.4.3.4 Synthesis of 1-nonylbenzimidazole, [Bz-76g]

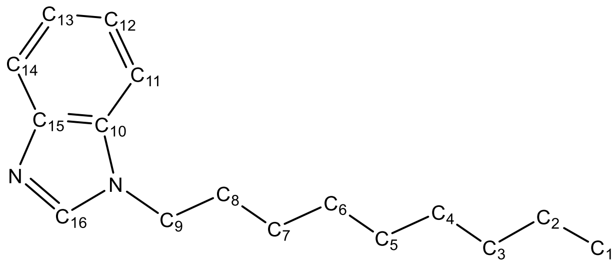

To a solution of benzimidazole **Bz-75** (2.95 g, 25.0 mmol) in acetonitrile (100 mL), potassium carbonate (5.00 g, 36.3 mmol) and tetraethylammonium iodide (0.65 g, 2.5 mmol) were added and the mixture was stirred for 1 hour at room temperature. Subsequently, 1-bromononane (5.18 g, 25.0 mmol) was added into the solution and the mixture was stirred for 7 days under reflux condition. Water (100 mL) was added to the mixture and the water phase was extracted three times with ethyl acetate (100 mL). The organic phase was washed with a saturated solution of sodium chloride and dried over anhydrous magnesium sulphate. Ethyl acetate was removed *in vacuo* and the reaction mixture was subjected to column chromatography (chloroform: ethanol = 95:5). The pure product was obtained as yellow liquid (3.34 g, 13.7 mmol, 54.8 %). **^{1}H-NMR** (300 MHz, $CDCl_3$): δ = 0.82 – 0.94 (*t*, 3 H, H1, $^3J_{H,H}$ = 6.7 Hz), 1.22 – 1.40 (*m*, 12 H, H2 – H7), 1.82 – 1.95 (*quin*, 2 H, H8, $^3J_{H,H}$ = 7.0 Hz), 4.13 – 4.22 (*t*, 2 H, H9, $^3J_{H,H}$ = 7.2 Hz), 7.24 – 7.35 (*m*, 2 H, aromatic), 7.37 – 7.45 (*m*, 1 H, aromatic) 7.78 – 7.86 (*m*, 1 H, aromatic) and 7.92 (*s*, 1 H, H 16) ppm. **^{13}C-NMR** (100 MHz, $CDCl_3$): δ = 14.07 (C1), 22.61 (C2), 26.80 (C3), 29.08 (C4), 29.16 (C5), 29.37 (C6), 29.79 (C7), 31.78 (C8), 45.10 (C9), 109.67, 120.32, 121.98, 122.76, 133.81 and 142.91 (aromatic), 143.84 (C16) ppm. MS (ESI) *m/z*: $[M+H]^+$ calcd. for $C_{16}H_{15}N_2$ 245.19, found 244.47. MS (ESI) *m/z*: $[M+H]^+$ calcd. for $C_{16}H_{15}N_2$ 245.19, found 244.47.

2.4.3.5 Synthesis of 1-decylbenzimidazole, [Bz-76h]

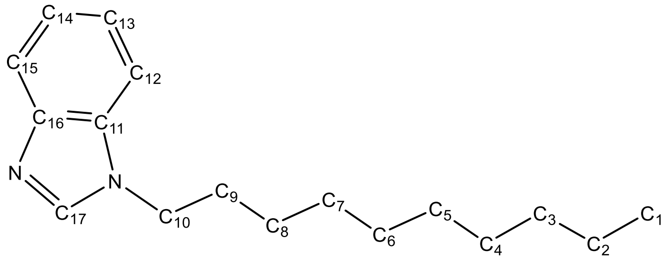

To a solution of benzimidazole **Bz-75** (2.95 g, 25.0 mmol) in acetonitrile (100 mL), potassium carbonate (5.00 g, 36.3 mmol) and tetraethylammonium iodide (0.65 g, 2.5 mmol) were added and the mixture was stirred for 1 hour at room temperature. Subsequently, 1-bromodecane (5.53 g, 25.0 mmol) was added into the solution and the mixture was stirred for 7 days under reflux condition. Water (100 mL) was added to the mixture and the water phase was extracted three times with ethyl acetate (100 mL). The organic phase was washed with a saturated solution of sodium chloride and dried over anhydrous magnesium sulphate. Ethyl acetate was removed *in vacuo* and the reaction mixture was subjected to column chromatography (chloroform: ethanol = 95:5). The pure product was obtained as yellow liquid (3.66 g, 14.2 mmol, 56.8 %). **^{1}H-NMR** (300 MHz, $CDCl_3$): δ = 0.74 – 0.87 (*t*, 3 H, H1, $^3J_{H,H}$ = 6.6 Hz), 1.08 – 1.33 (*m*, 14 H, H2 – H8), 1.72 – 1.87 (*quin*, 2 H, H9, $^3J_{H,H}$ = 6.9 Hz), 4.02 – 4.12 (*t*, 2 H, H10, $^3J_{H,H}$ = 7.2 Hz), 7.15 – 7.20 (*m*, 1 H, aromatic), 7.21 – 7.26 (*m*, 1 H, aromatic) 7.28 – 7.36 (*m*, 1 H, aromatic) 7.68 – 7.77 (*m*, 1 H, aromatic) and 7.81 (*s*, 1 H, H 17) ppm. **^{13}C-NMR** (100 MHz, $CDCl_3$): δ = 14.09 (C1), 22.65 (C2), 26.81 (C3), 29.08 (C4), 29.23 (C5), 29.41 (C6), 29.46 (C7), 29.80 (C8), 31.83 (C9), 45.11 (C10), 109.66, 120.36, 121.98, 122.75, 133.82 and 142.92 (aromatic), 143.86 (C17) ppm. MS (ESI) *m/z*: $[M+H]^+$ calcd. for $C_{17}H_{17}N_2$ 259.21, found 258.49.

2.4.4 Synthesis of pyridine-functionalised imidazolium salts

2.4.4.1 Synthesis of 1-hexyl-3-[phenyl(pyridin-2-yl)methyl]-1H-imidazol-3-ium chloride, [Im-71d]

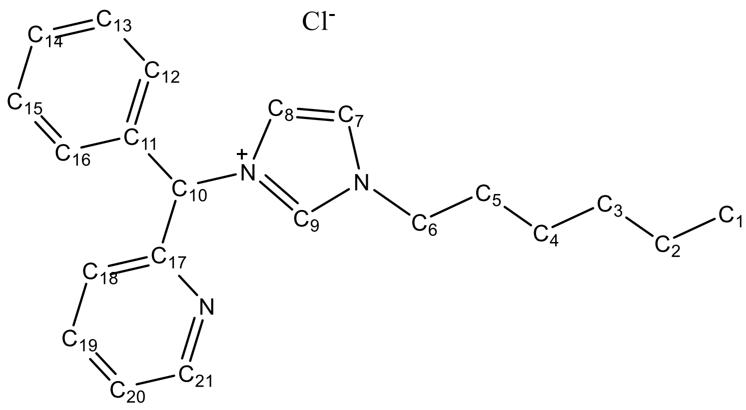

To a solution of compound **Im-76d** (1.87 g, 12.3 mmol) in acetonitrile (50 mL), 2-[chloro(phenyl)methyl]pyridine **74** (2.50 g, 12.3 mmol) was added and heated at refluxing temperature for 48 hours. The resulting mixture was reduced *in vacuo* to obtain brown oil. Three consecutive successive precipitations were conducted with chloroform and diethyl ether to purify the crude compound. The pure product was obtained as dark brownish liquid (2.34 g, 6.6 mmol, 53.6 %). **^{1}H-NMR** (300 MHz, $CDCl_3$): δ = 0.84 – 0.88 (*t*, 3 H, H1, $^3J_{H,H}$ = 6.9 Hz), 1.24 – 1.38 (*m*, 6 H, H2 – H4), 1.85 – 1.97 (*quin*, 2 H, H5, $^3J_{H,H}$ = 7.2 Hz), 4.22 – 4.32 (*t*, 2 H, H6, $^3J_{H,H}$ = 6.0 Hz), 7.21 (*s*, 1 H, aromatic), 7.33 – 7.42 (*m*, 4 H, aromatic), 7.78 (*s*, 1 H, aromatic), 7.80 – 7.87 (*m*, 2 H, aromatic), 7.98 (*s*, 1 H, aromatic), 8.57 – 8.63 (*d*, 1 H, aromatic, $^3J_{H,H}$ = 4.8 Hz) and 10.55 (*s*, 1 H, H9) ppm. **^{13}C-NMR** (100 MHz, $CDCl_3$): δ = 13.87 (C1), 22.35 (C2), 25.91 (C3), 30.04 (C4), 31.03 (C5), 50.27 (C6), 65.61 (C10), 120.16, 120.46, 122.80, 123.94, 125.01, 128.92, 129.49, 136.29, 137.71, 138.26 and 148.94 (aromatic) and 155.90 (C9) ppm. MS (ESI) *m/z*: $[M\text{-}Cl]^+$ calcd. for $C_{21}H_{26}N_3^+$ 320.21, found 319.93.

2.4.4.2 Synthesis of 1-heptyl-3-[phenyl(pyridin-2-yl)methyl]-1H-imidazol-3-ium chloride, [Im-71e]

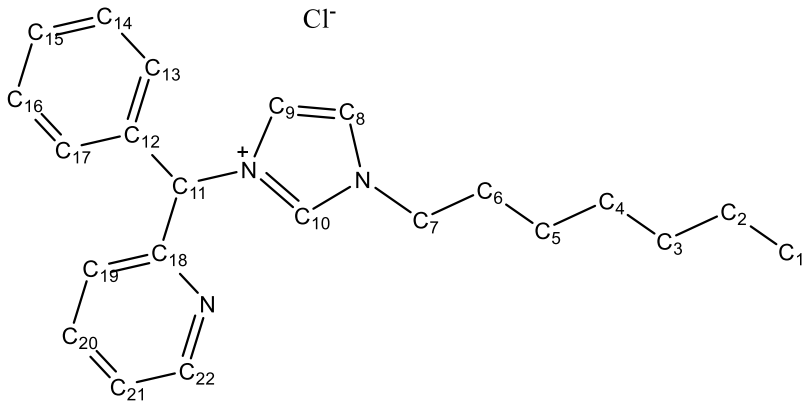

To a solution of compound **Im-76e** (2.05 g, 12.3 mmol) in acetonitrile (50 mL), 2-[chloro(phenyl)methyl]pyridine **74** (2.50 g, 12.3 mmol) was added and heated at refluxing temperature for 48 hours. The resulting mixture was reduced *in vacuo* to obtain brown oil. Three consecutive successive precipitations were conducted with chloroform and diethyl ether to purify the crude compound. The pure product was obtained as dark brownish oil (1.78 g, 5.3 mmol, 43.0 %). **^{1}H-NMR** (300 MHz, $CDCl_3$): δ = 0.79 – 0.93 (*m*, 6 H, H1), 1.18 – 1.40 (*m*, 16 H, H2 – H5), 1.79 – 1.98 (*quin*, 4 H, H6, $^3J_{H,H}$ = 6.0 Hz), 4.20 – 4.41 (*dt*, 4 H, H9, $^3J_{H,H}$ = 7.2 Hz, 28.5 Hz), 7.20 – 7.37 (*m*, 5 H, aromatic), 7.53 – 7.96 (*m*, 3 H, aromatic) 9.07 (*s*, 1 H, aromatic) and 10.23 – 10.39 (*d*, 1 H, H 10, $^3J_{H,H}$ = 30.0 Hz) ppm. **^{13}C-NMR** (100 MHz, $CDCl_3$): δ = 14.01 (C1), 22.42 (C2), 26.02 (C3), 30.15 (C4), 30.16 (C5), 31.21 (C6), 50.38 (C7) 65.77, 120.27, 120.57, 122.91, 124.05, 125.12, 129.03, 129.51, 136.41, 137.85, 138.40 and 149.20 (aromatic), 156.04 (C16) ppm. MS (ESI) *m/z*: $[M-Cl]^+$ calcd. for $C_{22}H_{28}N_3^+$ 334.23, found 333.93.

2.4.4.3 Synthesis of 1-octyl-3-[phenyl(pyridin-2-yl)methyl]-1H-imidazol-3-ium chloride, [Im-71f]

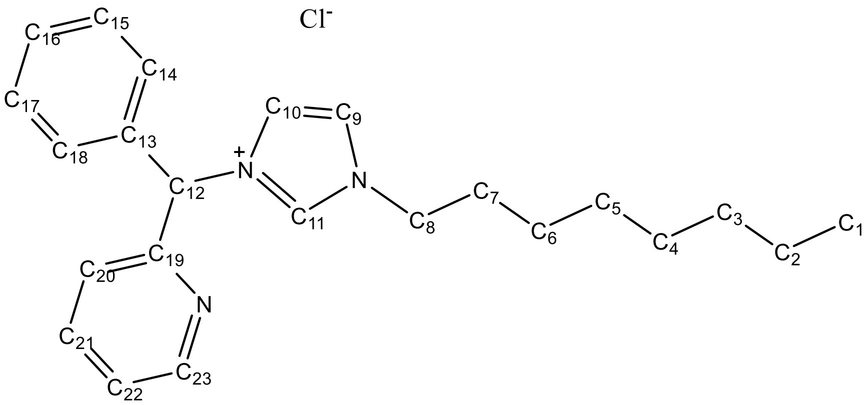

To a solution of compound **Im-76f** (2.22 g, 12.3 mmol) in acetonitrile (50 mL), 2-[chloro(phenyl)methyl]pyridine **74** (2.50 g, 12.3 mmol) was added and heated at refluxing temperature for 48 hours. The resulting mixture was reduced *in vacuo* to obtain brown oil. Three consecutive successive precipitations were conducted with chloroform and diethyl ether to purify the crude compound. The pure product was obtained as dark brownish oil (2.88 g, 7.5 mmol, 61.0 %). **^{1}H-NMR** (300 MHz, $CDCl_3$): δ = 0.81 – 0.92 (*m*, 6 H, H1), 1.16 – 1.39 (*m*, 20 H, H2 – H6), 1.82 – 1.98 (*quin*, 4 H, H7, $^{3}J_{H,H}$ = 6.0 Hz), 4.20 – 4.42 (*dt*, 4 H, H9, $^{3}J_{H,H}$ = 7.5 Hz, 28.5 Hz), 7.30 – 7.37 (*m*, 5 H, aromatic), 7.43 – 7.47 (*m*, 3 H, aromatic), 7.67 – 7.79 (*m*, 3 H, aromatic), 7.91 (*s*, 1 H, aromatic) and 10.48 (*s*, 1 H, H 11, $^{3}J_{H,H}$ = 39.0 Hz) ppm. **^{13}C-NMR** (100 MHz, $CDCl_3$): δ = 14.02 (C1), 22.53 (C2), 26.48 (C3), 28.99 (C4), 29.33 (C5), 29.47 (C6), 31.61 (C7), 47.89 (C8), 66.38, 112.64, 116.35, 124.01, 124.80, 126.73, 126.79, 128.85, 129.31, 134.99, 138.00, 142.96 and 149.51 (aromatic), and 154.59 (C23) ppm. MS (ESI) *m/z*: $[M-Cl]^+$ calcd. for $C_{23}H_{30}N_3^+$ 348.24, found 348.01.

2.4.4.4 Synthesis of 1-nonyl-3-[phenyl(pyridin-2-yl)methyl]-1H-imidazol-3-ium chloride, [Im-71g]

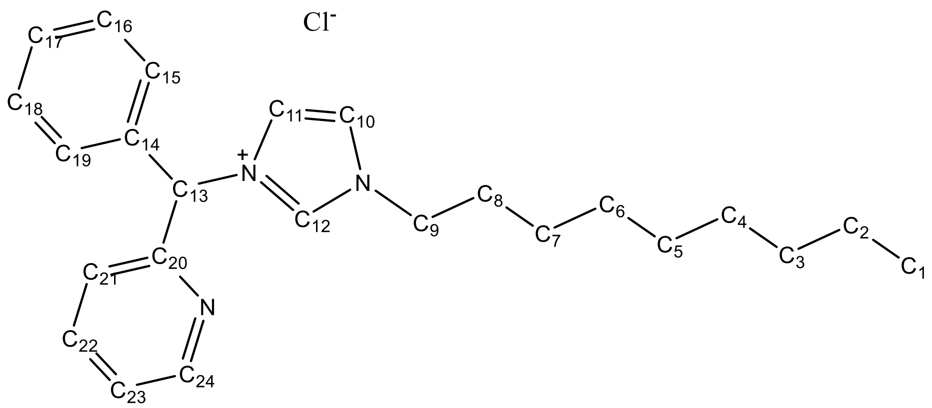

To a solution of compound **Im-76g** (2.39 g, 12.3 mmol) in acetonitrile (50 mL), 2-[chloro(phenyl)methyl]pyridine **74** (2.50 g, 12.3 mmol) was added and heated at refluxing temperature for 48 hours. The resulting mixture was reduced *in vacuo* to obtain brown oil. Three consecutive successive precipitations were conducted with chloroform and diethyl ether to purify the crude compound. The pure product was obtained as dark brownish oil (2.13 g, 5.4 mmol, 43.9 %). **^{1}H-NMR** (300 MHz, $CDCl_3$): δ = 0.82 – 0.93 (*m*, 6 H, H1), 1.19 – 1.39 (*m*, 24 H, H2 – H7), 1.84 – 1.98 (*quin*, 4 H, H8, $^{3}J_{H,H}$ = 5.1 Hz), 4.20 – 4.40 (*dt*, 4 H, H9, $^{3}J_{H,H}$ = 7.5 Hz, 36.0 Hz), 7.24 – 7.25 (*m*, 1 H, aromatic), 7.28 – 7.33 (*m*, 1 H, aromatic), 7.34 – 7.39 (*m*, 3 H, aromatic), 7.44 – 7.50 (*m*, 2 H, aromatic), 7.70 – 7.77 (*m*, 3 H, aromatic), 7.93 (*s*, 1 H, aromatic) and 10.70 (*s*, 1 H, H 12) ppm. **^{13}C-NMR** (100 MHz, $CDCl_3$): δ = 13.98 (C1), 22.51 (C2), 26.12 (C3), 28.82 (C4), 28.90 (C5), 29.05 (C6), 29.20 (C7), 31.67 (C8), 50.04 (C9), 65.64, 120.99, 122.01, 122.86, 123.73, 124.36, 126.94, 129.28, 136.35, 136.42, 137.54 and 149.42 (aromatic), and 154.91 (C24) ppm. MS (ESI) *m/z*: $[M-Cl]^+$ calcd. for $C_{24}H_{32}N_3^+$ 362.26, found 361.71.

2.4.4.5 Synthesis of 1-decyl-3-[phenyl(pyridin-2-yl)methyl]-1H-imidazol-3-ium chloride, [Im-71h]

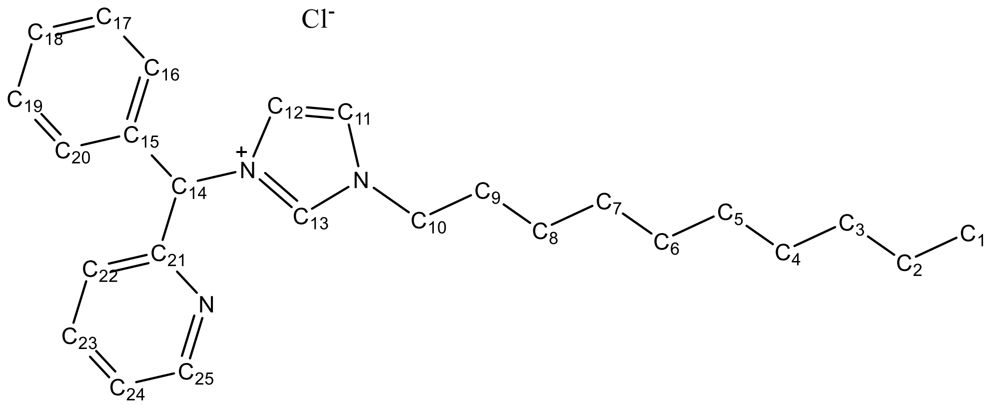

To a solution of compound **Im-76h** (2.56 g, 12.3 mmol) in acetonitrile (50 mL), 2-[chloro(phenyl)methyl]pyridine **74** (2.50 g, 12.3 mmol) was added and heated at refluxing temperature for 48 hours. The resulting mixture was reduced *in vacuo* to obtain brown oil. Three consecutive successive precipitations were conducted with chloroform and diethyl ether to purify the crude compound. The pure product was obtained as dark brownish oil (2.74 g, 6.7 mmol, 54.5 %). **^{1}H-NMR** (300 MHz, $CDCl_3$): δ = 0.80 – 0.95 (*m*, 6 H, H1), 1.15 – 1.42 (*m*, 28 H, H2 – H8), 1.81 – 1.98 (*quin*, 4 H, H9, $^{3}J_{H,H}$ = 8.4 Hz), 4.24 – 4.41 (*dt*, 4 H, H9, $^{3}J_{H,H}$ = 7.5 Hz, 21.0 Hz), 7.27 – 7.30 (*m*, 1 H, aromatic), 7.31 – 7.36 (*m*, 3 H, aromatic), 7.44 – 7.50 (*m*, 3 H, aromatic), 7.68 – 7.78 (*m*, 3 H, aromatic), 7.84 (*s*, 1 H, aromatic), 8.56 – 8.62 (*m*, 1 H, aromatic) and 10.30 (*s*, 1 H, H 12) ppm. **^{13}C-NMR** (100 MHz, $CDCl_3$): δ = 14.09 (C1), 22.64 (C2), 26.28 (C3), 29.03 (C4), 29.23 (C5), 29.40 (C6), 30.16 (C7), 30.32 (C8), 31.83 (C9), 50.12 (C10), 65.90, 121.01, 122.03, 122.82, 123.78, 124.46, 128.85, 129.32, 136.54, 137.04, 137.63 and 149.50 (aromatic), and 155.13 (C25) ppm. MS (ESI) *m/z*: $[M-Cl]^+$ calcd. for $C_{25}H_{34}N_3^+$ 376.28, found 375.98.

2.4.5 Synthesis of pyridine-functionalised benzimidazolium salts

2.4.5.1 Synthesis of 1-hexyl-3-[phenyl(pyridin-2-yl)methyl]-1H-benzimidazol-3-ium chloride, [Bz-71d]

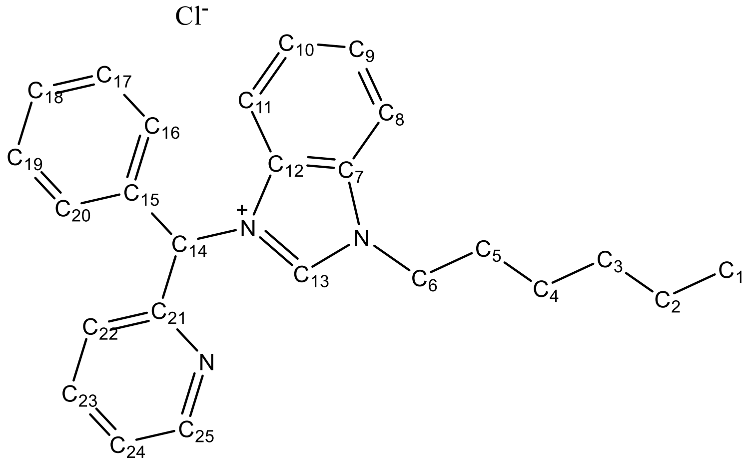

To a solution of compound **Bz-76d** (2.49 g, 12.3 mmol) in acetonitrile (50 mL), 2-[chloro(phenyl)methyl]pyridine **74** (2.50 g, 12.3 mmol) was added and heated at refluxing temperature for 96 hours. The resulting mixture was reduced *in vacuo* to about 20 mL, four equivalent of diethyl ether was added into the flask to yield pinkish red solid. (2.32 g, 5.7 mmol, 46.5 %). **^{1}H-NMR** (300 MHz, $CDCl_3$): δ = 0.80 – 0.90 (*t*, 3 H, H1, $^3J_{H,H}$ = 7.1 Hz), 1.21 – 1.48 (*m*, 6 H, H2 – H4), 1.97 – 2.10 (*quin*, 2 H, H5, $^3J_{H,H}$ = 7.5 Hz), 4.57 – 4.67 (*t*, 2 H, H6, $^3J_{H,H}$ = 7.5 Hz), 7.28 – 7.33 (*m*, 1 H, aromatic), 7.34 – 7.48 (*m*, 6 H, aromatic), 7.51 – 7.59 (*t*, 1 H, aromatic, $^3J_{H,H}$ = 8.4 Hz), 7.69 – 7.76 (*d*, 1 H, aromatic, $^3J_{H,H}$ = 8.4 Hz), 7.76 – 7.85 (*td*, 1 H, aromatic, $^3J_{H,H}$ = 1.8 Hz, 7.7 Hz) 7.85 – 7.91 (*d*, 1 H, aromatic, $^3J_{H,H}$ = 7.8 Hz), 7.93 (*s*, 1 H, aromatic), 8.51 – 8.56 (*dt*, 1 H, aromatic, $^3J_{H,H}$ = 0.8 Hz, 4.7 Hz) and 11.40 (*s*, 1 H, H13) ppm. **^{13}C-NMR** (100 MHz, $CDCl_3$): δ = 13.89 (C1), 22.38 (C2), 26.16 (C3), 29.28 (C4), 31.09 (C5), 47.79 (C6), 66.59, 112.50, 116.61, 123.99, 124.91, 126.63, 126.71, 128.81, 129.34, 131.52, 135.01, 137.96 and 143.42 (aromatic), and 154.68 (C25). MS (ESI) *m/z*: $[M\text{-}Cl]^+$ calcd. for $C_{25}H_{28}N_3^+$ 370.23, found 369.72.

2.4.5.2 Synthesis of 1-heptyl-3-[phenyl(pyridin-2-yl)methyl]-1H-benzimidazol-3-ium chloride, [Bz-71e]

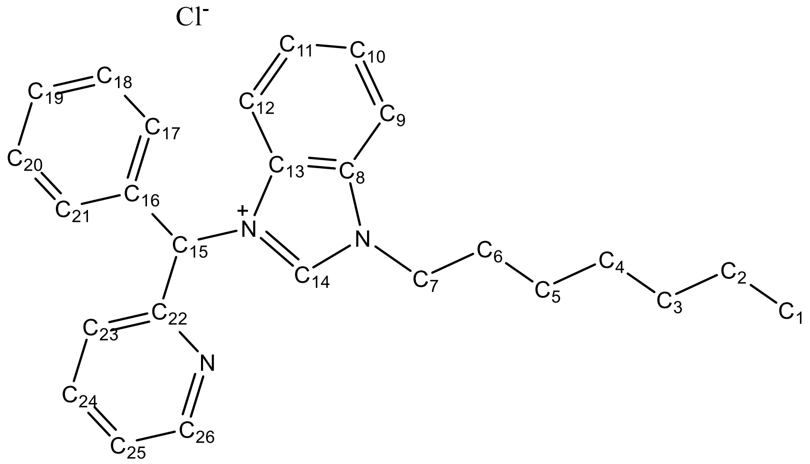

To a solution of compound **Bz-76e** (2.66 g, 12.3 mmol) in acetonitrile (50 mL), 2-[chloro(phenyl)methyl]pyridine **74** (2.50 g, 12.3 mmol) was added and heated at refluxing temperature for 96 hours. The resulting mixture was reduced *in vacuo* to about 20 mL, four equivalent of diethyl ether was added into the flask to yield pinkish red solid (1.78 g, 4.2 mmol, 34.1 %). **^{1}H-NMR** (300 MHz, $CDCl_3$): δ = 0.73 – 0.81 (m, 6 H, H1), 1.16 – 1.38 (m, 8 H, H2 – H5), 1.88 – 2.04 (m, 4 H, H5), 4.45 – 4.62 (m, 4 H, H7), 7.12 – 7.22 (m, 1 H, aromatic), 7.26 – 7.33 (m, 1 H, aromatic), 7.35 – 7.60 (m, 6 H, aromatic), 7.64 – 7.77 (m, 2 H, aromatic), 7.88 – 7.99 (m, 1 H, aromatic), 8.44 – 8.69 (m, 1 H, aromatic) 9.93 (s, 1 H, aromatic) and 11.20 (s, 1 H, H14) ppm. **^{13}C-NMR** (100 MHz, $CDCl_3$): δ = 13.98 (C1), 22.46 (C2), 26.47 (C3), 28.67 (C4), 29.50 (C5), 31.49 (C6), 47.77 (C7), 64.25 (C15), 111.84, 113.14, 116.26, 126.28, 126.54, 126.88, 126.99, 127.75, 128.15, 128.31, 130.94, 130.98, 140.54, 143.13 and 148.89 (aromatic), and 154.54 (C26). MS (ESI) *m/z*: $[M-Cl]^+$ calcd. for $C_{26}H_{30}N_3^+$ 384.24, found 383.77.

2.4.5.3 Synthesis of 1-octyl-3-[phenyl(pyridin-2-yl)methyl]-1H-benzimidazol-3-ium chloride, [Bz-71f]

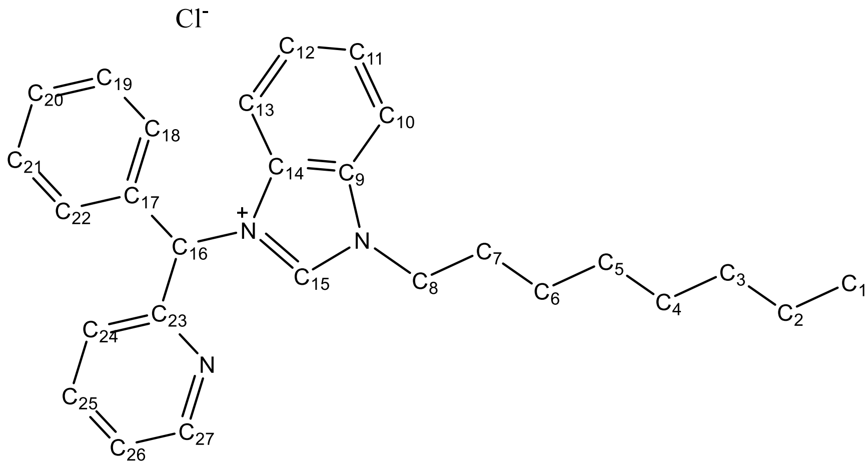

To a solution of compound **Bz-76f** (2.83 g, 12.3 mmol) in acetonitrile (50 mL), 2-[chloro(phenyl)methyl]pyridine **74** (2.50 g, 12.3 mmol) was added and heated at refluxing temperature for 96 hours. The resulting mixture was reduced *in vacuo* to about 20 mL, four equivalent of diethyl ether was added into the flask to yield pinkish red solid. (2.14 g, 4.9 mmol, 40.1 %). **^{1}H-NMR** (300 MHz, $CDCl_3$): δ = 0.73 – 0.84 (*t*, 3 H, H1, $^3J_{H,H}$ = 6.7 Hz), 1.19 – 1.40 (*m*, 10 H, H2 – H6), 1.90 – 2.04 (*quin*, 2 H, H7, $^3J_{H,H}$ = 7.4 Hz), 4.52 – 4.61 (*t*, 2 H, H8, $^3J_{H,H}$ = 7.5 Hz), 7.21 – 7.27 (*m*, 1 H, aromatic), 7.29 – 7.38 (*m*, 6 H, aromatic), 7.48 – 7.51 (*m*, 1 H, aromatic), 7.55 – 7.67 (*m*, 3 H, aromatic), 7.70 – 7.78 (*td*, 1 H, aromatic, $^3J_{H,H}$ = 1.8 Hz, 7.5 Hz) 7.78 – 7.83 (*d*, 1 H, aromatic, $^3J_{H,H}$ = 10.2 Hz), 7.83 (*s*, 1 H, aromatic), 8.45 – 8.50 (*dt*, 1 H, aromatic, $^3J_{H,H}$ = 0.6 Hz, 5.4 Hz) and 11.20 (*s*, 1 H, H15) ppm. **^{13}C-NMR** (100 MHz, $CDCl_3$): δ = 14.03 (C1), 22.55 (C2), 26.52 (C3), 28.96 (C4), 29.01 (C5), 29.36 (C6), 31.63 (C7), 47.85 (C8), 65.84 (C16), 112.53, 116.59, 124.00, 126.62, 126.70, 128.83, 129.29, 134.99, 137.95, 143.40 and 149.57 (aromatic), and 154.71 (C27). MS (ESI) *m/z*: $[M-Cl]^+$ calcd. for $C_{27}H_{32}N_3^+$ 398.26, found 398.96.

2.4.5.4 Synthesis of 1-nonyl-3-[phenyl(pyridin-2-yl)methyl]-1H-benzimidazol-3-ium chloride, [Bz-71g]

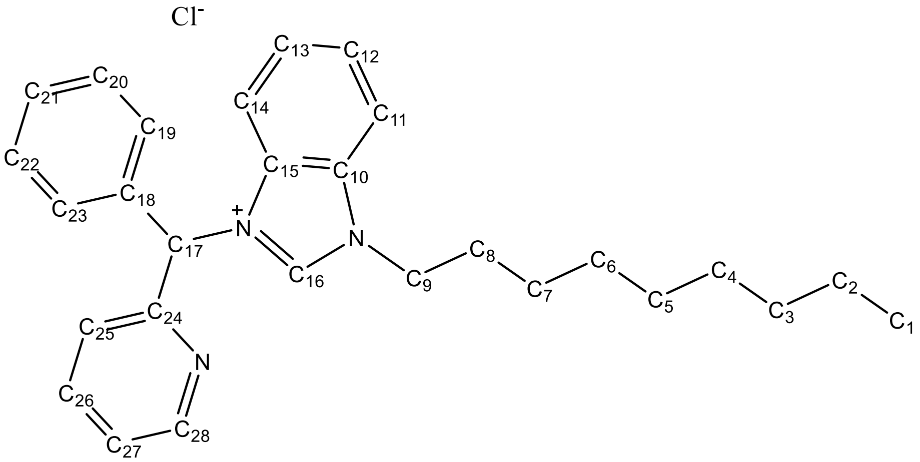

To a solution of compound **Bz-76g** (3.01 g, 12.3 mmol) in acetonitrile (50 mL), 2-[chloro(phenyl)methyl]pyridine **74** (2.50 g, 12.3 mmol) was added and heated at refluxing temperature for 96 hours. The resulting mixture was reduced *in vacuo* to about 20 mL, four equivalent of diethyl ether was added into the flask to yield pinkish red solid. (3.17 g, 7.8 mmol, 63.4 %). **^{1}H-NMR** (300 MHz, $CDCl_3$): δ = 0.71 – 0.84 (*m*, 6 H, H1), 1.12 – 1.41 (*m*, 24 H, H2 – H7), 1.90 – 2.03 (*quin*, 2 H, H8, $^{3}J_{H,H}$ = 7.5 Hz), 4.52 – 4.62 (*t*, 4 H, H9, $^{3}J_{H,H}$ = 7.5 Hz), 7.19 – 7.25 (*m*, 1 H, aromatic), 7.27 – 7.39 (*m*, 4 H, aromatic), 7.44 – 7.52 (*td*, 1 H, aromatic, $^{3}J_{H,H}$ = 0.9 Hz, 8.1 Hz), 7.56 – 7.68 (*m*, 4 H, aromatic), 7.70 – 7.75 (*dd*, 1 H, aromatic, $^{3}J_{H,H}$ = 1.8 Hz, 7.5 Hz) 7.76 – 7.81 (*d*, 1 H, aromatic, $^{3}J_{H,H}$ = 7.5 Hz), 7.84 (*s*, 1 H, aromatic), 8.44 – 8.49 (*ddd*, 1 H, aromatic, $^{3}J_{H,H}$ = 0.8 Hz, 1.8 Hz, 4.8 Hz) and 11.11 (*s*, 1 H, H16) ppm. **^{13}C-NMR** (100 MHz, $CDCl_3$): δ = 14.06 (C1), 22.59 (C2), 26.52 (C3), 29.00 (C4), 29.10 (C5), 29.31 (C6), 29.55 (C7), 31.75 (C8), 47.68 (C9), 66.74 (C17), 112.49, 113.05, 123.95, 124.87, 126.58, 126.67, 126.95, 128.81, 129.26, 131.36, 135.05, 137.84, 143.49 and 149.62 (aromatic), and 154.77 (C28). MS (ESI) *m/z*: $[M-Cl]^+$ calcd. for $C_{28}H_{34}N_3^+$ 412.28, found 411.73.

2.4.5.5 Synthesis of 1-decyl-3-[phenyl(pyridin-2-yl)methyl]-1H-benzimidazol-3-ium chloride, [Bz-71h]

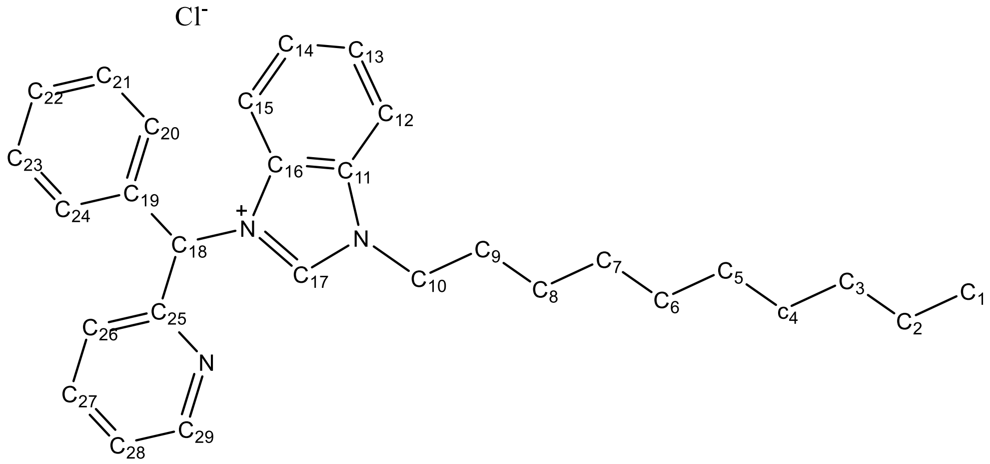

To a solution of compound **Bz-76h** (3.18 g, 12.3 mmol) in acetonitrile (50 mL), 2-[chloro(phenyl)methyl]pyridine **74** (2.50 g, 12.3 mmol) was added and heated at refluxing temperature for 96 hours. The resulting mixture was reduced *in vacuo* to about 20 mL, four equivalent of diethyl ether was added into the flask to yield pinkish red solid. (2.96 g, 6.4 mmol, 52.0 %). **^{1}H-NMR** (300 MHz, $CDCl_3$): δ = 0.76 – 0.84 (*m*, 6 H, H1), 1.11 – 1.41 (*m*, 28 H, H2 – H8), 1.91 – 2.03 (*quin*, 2 H, H9, $^{3}J_{H,H}$ = 7.8 Hz), 4.30 – 4.61 (*dt*, 4 H, H10, $^{3}J_{H,H}$ = 7.5 Hz, 62 Hz), 7.36 – 7.43 (*m*, 4 H, aromatic), 7.49 – 7.52 (*m*, 1 H, aromatic), 7.55 – 7.63 (*m*, 4 H, aromatic), 7.64 – 7.68 (*dd*, 1 H, aromatic, $^{3}J_{H,H}$ = 1.8 Hz, 7.8 Hz) 7.76 – 7.78 (*m*, 1 H, aromatic), 7.80 (*s*, 1 H, aromatic), 8.45 – 8.50 (*dq*, 1 H, aromatic, $^{3}J_{H,H}$ = 0.9 Hz, 5.4 Hz) and 11.21 (*s*, 1 H, H17) ppm. **^{13}C-NMR** (100 MHz, $CDCl_3$): δ = 14.09 (C1), 22.63 (C2), 26.53 (C3), 26.55 (C4), 29.00 (C5), 29.22 (C6), 29.36 (C7), 29.41 (C8), 31.81 (C9), 47.83 (C10), 66.76, 112.53, 116.57, 122.15, 122.88, 123.98, 124.85, 127.78, 128.31, 129.29, 135.01, 137.21, 137.90, 139.87, 143.41 and 149.63 (aromatic), and 154.75 (C29) ppm. MS (ESI) *m/z*: $[M-Cl]^+$ calcd. for $C_{29}H_{36}N_3^+$ 426.29, found 425.88.

2.4.6 Synthesis of silver NHC complex

2.4.6.1 Synthesis of [1-nonyl-3-[phenyl(pyridin-2-yl)methyl]-1H-imidazol-3-ium] silver bromide, [Im-77g-Br]

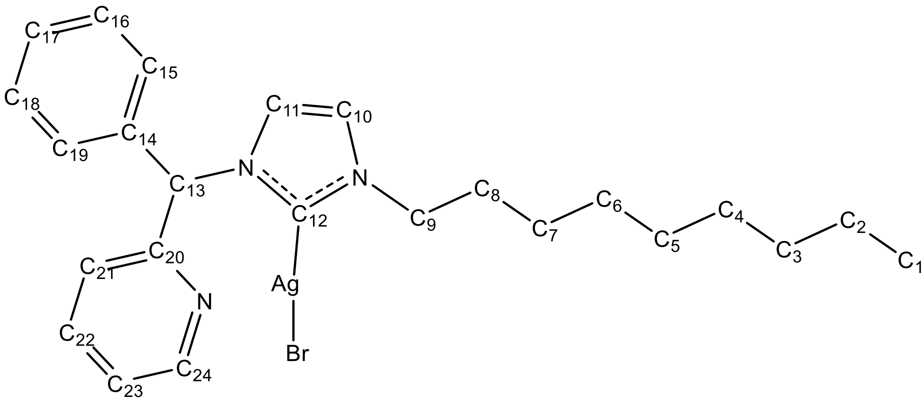

To a solution of compound **Im-71g-Br** (2.21 g, 5.0 mmol) in dichloromethane (50 mL), silver oxide (2.32 g, 10.0 mmol) was added in the dark and the reaction mixture was stirred at room temperature for 12 hours. The resulting mixture was filter through celite reduced *in vacuo* to obtain crude yellow oil. The crude oil was washed with diethyl ether and the diethyl ether layer was decanted and yielded complex **Im-77g-Br** in yellow oil (1.17 g, 2.1 mmol, 42.0 %). **^{1}H-NMR** (300 MHz, $CDCl_3$): δ = 0.84 – 0.94 (*m*, 6 H, H1), 1.20 – 1.37 (*m*, 24 H, H2 – H7), 1.75 – 1.87 (*m*, 4 H, H8), 3.89 – 4.13 (*dt*, 4 H, H9, $^3J_{H,H}$ = 7.2 Hz, 31.4 Hz), 6.89 – 6.99 (*m*, 3 H, aromatic), 7.13 – 7.19 (*m*, 2 H, aromatic), 7.25 – 7.40 (*m*, 5 H, aromatic), 7.71 – 7.79 (*td*, 1 H, aromatic, $^3J_{H,H}$ = 1.8 Hz, 7.8 Hz) and 8.62 – 8.67 (*dq*, 1 H, aromatic, $^3J_{H,H}$ = 0.9 Hz, 4.8 Hz) ppm. **^{13}C-NMR** (100 MHz, $CDCl_3$): δ = 14.08 (C1), 22.62 (C2), 26.46 (C3), 29.05 (C4), 29.13 (C5), 29.36 (C6), 31.07 (C7), 31.79 (C8), 47.05 (C9), 69.82, 120.44, 120.71, 121.52, 123.42, 123.70, 128.22, 128.70, 128.99, 137.40, 137.95, 149.97 (aromatic), and 157.15 (C24) ppm.

CHAPTER 3 EVALUATION OF ANTIMICROBIAL ACTIVITIES

3.1 Introduction

Antimicrobials are substances that are capable in suppressing or preventing pathogenic action of microbes, or even eliminating them. While there are many types of antimicrobials with different mechanism of action, they are often used in combinations to treat bacterial infections, and as prophylaxis to prevent initial or recurrence of an infection (Banin *et al* 2017). However, the abusive usage of these antimicrobials has caused them to lose effectiveness over time, as bacteria can evolve to survive under unfavourable conditions through acquiring antibiotics resistance (Munita & Arias 2016). Despites there are still drugs that can combat the tough bugs, the alarming phenomenon will eventually leave the medical officers with limited treatment options. Hence, there is a need of novel antimicrobials development to prevent any unwanted massacre in the future.

In this chapter, the synthesised compounds as discussed in **Chapter 2** were tested their antimicrobial properties using broth microdilution assay (BMD). A panel of clinically relevant microorganisms was selected, which involved eight Gram-positive and six Gram-negative bacteria, and three yeast species. Apart from the selected pathogenic bacteria, the rationale behind the inclusion of yeasts in the evaluation was due to the normalcy of yeast infection these days, also known as candidiasis, which affects mouth, genitals, and potentially blood. There are several methods published by the Clinical & Laboratory Standards Institute (CLSI) to evaluate the antimicrobial profiles of substances or compounds, which include broth dilution assay, broth microdilution assay, antimicrobial gradient diffusion method, well diffusion test, disk diffusion test et cetera. Broth microdilution assay was adopted in this study as it allows the generation of quantitative results (MIC and MBC values) with high reproducibility and operational convenience. Besides, the miniaturisation of the assay also allows the evaluation to be conducted at a much lower cost. Next, bacterial growth curves were plotted against *B. cereus* ATCC 14579 and *E. coli* ATCC 25922 with and without treatment of the lead compound (**Im-71g**) to estimate the suppressive capability over 24 hours. Besides, cell leakage assay was also performed to determine the release of intercellular components such as nucleic acid and proteins. The internal components will be measured spectrophotometrically.

3.2 Results and Discussion

3.2.1 Broth microdilution assay (BMD)

As mentioned in subchapter **3.1**, broth microdilution assay (BMD) was chosen as the method to evaluate the antimicrobial profiles of the synthesised compounds against a total of 15 pathogenic microorganisms, which include eight Gram-positive and six Gram-negative bacteria, and three yeast species (see **3.4 Experimental**). The antimicrobial properties were quantitatively reported in minimum inhibitory concentration (MIC) and minimum bactericidal concentration (MBC) values. MIC is the minimum concentration of a compound to inhibit the growth of microorganisms, while MBC is the minimum concentration of a compound to eliminate the tested microorganisms. The antimicrobial profiles of each synthesised compounds along with previously synthesised compounds **Im-71a – c** were tabulated in **Table 14a – c**. Due to the highly lipophilic character of the synthesised compounds, the solubility possessed a rather great challenge. Hence, the stock solutions of the synthesised compounds were prepared with 10 % DMSO in phosphate-buffered saline solution. The final working concentration of DMSO in the 96-well microtiter plate upon addition of all necessary contents was reduced to 2.5 %. Solvent control was conducted against all the microorganisms, and it showed that the DMSO at 2.5 % did not have effect on the growth of microorganisms.

In this study, two commercially available antibiotics namely chloramphenicol (CHL) and cycloheximide (CHX) were used as the reference drugs in the antimicrobial profile evaluation. Chloramphenicol is a broad-spectrum antibiotic that eliminates wide range of bacteria through inhibiting the protein synthesis by binding to the bacterial 50S ribosomal subunit. Cycloheximide on the other hand, is a common antifungal agent used to treat yeast infection which eliminates the yeast *via* inhibition of protein synthesis and induces apoptosis.

Table 14a. Determination of minimum inhibitory concentration (MIC) and minimum bactericidal concentration (MBC) in µg/mL of synthesised compounds against the chosen microorganism strains (CHL – Chloramphenicol; CHX – Cycloheximide).

Compound	*B. cereus* ATCC 14579		*B. subtilis* ATCC 8188		MSSA ATCC 29213		MSSA ATCC 6538p		MRSA ATCC 43300	
	Minimum inhibitory concentration (µg/mL)									
	MIC	MBC	MIC	MBC	MIC	MBC	MIC	MBC	MIC	MBC
74	> 1000	> 1000	> 1000	> 1000	> 1000	> 1000	> 1000	> 1000	> 1000	> 1000
1-bromohexane	> 1000	> 1000	> 1000	> 1000	> 1000	> 1000	> 1000	> 1000	> 1000	> 1000
1-bromoheptane	> 1000	> 1000	> 1000	> 1000	> 1000	> 1000	> 1000	> 1000	> 1000	> 1000
1-bromooctane	> 1000	> 1000	> 1000	> 1000	> 1000	> 1000	> 1000	> 1000	> 1000	> 1000
1-bromononane	> 1000	> 1000	> 1000	> 1000	> 1000	> 1000	> 1000	> 1000	> 1000	> 1000
1-bromodecane	> 1000	> 1000	> 1000	> 1000	> 1000	> 1000	> 1000	> 1000	> 1000	> 1000
Im-76a*	> 1000	> 1000	> 1000	> 1000	> 1000	> 1000	> 1000	> 1000	> 1000	> 1000
Im-76d	1000.00	> 1000	1000.00	> 1000	1000.00	> 1000	1000.00	> 1000	1000.00	> 1000
Im-76e	62.50	125.00	62.50	125.00	250.00	500.00	125.00	500.00	250.0	1000.00
Im-76f	62.50	125.00	31.25	62.50	62.50	500.00	62.50	500.00	62.50	500.00
Im-76g	7.81	31.25	7.81	15.63	15.63	62.50	7.81	62.50	7.81	62.50
Im-76h	125.00	250.00	250.00	250.00	250.00	> 1000	250.0	1000.00	250.0	> 1000
Bz-76a*	> 1000	> 1000	> 1000	> 1000	> 1000	> 1000	> 1000	> 1000	> 1000	> 1000
Bz-76d	250.00	500.00	250.00	500.00	500.00	1000.00	500.00	1000.00	500.00	1000.00
Bz-76e	250.00	500.00	250.00	500.00	500.00	500.00	500.00	500.00	500.00	500.00
Bz-76f	125.00	500.00	250.00	500.00	250.00	500.00	125.00	500.00	250.00	500.00
Bz-76g	3.91	> 1000	3.91	> 1000	3.91	> 1000	3.91	> 1000	7.81	> 1000
Bz-76h	3.91	> 1000	3.91	> 1000	7.81	> 1000	3.91	> 1000	7.81	> 1000
Im-71a**	1410.00	1410.00	1410.00	> 1410	707.00	1410.00	707.00	1410.00	1410.00	1410.00
Im-71d	250.00	500.00	250.00	500.00	250.0	1000.00	250.0	1000.00	500.00	1000.00
Im-71e	62.50	125.00	62.50	250.00	62.50	125.00	31.25	125.00	62.50	250.00
Im-71f	31.25	125.00	62.50	125.00	31.25	125.00	31.25	125.00	31.25	125.00
Im-71g	15.63	62.50	7.81	31.25	15.63	31.25	7.81	31.25	15.63	31.25
Im-71h	125.00	1000.00	125.00	500.00	31.25	250.00	31.25	125.00	15.63	125.00
Bz-71a**	> 1414	> 1414	> 1410	> 1410	> 1410	> 1410	> 1410	> 1410	> 1410	> 1410
Bz-71d	62.50	> 1000	62.50	> 1000	125.00	> 1000	125.00	> 1000	125.00	> 1000
Bz-71e	62.50	> 1000	62.50	> 1000	125.00	> 1000	62.50	> 1000	125.00	> 1000
Bz-71f	62.50	> 1000	62.50	> 1000	62.50	> 1000	62.50	> 1000	62.50	> 1000
Bz-71g	3.91	> 1000	3.91	> 1000	3.91	> 1000	3.91	> 1000	3.91	> 1000
Bz-71h	3.91	> 1000	3.91	> 1000	7.81	> 1000	7.81	> 1000	7.81	> 1000
CHL***	1.94	> 16.20	1.94	> 16.20	8.08	> 16.20	8.08	> 16.20	8.08	> 16.20
CHX***	> 14.10	> 14.10	> 14.10	> 14.10	> 14.10	> 14.10	> 14.10	> 14.10	> 14.10	> 14.10

Abbreviation: CHL – Chloramphenicol, CHX – Cycloheximide

** Commercially available*

*** Results obtained from (Choo et al 2018)*

****Results are expressed in ng/mL*

Table 14b. Determination of minimum inhibitory concentration (MIC) and minimum bactericidal concentration (MBC) in μg/mL of synthesised compounds against the chosen microorganism strains (CHL – Chloramphenicol; CHX – Cycloheximide).

Compound	Minimum inhibitory concentration (μg/mL)									
	MRSA ATCC 33591		*E. faecalis* ATCC 29212		VRE ATCC 700802		*E. coli* ATCC 25922		*K. pneumoniae* ATCC 10031	
	MIC	MBC	MIC	MBC	MIC	MBC	MIC	MBC	MIC	MBC
74	> 1000	> 1000	> 1000	> 1000	> 1000	> 1000	> 1000	> 1000	> 1000	> 1000
1-bromohexane	> 1000	> 1000	> 1000	> 1000	> 1000	> 1000	> 1000	> 1000	> 1000	> 1000
1-bromoheptane	> 1000	> 1000	> 1000	> 1000	> 1000	> 1000	> 1000	> 1000	> 1000	> 1000
1-bromooctane	> 1000	> 1000	> 1000	> 1000	> 1000	> 1000	> 1000	> 1000	> 1000	> 1000
1-bromononane	> 1000	> 1000	> 1000	> 1000	> 1000	> 1000	> 1000	> 1000	> 1000	> 1000
1-bromodecane	> 1000	> 1000	> 1000	> 1000	> 1000	> 1000	> 1000	> 1000	> 1000	> 1000
Im-76a*	> 1000	> 1000	> 1000	> 1000	> 1000	> 1000	> 1000	> 1000	> 1000	> 1000
Im-76d	1000.00	> 1000	> 1000	> 1000	> 1000	> 1000	500.00	> 1000	500.00	> 1000
Im-76e	62.50	500.00	250.0	500.00	250.0	500.00	62.50	250.00	125.00	250.00
Im-76f	31.25	250.00	125.00	250.00	125.00	250.00	31.25	125.00	62.50	125.00
Im-76g	7.81	62.50	15.63	62.50	31.25	62.50	31.25	62.50	15.63	31.25
Im-76h	500.00	> 1000	> 1000	> 1000	> 1000	> 1000	500.00	> 1000	500.00	> 1000
Bz-76a*	> 1000	> 1000	> 1000	> 1000	> 1000	> 1000	> 1000	> 1000	> 1000	> 1000
Bz-76d	500.00	1000.00	1000.00	> 1000	500.00	1000.00	> 1000	> 1000	500.00	1000.00
Bz-76e	500.00	500.00	1000.00	1000.00	500.00	500.00	> 1000	> 1000	500.00	1000.00
Bz-76f	250.00	500.00	500.00	1000.00	125.00	500.00	> 1000	> 1000	250.00	500.00
Bz-76g	3.91	> 1000	7.81	62.50	7.81	> 1000	> 1000	> 1000	7.81	> 1000
Bz-76h	7.81	> 1000	7.81	500.00	15.63	> 1000	> 1000	> 1000	125.00	> 1000
Im-71a**	1410	> 1414	> 1410	> 1410	> 1410	> 1410	> 1410	> 1410	> 1410	> 1410
Im-71d	500.00	1000.00	500.00	1000.00	500.00	1000.00	> 1000	> 1000	500.00	1000.00
Im-71e	62.50	250.00	250.0	500.00	500.00	1000.00	62.50	250.00	250.00	500.00
Im-71f	31.25	125.00	62.50	250.00	125.00	500.00	62.50	125.00	125.00	250.00
Im-71g	31.25	62.50	7.81	125.00	31.25	125.00	62.50	125.00	125.00	125.00
Im-71h	62.50	500.00	250.0	1000.00	250.0	> 1000	1000.00	> 1000	250.00	250.00
Bz-71a**	> 1414	> 1414	> 1410	> 1410	> 1410	> 1410	> 1410	> 1410	> 1410	> 1410
Bz-71d	62.50	> 1000	500.00	1000.00	500.00	> 1000	1000.00	> 1000	125.00	> 1000
Bz-71e	62.50	> 1000	500.00	1000.00	500.00	> 1000	1000.00	> 1000	125.00	> 1000
Bz-71f	62.50	> 1000	125.00	500.00	250.00	> 1000	500.00	1000.00	31.25	> 1000
Bz-71g	3.91	> 1000	3.91	125.00	7.81	> 1000	15.63	250.00	7.81	> 1000
Bz-71h	7.81	> 1000	3.91	250.0	7.81	> 1000	31.25	1000.00	31.25	> 1000
CHL***	8.08	> 16.20	16.20	> 16.20	16.20	> 16.20	8.08	> 16.20	0.97	0.97
CHX***	> 14.10	> 14.10	> 14.10	> 14.10	> 14.10	> 14.10	> 14.10	> 14.10	> 14.10	> 14.10

Abbreviation: CHL – Chloramphenicol, CHX – Cycloheximide

** Commercially available*

*** Results obtained from (Choo et al 2018)*

****Results are expressed in ng/mL*

Table 14c. Determination of minimum inhibitory concentration (MIC) and minimum bactericidal concentration (MBC) in µg/mL of synthesised compounds against the chosen microorganism strains (CHL – Chloramphenicol; CHX – Cycloheximide).

Compound	Minimum inhibitory concentration (µg/mL)									
	P. aeruginosa ATCC 10145		*S. flexneri* ATCC 12022		*C. albicans* IMR		*C. albicans* Clinical isolates		*C. tropicalis* Clinical isolates	
	MIC	MBC	MIC	MBC	MIC	MBC	MIC	MBC	MIC	MBC
74	> 1000	> 1000	> 1000	> 1000	> 1000	> 1000	> 1000	> 1000	> 1000	> 1000
1-bromohexane	> 1000	> 1000	> 1000	> 1000	> 1000	> 1000	> 1000	> 1000	> 1000	> 1000
1-bromoheptane	> 1000	> 1000	> 1000	> 1000	> 1000	> 1000	> 1000	> 1000	> 1000	> 1000
1-bromooctane	> 1000	> 1000	> 1000	> 1000	> 1000	> 1000	> 1000	> 1000	> 1000	> 1000
1-bromononane	> 1000	> 1000	> 1000	> 1000	> 1000	> 1000	> 1000	> 1000	> 1000	> 1000
1-bromodecane	> 1000	> 1000	> 1000	> 1000	> 1000	> 1000	> 1000	> 1000	> 1000	> 1000
Im-76a*	> 1000	> 1000	> 1000	> 1000	> 1000	> 1000	> 1000	> 1000	> 1000	> 1000
Im-76d	1000.00	> 1000	250.00	500.00	> 1000	> 1000	> 1000	> 1000	> 1000	> 1000
Im-76e	500.00	> 1000	62.50	250.00	> 1000	> 1000	> 1000	> 1000	> 1000	> 1000
Im-76f	500.00	> 1000	62.50	125.00	> 1000	> 1000	> 1000	> 1000	> 1000	> 1000
Im-76g	500.00	> 1000	31.25	62.50	> 1000	> 1000	> 1000	> 1000	> 1000	> 1000
Im-76h	1000.00	> 1000	500.00	500.00	> 1000	> 1000	> 1000	> 1000	> 1000	> 1000
Bz-76a*	> 1000	> 1000	> 1000	> 1000	> 1000	> 1000	> 1000	> 1000	> 1000	> 1000
Bz-76d	> 1000	> 1000	> 1000	> 1000	> 1000	> 1000	> 1000	> 1000	> 1000	> 1000
Bz-76e	> 1000	> 1000	> 1000	> 1000	> 1000	> 1000	> 1000	> 1000	> 1000	> 1000
Bz-76f	> 1000	> 1000	> 1000	> 1000	> 1000	> 1000	> 1000	> 1000	> 1000	> 1000
Bz-76g	> 1000	> 1000	> 1000	> 1000	> 1000	> 1000	> 1000	> 1000	> 1000	> 1000
Bz-76h	> 1000	> 1000	> 1000	> 1000	> 1000	> 1000	> 1000	> 1000	> 1000	> 1000
Im-71a**	> 1410	> 1410	1410.00	1410.00	707.00	1410.00	1410.00	> 1410	1410.00	> 1410
Im-71d	> 1000	> 1000	500.00	1000.00	> 1000	> 1000	> 1000	> 1000	> 1000	> 1000
Im-71e	> 1000	> 1000	250.00	500.00	> 1000	> 1000	> 1000	> 1000	> 1000	> 1000
Im-71f	> 1000	> 1000	125.00	250.00	> 1000	> 1000	> 1000	> 1000	> 1000	> 1000
Im-71g	> 1000	> 1000	125.00	125.00	> 1000	> 1000	> 1000	> 1000	> 1000	> 1000
Im-71h	> 1000	> 1000	1000.00	1000.00	> 1000	> 1000	> 1000	> 1000	> 1000	> 1000
Bz-71a**	> 1410	> 1410	> 1410	> 1410	> 1410	> 1410	> 1410	> 1410	> 1410	> 1410
Bz-71d	> 1000	> 1000	500.00	> 1000	250.00	> 1000	250.00	> 1000	125.00	> 1000
Bz-71e	> 1000	> 1000	500.00	> 1000	250.00	> 1000	250.00	> 1000	125.00	> 1000
Bz-71f	> 1000	> 1000	250.00	1000.00	125.00	> 1000	31.25	> 1000	125.00	> 1000
Bz-71g	250.00	1000.00	31.25	500.00	15.63	> 1000	3.91	> 1000	7.81	> 1000
Bz-71h	250.00	> 1000	31.25	> 1000	500.00	> 1000	250.00	> 1000	500.00	> 1000
CHL***	> 16.20	> 16.20	8.08	16.20	> 16.20	> 16.20	> 16.20	> 16.20	> 16.20	> 16.20
CHX***	> 14.10	> 14.10	> 14.10	> 14.10	14.10	14.10	14.10	14.10	14.10	14.10

Abbreviation: CHL – Chloramphenicol, CHX – Cycloheximide

** Commercially available*

*** Results obtained from (Choo et al 2018)*

****Results are expressed in ng/mL*

Based on **Table 14a – c**, most of the synthesised compounds display moderate antimicrobial activities against the chosen bacterial strains, with the exception of compound **Im-71g** and **Bz-71g** which showed good bacteriostatic activities as low as 7.81 µg/mL (20.0 nM) and 3.91 µg/mL (8.7 nM). As expected, as the number of carbons in the alkyl chain increased (up to $C_n = 9$), the antimicrobial properties increase. A longer alkyl chain eases the integration of the hydrocarbon alkyl chain with the lipid bilayer of bacterial cell wall through the hydrophobic and van der Waal's interactions (Birnie *et al* 2000; Patrick 2013). Besides, longer alkyl chain has better lipophilic property which results in increased in affinity of the compound to the liposome membrane of microorganisms, thus promoting the interactions between the microorganism and the compound (de Almeida *et al* 2009). As mentioned earlier, a higher CLog P value indicates a higher lipophilicity of the compound, hence a better penetration and permeation are expected. Hence, **Im-71h** and **Bz-71h** with CLog P value of 3.046 and 4.094 respectively, should possess a much better antimicrobial profile than **Im-71g** and **Bz-71g** with CLog P value of 2.602 and 3.650, respectively. However, a retardation in the antimicrobial property of the compound when the chain length is increased to 10 carbons was observed in both imidazole-derived and benzimidazole-derived salts from 7.81 to 31.25 µg/mL and 3.91 to 7.81 µg/mL, respectively, as demonstrated by **Im-71g** and **Bz-71g** against *S. aureus*, which the trend is similar to their parent imidazole and benzimidazole derivatives. This is due to the high lipophilicity of the alkyl chain which hindered the diffusion of the compound into the targeted cell membrane, therefore triggering a weaker immune response. Hence, it can be deduced that the "cut-off" point for **Im-71** and **Bz-71** are nine carbons.

Comparing to our previously reported pyridine-functionalised imidazolium salts **Im-71a – c**, the salts bearing a longer alkyl chain showed better antimicrobial activities, with the increment of at least 160-fold, from 1.25 mM (**Im-71c**) to 2×10^{-5} mM (**Im-71g**). Besides, the pyridine functionality also showed superiority in the antimicrobial properties. For instance, a study was conducted on ester- and amide-functionalised imidazolium salts, where the lowest MIC values reported for each was 75 µg/mL and 9.375 µg/mL respectively against the selected microorganisms (Kanjilal *et al* 2009). Moreover, a different group worked on alcohol-functionalised imidazolium salts and the lowest MIC reported was 8 µg/mL (Demberelnyamba *et al* 2004). The excellent antimicrobial property of **Im-71g** and **Bz-71g** with MIC values of 7.81 µg/mL and 3.91

µg/mL respectively, had shown the promising approach of pyridine functionalisation in drug design. Despite the great antimicrobial activities were observed, the antimicrobial profiles of this class of pyridine-functionalised imidazolium salts were inferior to a class of dialkyl substituted imidazolium salts, where the MIC values were found to be as low as 0.013 µg/mL (Zheng *et al* 2016).

Based on **Table 14a – c**, **Bz-71** have better bacteriostatic properties of the compounds, but the bactericidal properties of the benzimidazole-derived compounds remained weaker than their imidazolium counter parts. For examples, **Bz-71** showed MIC values as low as 3.91 µg/mL against the tested microorganisms, whereas **Im-71** showed lowest MIC values of 7.81 µg/mL. However, **Bz-71** were almost non-bactericidal at highest tested concentration (MBC values > 1000 µg/mL) while **Im-71** showed MBC values as low as 31.25 µg/mL against the tested microorganisms. This is rather an interesting finding which requires additional studies as there is no related evidence found in the scholarly database. Interestingly, **Bz-71e – h** were active against all three yeast strains with MIC values as low as 3.91 µg/mL, in which their imidazolium counter parts **Im-71e – h** did not display any activity. With the great antiyeast properties of benzimidazole-derived vitamin B12, it is believed that benzimidazolium salts would possess similar antiyeast property and be much more effective against yeasts as compared to the imidazolium salts (Woolley 1944).

Moreover, **Im-71** have shown almost similar strength (lowest MIC of 7.81 µg/mL) in antimicrobial properties against the *Staphylococcus* species and *Enterococcus* species, but generally weaker than their parent imidazole **Im-75** against the other bacterial strains (lowest MIC of **Im-71** to **Im-75**; 15.63 to 7.81 µg/mL). On the other hand, **Bz-71** showed improved bacteriostatic properties against all tested microorganisms, including the yeast strains, as compared to their parent benzimidazole **Bz-75** (lowest MIC of 500.00 to 31.25 µg/mL against *S. flexneri*, and > 1000 to 250 µg/mL against *C. albicans*). However, the bactericidal properties of **Bz-71** are weaker than **Bz-75**. This finding is in line with the reported literature, where (benz)imidazolium salts tend to self-assemble, limiting the rate of diffusion to the cell surface. This would result in weaker permeability and lower bioavailability at the site of action, hence triggering a weaker immune response (Łuczak *et al* 2010).

3.2.2 Bacterial growth curve

The lead compounds, **Im-71g** and **Bz-71g**, were selected to study their killing nature. *B. cereus* ATCC 14579 and *E. coli* ATCC 25922 were chosen and cultured overnight in the presence of the compounds at various concentrations, ranging from 1.00 mg/mL to 3.91 mg/mL. As the bacterial cultures were growing, the absorbance readings were measured spectrophotometrically every 1-hour interval at 620 nm. The absorbance values were converted into culture density (untreated bacteria set to be 100 % at 21st hour). The growth curves for each tested compound against each bacterial strain were plotted as shown in **Figure 36a – d**.

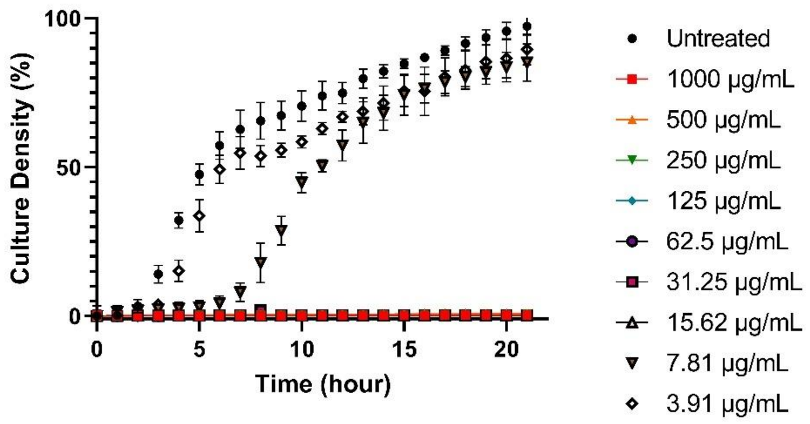

Figure 36a. Growth curve of *B. cereus* ATCC 14579 over 21 hours cultured in MHB containing compound **Im-71g**.

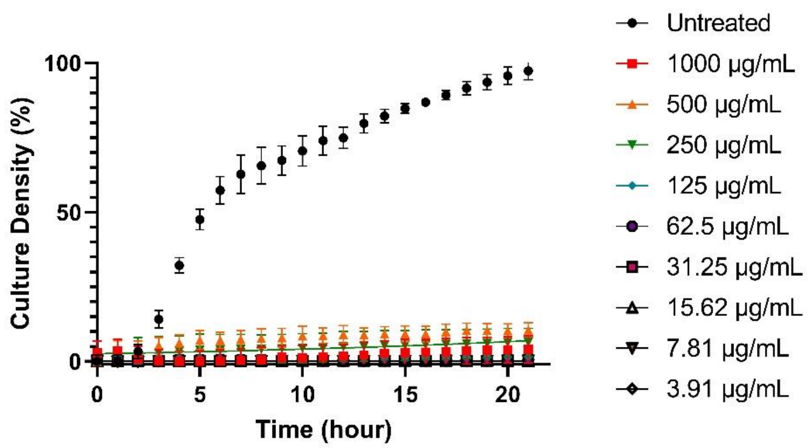

Figure 36b. Growth curve of *B. cereus* ATCC 14579 over 21 hours cultured in MHB containing compound **Bz-71g**.

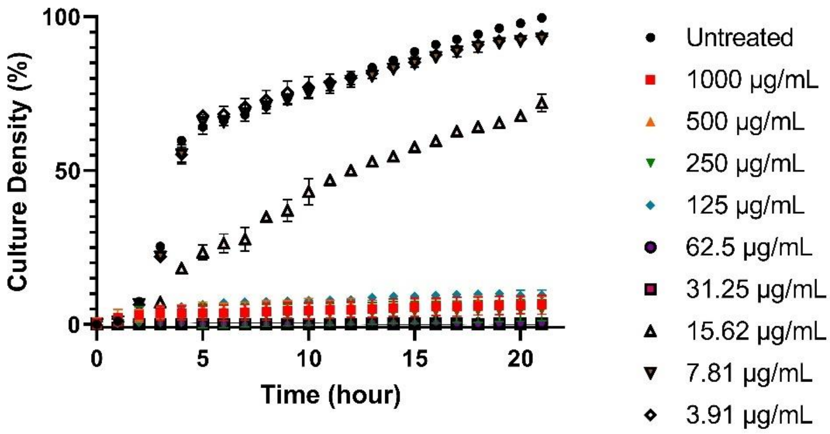

Figure 36c. Growth curve of *E. coli* ATCC 25922 over 21 hours cultured in MHB containing compound **Im-71g**.

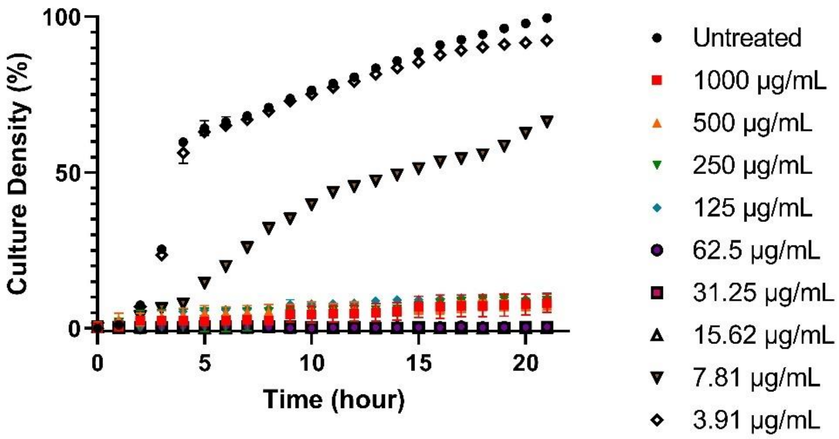

Figure 36d. Growth curve of *E. coli* ATCC 25922 over 21 hours cultured in MHB containing compound **Bz-71g**.

Based on **Figure 36a – d**, it was observed that the tested compounds acted immediately upon exposing to the bacterial cultures. Despite **Im-71g** was found to have MIC values against *B. cereus* and *E. coli* at 3.71 and 7.81 µg/mL respectively as shown in broth microdilution assay, the sub-MIC (concentration that is half of the MIC) of **Im-71g** against *B. cereus* and *E. coli* at 7.81 and 15.63 µg/mL were found to retard the growth of the bacterial culture. As shown in **Figure 36a** and **Figure 36c**, the log phase of *B. cereus* and *E. coli* was delayed by four and one hour(s) respectively, upon exposing to **Im-71g**. Meanwhile, since the MIC of **Bz-71g** against *B. cereus* was 3.71 µg/mL, the sub-MIC profile was not able to be determined from the graph. However, it was still visible that the log phase of *E. coli* was delayed by two hours upon exposed to **Bz-71g** as shown in **Figure 36d**.

3.2.3 Cell leakage assay

Antimicrobial compounds such as antimicrobial peptides can pierce through the target cell membrane to induce cellular leakage of the entrapped intracellular contents. As previously described briefly in subchapter **1.4**, an increased alkyl chain length could attribute to the overall lipophilicity character of the compound, allowing the alkyl side chain to pierce through the bacterial cell wall more effectively. Since nonyl-substituted (benz)imidazolium salts **Im-71g** and **Bz-71g** were found to be the most potent among all the synthesised compounds, they were employed in cell leakage assay. Based on **Figure 37**, it was observed that the absorbance readings for both nucleic acid and protein leakages increased over the course of 6-hour incubation. This indicated that both the **Im-71g** and **Bz-71g** pierced through the bacterial cell wall, thus leading to the leakage of intercellular components from the tested bacteria. There was no obvious trend to conclude that the penetration is a time-dependent mechanism, as there was a drop in absorbance reading at 4th hour for *B. cereus* treated with **Im-71g**. Meanwhile, the benzimidazolium-derived salts generally potrayed weaker penetrations as supported by the data collected from this assay. This could be explained by the electron-withdrawing nature of extended π-conjugation that reduces the binding affinity of the benzimidazolium salts. These results also corresponded to the broth microdilution assay in which where imidazolium salts were generally more bactericidal than the benzimidazolium analogues.

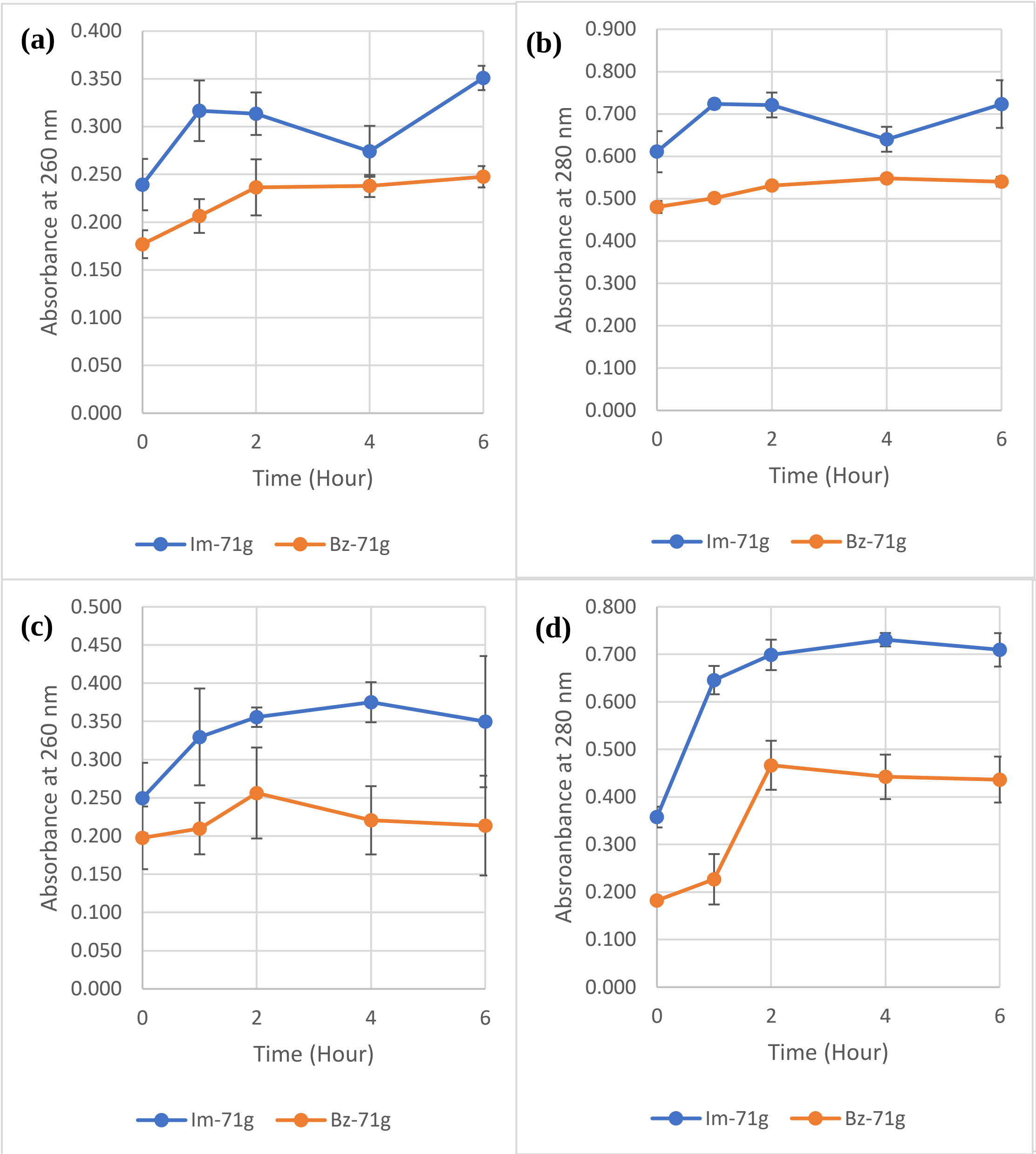

Figure 37. Leakage of nucleic acid (260 nm) **(a)** and proteins (280 nm) **(b)** from *B. cereus* ATCC 14579 and leakage of nucleic acid (260 nm) **(c)** and proteins (280 nm) **(d)** from *E. coli* ATCC 25922 after treated with 1 × MIC of **Im-71g** and **Bz-71g** for 6 hours. The absorbance was reported in mean. The assay was performed in triplicates.

3.3 Conclusion

This chapter discussed the antimicrobial profiles of all the synthesised (benz)imidazolium salts. Their respective antimicrobial profiles were evaluated against a panel of clinically pathogenic microorganisms, which include eight Gram-positive and six Gram-negative bacteria, and three yeast species, using broth microdilution assay. Compound **Im-71g** and **Bz-71g** which showed good bacteriostatic activities as low as 7.81 µg/mL (20.0 nM) and 3.91 µg/mL (8.7 nM). The results revealed that the length of alkyl chain influenced the antimicrobial properties of the compounds, where increasing alkyl chain length enhances the antimicrobial properties of the compounds against the tested microorganisms. However, a "cut-off" point was determined, where alkyl chain with more than nine carbons (i.e., decyl-) possessed weaker antimicrobial properties. This was due to the high lipophilic moiety that faced challenge in diffusing through the hydrophilic membrane, hence triggering a slower and weaker immune response. Generally, **Im-76d – h** showed higher MIC values than their benzimidazolium analogues, **Bz-76d – h**, but lower MBC values were seen in **Im-76d – h**. Similar trend of finding can also be seen in the **Im-71d – h** and **Bz-71d – h**. Bacterial growth curves for *B. cereus* and *E. coli* treated with **Im-71g** and **Bz-71g** respectively were plotted and revealed that the compounds acted immediately the moment the bacteria cultures were exposed to the tested compounds. Besides, the sub-MIC of both compounds also showed the potential of suppressing the growth of the bacterial cultures. Moreover, cell leakage assay was also conducted and showed that the intercellular components were released from the bacterial cells when exposed to **Im-71g** and **Bz-71g**. This result was in line with the bacterial growth curve study, where the killing of bacterial took place at the moment the bacterial cultures were exposed to the tested compounds.

3.4 Experimental

3.4.1 Microorganisms

The broth microdilution assay was conducted using the microorganisms tabulated in **Table 15** to determine the antimicrobial profiles of the synthesised compounds.

Table 15. List of microorganism strains to be used in this study to determine the antimicrobial profiles of the synthesised compounds.

Group	Strain	Microorganism
Gram-positive	ATCC 14579	*Bacillus cereus*
	ATCC 8188	*Bacillus subtilis*
	ATCC 29213	Methicillin-sensitive *Staphylococcus aureus* (MSSA)
	ATCC 6538p	Methicillin-sensitive *Staphylococcus aureus* (MSSA)
	ATCC 43300	Methicillin-resistant *Staphylococcus aureus* (MRSA)
	ATCC 33591	Methicillin-resistant *Staphylococcus aureus* (MRSA)
	ATCC 29212	*Enterecoccus faecalis*
	ATCC 700802	Vancomycin-resistant *Enterococcus faecalis* (VRE)
Gram-negative	ATCC 25922	*Escherichia coli*
	ATCC 10031	*Klebsiella pneumoniae*
	ATCC 10145	*Pseudomonas aeruginosa*
	ATCC 12022	*Shigella flexneri*
Yeast	IMR	*Candida albicans*
	Clinical isolate	*Candida albicans*
	Clinical isolate	*Candida tropicalis*

3.4.2 Broth microdilution assay (BMD)

Broth microdilution assay was conducted using 96-well microtiter plates as per shown in the protocol provided by Clinical & Laboratory Standards Institute (CLSI, 2012) with slight modifications. The synthesised compounds were prepared in 10 % DMSO in PBS solution. Positive controls used in this study were chloramphenicol (0.25 mg/mL) for bacterial strains and cycloheximide (1.00 mg/mL) for yeast species. Three negative controls were used, namely blank control (MHB broth only), solvent control (MHB and 2.5 % DMSO only), and sterility control (MHB and compound only). The microorganisms were freshly cultured on MHA and inoculated into MHB. The overnight cultures in MHB were adjusted to match 0.5 McFarland Standard and 100-fold diluted with MHB. The 96-well microtiter plates were charged with synthesised compounds per the protocol provided by CLSI with final working concentration ranging from 1.00 mg/mL to 3.91 μg/mL. Then, the diluted microorganism suspensions were added into each well and the 96-well microtiter plates were allowed to incubate at 37 °C for 24 hours. The well with the lowest concentration where no growth was observed (non-turbid) was determined as the minimum inhibitory concentration (MIC). The clear wells were restreaked onto fresh MHA and incubated overnight. The lowest concentration where the microorganisms did not grow on MHA was determined as the minimum bactericidal concentration (MBC). All the experiments were conducted in triplicates.

3.4.3 Bacterial growth curve

Two selected microorganisms namely *B. cereus* ATCC 14579 and *E. coli* ATCC 25922 were used for the study of bacterial growth curve. Overnight bacteria cultures in MHB were adjusted to match 0.5 McFarland standard. Bacteria were incubated with different concentrations of **Im-71g** in Tecan Infinite® M200 PRO where the absorbance of bacterial suspensions were recorded spectrophotometrically at 625 nm at one-hour interval for 24 hours. The growth curves were plotted. The experiment was performed in triplicates.

3.4.4 Cell leakage assay

Cell leakage assay was performed based on literature method with slight modifications (Ong *et al* 2015). The leakage of the intercellular components due to bacterial cell membrane rupture was measured spectrophotometrically at 260 nm and 280 nm for nucleic acids and proteins, respectively. Briefly, *B. cereus* ATCC 14579 and *E. coli* ATCC 25922 were cultured overnight in MHB. The bacterial cells were harvested *via* centrifugation (10,000 × g, 15 minutes) at room temperature, washed twice, and resuspended in sterile phosphate-buffered saline solution. The bacterial suspensions were then adjusted to OD_{600} of 1.5. At time $t = 0^{th}$ hour, MIC of **Im-71g** and **Bz-71g** were added to the adjusted bacterial suspension. Untreated cultures of *B. cereus* and *E. coli* and separate vials containing bacterial suspension treated with DMSO were used as negative controls. Aliquots of the treated bacterial suspension (200 µL) was removed at regular time interval (0^{th}, 1^{st}, 2^{nd}, 4^{th}, and 6^{th} hour). Cell supernatants were obtained *via* centrifugation (6000 × g, 5 minutes). The absorbance of bacterial cell supernatant at 260 nm and 280 nm was measured using Tecan NanoQuant Plate^{TM}. The experiment was performed in triplicates.

CHAPTER 4 EVALUATION OF CELL CYTOTOXICITY

4.1 Introduction

Despite maximum effort was put in clinical research and trials of promising therapies, cancer remains one of the leading causes of morbidity and mortality for the past decades (Bailar & Gornik 1997). The occurrence of cancers are due to somatic mutations in the cells, particularly in the ‘cancer gene’, activating a competitive advantage that allows these mutated cells to proliferate and grow more rapidly, even in less favourable conditions, than non-cancerous cells (Weinberg 1996). The cell cycle of a non-cancerous cells involves programmed cell death, also known as apoptosis, when the cells are eliminated when damaged or no longer needed, whereas the growth of cancer cells is not regulated, and they are capable of proliferate uncontrollably with the possibility of invading neighbouring tissues and eventually metastasise to other organs (Tandon *et al* 2019; Vucic 2008). There are many types of cancers that have been identified, where those that are accountable for most cancer-associated deaths are such as lungs, breast, colorectal, stomach, and liver cancers (WHO 2014).

Early in the 1840s, an Italian chemist Michele Peyrone (1813 – 1883) successfully synthesised *cis*-diamminedichloroplatinum(II), or commonly known as cisplatin, the basis of today’s most commonly used family of anticancer drugs (Kauffman *et al* 2010). However, its anticancer properties were only discovered later in 1965 by a biophysical chemist, Barnett Rosenberg. The discovery of cisplatin has completely turned the tide on how some cancers were being treated, greatly reducing the mortality rate of several cancer cases, especially testicular cancer. Nonetheless, the severe side effects of cisplatin which include nausea and nephrotoxicity have limited the dose of the drug that can be prescribed to patients (Arany & Safirstein 2003). As a result, many cancer cases ended up being treated with less-than-optimal doses and this leads to the development of cisplatin-resistance in several cancers. Such alarming issue has urged the need in searching for alternative compounds to be used in cancer treatment. While several research groups focus on developing the third generation of cisplatin such as satraplatin and picoplatin, organic compounds such as imidazolium salts have also created a new wave of interest, bringing them to the forefront in drug discovery (Olszewski & Hamilton 2010; Wong & Giandomenico 1999).

In this chapter, cytotoxicity profiles of the synthesised (benz)imidazolium salts were reported and discussed. MTT cell viability assay will be carried out to evaluate the cytotoxicity profiles of the synthesised (benz)imidazolium salts against a list of human carcinoma cell lines, such as oral (H103), breast (MCF-7), colon (HCT-116) and skin (HT1080) cancer cells. The synthesised (benz)imidazolium salts were also tested against a series of human non-cancerous cell lines such as skin keratinocytes (HaCaT), lung epithelial cells (Beas2B) for selectivity index study. Furthermore, DCFDA intracellular reactive oxygen species (ROS) assay was also performed using HCT-116 to identify the mode of action of the synthesised (benz)imidazolium salts.

4.2 Results and Discussion

4.2.1 Cell cytotoxicity of pyridine-functionalised (benz)imidazolium salts

MTT cell viability assay was performed to determine the cell cytotoxicity profiles of the synthesised (benz)imidazolium salts. When viable cells are exposed to MTT dye, the mitochondrial dehydrogenase of the cells reduces the MTT tetrazolium dyes into blue formazan crystals. Hence, the higher concentration of blue formazan crystal indicates higher cell viability.

In this study, four selected human carcinoma cell lines, including H103 (oral squamous carcinoma), HCT-116 (colorectal epithelial carcinoma), MCF-7 (breast epithelial carcinoma), and HT1080 (skin fibrosarcoma) were treated to various concentrations of synthesised (benz)imidazolium salts, ranging from 1.0 to 4.0 µM for 24 hours before loading the MTT dye. The absorbance values based on the dissolved formazan were converted to their respective cell viability at different concentration to generate cell viability-concentration plots. The cytotoxicity profiles of the synthesised (benz)imidazolium salts were expressed in terms of IC_{50} or half maximal inhibitory concentration, where 50 % of the cell growth were inhibited by the compounds. The IC_{50} values were summarised and tabulated in **Table 16**. Cisplatin was used as the positive control due to its clinically proven cytotoxicity.

Table 16. Cell cytotoxicity of the synthesised compounds against selected human carcinoma cell lines, reported as IC_{50} in µM.

	IC_{50} (µM)			
	HT1080	HCT-116	H103	MCF-7
Im-71d	> 4.00	3.30 ± 0.18	3.49 ± 0.04	3.70 ± 0.20
Im-71e	> 4.00	3.06 ± 0.12	3.08 ± 0.10	3.65 ± 0.03
Im-71f	3.80 ± 0.41	2.17 ± 0.09	2.53 ± 0.03	2.39 ± 0.07
Im-71g	1.68 ± 0.15	1.40 ± 0.06	1.99 ± 0.02	2.38 ± 0.07
Im-71h	1.07 ± 0.07	0.71 ± 0.03*	1.80 ± 0.14	2.00 ± 0.08
Bz-71d	> 4.00	3.85 ± 0.25	3.70 ± 0.11	> 4.00
Bz-71e	> 4.00	3.36 ± 0.44	3.28 ± 0.31	> 4.00
Bz-71f	3.15 ± 0.15	3.13 ± 0.11	2.53 ± 0.04	3.07 ± 0.07
Bz-71g	2.86 ± 0.15	2.43 ± 0.20	2.20 ± 0.07	2.62 ± 0.10
Bz-71h	1.92 ± 0.20	1.23 ± 0.04	1.99 ± 0.12	1.55 ± 0.07
Cisplatin	N/A	10.78 ± 0.21	6.16 ± 0.04	19.78 ± 0.21

**The value was based on extrapolation using the regression curve due to the high cytotoxicity of the compound against the cell line.*

Based on **Table 16**, all the synthesised imidazolium salts and benzimidazolium salts were cytotoxic to the selected human carcinoma cell lines ranging from 0.71 to 3.80 µM, except for **Im-71d – e** against HT1080 and **Bz-71d – e** against HT1080 and MCF-7 where no cytotoxicity was observed at highest tested concentration (4.00 µM). The findings were in agreement to several published reports where imidazolium salts may have cytotoxicity against selected cell lines with IC_{50} values ranging from 3 – 30 µM (Wright *et al* 2015; Yang *et al* 2019). As mentioned in subchapter **1.4**, the previously synthesised imidazolium salts **Im-71a** (*N*-methyl), **Im-71b** (*N*-phenyl), and **Im-71c** (*N*-*tert*-butyl) did not show any cytotoxicity at even higher concentration (40.00 µM). The results have supported the initial hypothesis, where increasing the carbon number of the alkyl chain length will enhance the biological properties. For instance, the lengthening of the alkyl chain length in imidazolium salt derivatives against HCT-116 showed increment in IC_{50} value from 3.30 µM (six carbon) to 0.71 µM (10 carbon). These findings can be evident and supported by other studies where better anticancer properties can be seen in compound bearing a longer alkyl side chain up to 20 carbons (Komeda *et al* 2017; Laha *et al* 2018; Takahashi *et al* 2006; Zheng *et al* 2016). These findings were also corresponded to reported literatures, where compounds containing imidazole moieties display anticancer characters that target cancer cells differently, which include DNA, vascular endothelial growth factor, mitotic microtubules, histone deacetylases, receptor tyrosine kinases, topoisomerases et cetera (Ali *et al* 2015; Ali *et al* 2017; Chen *et al* 2008). Unlike antimicrobial profiles, (benz)imidazolium salts bearing a decyl *R*-group produced better cytotoxic properties. This could be due to the difference in the combined hydrophobicity and electrostatics interactions of the surfactants on the mammalian cells and on the bacterial cells (Zhang *et al* 2015).

Like the mode of action in killing the bacterial cells, the tested compounds primarily acted on cancer cells *via* penetration of cell membrane, which was evident from the enhanced cytotoxicity profiles from increasing carbon chain length. The increased carbon chain length elevated the lipophilicity of the compound, which enabled a better binding affinity of the compound to the cellular membrane (Fatima *et al* 2017). As lipids are one of the major constituents of cell and mitochondrial membrane, it was assumed that the increased lipophilicity of the compounds increased the bioavailability of the compounds to invade the cells where they can produce cytotoxicity by inhibiting cellular respiration and causing loss of adenosine triphosphate (Iqbal *et al* 2013; Schenkel & Bakovic 2014). Hence, a higher calculated log P value of the compound will be expected to demonstrate more cytotoxic profile due to its high lipophilicity. This statement was supported by the experimental data, where **Im-71h** with CLog P value of 3.046 showed better cytotoxic profile than **Im-71d** with CLog P value of 1.268, and **Bz-71h** with CLog P value of 4.094 was more cytotoxic to the cell lines than **Bz-71d** with CLog P value of 2.316. Furthermore, it was also worth noting that most tested compounds showed better inhibition of proliferation at lower concentration when compared to the commercially used cisplatin.

In addition, it was also observable that all benzimidazolium salts have slightly weaker cytotoxicity when compared to their imidazolium salt analogues as shown in **Table 16**, where imidazolium salt analogues were about two-fold more cytotoxic than benzimidazolium salt analogues against HT1080 and HCT-116 with IC_{50} value of 1.07 and 0.71 µM respectively. Since the same observations were obtained for both antimicrobial and cell cytotoxicity profiles, it can be deduced that the extended π-conjugation in benzimidazolium salts with such functional groups will yield poorer biological properties. Despite of the higher CLog P value calculated for **Bz-71h** (4.094) than **Im-71h** (3.046), the poorer cytotoxic profiles could be explained by that extended π-conjugation reduced the water-solubility, which leads to inaccurate subcellular targeting and obstacles to penetration through the biological barrier such as plasma membrane and capillary endothelium (Tian *et al* 2017). However, such statement may not comply to other types of imidazolium salts or their NHC complexes where, for instance, a sulfonated benzimidazolium-derived copper NHC complex appeared to be more cytotoxic to the tested cancer cell line than its imidazolium analogue. Hence, there is scarce evidence to deduce how the extended π-conjugation in benzimidazolium salts influence the cell cytotoxicity.

4.2.2 Selectivity index study

Despite that the cytotoxic profiles of tested (benz)imidazolium salts against the selected cell lines were remarkable, low toxicity to non-cancerous cells was required to ensure the compounds only selectively targeting the cancer cells. Hence, a selectivity index study was conducted to compare the cytotoxicity profiles of these compounds against both cancer cells and non-cancerous cells. In this selectivity index study, two non-cencerous cell lines were selected, namely HaCaT (human skin keratinocytes) and Beas2B (human lung epithelial cells). The selection of these human cell lines was to explore the prospects of potential drug delivery route in the future, which include but not limited to, oral administration, dermal or transdermal delivery, pulmonary delivery, or intravenously. The cytotoxicity profiles of synthesised (benz)imidazolium salts against HaCaT and Beas2B were recorded and tabulated in **Table 17**. Like the assay against the cancer cells, a dose-dependent trend can be seen from the result based on **Table 17**. Unanticipatedly, the IC_{50} values against HaCaT and Beas2B were neither significantly higher nor lower than that of against the cancer cells as shown in **Table 16**.

Table 17. Cell cytotoxicity of the synthesised compounds against selected human non-cancerous cell lines, reported as IC_{50} in µM.

	IC_{50} (µM)	
	Beas2B	HaCaT
Im-71d	> 4.00	3.58 ± 0.09
Im-71e	> 4.00	3.11 ± 0.15
Im-71f	3.20 ± 0.17	2.82 ± 0.06
Im-71g	2.73 ± 0.06	2.38 ± 0.03
Im-71h	2.15 ± 0.02	2.07 ± 0.06
Bz-71d	> 4.00	3.85 ± 0.04
Bz-71e	> 4.00	3.19 ± 0.10
Bz-71f	3.41 ± 0.04	2.84 ± 0.04
Bz-71g	3.12 ± 0.04	2.60 ± 0.06
Bz-71h	2.39 ± 0.05	1.20 ± 0.01

The selectivity index (SI) is defined as the cytotoxic selectivity of the tested compound against cancer cells from non-cancerous cells. It can be calculated from the ratio of IC_{50} values obtained from those against the cancer cells to IC_{50} values obtained from those against the non-cancerous cells. Compound with SI value higher than 3 is deduced as compound with high selectivity towards the targeted cells instead of the non-targeted cells, in this case, which are the cancerous cells and non-cancerous cells respectively, while SI value between 1 and 3 indicates moderate inhibition of cancer cells survival than non-cancerous cells (Indrayanto *et al* 2020). In this study, the SI values were calculated based on the IC_{50} values of four cancer cell lines and a non-cancerous cell line at a time. The SI values of the tested compounds towards HaCaT and Beas2B were tabulated in **Table 18** and **Table 19**, respectively.

Table 18. Selectivity index (SI) of selected compounds for lung epithelial cells (Beas2B) against skin cancer (HT1080), colon cancer (HCT-116), oral cancer (H103) and breast cancer (MCF-7).

Compound tested	Selectivity Index (SI) towards BEAS2B			
	HT1080	HCT-116	H103	MCF-7
Im-71d	ND	ND	ND	ND
Im-71e	ND	ND	ND	ND
Im-71f	0.84	1.47	1.26	1.34
Im-71g	1.63	1.95	1.37	1.15
Im-71h	2.01	3.03	1.19	1.08
Bz-71d	ND	ND	ND	ND
Bz-71e	ND	ND	ND	ND
Bz-71f	1.08	1.09	1.35	1.11
Bz-71g	1.09	1.28	1.42	1.19
Bz-71h	1.23	1.94	1.20	1.54

**ND = not determined*

Table 19. Selectivity index (SI) of selected compounds for skin keratinocytes (HaCaT) against skin cancer (HT1080), colon cancer (HCT-116), oral cancer (H103) and breast cancer (MCF-7).

Compound tested	Selectivity Index (SI) towards HaCaT			
	HT1080	HCT-116	H103	MCF-7
Im-71d	ND	1.08	1.03	0.97
Im-71e	ND	1.02	1.01	0.85
Im-71f	0.74	1.30	1.11	1.18
Im-71g	1.42	1.70	1.20	1.00
Im-71h	1.93	2.92	1.15	1.04
Bz-71d	ND	1.00	1.04	ND
Bz-71e	ND	0.95	0.97	ND
Bz-71f	0.90	0.91	1.12	0.93
Bz-71g	0.91	1.07	1.18	0.99
Bz-71h	0.63	0.98	0.60	0.50

**ND = not determined*

Based on **Table 18** and **Table 19**, all tested compounds did not have distinct selectivity towards neither of the human non-cancerous cell lines. The SI values for most compounds were close to 1, which indicated that the compounds inhibited both cancer cells and non-cancerous cells equally. Notably, **Im-71h** was the only candidate that portrayed selectivity index of close to 3 against HCT-116 and approximately 2 against HT1080, towards Beas2B and HaCaT cell lines. On the other hand, **Im-71g** also demonstrated moderate SI value of 2 against HCT-116 towards Beas2B and HaCaT cell lines. Despite most of the SI values obtained were close to 1, this phenomenon could be explained by the fast-doubling time of HaCaT and Beas2B, which were approximately 24 to 36 hours and these are similar to the doubling time of all cancer cell lines employed in this study. As a result, these fast-growing non-cancerous cells were greatly inhibited by the tested (benz)imidazolium salts even at low concentrations. Therefore, by employing a slow-growing cell line such as CCD841CON, a colorectal epithelial cell line, the antiproliferative properties of the compounds could be neglected, which eventually gives off a better selectivity index (Flis & SPŁAWIŃSKI 2009; Haque *et al* 2016; Mahavorasirikul *et al* 2010; Peña-Morán *et al* 2016). Moreover, based on our previous study, cisplatin was found to have low SI values towards the HaCaT and Beas2B (SI < 1). This explained the reason behind the severe adverse side effects that were observed in the cancer patients when cisplatin was administered. Like cisplatin, the remarkable cell cytotoxicity profiles of tested (benz)imidazolium salts could also be due to their high toxicities against the human non-cancerous cell lines.

4.2.3 DCFDA Intracellular ROS assay

DCFDA (2',7'-dichlorodihydrofluorescein diacetate) was used to determine the level of intracellular reactive oxygen species (ROS) production/reduction. This assay was to probe the possible mode of cell cytotoxicity of the synthesised compounds *via* the production of ROS intracellularly. In this study, HCT-116 was employed as the model to study the ROS level production/reduction. Like MTT assay, HCT-116 was treated to various concentrations of synthesised (benz)imidazolium salts, ranging from 1.0 to 4.0 µM for 24 hours before loading the DFCDA fluorescent probe. The DCFDA will be converted into non-fluorogenic intermediate by the cellular esterase, which are prone to oxidation by the surrounding ROS to form 2',7'-dichlorofluorescein (DCF) as shown in **Scheme 20**. The fluorescence generated is directly proportional to the concentration of DCF, which indicates the ROS production/reduction in the cells. The assay was performed in triplicates and the results were summarised in **Figure 35a – c**.

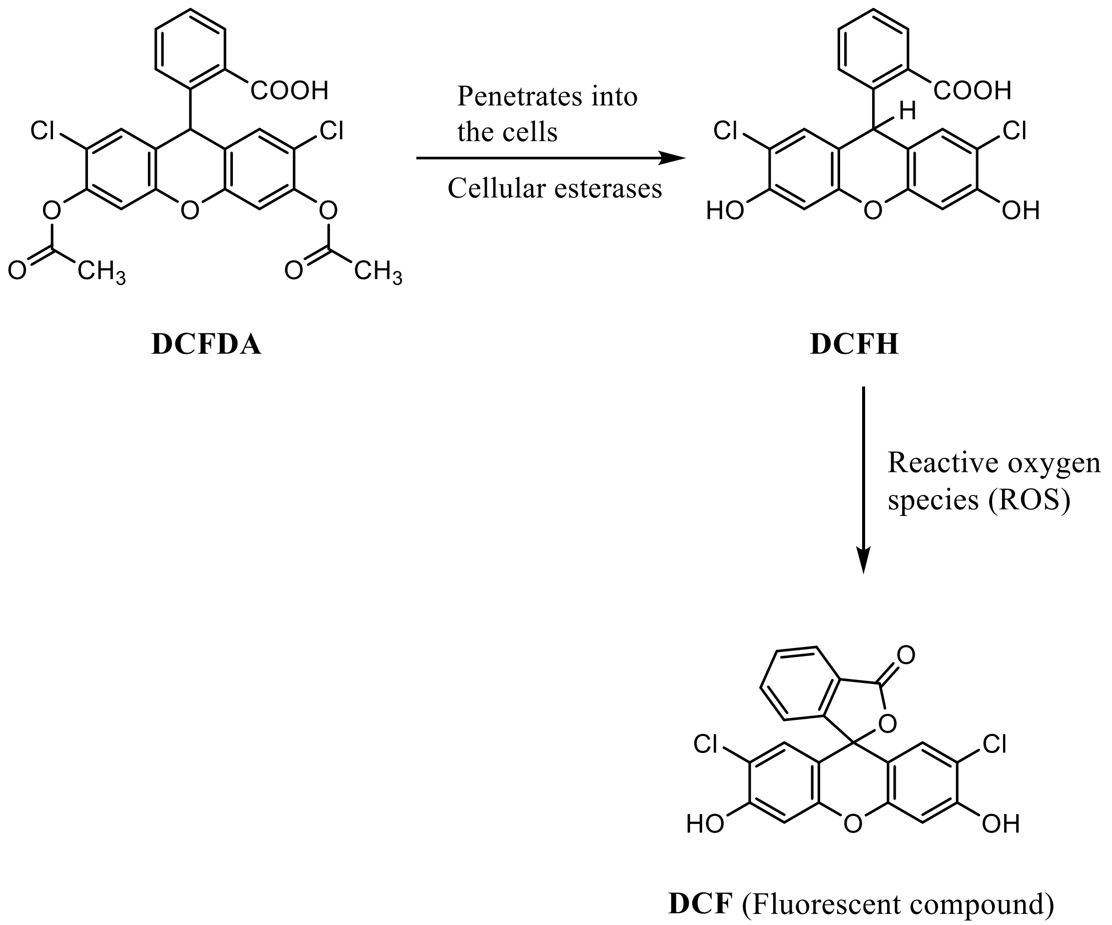

Scheme 20. Conversion of DCFDA into fluorescent DCF by the cellular esterases and ROS.

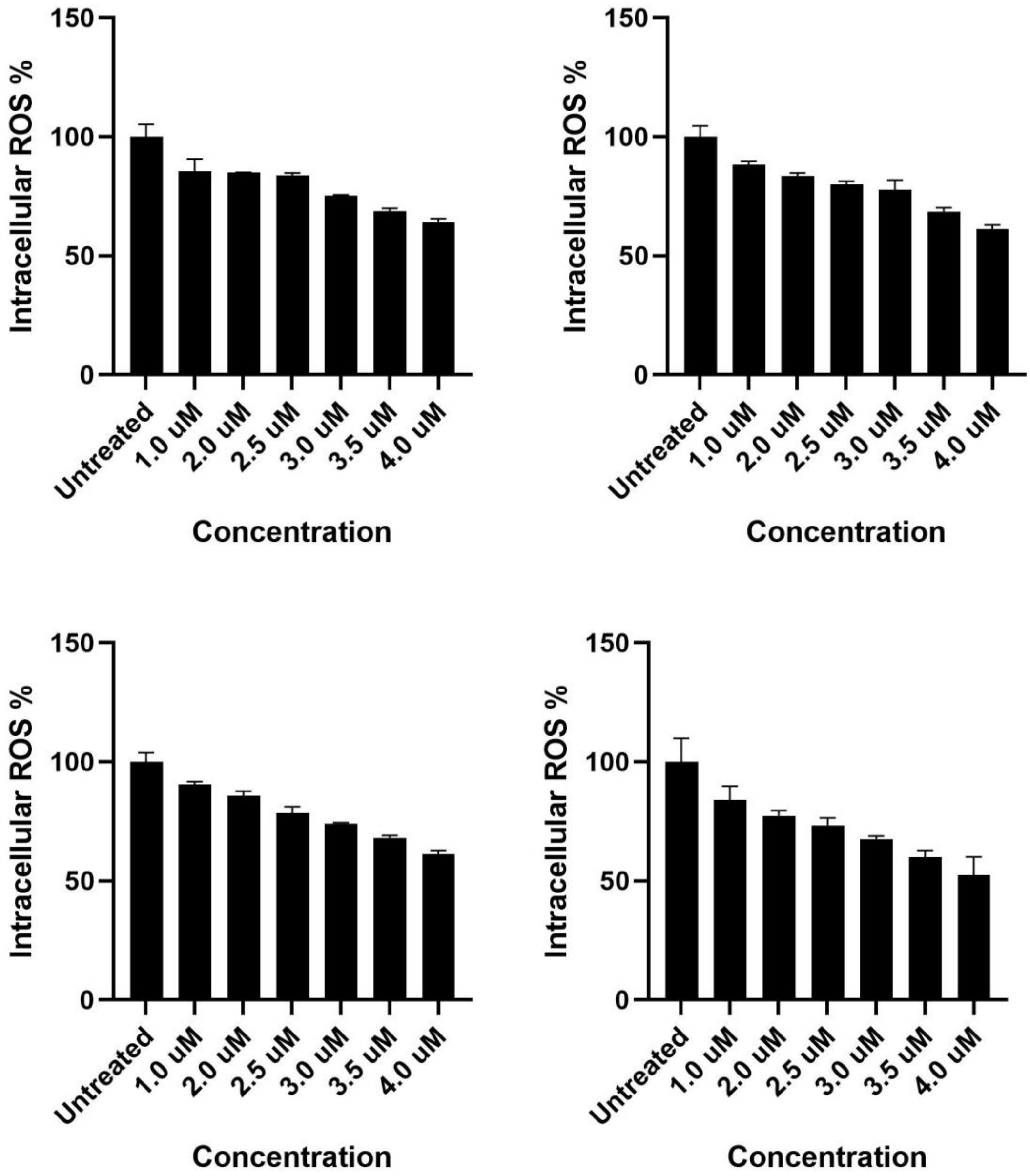

Figure 38a. The intracellular ROS % of HCT-116 after 24 hours of exposure to the tested compound at various concentration ranging from 1.0 to 4.0 µM: (a) **Im-71d**; (b) **Im-71e**; (c) **Im-71f**; (d) **Im-71g**.

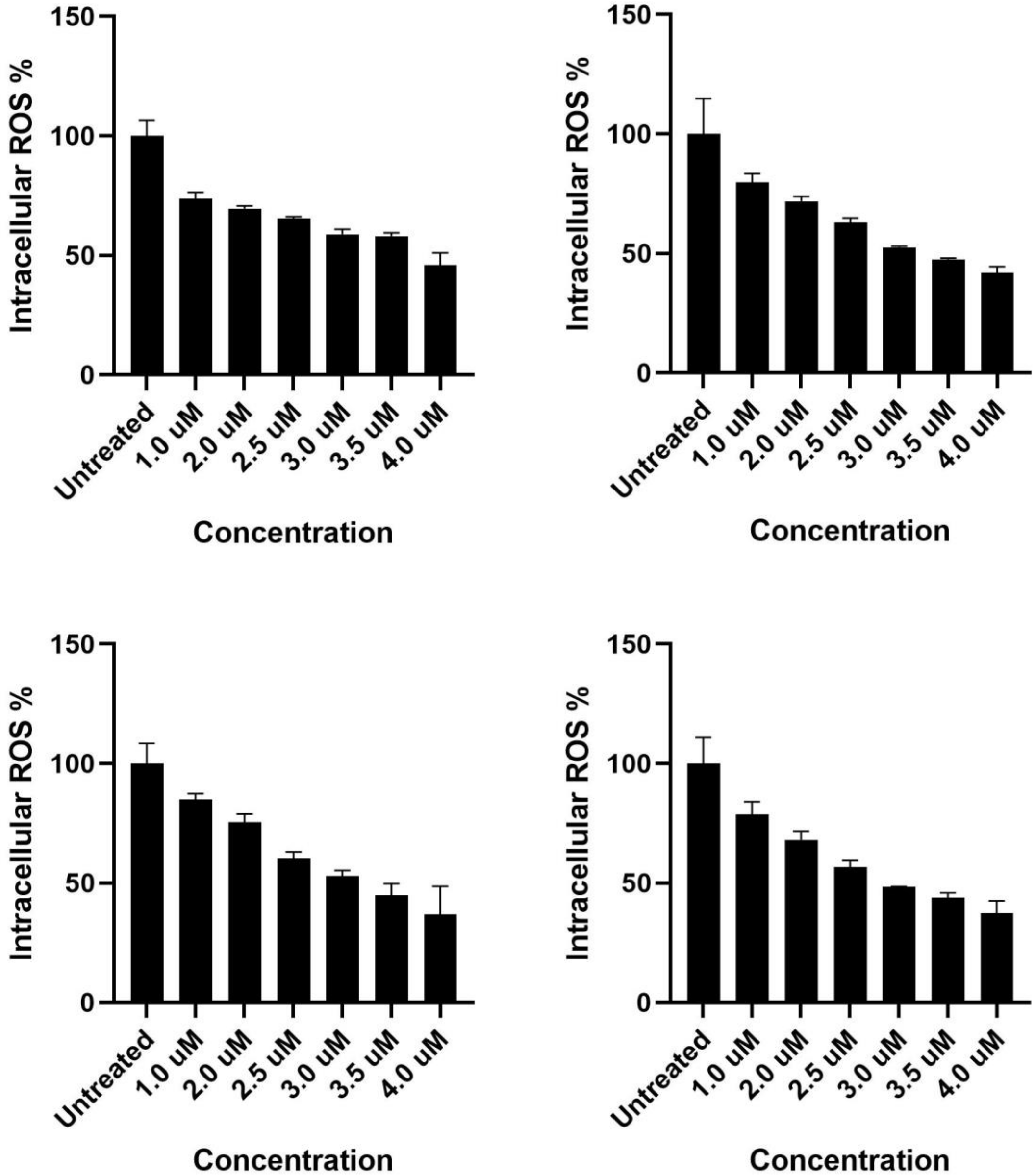

Figure 38b. The intracellular ROS % of HCT-116 after 24 hours of exposure to the tested compound at various concentration ranging from 1.0 to 4.0 µM: (a) **Im-71h**; (b) **Bz-71d**; (c) **Bz-71e**; (d) **Bz-71f**.

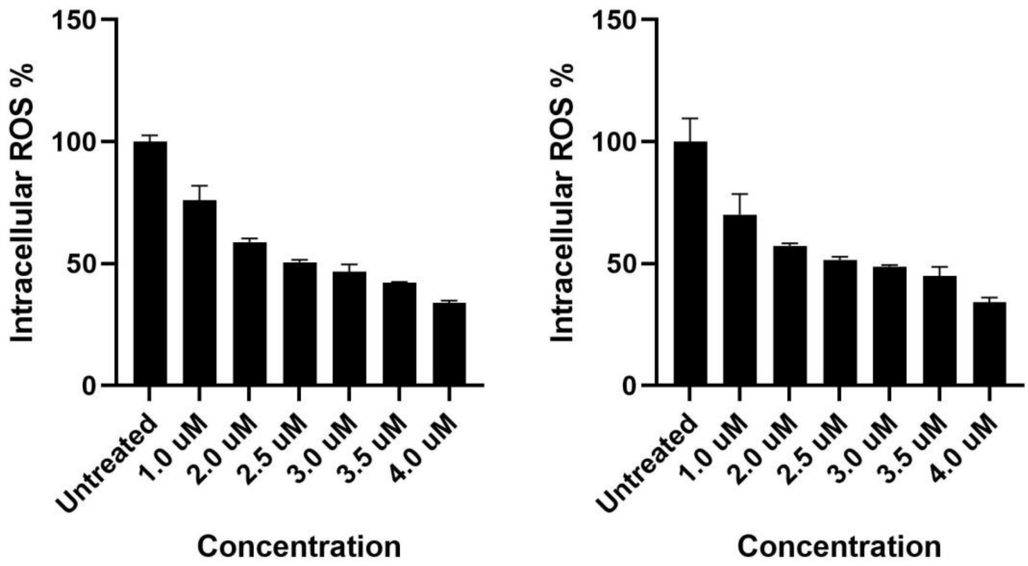

Figure 38c. The intracellular ROS % of HCT-116 after 24 hours of exposure to the tested compound at various concentration ranging from 1.0 to 4.0 µM: (a) **Bz-71g**; (b) **Bz-71h**.

Based on **Figure 38a – c**, it was observed that all tested compounds reduced the intracellular ROS %. Generally, imidazolium salts **Im-71d – h** did not exhibit an obvious dose-dependent manner, however, only **Im-71h** was able to reduce the ROS level by 53 % at 4.0 µM. Unlike **Bz-71d – h**, the tested compounds displayed a dose-dependent manner, where 4.0 µM of **Bz-71d – h** reduced the ROS level by 56 %, 63 %, 61 %, 72 % and 71 % in respect to the increasing carbon chain length. However, there was no significant influence of the increasing alkyl chain length on the ROS reduction level, which deduced that the main ROS scavenging site of the compound was not the alkyl chain. This could be explained by the electron-rich extended π-conjugation in benzimidazolium salts which can donate electrons to reduce free radicals or react with the free radicals to terminate the radical chain reaction (Lindsay 2007). The better ROS reduction activity can also explain the poorer antimicrobial and cytotoxicity profiles of benzimidazolium salts against the selected cancer cells, where the compounds acted in such a way where they protected the treated cells from oxidative stress (Świętek *et al* 2019). Besides, it was also well known that azole compounds are antioxidative in nature as reported by numerous studies, this supported our findings on the reduction of intracellular ROS level (Cindrić *et al* 2019; Haque *et al* 2013; Ranjith 2016).

Nevertheless, as ROS is recognised as the double-edge sword, where it acts as one of the important regulatory factors that contributed to the growth of cancer cells, it is speculated that by enhancing the antioxidant potentials of the synthesised compounds through further modification of the functional moiety could turn the tide and inhibit the growth of cancer cells (Wang & Yi 2008). This strategy is evident in reported studies where overexpression of a strong ROS scavenging enzymes such as glutathione peroxidase or catalase inhibited the growth of cancer cells (Liu *et al* 2006; Nelson *et al* 2006; Venkataraman *et al* 2005).

4.3 Conclusion

This chapter discussed the cell cytotoxicity profiles of all the synthesised (benz)imidazolium salts. Their respective cytotoxicity profiles were evaluated against a list of selected human carcinoma cell lines, which include H103 (oral squamous carcinoma), HCT-116 (colorectal epithelial carcinoma), MCF-7 (breast epithelial carcinoma) and HT1080 (skin fibrosarcoma) using MTT cell viability assay. The results revealed that the alkyl side chain greatly influenced the cytotoxicity of the compounds, where increasing alkyl chain length enhanced the cytotoxicity against the tested cell lines. From the study, it was found that the IC_{50} of **Im-71h** against HCT-116 was 0.71 μM, that is 15-fold more effective than cisplatin. **Im-71h** also showed great selectivity index (SI > 3) towards HaCaT and Beas2B cell lines. However, all the other compounds did not comply to the similar result, where they did not portray any selectivity towards the HaCaT and Beas2B cell lines. The DCFDA intracellular ROS assay revealed that the benzimidazolium salts **Bz-71d – h** were generally better radical scavengers due to the electron-rich extended π-conjugated system. A dose-dependent trend was observed in treatment with benzimidazolium salts but not in those treated with imidazolium salts. **Bz-71h** reduced the ROS level by 71 % at 4.0 μM whereas similar concentration of **Im-71h** was only able to reduce the ROS level by 53 %. The better radical scavenging properties of benzimidazolium salts also explained the poorer antimicrobial and cell cytotoxicity profiles as they were shielding the treated cells from oxidative stress.

4.4 Experimental

4.4.1 Cell lines

The list of human carcinoma cell lines and human non-cancerous cell lines used in this study was tabulated in **Table 20**.

Table 20. List of cell lines to be used in this study.

Group	Cell lines	Cell type
Human carcinoma	HCT-116	Colorectal epithelial carcinoma
	H103	Oral squamous carcinoma
	MCF-7	Breast epithelial adenocarcinoma
	HT1080	Skin fibrosarcoma
Human non-cancerous cell	HaCaT	Skin keratinocytes
	BEAS2B	Lung epithelial cells

4.4.2 Maintenance of cell culture

The cell culture media used to culture and to maintain the human carcinoma cell lines and non-cancerous cell lines were as shown in **Table 21** below.

Table 21. List of cell culture media required by the respective cell lines.

Group	Cell lines	Cell culture medium
Human carcinoma	HCT-116	Roswell Park Memorial Institute (RPMI)
	H103	Dulbecco's Modified Eagle Medium-F12 (DMEM-F12)
	MCF-7	Dulbecco's Modified Eagle Medium (DMEM)
	HT1080	Dulbecco's Modified Eagle Medium (DMEM)
Human non-cancerous cell	HaCaT	Dulbecco's Modified Eagle Medium (DMEM)
	BEAS2B	Roswell Park Memorial Institute (RPMI)

The cell culture media were supplemented with sodium hydrogen carbonate, 10 % foetal bovine serum (FBS), 100 U/mL penicillin and 100 µg/mL streptomycin in culture flasks. In addition, DMEM-F12 medium for H103 was added with 0.5 µg/mL of sodium hydrocortisone succinate. Prior to cell-based assay, all cell lines were maintained at 37 °C, 5 % CO_2 and 95 % humidity. Cells that have a confluency of 70 – 80 % were chosen for cell seeding purpose. The old medium was carefully removed from the cell culture flasks. The cells were then washed three times with sterile phosphate-buffered saline (PBS) solution. The cells were incubated in the presence of 0.05 % trypsin-EDTA solution at 37 °C and 5 % CO_2 for 1 – 15 minutes depending on the type of cells. The flasks containing the cells were then gently tapped to facilitate the cell segregation and observed using an inverted microscope to ensure complete segregation. Trypsin activity was then terminated by addition of fresh complete media containing 10 % FBS. The cells were then counted and diluted to obtain a final working concentration of 50,000 – 100,000 cells/mL for cell seeding in the microtiter plate (100 µL of cell suspension per well).

4.4.3 MTT cell viability assay

MTT (3-(4,5-dimethylthiazol-2-yl)-2,5-diphenyltetrazolium bromide) cell viability assay was performed to evaluate the cell cytotoxicity profiles of the synthesised compounds. The compounds tested were prepared in PBS solution containing 2 % DMSO. The cells were seeded in 96-well microtiter plate at a density of 5,000 to 10,000 cells/well in 100 µL cell culture medium and incubated at 37 °C (5 % CO_2). After 24 hours of seeding, the medium was removed and the cells were further incubated with freshly prepared medium containing compound of interest with various concentration ranging from 1.0, 2.0, 2.5, 3.0, 3.5 and 4.0 µM at 37 °C for 24 hours. After incubation, 10 µL of MTT dye (5 mg/mL in PBS) was added into each well. The plates were incubated again for 4 hours in the CO_2 incubator at 37 °C. After that, the MTT-containing medium was removed, and the purple formazan crystals formed were dissolved in 100 µL of dimethyl sulfoxide. The plates were then measured spectrophotometrically at 570 nm, with reference wavelength at 620 nm. The cell viability was determined by using the formula: Cell viability % = (optical density of sample / optical density of control) × 100 (solvent controls set to 100 % viable cells). IC_{50} value was defined as the concentration where 50 % inhibition of proliferation on the tested cell lines. The experiment was carried out in three technical replicates and two biological replicates. Positive control results were adopted from our previous finding as reference in this study.

4.4.3 DCFDA intracellular ROS assay

DCFDA (2’,7’-dichlorodihydrofluorescein diacetate) intracellular ROS assay was performed to evaluate the intracellular reactive oxygen species level after treated with the compounds. HCT-116 colorectal carcinoma was seeded at a cell density of 5,000 cells/well in 100 µL RPMI and incubated at 37 °C (5 % CO_2). After 24 hours of seeding, the medium was removed and the cells were further incubated with freshly prepared medium containing compound of interest with various concentration ranging from 1.0, 2.0, 2.5, 3.0, 3.5 and 4.0 µM at 37 °C for 24 hours. After incubation, the media was decanted, and 100 µL of 10 µM DCFDA in PBS was added into each well and incubated in CO_2 incubator for 45 minutes. The fluorescence intensity was measure at excitation and emission wavelength of 485 and 535 nm, respectively. The influence of tested compound on ROS production/reduction was reported as the percentage of reactive oxygen species in relative to the untreated culture. The percentage of ROS production/reduction was calculated using the formula: % ROS = (fluorescence intensity of sample / fluorescence intensity of control) × 100 (solvent control set to 100 % viable cells). The experiment was carried out in three technical replicates.

CHAPTER 5 SUMMARY AND FUTURE STUDIES

5.1 Summary

In this research project, a series of pyridine-functionalised imidazolium and benzimidazolium salts (**Im-71d – h** and **Bz-71d – h**), and their parent imidazole and benzimidaole derivatives (**Im-76d – h** and **Bz-76d – h**) were synthesised and characterised utilising both proton (^{1}H) and carbon (^{13}C) nuclear magnetic resonance (NMR) spectroscopy and mass spectrometry (MS). A total of 20 compounds (where 10 were novel compounds) were successfully synthesised using the conventional heating method. Moreover, all (benz)imidazole and their respective salts were also synthesised using microwave irradiation. Based on the study, it was found that the reaction duration of alkylation can be shorted from five days to three hours, and from two days to 30 minutes, respectively, for synthesis of (benz)imidazole derivatives, and synthesis of (benz)imidazolium salts, respectively. Besides, silver NHC complex derived from **Im-71g-Br** was also synthesised and characterised. However, the biological properties were not evaluated due to its structural instability and sensitivity to light. Attempt to crystallise the silver NHC **Ag-Im-77a-PF$_6$** afforded crystal of **Im-71a-PF$_6$** instead. Its molecular structure was studied and reported in subchapter **2.2.1.3**. A computational study was also conducted, namely the Lipinski's Rule of 5 analysis, to determine the "drugability" of the synthesised compounds. All (benz)imidazolium salts were found to comply to the Lipinski's Ro5 rules, where they are presumed to be orally active.

The evaluation of antimicrobial activities of these compounds revealed that the increasing carbon chain length at the *N*-wingtip (where C_n = 6, 7, 8, 9, 10) enhanced the antimicrobial activities up to nine carbon (nonyl-), and the activities fell when the carbon chain length was 10 carbon (decyl-). This "cut-off" point was due to the immoderate lipophilicity of the alkyl chain length which caused the compound to bind stronger to the membrane, slowing the diffusion rate, thus retarding the immune response. Overall, **Im-71g** (C_n = 9) possessed the best antimicrobial activities with MIC values and MBC values as low as 7.81 µg/mL and 31.3 µg/mL respectively, against *B. subtilis* and one of the MSSA strains. In short, it can be concluded that the alkyl chain length influenced the overall antimicrobial activities of the compound. Besides, the extended π-conjugation at the imidazolylidene played a role in the overall antimicrobial activities as well. Comparing to their imidazole derivatives, **Bz-75d – h** and their salts, **Bz-71d – h** were more bacteriostatic to the tested microorganisms (showed lower MIC values), however, their bactericidal properties remained weaker (showed higher or no MBC values). Bacterial growth curves analysis for **Im-71g** and **Bz-71g** revealed that the compounds acted immediately the moment the bacteria cultures were exposed to the tested compounds. Besides, the sub-MIC of both compounds also showed the potential of suppressing the growth of the bacterial cultures. Moreover, cell leakage assay also showed that the intercellular components were released from the bacterial cells when exposed to **Im-71g** and **Bz-71g** in a non-time-dependent manner, which was in line with the bacterial growth curve study, where the killing of bacterial took place at the moment the bacterial cultures were exposed to the tested compounds.

Subsequently, the cell cytotoxicity evaluation of all the synthesised (benz)imidazolium salts was performed against a list of selected human carcinoma cell lines, which include H103 (oral squamous carcinoma), HCT-116 (colorectal epithelial carcinoma), MCF-7 (breast epithelial carcinoma) and HT1080 (skin fibrosarcoma) using MTT cell viability assay. The results revealed that increasing alkyl chain length enhanced the cytotoxicity against the tested cell lines. From the study, it was found that the IC_{50} of **Im-71h** against HCT-116 was 0.71 μM, that is 15-fold more effective than cisplatin. **Im-71h** also showed great selectivity index (SI > 3) towards HaCaT and Beas2B cell lines. However, all the other compounds did not comply to the similar result, where they did not portray any selectivity towards the HaCaT and Beas2B cell lines. The DCFDA intracellular ROS assay revealed that the benzimidazolium salts **Bz-71d – h** were generally better radical scavengers due to the electron-rich extended π-conjugated system. A dose-dependent trend was observed in treatment with benzimidazolium salts but not in those treated with imidazolium salts. **Bz-71h** reduced the ROS level by 71 % at 4.0 μM whereas similar concentration of **Im-71h** was only able to reduce the ROS level by 53 %. The better radical scavenging properties of benzimidazolium salts also explained the poorer antimicrobial and cell cytotoxicity profiles as they were shielding the treated cells from oxidative stress.

In summary, the alkyl chain length had an influence on the biological properties (antimicrobial and cell cytotoxicity) of the compound. However, increasing the alkyl chain length did not affect the radical scavenging properties. The extended π-conjugation also had an influence on the biological applications. Most importantly, this study contributed to the scarce information available for pyridine-functionalised (benz)imidazolium salts on the database, where lots of studies on azolium salts were dialkyl-substituted. The deployment of microwave technology in the synthesis was also optimised and reported.

5.2 Future studies

Despite excellent biological properties were observed in the synthesised (benz)imidazolium salts, it is regretful to mention that there were several parts of the study affected by the ongoing COVID pandemic. The periodic access restrictions to the research laboratory and cease of operation of several facilities had greatly impacted the quality of this work. The items listed in the following can be considered in the future to improve the quality or extend the boundary of this research:

1. The temperature range adopted for VT-NMR analysis shall be increased to identify the coalescence temperature.

2. Synthesis of silver NHC complexes using the synthesised (benz)imidazolium salts as the ligands should presumably enhance the over biological properties. However, a proper facility (dark room) is recommended as the purification and evaporation will be performed without the aluminium foil, where the light energy begins to attack the resulting samples.

3. Determination of mode of actions on the antimicrobial profiles of synthesised compounds can be extended into the following:
    a. Time-kill kinetics assay
    From the present bacterial growth curve study, it was found that the compounds reacted immediately the moment the bacterial cultures were exposed to. Hence, a time-kill kinetics assay would be able to accurately tell the rate of killing of the tested compounds against the microorganisms.
    b. Scanning electron microscopy (SEM)
    From the present intercellular component leakage study, it was found that the treated bacterial released the cellular nucleic acids and proteins. Using SEM can further investigate on the cell surface morphology to observe the disrupted membrane.

c. Confocal laser scanning microscopy assay

Like SEM analysis, confocal laser scanning microscopy can be used to image the integrity of bacterial membrane.

4. Determination of mode of actions on the cell cytotoxicity profiles of synthesised compounds can be extended into the following:

   a. Flow cytometry analysis

      Using a flow cytometry, the cells undergo apoptosis can be imaged and DNA fragmentation can be observed using propidium iodide stain.

   b. Cell cycle analysis

      Antibodies can be deployed to determine the cell cycle stage where the cells are arrested by the tested compounds.

REFERENCE

Abiramasundari A., Sudarsanam V., Vasu K. K. (2015) Characterization of the degradation products of bambuterol using LCMS-QTOF and NMR, *Analytical Methods*, 7(18): 7659-7673.

Alanis A. J. (2005) Resistance to antibiotics: are we in the post-antibiotic era?, *Archives of medical research*, 36(6): 697-705.

Alexander J. W. (2009) History of the medical use of silver, *Surgical infections*, 10(3): 289-292.

Ali I., Nadeem Lone M., A Al-Othman Z., Al-Warthan A., Marsin Sanagi M. (2015) Heterocyclic scaffolds: centrality in anticancer drug development, *Current drug targets*, 16(7): 711-734.

Ali I., Lone M. N., Aboul-Enein H. Y. (2017) Imidazoles as potential anticancer agents, *MedChemComm*, 8(9): 1742-1773.

Angelucci L., Bolle P. Considerations on biochemical studies with trazodone. Trazodone: Karger Publishers; 1974. p. 65-75.

Arany I., Safirstein R. L., editors. Cisplatin nephrotoxicity. Seminars in nephrology; 2003:23: Elsevier.

Arduengo III A. J., Harlow R. L., Kline M. (1991) A stable crystalline carbene, *Journal of the American Chemical Society*, 113(1): 361-363.

Ashley E. S. D. (2010) Pharmacology of azole antifungal agents, *Antifungal therapy*, 199-218.

Astruc D. (2011) The 2010 Chemistry Nobel Prize to RF Heck, E. Negishi, and A. Suzuki for palladium-catalyzed cross-coupling reactions, *Analytical and bioanalytical chemistry*, 399(5): 1811-1814.

Atif M., Bhatti H. N., Haque R. A., Iqbal M. A., Khadeer M. B. A., Majid A. M. S. A. (2020) Synthesis, Structure, and Anticancer Activity of Symmetrical and Non-symmetrical Silver (I)-N-Heterocyclic Carbene Complexes, *Applied Biochemistry and Biotechnology*, 1-19.

Bailar J. C., Gornik H. L. (1997) Cancer undefeated, *New England Journal of Medicine*, 336(22): 1569-1574.

Banin E., Hughes D., Kuipers O. P. (2017) Bacterial pathogens, antibiotics and antibiotic resistance, *FEMS microbiology reviews*, 41(3): 450-452.

Baratta W., Herrmann W. A., Rigo P., Schwarz J. (2000) Convenient syntheses of novel ruthenium catalysts bearing N-heterocyclic carbenes, *Journal of Organometallic Chemistry*, 593(489-493.

Berk Z. Food process engineering and technology: Academic Press; 2018.

Berthod A., Ruiz-Angel M. J., Huguet S. (2005) Nonmolecular solvents in separation methods: dual nature of room temperature ionic liquids, *Analytical chemistry*, 77(13): 4071-4080.

Birnie C. R., Malamud D., Schnaare R. L. (2000) Antimicrobial evaluation of N-alkyl betaines and N-alkyl-N, N-dimethylamine oxides with variations in chain length, *Antimicrobial agents and chemotherapy*, 44(9): 2514-2517.

Boehme C., Frenking G. (1998) N-Heterocyclic carbene, silylene, and germylene complexes of MCl (M= Cu, Ag, Au). A theoretical study1, *Organometallics*, 17(26): 5801-5809.

Bonnet L. G., Douthwaite R. E., Kariuki B. M. (2003) Synthesis of new chiral N-heterocyclic carbene− imine ligands and their application to an asymmetric allylic alkylation reaction, *Organometallics*, 22(21): 4187-4189.

Bornemann D., Schlemper L., Trapp N., Togni A. (2020) Expanding the Scope of Water-Stable Rhenium (V)-NHC Complexes–Synthesis, Characterization, and Derivatization, *European journal of inorganic chemistry*, 2020(11-12): 1004-1010.

Borowiecki P., Milner-Krawczyk M., Brzezińska D., Wielechowska M., Plenkiewicz J. (2013) Synthesis and antimicrobial activity of imidazolium and triazolium chiral ionic liquids, *Eur J Org Chem*, 2013(712-720.

Breslow R. N-Heterocyclic carbenes in organocatalysis: John Wiley & Sons; 2019.

Bruice P. Y. Organic chemistry. 7th ed. ed: Boston : Pearson; 2014.

Burnier M., Wuerzner G. (2011) Pharmacokinetic evaluation of losartan, *Expert opinion on drug metabolism & toxicology*, 7(5): 643-649.

Castagnolo D., De Logu A., Radi M., Bechi B., Manetti F., Magnani M., Supino S., Meleddu R., Chisu L., Botta M. (2008) Synthesis, biological evaluation and SAR study of novel pyrazole analogues as inhibitors of Mycobacterium tuberculosis, *Bioorganic & medicinal chemistry*, 16(18): 8587-8591.

Castagnolo D., Manetti F., Radi M., Bechi B., Pagano M., De Logu A., Meleddu R., Saddi M., Botta M. (2009) Synthesis, biological evaluation, and SAR study of novel pyrazole analogues as inhibitors of Mycobacterium tuberculosis: part 2.

Synthesis of rigid pyrazolones, *Bioorganic & medicinal chemistry*, 17(15): 5716-5721.

Çetinkaya B., Çetinkaya E., Küçükbay H., Durmaz R. (1996) Antimicrobial activity of carbene complexes of rhodium (I) and ruthenium (II), *ARZNEIMITTEL FORSCHUNG*, 46(821-823.

Chai Y., Wang L., Wang L. (2016) How does a C□ C double bond cleave in the gas phase? Fragmentation of protonated ketotifen in mass spectrometry, *Journal of Mass Spectrometry*, 51(12): 1105-1110.

Chauvin Y., Einloft S., Olivier H. (1995) Catalytic dimerization of propene by nickel-phosphine complexes in 1-butyl-3-methylimidazolium chloride/AlEtxCl3-x (x= 0, 1) ionic liquids, *Industrial & engineering chemistry research*, 34(4): 1149-1155.

Chen J., Wang Z., Lu Y., Dalton J. T., Miller D. D., Li W. (2008) Synthesis and antiproliferative activity of imidazole and imidazoline analogs for melanoma, *Bioorganic & medicinal chemistry letters*, 18(11): 3183-3187.

Chiang M., Li Y., Krishnan D., Sumod P., Ng K. H., Leung P. H. Synthesis and Characterisation of a Novel Chiral Bidentate Pyridine-N-Heterocyclic Carbene-Based Palladacycle. Wiley Online Library; 2010.

Choo K. B., Mah W. L., Lee S. M., Lee W. L., Cheow Y. L. (2018) Palladium complexes of bidentate pyridine N-heterocyclic carbenes: Optical resolution, antimicrobial and cytotoxicity studies, *Applied Organometallic Chemistry*, 32(8): e4377.

Choo K. B., Lee S. M., Lee W. L., Cheow Y. L. (2019) Synthesis, characterization, in vitro antimicrobial and anticancer studies of new platinum N-heterocyclic carbene (NHC) complexes and unexpected nickel complexes, *Journal of Organometallic Chemistry*, 898(120868.

Cindrić M., Sović I., Mioč M., Hok L., Boček I., Roškarić P., Butković K., Martin-Kleiner I., Starčević K., Vianello R. (2019) Experimental and Computational Study of the Antioxidative Potential of Novel Nitro and Amino Substituted Benzimidazole/Benzothiazole-2-Carboxamides with Antiproliferative Activity, *Antioxidants*, 8(10): 477.

Correa A., Nolan S. P., Cavallo L. N-heterocyclic carbene complexes of Au, Pd, and Pt as effective catalysts in organic synthesis. Computational mechanisms of Au and Pt catalyzed reactions: Springer; 2011. p. 131-155.

Cui B., Zheng B. L., He K., Zheng Q. Y. (2003) Imidazole alkaloids from lepidium m eyenii, *Journal of natural products*, 66(8): 1101-1103.

de Almeida C. G., Diniz C. G., Silva V. L., Saraiva M. F., Le Hyaric M., de Almeida M. V. (2009) Antibacterial activity of lipophilic fluoroquinolone derivatives, *Medicinal Chemistry*, 5(5): 419-421.

de Frémont P., Marion N., Nolan S. P. (2009) Carbenes: Synthesis, properties, and organometallic chemistry, *Coordination chemistry reviews*, 253(7-8): 862-892.

Debus H., Liebigs S. (1858) Synthesis of 2, 2'-imidazole, *Liebigs Ann Chem*, 107(199-208.

Demberelnyamba D., Kim K.-S., Choi S., Park S.-Y., Lee H., Kim C.-J., Yoo I.-D. (2004) Synthesis and antimicrobial properties of imidazolium and pyrrolidinonium salts, *Bioorganic & medicinal chemistry*, 12(5): 853-857.

Derat E., Maestri G. (2013) Understanding palladium complexes structures and reactivities: beyond classical point of view, *Wiley Interdisciplinary Reviews: Computational Molecular Science*, 3(6): 529-541.

Di Marco L., Hans M., Delaude L., Monbaliu J. C. M. (2016) Continuous-Flow N-Heterocyclic Carbene Generation and Organocatalysis, *Chemistry–A European Journal*, 22(13): 4508-4514.

Drake P. L., Hazelwood K. J. (2005) Exposure-related health effects of silver and silver compounds: a review, *The Annals of occupational hygiene*, 49(7): 575-585.

Eloy L., Jarrousse A. S., Teyssot M. L., Gautier A., Morel L., Jolivalt C., Cresteil T., Roland S. (2012) Anticancer activity of silver–N-heterocyclic carbene complexes: Caspase-independent induction of apoptosis via mitochondrial apoptosis-inducing factor (AIF), *ChemMedChem*, 7(5): 805-814.

Fatima T., Haque R. A., Iqbal M. A., Ahmad A., Hassan L. E. A., Taleb-Agha M., Ahamed M. B. K., Majid A. A., Razali M. R. (2017) Tetra N-heterocyclic carbene dinuclear silver (I) complexes as potential anticancer agents: Synthesis and in vitro anticancer studies, *Journal of Organometallic Chemistry*, 853(122-135.

Fatima T., Haque R. A., Razali M. R., Ahmad A., Asif M., Khadeer Ahamed M. B., Abdul Majid A. (2017) Effect of lipophilicity of wingtip groups on the anticancer potential of mono N-heterocyclic carbene silver (I) complexes: Synthesis, crystal structures and in vitro anticancer study, *Applied Organometallic Chemistry*, 31(10): e3735.

Flis S., SPŁAWIŃSKI J. (2009) Inhibitory effects of 5-fluorouracil and oxaliplatin on human colorectal cancer cell survival are synergistically enhanced by sulindac sulfide, *Anticancer research*, 29(1): 435-441.

Fox C. L. (1968) Silver sulfadiazine—a new topical therapy for pseudomonas in burns: therapy of pseudomonas infection in burns, *Archives of surgery*, 96(2): 184-188.

Frenking G., Solà M., Vyboishchikov S. F. (2005) Chemical bonding in transition metal carbene complexes, *Journal of Organometallic Chemistry*, 690(24-25): 6178-6204.

Garella D., Borretto E., Di Stilo A., Martina K., Cravotto G., Cintas P. (2013) Microwave-assisted synthesis of N-heterocycles in medicinal chemistry, *MedChemComm*, 4(10): 1323-1343.

Garner M. E., Niu W., Chen X., Ghiviriga I., Abboud K. A., Tan W., Veige A. S. (2015) N-heterocyclic carbene gold (I) and silver (I) complexes bearing functional groups for bio-conjugation, *Dalton transactions*, 44(4): 1914-1923.

Garrison J. C., Youngs W. J. (2005) Ag (I) N-heterocyclic carbene complexes: synthesis, structure, and application, *Chemical reviews*, 105(11): 3978-4008.

Gedye R., Smith F., Westaway K. (1986) Microwave assisted syntheses in household microwave ovens, *Tetrahedron Letters*, 27(3): 279-283.

Gedye R. N., Smith F. E., Westaway K. C. (1988) The rapid synthesis of organic compounds in microwave ovens, *Canadian Journal of Chemistry*, 66(1): 17-26.

Giguere R. J., Bray T. L., Duncan S. M., Majetich G. (1986) Application of commercial microwave ovens to organic synthesis, *Tetrahedron Letters*, 27(41): 4945-4948.

Glushkov V., Arapov K., Kotelev M., Rudowsky K., Suponitsky K. Y., Gorbunov A., Maiorova O., Slepukhin P. (2012) N-heterocyclic carbenes. IV. 1synthesis of symmetrical and unsymmetrical imidazolium salts with abietane moiety, *Heteroatom Chemistry*, 23(1): 5-15.

Gök Y., Akkoç S., Albayrak S., Akkurt M., Tahir M. N. (2014) N-Phenyl-substituted carbene precursors and their silver complexes: synthesis, characterization and antimicrobial activities, *Applied Organometallic Chemistry*, 28(4): 244-251.

Gravel J., Schmitzer A. (2017) Imidazolium and benzimidazolium-containing compounds: from simple toxic salts to highly bioactive drugs, *Organic & Biomolecular Chemistry*, 15(5): 1051-1071.

Greenberg M. J. (1980) The importance of hydrophobic properties of organic compounds on their taste intensities: a quantitative structure-taste-intensity study, *Journal of Agricultural and Food Chemistry*, 28(3): 562-566.

Grepioni F., Cojazzi G., Draper S. M., Scully N., Braga D. (1998) Crystal Forms of Hexafluorophosphate Organometallic Salts and the Importance of Charge-Assisted C− H---F Hydrogen Bonds, *Organometallics*, 17(3): 296-307.

Grubbs R. H. (2004) Olefin metathesis, *Tetrahedron*, 60(34): 7117-7140.

Gupta R. R., Kumar M., Gupta V. Heterocyclic Chemistry: Volume II: Five-Membered Heterocycles: Springer Science & Business Media; 2013.

Hans M., Lorkowski J., Demonceau A., Delaude L. (2015) Efficient synthetic protocols for the preparation of common N-heterocyclic carbene precursors, *Beilstein journal of organic chemistry*, 11(1): 2318-2325.

Hansch C., Björkroth J., Leo A. (1987) Hydrophobicity and central nervous system agents: on the principle of minimal hydrophobicity in drug design, *Journal of pharmaceutical sciences*, 76(9): 663-687.

Hantzsch A. (1888) Synthese von thiazolen und oxazolen, *Berichte der deutschen chemischen Gesellschaft*, 21(1): 942-946.

Haque R. A., Hasanudin N., Iqbal M. A., Ahmad A., Hashim S., Abdul Majid A., Ahamed M. B. K. (2013) Synthesis, crystal structures, in vitro anticancer, and in vivo acute oral toxicity studies of bis-imidazolium/benzimidazolium salts and respective dinuclear Ag (I)-N-heterocyclic carbene complexes, *Journal of Coordination Chemistry*, 66(18): 3211-3228.

Haque R. A., Iqbal M. A., Asekunowo P., Majid A. A., Ahamed M. B. K., Umar M. I., Al-Rawi S. S., Al-Suede F. S. R. (2013) Synthesis, structure, anticancer, and antioxidant activity of para-xylyl linked bis-benzimidazolium salts and respective dinuclear Ag (I) N-heterocyclic carbene complexes (Part-II), *Medicinal Chemistry Research*, 22(10): 4663-4676.

Haque R. A., Choo S. Y., Budagumpi S., Iqbal M. A., Abdullah A. A.-A. (2015) Silver (I) complexes of mono-and bidentate N-heterocyclic carbene ligands: synthesis, crystal structures, and in vitro antibacterial and anticancer studies, *European journal of medicinal chemistry*, 90(82-92.

Haque R. A., Ghdhayeb M. Z., Budagumpi S., Ahamed M. B. K., Majid A. M. A. (2016) Synthesis, crystal structures, and in vitro anticancer properties of new N-heterocyclic carbene (NHC) silver (I)-and gold (I)/(III)-complexes: a rare example of silver (I)–NHC complex involved in redox transmetallation, *RSC advances*, 6(65): 60407-60421.

Haziz U. F., Haque R. A., Amirul A., Shaheeda N., Razali M. R. (2016) Synthesis, structures and antibacterial studies of non-functionalized and nitrile-functionalized bis-benzimidazolium salts and respective dinuclear silver (I)-N-heterocyclic carbene complexes, *Polyhedron*, 117(628-636.

Hendricks S., Wulf O., Hilbert G., Liddel U. (1936) Hydrogen bond formation between hydroxyl groups and nitrogen atoms in some organic compounds, *Journal of the American Chemical Society*, 58(10): 1991-1996.

Herrmann W. A., Böhm V. P., Reisinger C.-P. (1999) Application of palladacycles in Heck type reactions, *Journal of Organometallic Chemistry*, 576(1-2): 23-41.

Herrmann W. A. (2002) N-heterocyclic carbenes: a new concept in organometallic catalysis, *Angewandte Chemie International Edition*, 41(8): 1290-1309.

Hindi K. M., Panzner M. J., Tessier C. A., Cannon C. L., Youngs W. J. (2009) The Medicinal applications of imidazolium carbene− metal complexes, *Chemical reviews*, 109(8): 3859-3884.

Hopkinson M. N., Richter C., Schedler M., Glorius F. (2014) An overview of N-heterocyclic carbenes, *Nature*, 510(7506): 485-496.

Hosseini M., Stiasni N., Barbieri V., Kappe C. O. (2007) Microwave-assisted asymmetric organocatalysis. A probe for nonthermal microwave effects and the concept of simultaneous cooling, *The Journal of organic chemistry*, 72(4): 1417-1424.

Hryniewicka A., Malinowska M., Hauschild T., Pieczul K., Morzycki J. W. (2019) Synthesis and antimicrobial properties of steroid-based imidazolium salts, *The Journal of steroid biochemistry and molecular biology*, 189(65-72.

Hryniewicka A., Niemirowicz-Laskowska K., Wielgat P., Car H., Hauschild T., Morzycki J. W. (2021) Dehydroepiandrosterone derived imidazolium salts and their antimicrobial efficacy, *Bioorganic Chemistry*, 108(104550.

Hu X., Tang Y., Gantzel P., Meyer K. (2003) Silver Complexes of a Novel Tripodal N-Heterocyclic Carbene Ligand: Evidence for Significant Metal− Carbene π-Interaction, *Organometallics*, 22(4): 612-614.

Huggins M. T., Kesharwani T., Buttrick J., Nicholson C. (2020) Variable Temperature NMR Experiment Studying Restricted Bond Rotation, *Journal of Chemical Education*, 97(5): 1425-1429.

Hussaini S. Y., Haque R. A., Agha M. T., Abdul Majid A., Razali M. R. (2018) Synthesis, structures and anticancer studies of symmetrically and non-symmetrically aliphatic nitrile functionalized silver (I)-N-heterocyclic carbene and palladium (II)-N-heterocyclic carbene complexes, *Inorganic and Nano-Metal Chemistry*, 48(4-5): 247-256.

Igau A., Grutzmacher H., Baceiredo A., Bertrand G. (1988) Analogous. alpha.,. alpha.'-bis-carbenoid, triply bonded species: synthesis of a stable. lambda. 3-phosphino carbene-. lambda. 5-phosphaacetylene, *Journal of the American Chemical Society*, 110(19): 6463-6466.

Indrayanto G., Putra G. S., Suhud F. (2020) Validation of in-vitro bioassay methods: Application in herbal drug research, *Profiles of Drug Substances, Excipients, and Related Methodology*, 46(273-307.

Iqbal M. A., Haque R. A., Budagumpi S., Ahamed M. B. K., Majid A. M. A. (2013) Short metal–metal separations and in vitro anticancer studies of a new dinuclear silver (I)-N-heterocyclic carbene complex of para-xylyl-linked bis-benzimidazolium salt, *Inorganic Chemistry Communications*, 28(64-69.

Iqbal M. A., Haque R. A., Nasri S. F., Majid A. A., Ahamed M. B. K., Farsi E., Fatima T. (2013) Potential of silver against human colon cancer:(synthesis, characterization and crystal structures of xylyl (Ortho, meta, & Para) linked bis-benzimidazolium salts and Ag (I)-NHC complexes: In vitro anticancer studies), *Chemistry Central Journal*, 7(1): 1-17.

Jagtap S. (2017) Heck reaction—state of the art, *Catalysts*, 7(9): 267.

Johnson N. A., Southerland M. R., Youngs W. J. (2017) Recent developments in the medicinal applications of silver-NHC complexes and imidazolium salts, *Molecules*, 22(8): 1263.

Kanjilal S., Sunitha S., Reddy P. S., Kumar K. P., Murty U. S., Prasad R. B. (2009) Synthesis and evaluation of micellar properties and antimicrobial activities of imidazole-based surfactants, *European journal of lipid science and technology*, 111(9): 941-948.

Kauffman G. B., Pentimalli R., Hall M. D. (2010) Michele Peyrone (1813-1883), Discoverer of Cisplatin, *Platinum Metals Review*, 54(4): 250-256.

Keglevich G., Grun A., Balint E. (2013) Microwave Irradiation and Phase Transfer Catalysis in C-, O-and N-Alkylation Reactions, *Current Organic Synthesis*, 10(5): 751-763.

Kim H., Kang S. K. (2014) Crystal structure of phenyl (pyridin-2-yl) methanol, *Acta Crystallographica Section E: Structure Reports Online*, 70(9): o947-o947.

Klasen H. (2000) A historical review of the use of silver in the treatment of burns. II. Renewed interest for silver, *Burns*, 26(2): 131-138.

Knapp A. R., Panzner M. J., Medvetz D. A., Wright B. D., Tessier C. A., Youngs W. J. (2010) Synthesis and antimicrobial studies of silver N-heterocyclic carbene complexes bearing a methyl benzoate substituent, *Inorganica chimica acta*, 364(1): 125-131.

Komeda S., Yoneyama H., Uemura M., Muramatsu A., Okamoto N., Konishi H., Takahashi H., Takagi A., Fukuda W., Imanaka T. (2017) Specific Conformational Change in Giant DNA Caused by Anticancer Tetrazolato-Bridged Dinuclear Platinum (II) Complexes: Middle-Length Alkyl Substituents Exhibit Minimum Effect, *Inorganic chemistry*, 56(2): 802-811.

Kumar V., Malhotra S. V. (2008) Synthesis of nucleoside-based antiviral drugs in ionic liquids, *Bioorganic & medicinal chemistry letters*, 18(20): 5640-5642.

Laha P., De U., Chandra F., Dehury N., Khullar S., Kim H. S., Patra S. (2018) Alkyl chain-modified cyclometalated iridium complexes as tunable anticancer and imaging agents, *Dalton transactions*, 47(44): 15873-15881.

Lamberth C., Dinges J. Bioactive heterocyclic compound classes: pharmaceuticals: John Wiley & Sons; 2012.

Lee J. W., Lee J. H., Son H. J., Choi Y. K., Yoon G. J., Park M. H. (1996) One Pot Synthesis of Oxazolidinones by Tosylation or Mesylation of N-Boc-β-Amino Alcohols, *Synthetic communications*, 26(1): 83-88.

Li S., Yang F., Lv T., Lan J., Gao G., You J. (2014) Synthesis of unsymmetrical imidazolium salts by direct quaternization of N-substituted imidazoles using arylboronic acids, *Chemical Communications*, 50(30): 3941-3943.

Liang J., Li J., Zhou C., Jia W., Song H., Zhang L., Zhao F., Lee B. P., Liu B. (2019) In situ synthesis of biocompatible imidazolium salt hydrogels with antimicrobial activity, *Acta biomaterialia*, 99(133-140.

Lidström P., Tierney J., Watheyb B., Westmana J. (2001) Microwave assisted organic synthesisĐa review, *Tetrahedron*, 57(9225-9283.

Liebman J. F., Greenberg A. From atoms to polymers: VCH Publishers; 1989.

Lindsay R. C. Food additives. Fennema's food chemistry: CRC Press; 2007. p. 701-762.

Lis R., Morgan Jr T. K., DeVita R. J., Davey D. D., Lumma Jr W. C., Wohl R. A., Diamond J., Wong S. S., Sullivan M. E. (1987) Synthesis and antiarrhythmic activity of novel 3-alkyl-1-[. omega.-[4-[(alkylsulfonyl) amino] phenyl]-. omega.-hydroxyalkyl]-1H-imidazolium salts and related compounds, *Journal of medicinal chemistry*, 30(4): 696-704.

Liu J., Du J., Zhang Y., Sun W., Smith B. J., Oberley L. W., Cullen J. J. (2006) Suppression of the malignant phenotype in pancreatic cancer by overexpression of phospholipid hydroperoxide glutathione peroxidase, *Human gene therapy*, 17(1): 105-116.

Liu W., Gust R. (2013) Metal N-heterocyclic carbene complexes as potential antitumor metallodrugs, *Chemical Society Reviews*, 42(2): 755-773.

Łuczak J., Jungnickel C., Łącka I., Stolte S., Hupka J. (2010) Antimicrobial and surface activity of 1-alkyl-3-methylimidazolium derivatives, *Green chemistry*, 12(4): 593-601.

Mahavorasirikul W., Viyanant V., Chaijaroenkul W., Itharat A., Na-Bangchang K. (2010) Cytotoxic activity of Thai medicinal plants against human cholangiocarcinoma, laryngeal and hepatocarcinoma cells in vitro, *BMC complementary and alternative medicine*, 10(1): 1-8.

Mallakpour S., Dinari M. Ionic liquids as green solvents: progress and prospects. Green solvents II: Springer; 2012. p. 1-32.

Manikannan R., Venkatesan R., Muthusubramanian S., Yogeeswari P., Sriram D. (2010) Pyrazole derivatives from azines of substituted phenacyl aryl/cyclohexyl sulfides and their antimycobacterial activity, *Bioorganic & medicinal chemistry letters*, 20(23): 6920-6924.

Marion N., Díez-González S., Nolan S. P. (2007) N-heterocyclic carbenes as organocatalysts, *Angewandte Chemie International Edition*, 46(17): 2988-3000.

Matsumura Y., Yoshikata K., Kunisaki S.-i., Tsuchido T. (2003) Mode of bactericidal action of silver zeolite and its comparison with that of silver nitrate, *Appl Environ Microbiol*, 69(7): 4278-4281.

Medvetz D. A., Hindi K. M., Panzner M. J., Ditto A. J., Yun Y. H., Youngs W. J. (2008) Anticancer activity of Ag (I) N-heterocyclic carbene complexes derived from 4, 5-dichloro-1H-imidazole, *Metal-based drugs*, 2008(

Melaiye A., Simons R. S., Milsted A., Pingitore F., Wesdemiotis C., Tessier C. A., Youngs W. J. (2004) Formation of water-soluble pincer silver (I)− carbene complexes: a novel antimicrobial agent, *Journal of medicinal chemistry*, 47(4): 973-977.

Melaiye A., Sun Z., Hindi K., Milsted A., Ely D., Reneker D. H., Tessier C. A., Youngs W. J. (2005) Silver (I)− imidazole cyclophane gem-diol complexes encapsulated by electrospun tecophilic nanofibers: Formation of nanosilver particles and antimicrobial activity, *Journal of the American Chemical Society*, 127(7): 2285-2291.

Mishra R., Ganguly S. (2012) Imidazole as an anti-epileptic: an overview, *Medicinal Chemistry Research*, 21(12): 3929-3939.

Mumtaz A., Saeed A., Fatima N., Dawood M., Rafique H., Iqbal J. (2016) Imidazole and its derivatives as potential candidates for drug development, *Bangladesh Journal of Pharmacology*, 11(4): 756-764.

Munita J. M., Arias C. A. (2016) Mechanisms of antibiotic resistance, *Virulence mechanisms of bacterial pathogens*, 481-511.

Nawrocki J. (1997) The silanol group and its role in liquid chromatography, *Journal of Chromatography A*, 779(1-2): 29-71.

Nelson S. K., Bose S. K., Grunwald G. K., Myhill P., McCord J. M. (2006) The induction of human superoxide dismutase and catalase in vivo: a fundamentally new approach to antioxidant therapy, *Free Radical Biology and Medicine*, 40(2): 341-347.

Nguyen L. A., He H., Pham-Huy C. (2006) Chiral drugs: an overview, *International journal of biomedical science: IJBS*, 2(2): 85.

Nüchter M., Ondruschka B., Bonrath W., Gum A. (2004) Microwave assisted synthesis–a critical technology overview, *Green chemistry*, 6(3): 128-141.

Oehninger L., Stefanopoulou M., Alborzinia H., Schur J., Ludewig S., Namikawa K., Muñoz-Castro A., Köster R. W., Baumann K., Wölfl S. (2013) Evaluation of arene ruthenium (II) N-heterocyclic carbene complexes as organometallics interacting with thiol and selenol containing biomolecules, *Dalton transactions*, 42(5): 1657-1666.

Öfele K. (1968) 1, 3-Dimethyl-4-imidazolinyliden-(2)-pentacarbonylchrom ein neuer Übergangsmetall-carben-komplex, *Journal of Organometallic Chemistry*, 12(3): P42-P43.

Olszewski U., Hamilton G. (2010) A better platinum-based anticancer drug yet to come?, *Anti-Cancer Agents in Medicinal Chemistry (Formerly Current Medicinal Chemistry-Anti-Cancer Agents)*, 10(4): 293-301.

Ong K. S., Yule C. M., Lee S. M. (2015) Antimicrobial producing bacteria isolated from tropical peat swamp soil, *Malaysian Journal of Microbiology*, 11(Special issue2): 170-175.

Panzner M. J., Hindi K. M., Wright B. D., Taylor J. B., Han D. S., Youngs W. J., Cannon C. L. (2009) A theobromine derived silver N-heterocyclic carbene: synthesis, characterization, and antimicrobial efficacy studies on cystic fibrosis relevant pathogens, *Dalton transactions*, 35): 7308-7313.

Patrick G. L. An introduction to medicinal chemistry: Oxford university press; 2013.

Peña-Morán O. A., Villarreal M. L., Álvarez-Berber L., Meneses-Acosta A., Rodríguez-López V. (2016) Cytotoxicity, post-treatment recovery, and selectivity analysis of naturally occurring podophyllotoxins from Bursera fagaroides var. fagaroides on breast cancer cell lines, *Molecules*, 21(8): 1013.

Pernak J., Sobaszkiewicz K., Foksowicz-Flaczyk J. (2004) Ionic liquids with symmetrical dialkoxymethyl-substituted imidazolium cations, *Chemistry–A European Journal*, 10(14): 3479-3485.

Perry M. C., Cui X., Powell M. T., Hou D.-R., Reibenspies J. H., Burgess K. (2003) Optically active iridium imidazol-2-ylidene-oxazoline complexes: preparation and use in asymmetric hydrogenation of arylalkenes, *Journal of the American Chemical Society*, 125(1): 113-123.

Pozharskii A. F., Soldatenkov A. T., Katritzky A. R. Heterocycles in life and society: an introduction to heterocyclic chemistry, biochemistry and applications: John Wiley & Sons; 2011.

Qian W., Texter J., Yan F. (2017) Frontiers in poly (ionic liquid) s: syntheses and applications, *Chemical Society Reviews*, 46(4): 1124-1159.

Ramnial T. The chemistry of imidazolium salts and phosphonium-based ionic liquids: Department of Chemistry-Simon Fraser University; 2006.

Ramos-Lima F. J., Moneo V., Quiroga A. G., Carnero A., Navarro-Ranninger C. (2010) The role of p53 in the cellular toxicity by active trans-platinum complexes containing isopropylamine and hydroxymethylpyridine, *European journal of medicinal chemistry*, 45(1): 134-141.

Ranjith R. (2016) The chemistry and biological significance of imidazole, benzimidazole, benzoxazole, tetrazole and quinazolinone nucleus, *Journal of Chemical and pharmaceutical Research*, 8(5): 505-526.

Reedijk B. J. (2008) Metal-ligand exchange kinetics in platinum and ruthenium complexes, *Platinum Metals Review*, 52(1): 2-11.

Reid V. R., Crank J. A., Armstrong D. W., Synovec R. E. (2008) Characterization and utilization of a novel triflate ionic liquid stationary phase for use in comprehensive two-dimensional gas chromatography, *Journal of separation science*, 31(19): 3429-3436.

Reinhardt A., Horn M., Schmauck J. P. g., Brohl A., Giernoth R., Oelkrug C., Schubert A., Neundorf I. (2014) Novel imidazolium salt–peptide conjugates and their antimicrobial activity, *Bioconjugate chemistry*, 25(12): 2166-2174.

Riduan S. N., Zhang Y. (2013) Imidazolium salts and their polymeric materials for biological applications, *Chemical Society Reviews*, 42(23): 9055-9070.

Roymahapatra G., M Mandal S., F Porto W., Samanta T., Giri S., Dinda J., L Franco O., K Chattaraj P. (2012) Pyrazine functionalized Ag (I) and Au (I)-NHC complexes are potential antibacterial agents, *Current medicinal chemistry*, 19(24): 4184-4193.

Rubio-Pérez L., Azpíroz R., Di Giuseppe A., Polo V., Castarlenas R., Pérez-Torrente J. J., Oro L. A. (2013) Pyridine-Enhanced Head-to-Tail Dimerization of Terminal Alkynes by a Rhodium–N-Heterocyclic-Carbene Catalyst, *Chemistry–A European Journal*, 19(45): 15304-15314.

Ruiz-Angel M., Carda-Broch S., Berthod A. (2006) Ionic liquids versus triethylamine as mobile phase additives in the analysis of β-blockers, *Journal of Chromatography A*, 1119(1-2): 202-208.

Sabounchei S. J., Hosseinzadeh M., Panahimehr M., Nematollahi D., Khavasi H. R., Khazalpour S. (2015) A palladium–phosphine catalytic system as an active and recycable precatalyst for Suzuki coupling in water, *Transition Metal Chemistry*, 40(6): 657-663.

Safari J., Naeimi H., Khakpour A. A., Jondani R. S., Khalili S. D. (2007) A rapid and efficient method for synthesis of new 3-arylideneisobenzofuran-1 (3H)-one derivatives catalyzed by acetic anhydride under solvent-free and microwave conditions, *Journal of Molecular Catalysis A: Chemical*, 270(1-2): 236-240.

Samantaray M. K., Katiyar V., Roy D., Pang K., Nanavati H., Stephen R., Sunoj R. B., Ghosh P. (2006) A Cationic (N-Heterocyclic carbene) silver Complex as Catalyst for Bulk Ring-Opening Polymerization of l-Lactides, *European journal of inorganic chemistry*, 2006(15): 2975-2984.

Schenkel L. C., Bakovic M. (2014) Formation and regulation of mitochondrial membranes, *International journal of cell biology*, 2014(

Selvarajoo P. D., Haque R. A., Haziz U. F., Avicor S. W., Wajidi M. F., Razali M. R. (2017) Dinuclear silver (I)-N-heterocyclic carbene complexes: Synthesis, characterization and larvicidal activity of bis-imidazolium dinuclear silver (I)-N-heterocyclic carbene complexes, *Journal of inorganic biochemistry*, 175(232-238.

Sharhan O., Heidelberg T., Hashim N. M., Salman A. A., Ali H. M., Jayash S. N. (2018) Synthesis and biological study of acridine-based imidazolium salts, *RSC advances*, 8(68): 38995-39004.

Shih W.-C., Wang C.-H., Chang Y.-T., Yap G. P., Ong T.-G. (2009) Synthesis and structure of an amino-linked N-heterocyclic carbene and the reactivity of its aluminum adduct, *Organometallics*, 28(4): 1060-1067.

Shmidt M. S., Reverdito A. M., Kremenchuzky L., Perillo I. A., Blanco M. M. (2008) Simple and efficient microwave assisted N-alkylation of isatin, *Molecules*, 13(4): 831-840.

Slimani I., Chakchouk-Mtibaa A., Mellouli L., Mansour L., Ozdemir I., Gürbüz N., Hamdi N. (2020) Novel N-Heterocyclic Carbene Silver (I) Complexes: Synthesis, Structural Characterization, Antimicrobial and Cytotoxicity Potential Studies, *Journal of the Brazilian Chemical Society*, 31(10): 2058-2070.

Starks C. M., Liotta C. L., Halpern M. E. Phase-transfer catalysis: Fundamentals I. Phase-Transfer Catalysis: Springer; 1994. p. 23-47.

Steinman R. A., Brufsky A. M., Oesterreich S. (2012) Zoledronic acid effectiveness against breast cancer metastases-a role for estrogen in the microenvironment?, *Breast Cancer Research*, 14(5): 1-9.

Storr T., Thompson K. H., Orvig C. (2006) Design of targeting ligands in medicinal inorganic chemistry, *Chemical Society Reviews*, 35(6): 534-544.

Stromyer M. L., Southerland M. R., Satyal U., Sikder R. K., Weader D. J., Baughman J. A., Youngs W. J., Abbosh P. H. (2020) Synthesis, characterization, and biological activity of a triphenylphosphonium-containing imidazolium salt against select bladder cancer cell lines, *European journal of medicinal chemistry*, 185(111832.

Świętek M., Lu Y.-C., Konefał R., Ferreira L. P., Cruz M. M., Ma Y.-H., Horák D. (2019) Scavenging of reactive oxygen species by phenolic compound-modified maghemite nanoparticles, *Beilstein journal of nanotechnology*, 10(1): 1073-1088.

Takahashi N., Honda T., Ohba T. (2006) Anticancer and superoxide scavenging activities of p-alkylaminophenols having various length alkyl chains, *Bioorganic & medicinal chemistry*, 14(2): 409-417.

Tandon R., Singh I., Luxami V., Tandon N., Paul K. (2019) Recent advances and developments of in vitro evaluation of heterocyclic moieties on cancer cell lines, *The Chemical Record*, 19(2-3): 362-393.

Thrash B., Uthayathas S., Karuppagounder S. S., Suppiramaniam V., Dhanasekaran M., editors. Paraquat and maneb induced neurotoxicity. PROCEEDINGS-WESTERN PHARMACOLOGY SOCIETY; 2007:50: [Western Pharmacology Society]; 1998.

Tian X., Zhang Q., Zhang M., Uvdal K., Wang Q., Chen J., Du W., Huang B., Wu J., Tian Y. (2017) Probe for simultaneous membrane and nucleus labeling in living cells and in vivo bioimaging using a two-photon absorption water-soluble Zn (II) terpyridine complex with a reduced π-conjugation system, *Chemical Science*, 8(1): 142-149.

Tripathy H., Krishnanand S., Adhikary L., Chandrashekar J. (2010) Microwave assisted parallel synthesis of 1, 4, 5-tri substituted imidazoles and their pharmacological evaluation, *Research Journal of Pharmaceutical, Biological and Chemical Sciences*, 1(4):

Van der Burg W., Bonta I., Delobelle J., Ramon C., Vargaftig B. (1970) Novel type of substituted piperazine with high antiserotonin potency, *Journal of medicinal chemistry*, 13(1): 35-39.

Venkataraman S., Jiang X., Weydert C., Zhang Y., Zhang H. J., Goswami P. C., Ritchie J. M., Oberley L. W., Buettner G. R. (2005) Manganese superoxide dismutase overexpression inhibits the growth of androgen-independent prostate cancer cells, *Oncogene*, 24(1): 77-89.

Vervoort R. J., Maris F., Hindriks H. (1992) Comparison of high-performance liquid chromatographic methods for the analysis of basic drugs, *Journal of Chromatography A*, 623(2): 207-220.

Vucic D. (2008) Editorial [Apoptotic Pathways as Targets for Therapeutic Intervention Guest Editor: Domagoj Vucic], *Current cancer drug targets*, 8(2): 86-86.

Wang J., Yi J. (2008) Cancer cell killing via ROS: to increase or decrease, that is the question, *Cancer biology & therapy*, 7(12): 1875-1884.

Wang Q., Baker G. A., Baker S. N., Colón L. A. (2006) Surface confined ionic liquid as a stationary phase for HPLC, *Analyst*, 131(9): 1000-1005.

Wang X.-Q., Liu L.-X., Li Y., Sun C.-J., Chen W., Li L., Zhang H.-B., Yang X.-D. (2013) Design, synthesis and biological evaluation of novel hybrid compounds of imidazole scaffold-based 2-benzylbenzofuran as potent anticancer agents, *European journal of medicinal chemistry*, 62(111-121.

Wanzlick H. W., Schönherr H. J. (1968) Direct synthesis of a mercury salt-carbene complex, *Angewandte Chemie International Edition in English*, 7(2): 141-142.

Wasserscheid P., Welton T. Ionic liquids in synthesis: John Wiley & Sons; 2008.

Weader D. (2020) Synthesis, Characterization, and Biological Activity of Imidazolium Salts,

Weinberg R. A. (1996) How cancer arises, *Scientific American*, 275(3): 62-70.

WHO. Antimicrobial resistance: global report on surveillance: World Health Organization; 2014.

Wilkes J. S., Levisky J. A., Wilson R. A., Hussey C. L. (1982) Dialkylimidazolium chloroaluminate melts: a new class of room-temperature ionic liquids for electrochemistry, spectroscopy and synthesis, *Inorganic chemistry*, 21(3): 1263-1264.

Williams N. A., Merzouk M., Hitchcock P. B. (2010) Synthesis of Silver (I) Complexes of Iminoalkyl Functionalised ?-Heterocyclic Carbenes, *International Journal of Inorganic Chemistry*, 2010(

Wong E., Giandomenico C. M. (1999) Current status of platinum-based antitumor drugs, *Chemical reviews*, 99(9): 2451-2466.

Woolley D. (1944) Some biological effects produced by benzimidazole and their reversal by purines, *J biol Chem*, 152(225232.2):

Wright B. D., Deblock M. C., Wagers P. O., Duah E., Robishaw N. K., Shelton K. L., Southerland M. R., DeBord M. A., Kersten K. M., McDonald L. J. (2015) Antitumor activity of lipophilic imidazolium salts on select NSCLC cell lines, *Medicinal Chemistry Research*, 24(7): 2838-2861.

Wynne J., Malacoff R. F., Benotti J. R., Curfman G. D., Grossman W., Holman B. L., Smith T. W., Braunwald E. (1980) Oral amrinone in refractory congestive heart failure, *The American journal of cardiology*, 45(6): 1245-1249.

Yamatsu K., Kaneko T., Yamanishi Y., Kitahara A., Ohtake S. A possible mechanism of central action of trazodone in rats. Trazodone: Karger Publishers; 1974. p. 11-17.

Yang J.-L., Ma Y.-H., Li Y.-H., Zhang Y.-P., Tian H.-C., Huang Y.-C., Li Y., Chen W., Yang L.-J. (2019) Design, Synthesis, and Anticancer Activity of Novel Trimethoxyphenyl-Derived Chalcone-Benzimidazolium Salts, *ACS omega*, 4(23): 20381-20393.

Yang X.-D., Zeng X.-H., Zhang Y.-L., Qing C., Song W.-J., Li L., Zhang H.-B. (2009) Synthesis and cytotoxic activities of novel phenacylimidazolium bromides, *Bioorganic & medicinal chemistry letters*, 19(7): 1892-1895.

Yaşar Ş., Köprülü T. K., Tekin Ş., Yaşar S. (2018) Sulfonated N-heterocyclic carbine-silver (I) complexes: Synthesis, characterisation and biological evaluation, *Applied Organometallic Chemistry*, 32(2): e4016.

Zhang C., Ding Z., Suhaimi N.-A. M., Kng Y. L., Zhang Y., Zhuo L. (2009) A class of imidazolium salts is anti-oxidative and anti-fibrotic in hepatic stellate cells, *Free radical research*, 43(10): 899-912.

Zhang L., Peng X. M., Damu G. L., Geng R. X., Zhou C. H. (2014) Comprehensive review in current developments of imidazole-based medicinal chemistry, *Medicinal research reviews*, 34(2): 340-437.

Zhang S., Ding S., Yu J., Chen X., Lei Q., Fang W. (2015) Antibacterial activity, in vitro cytotoxicity, and cell cycle arrest of gemini quaternary ammonium surfactants, *Langmuir*, 31(44): 12161-12169.

Zhang Y., Chan J. Y. G. (2010) Sustainable chemistry: imidazolium salts in biomass conversion and CO 2 fixation, *Energy & Environmental Science*, 3(4): 408-417.

Zheng Z., Xu Q., Guo J., Qin J., Mao H., Wang B., Yan F. (2016) Structure–antibacterial activity relationships of imidazolium-type ionic liquid monomers, poly (ionic liquids) and poly (ionic liquid) membranes: effect of alkyl chain length and cations, *ACS applied materials & interfaces*, 8(20): 12684-12692.

Zhou C.-H., Zhang Y.-Y., Yan C.-Y., Wan K., Gan L.-L., Shi Y. (2010) Recent researches in metal supramolecular complexes as anticancer agents, *Anti-Cancer Agents in Medicinal Chemistry (Formerly Current Medicinal Chemistry-Anti-Cancer Agents)*, 10(5): 371-395.

Zhou C., Gan L., Zhang Y., Zhang F., Wang G., Jin L., Geng R. (2009) Review on supermolecules as chemical drugs, *Science in China Series B: Chemistry*, 52(4): 415-458.

Zhuang R.-T., Lin W.-J., Zhuang R. R., Hwang W.-S. (2013) Hg (II), Ag (I) and Au (I) complexes with aniline or pyridine-functionalized N-heterocyclic carbene, *Polyhedron*, 51(132-141.

APPENDIX 1: X-RAY CRYSTALLOGRAPHIC DATA

Table A1.1. Crystallographic data of **Im-71a-PF_6**.

Formula	$C_{16}H_{16}N_3PF_6$
Formula weight	395.29
Crystal system	Triclinic
Space group	*P*-1
Temperature (K)	100
a, b, c (Å)	8.5368(19), 10.2143(3), 10.9118(3)
α, β, γ (°)	65.377(2), 85.113(2), 80.762(2)
V (Å^3)	853.56(4)
Z	2
Radiation type	Cuκα
μ (mm^{-1})	2.07
Crystal size (mm)	0.10 × 0.06 × 0.04
No. of measured, independent and observed [$I \geq 2u(I)$] reflections	20346, 3046, 2744
R_{int}	0.037
R_1	0.044
wR_2	0.130
$\Delta\rho_{max}$, $\Delta\rho_{min}$ (e Å^{-3})	0.78, - 0.72

APPENDIX 2: NMR SPECTRAL DATA

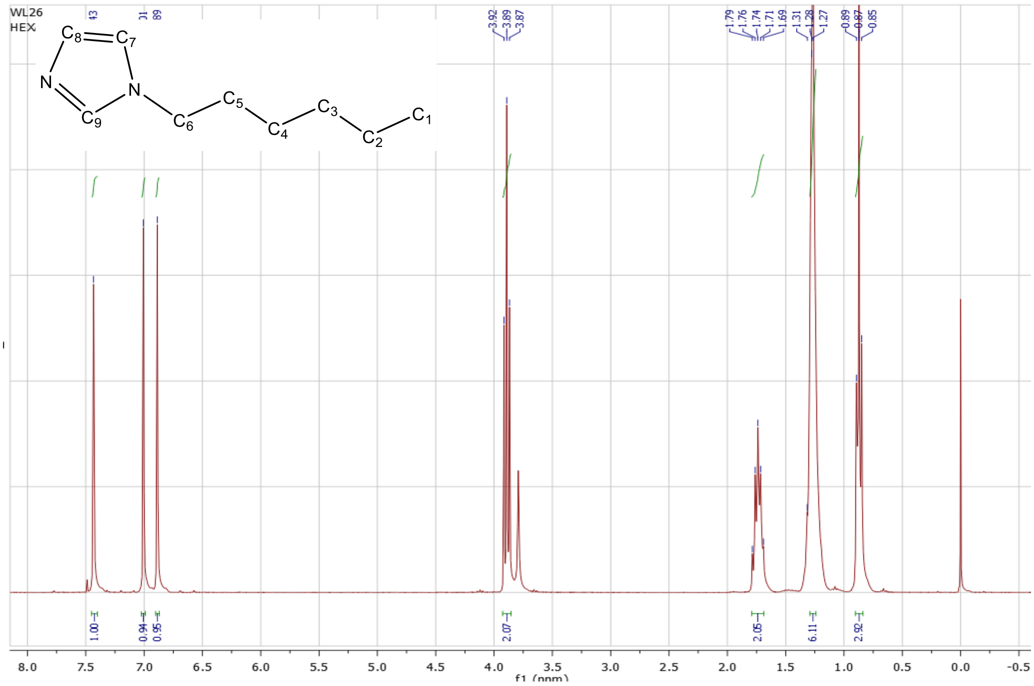

Figure A2.1. ^{1}H-NMR spectrum for compound **Im-76d**.

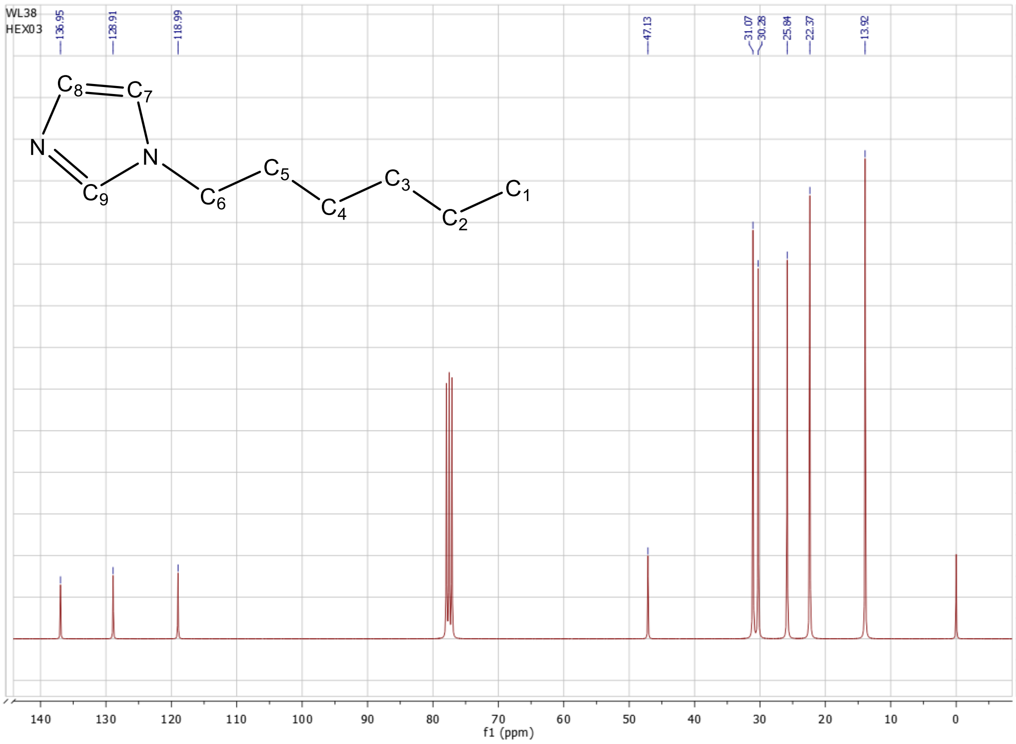

Figure A2.2. ^{13}C-NMR spectrum for compound **Im-76d**.

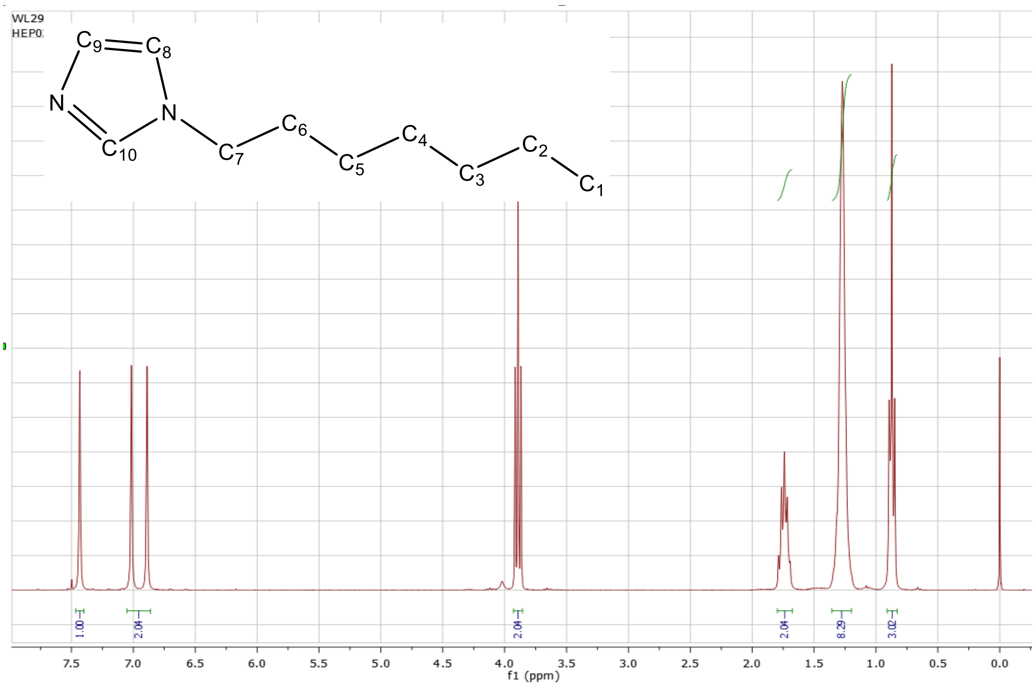

Figure A2.3. ^{1}H-NMR spectrum for compound **Im-76e**.

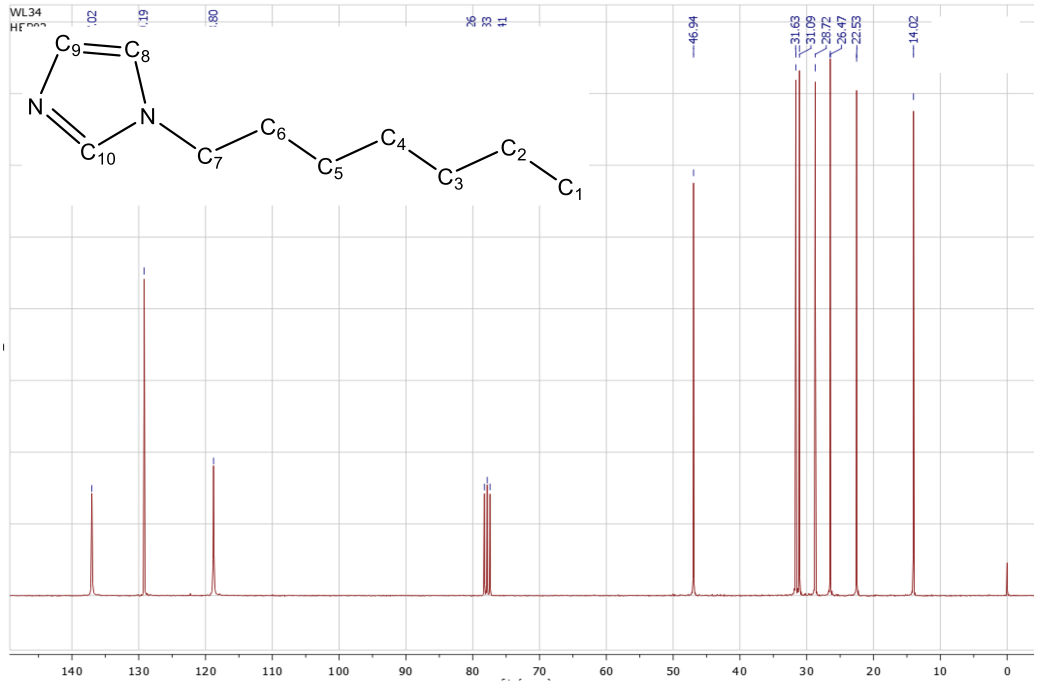

Figure A2.4. ^{13}C-NMR spectrum for compound **Im-76e**.

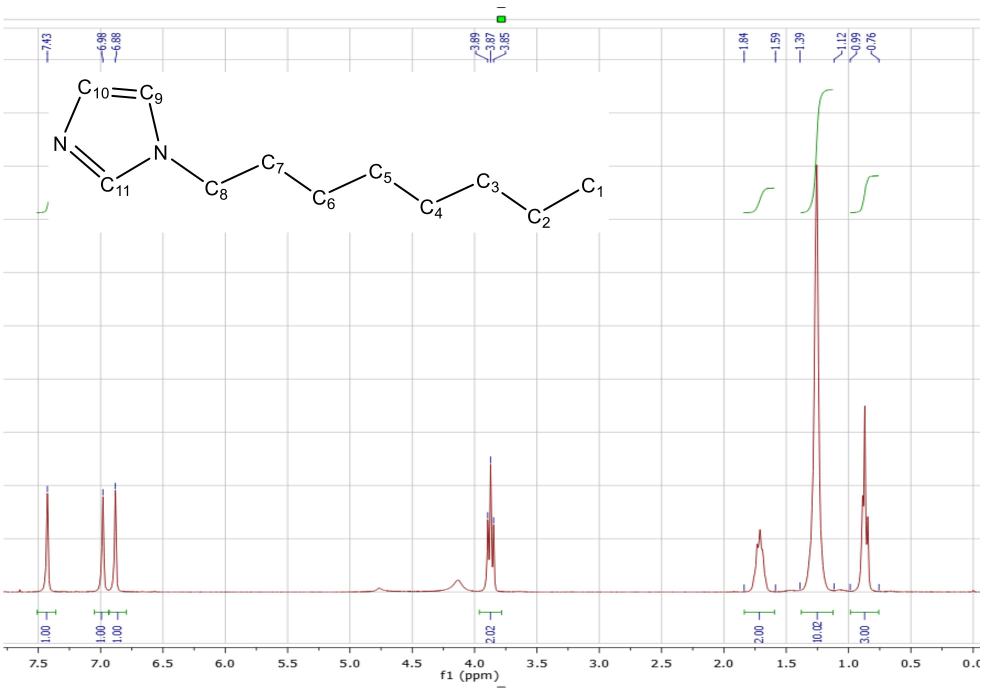

Figure A2.5. ^{1}H-NMR spectrum for compound **Im-76f**.

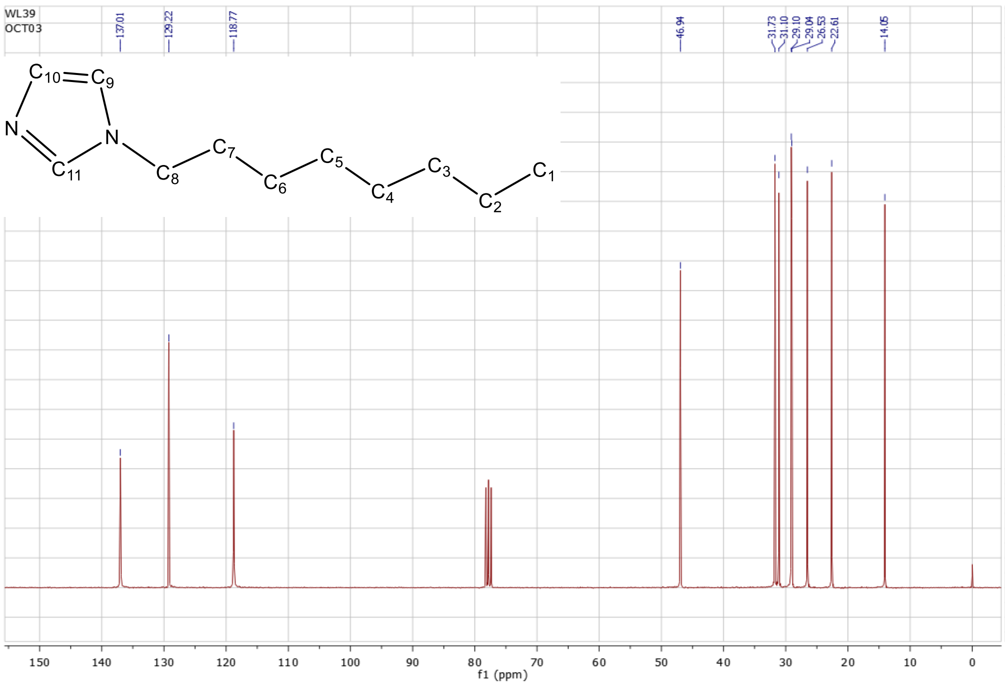

Figure A2.6. ^{13}C-NMR spectrum for compound **Im-76f**.

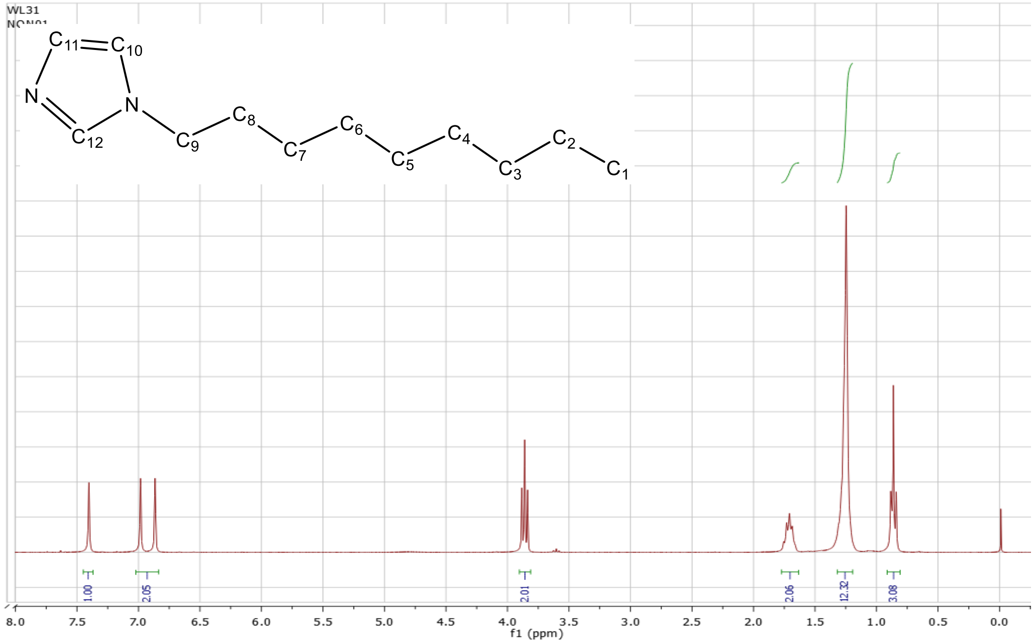

Figure A2.7. ^{1}H-NMR spectrum for compound **Im-76g**.

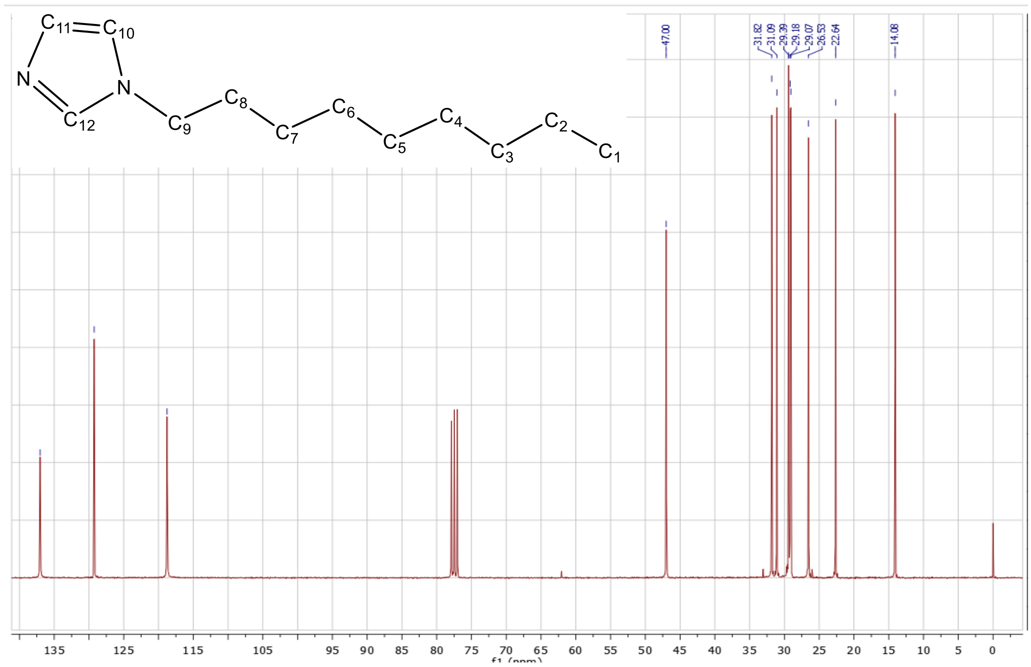

Figure A2.8. ^{13}C-NMR spectrum for compound **Im-76g**.

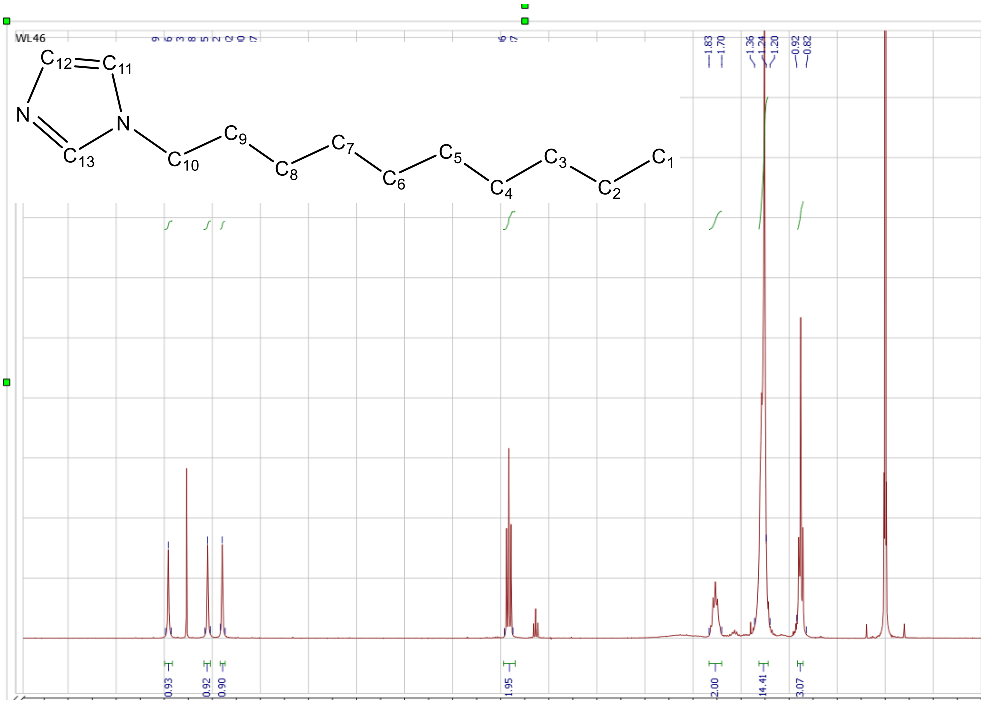

Figure A2.9. ^{1}H-NMR spectrum for compound **Im-76h**.

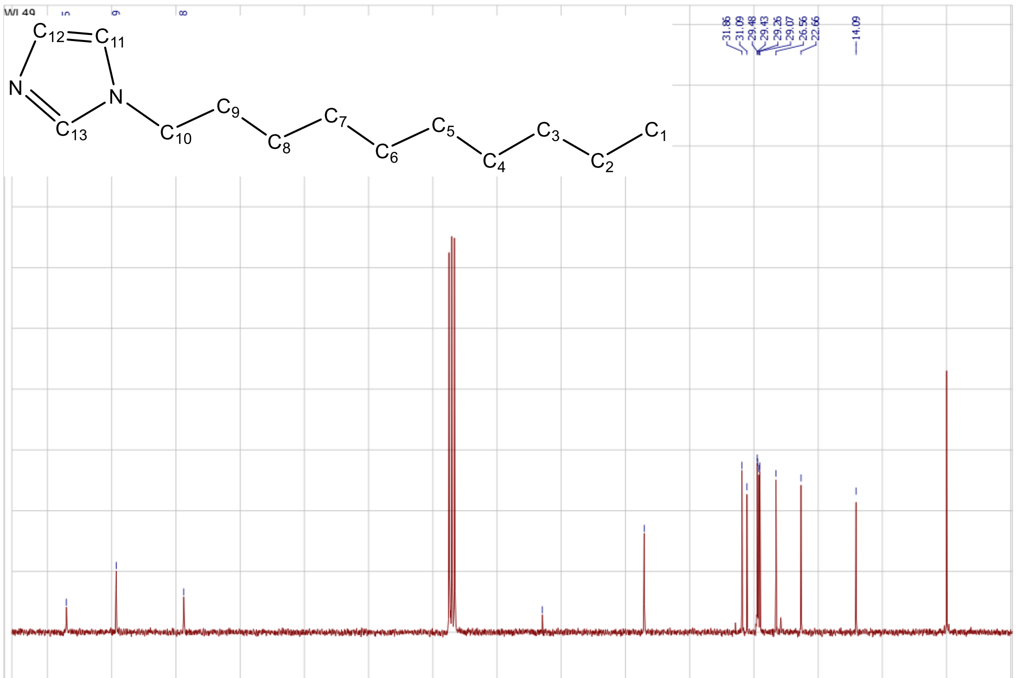

Figure A2.10. ^{13}C-NMR spectrum for compound **Im-76h**.

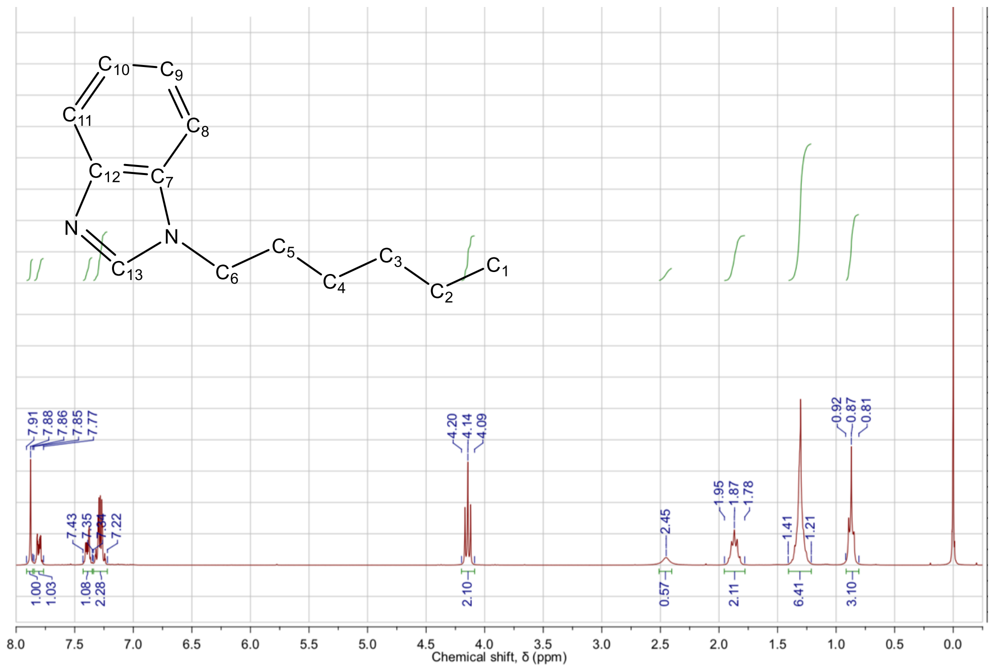

Figure A2.11. ^{1}H-NMR spectrum for compound **Bz-76d**.

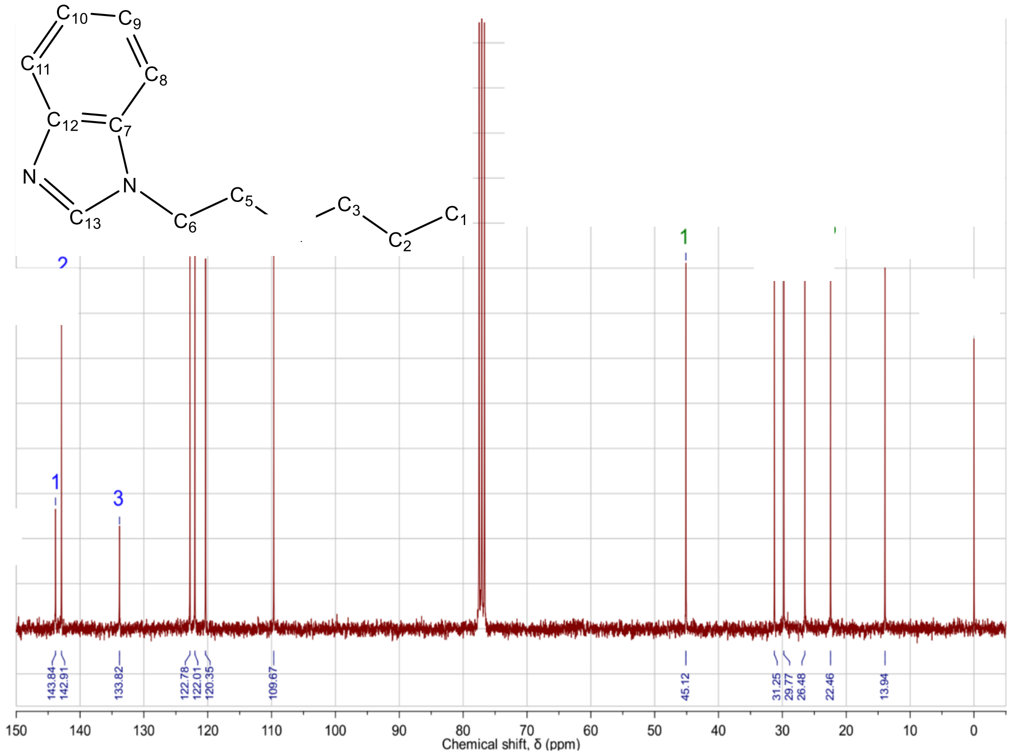

Figure A2.12. ^{13}C-NMR spectrum for compound **Bz-76d.**

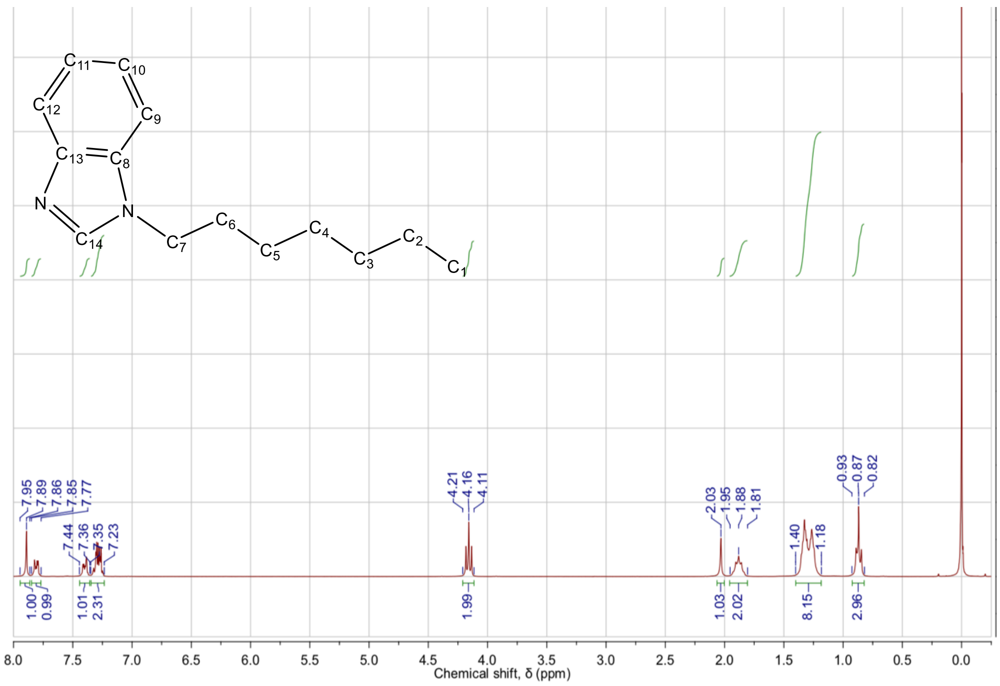

Figure A2.13. ^{1}H-NMR spectrum for compound **Bz-76e.**

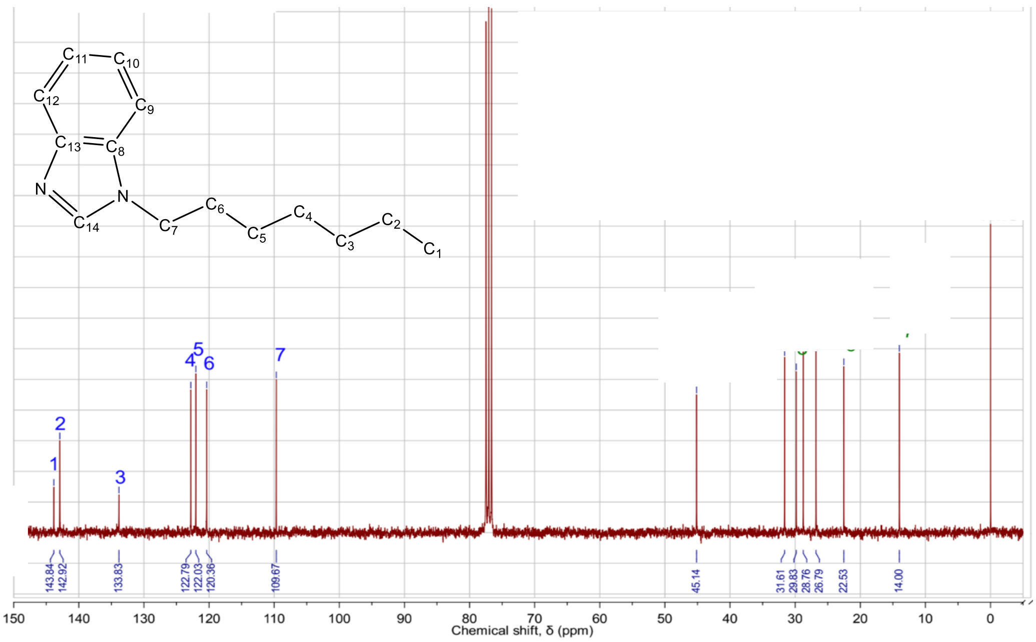

Figure A2.14. ^{13}C-NMR spectrum for compound **Bz-76e**.

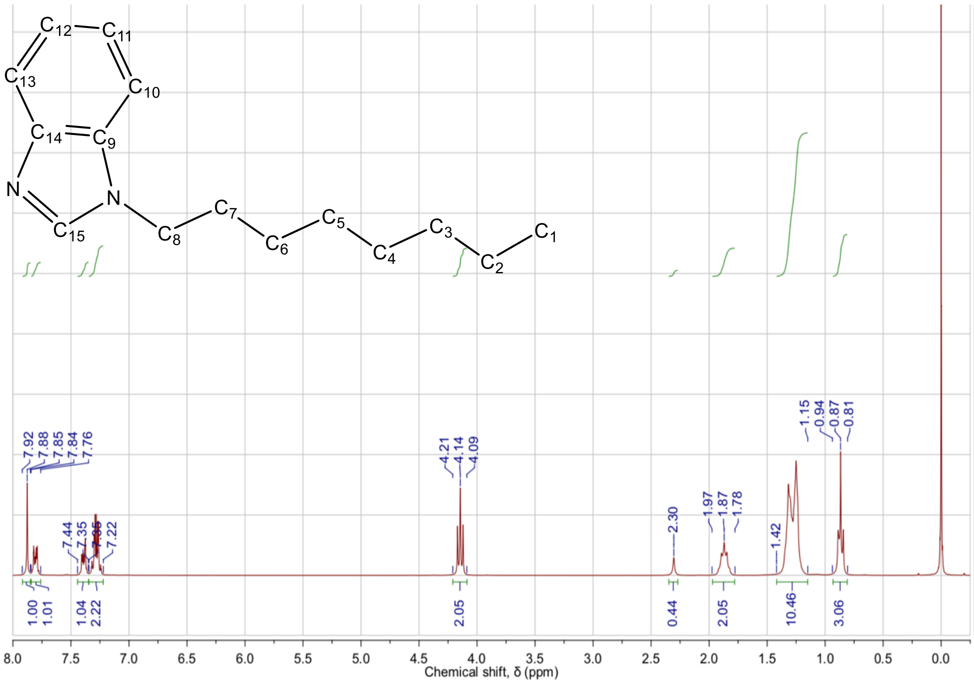

Figure A2.15. ^{1}H-NMR spectrum for compound **Bz-76f.**

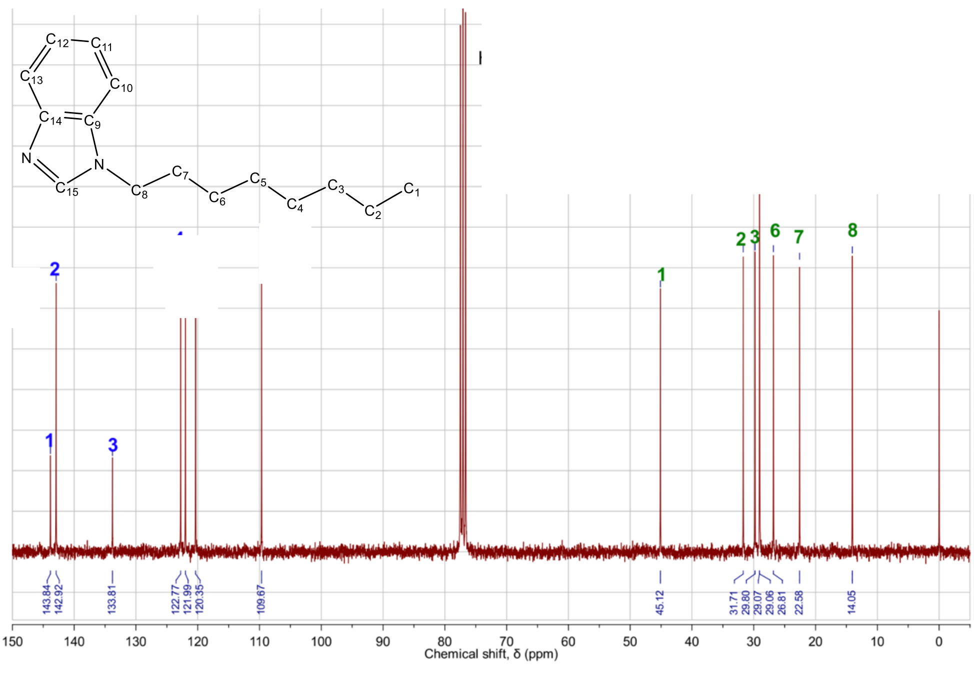

Figure A2.16. ^{13}C-NMR spectrum for compound **Bz-76f.**

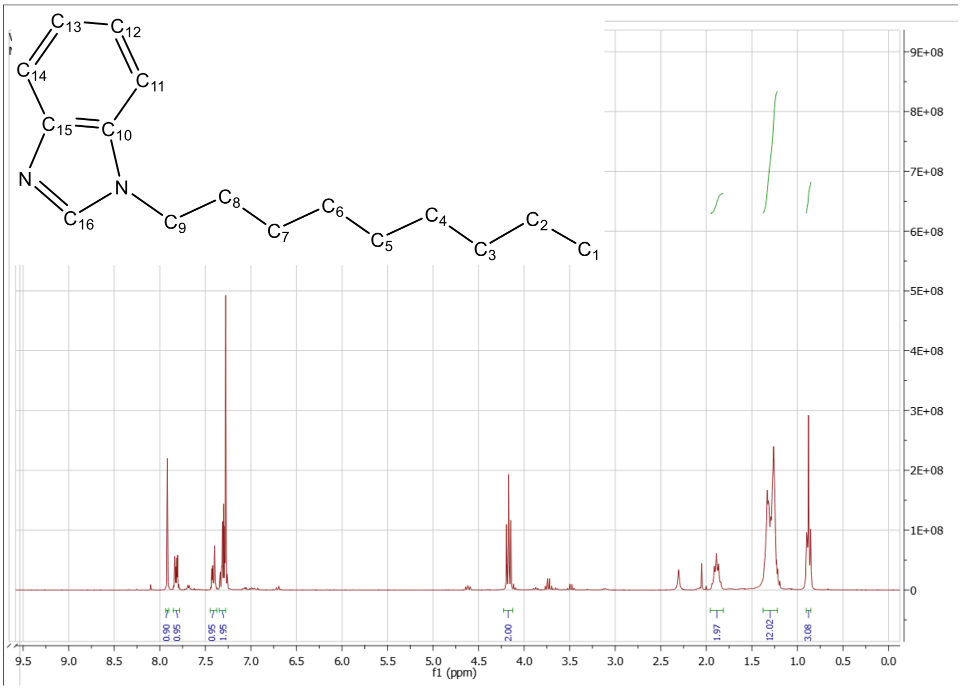

Figure A2.17. ^{1}H-NMR spectrum for compound **Bz-76g.**

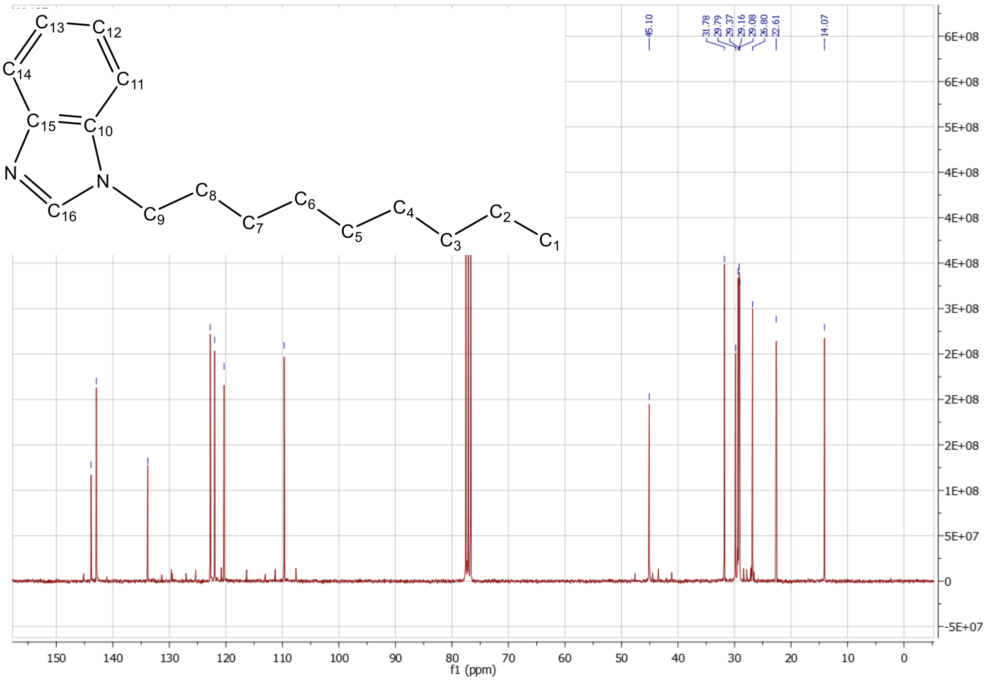

Figure A2.18. ^{13}C-NMR spectrum for compound **Bz-76g.**

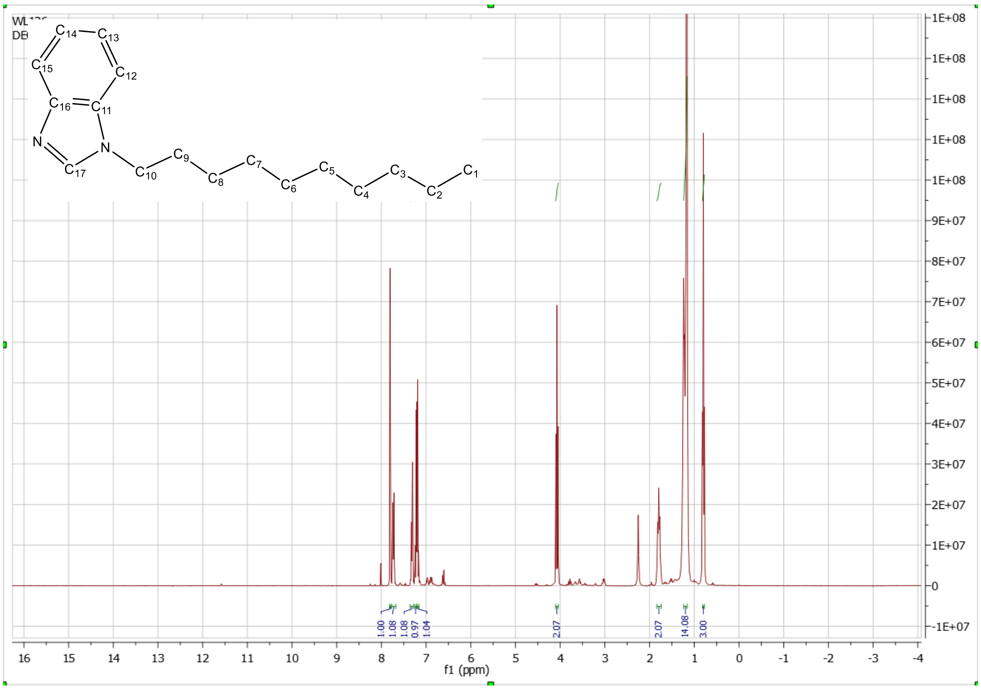

Figure A2.19. ^{1}H-NMR spectrum for compound **Bz-76h.**

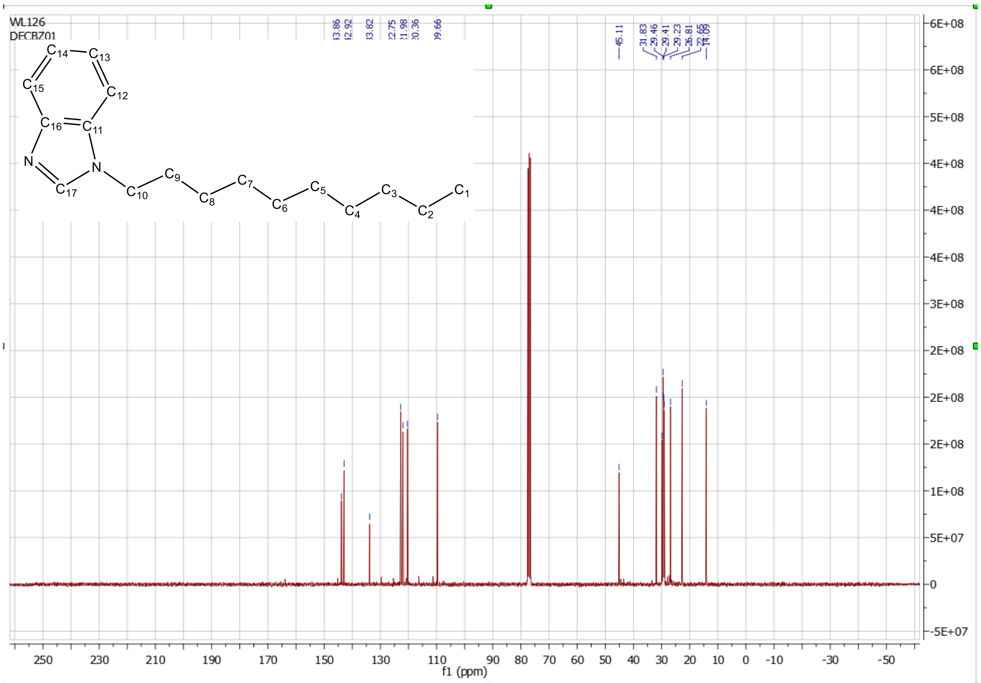

Figure A2.20. ^{13}C-NMR spectrum for compound **Bz-76h.**

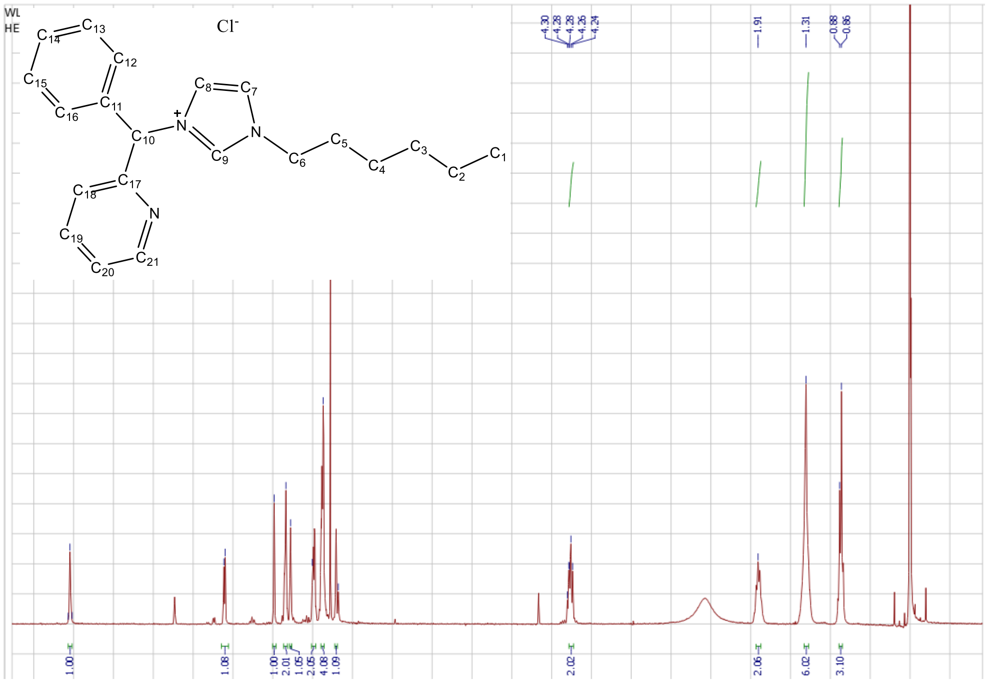

Figure A2.21. ^{1}H-NMR spectrum for compound **Im-71d**.

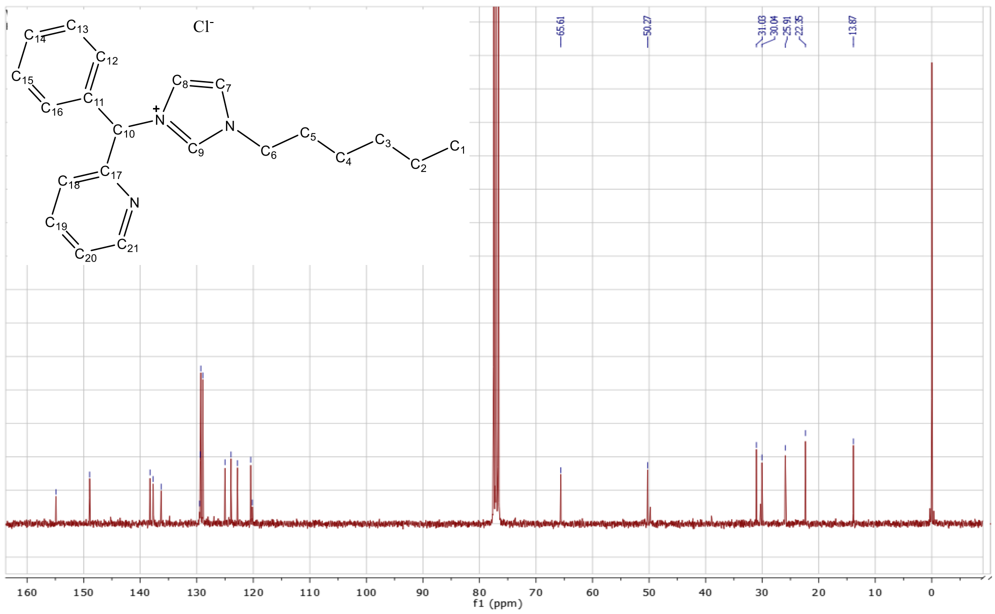

Figure A2.22. ^{13}C-NMR spectrum for compound **Im-71d**.

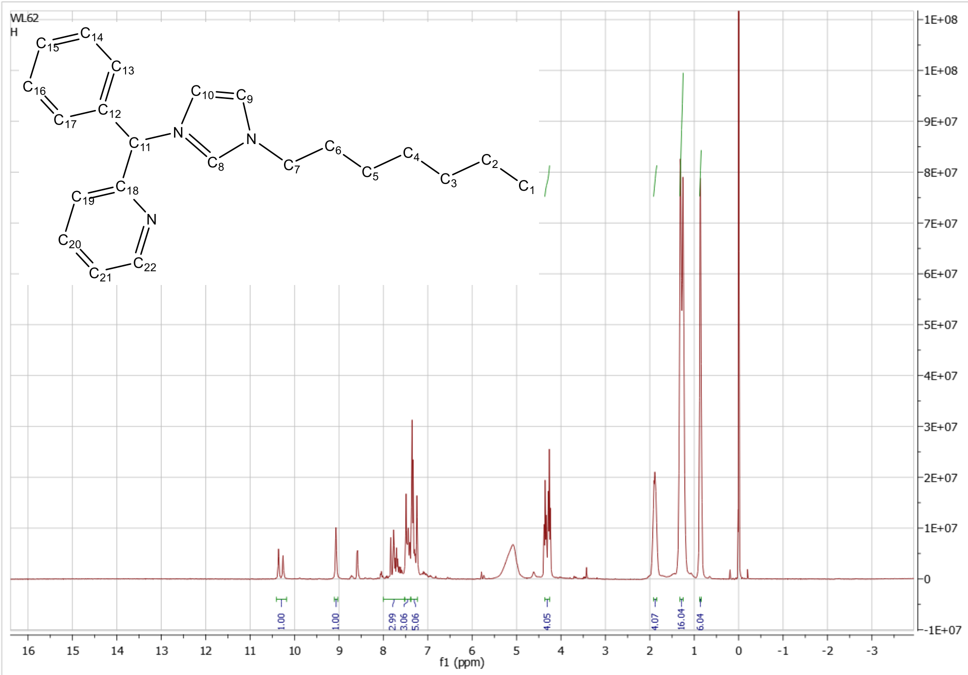

Figure A2.23. ^{1}H-NMR spectrum for compound **Im-71e.**

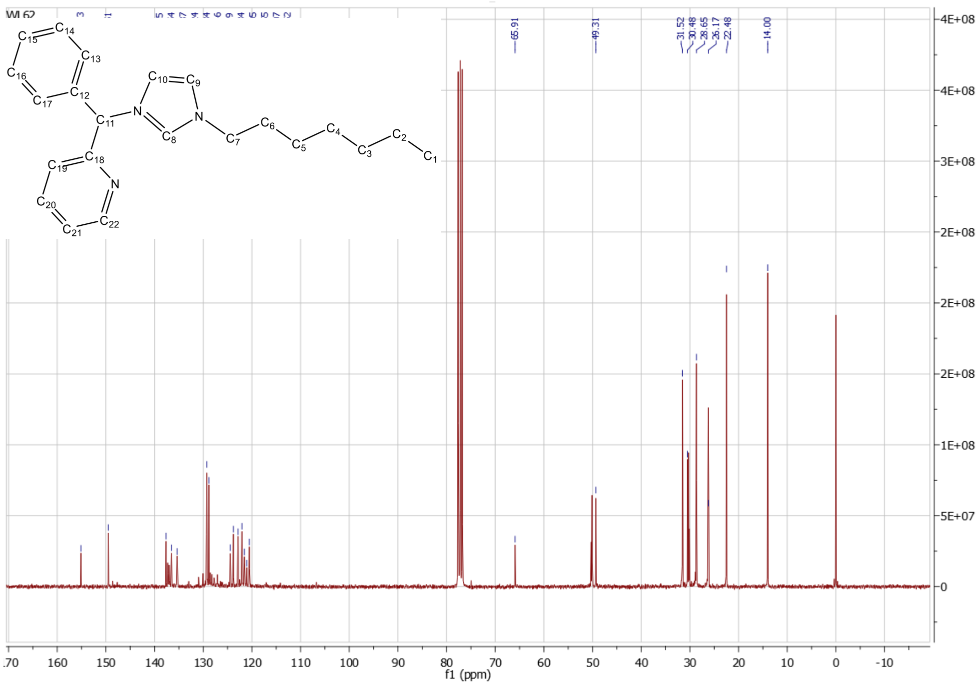

Figure A2.24. ^{13}C-NMR spectrum for compound **Im-71e.**

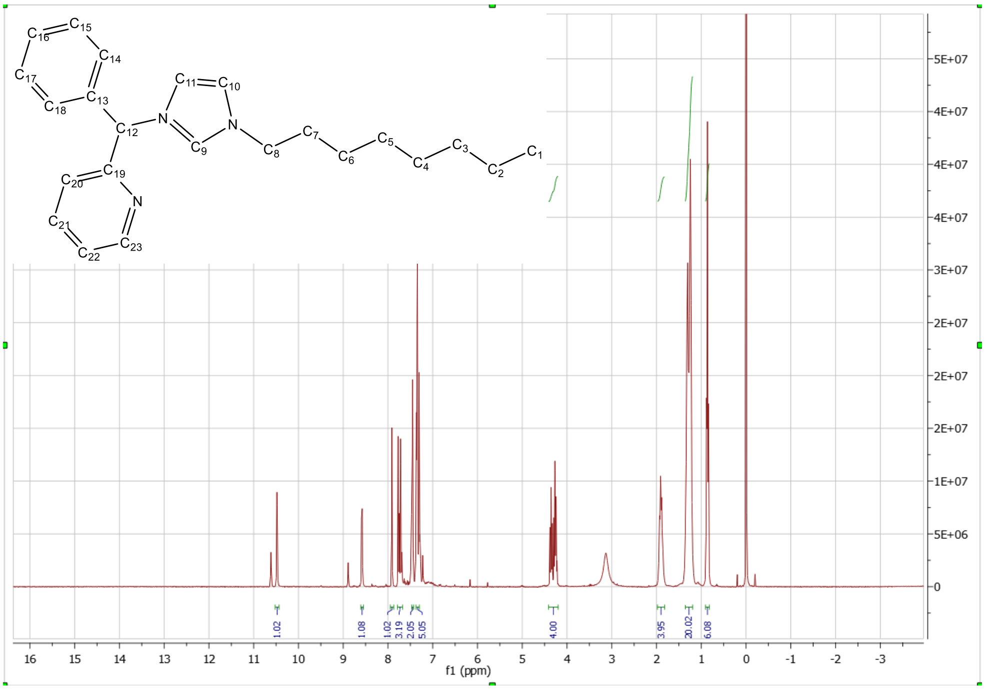

Figure A2.25. ^{1}H-NMR spectrum for compound **Im-71f.**

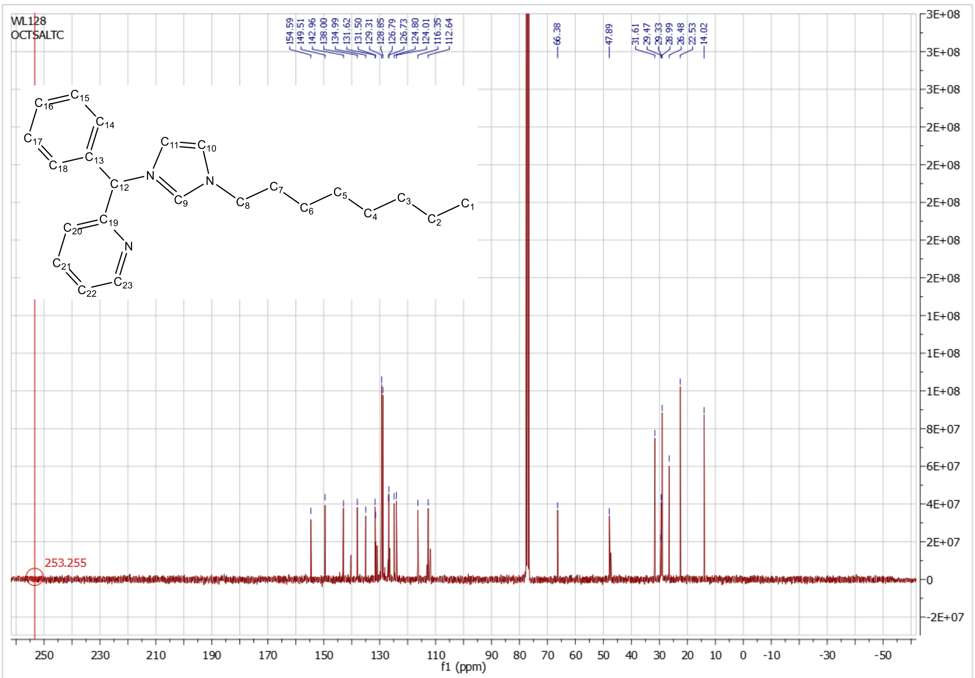

Figure A2.26. ^{13}C-NMR spectrum for compound **Im-71f.**

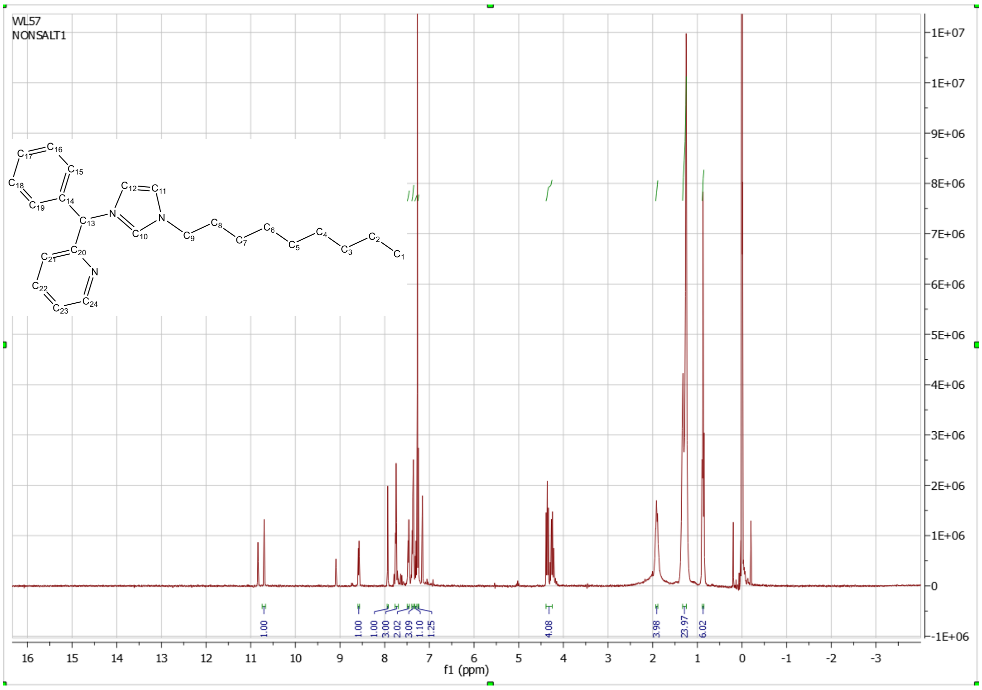

Figure A2.27. ^{1}H-NMR spectrum for compound **Im-71g.**

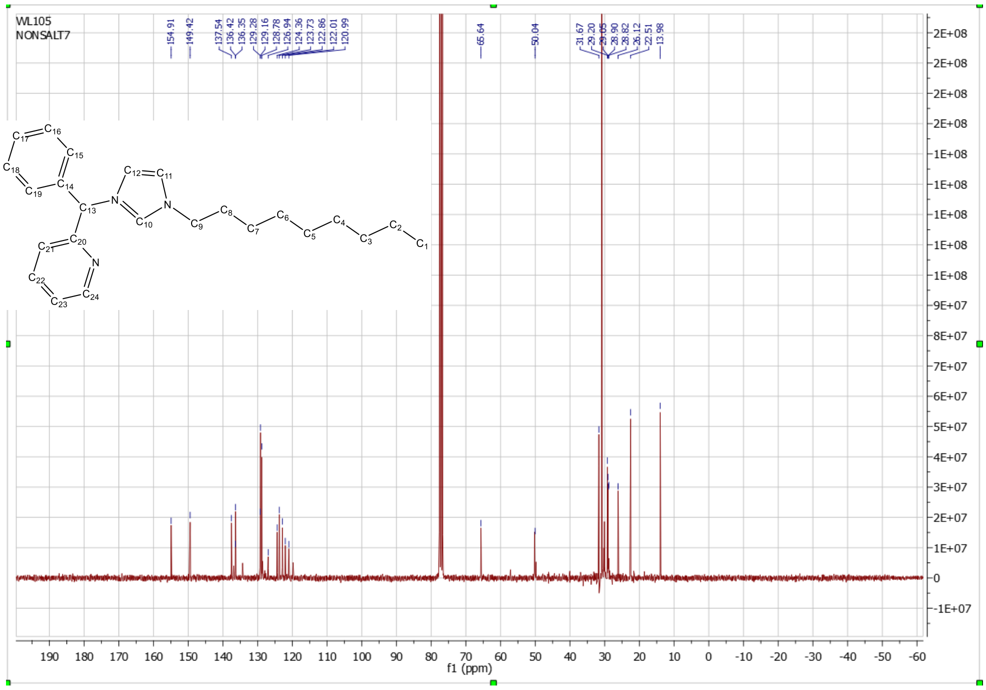

Figure A2.28. ^{13}C-NMR spectrum for compound **Im-71g.**

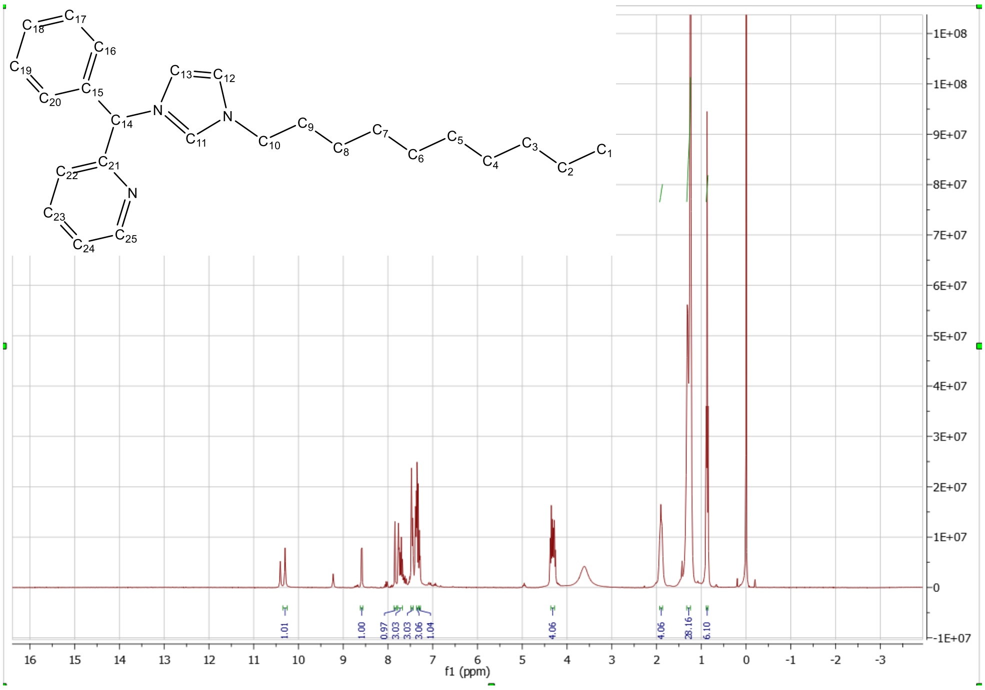

Figure A2.29. ^{1}H-NMR spectrum for compound **Im-71h.**

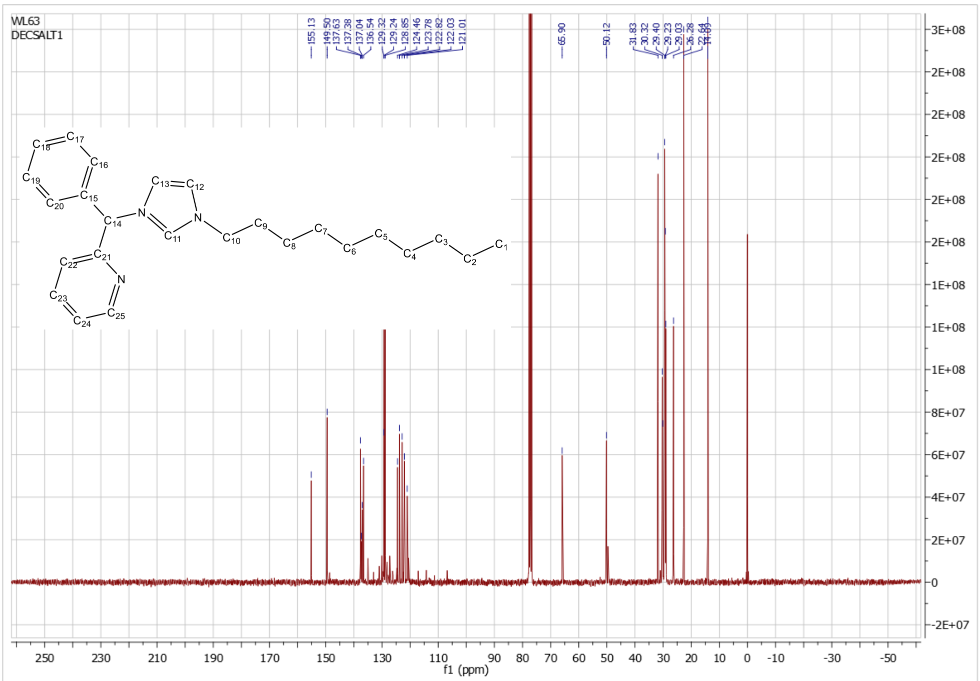

Figure A2.30. ^{13}C-NMR spectrum for compound **Im-71h.**

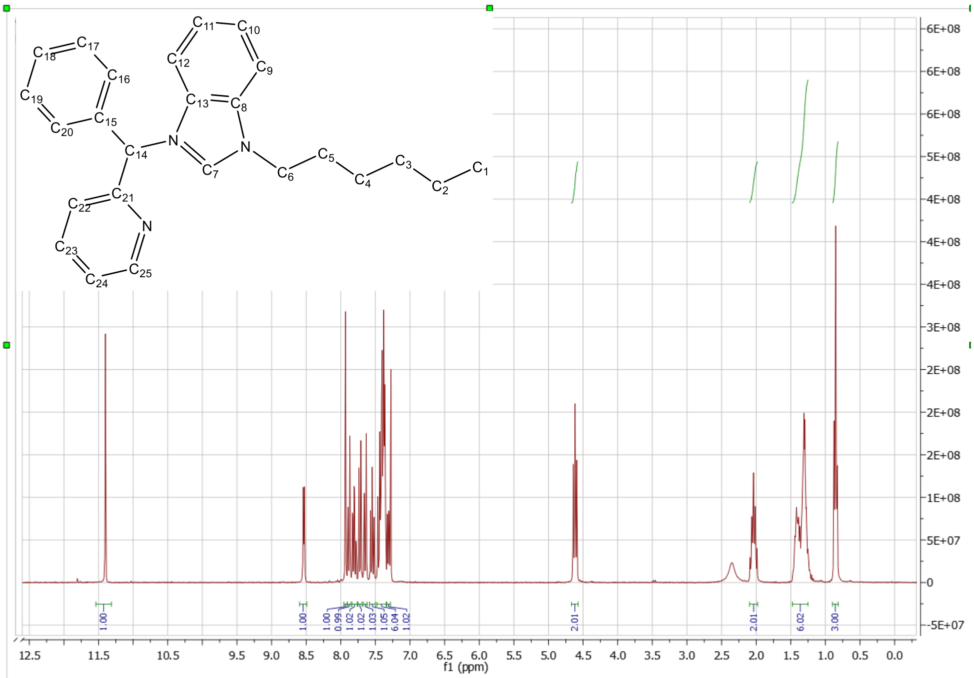

Figure A2.31. ^{1}H-NMR spectrum for compound **Bz-71d.**

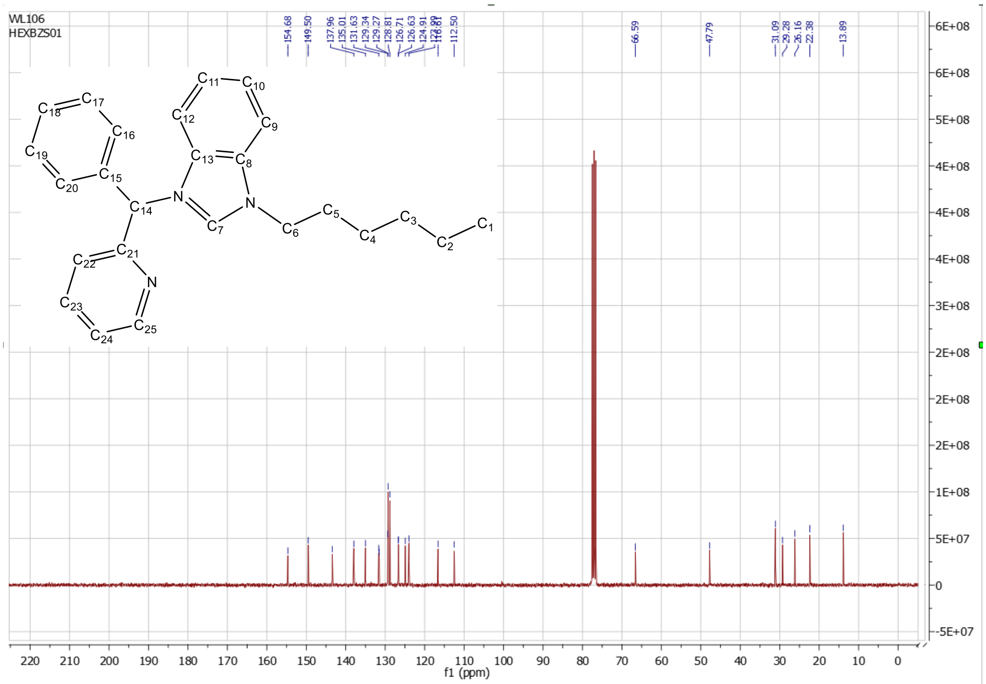

Figure A2.32. ^{13}C-NMR spectrum for compound **Bz-71d.**

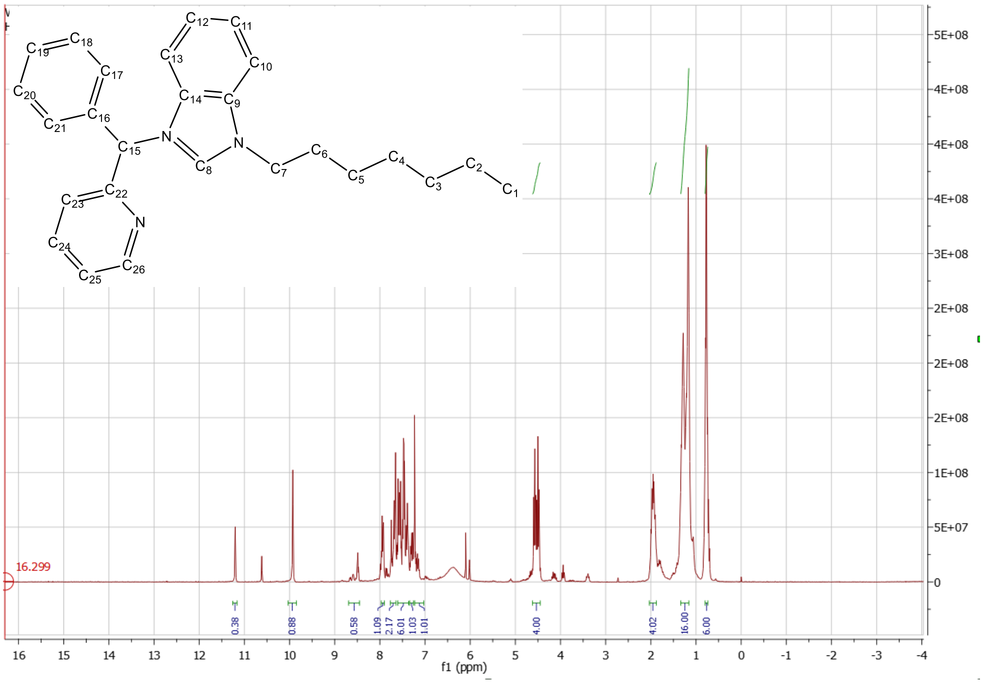

Figure A2.33. ^{1}H-NMR spectrum for compound **Bz-71e.**

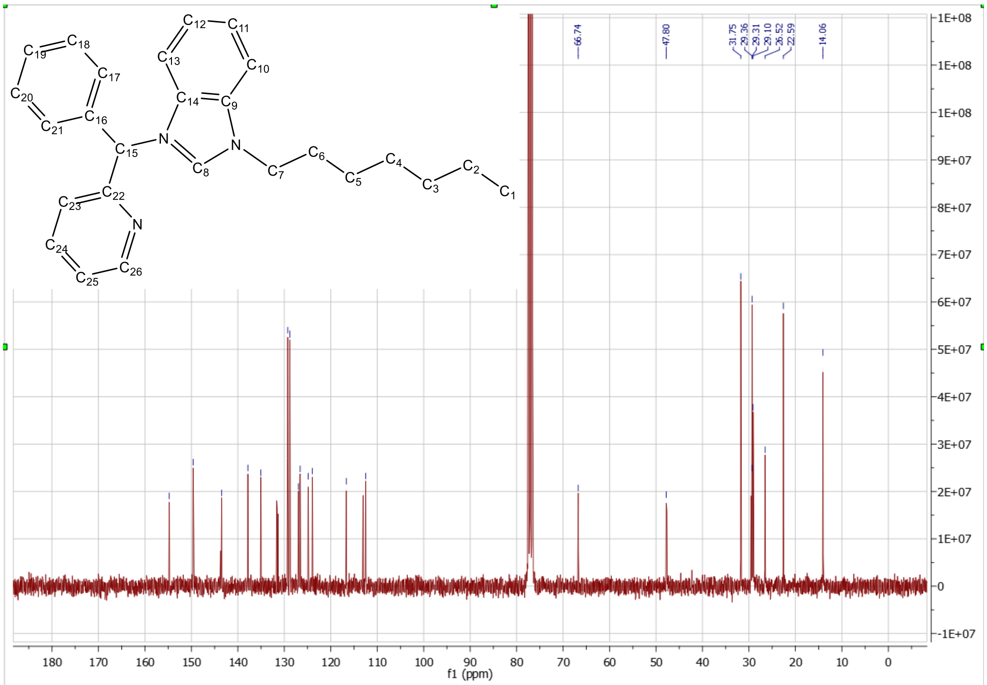

Figure A2.34. ^{13}C-NMR spectrum for compound **Bz-71e.**

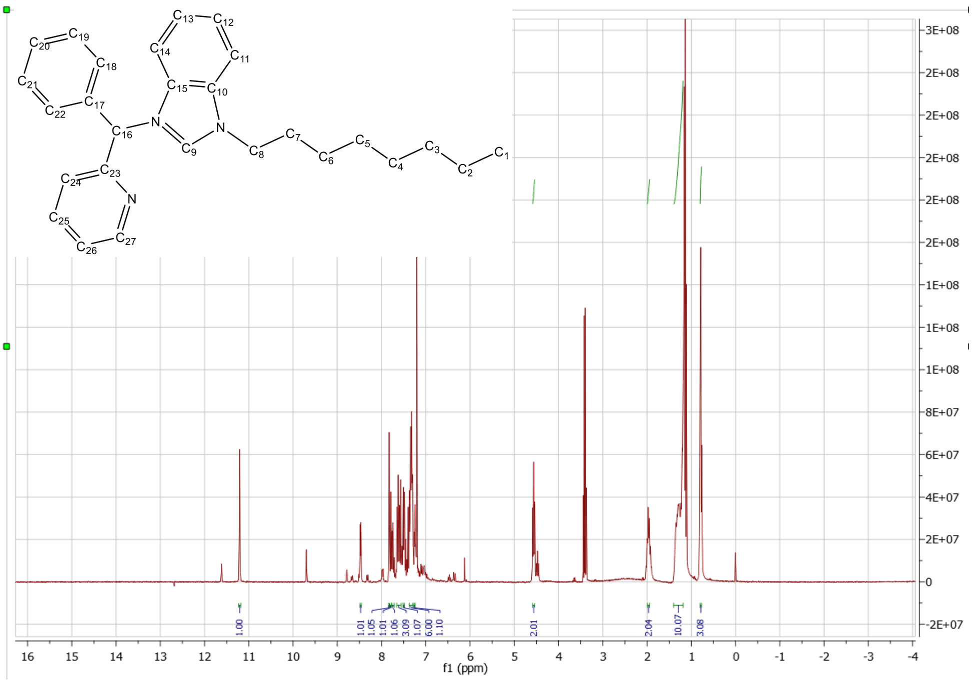

Figure A2.35. ^{1}H-NMR spectrum for compound **Bz-71f.**

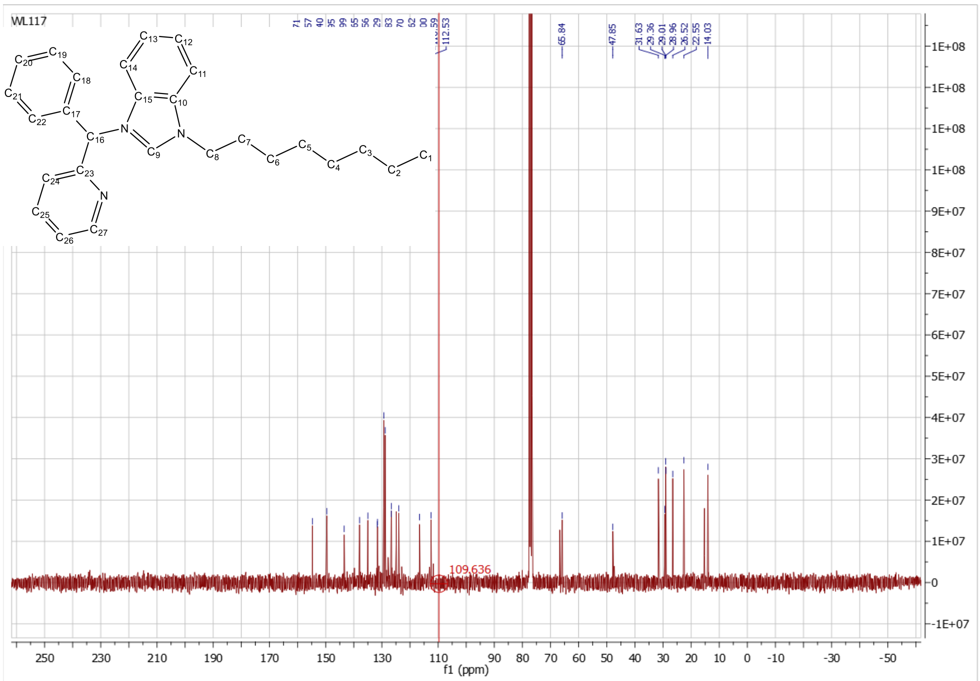

Figure A2.36. ^{13}C-NMR spectrum for compound **Bz-71f.**

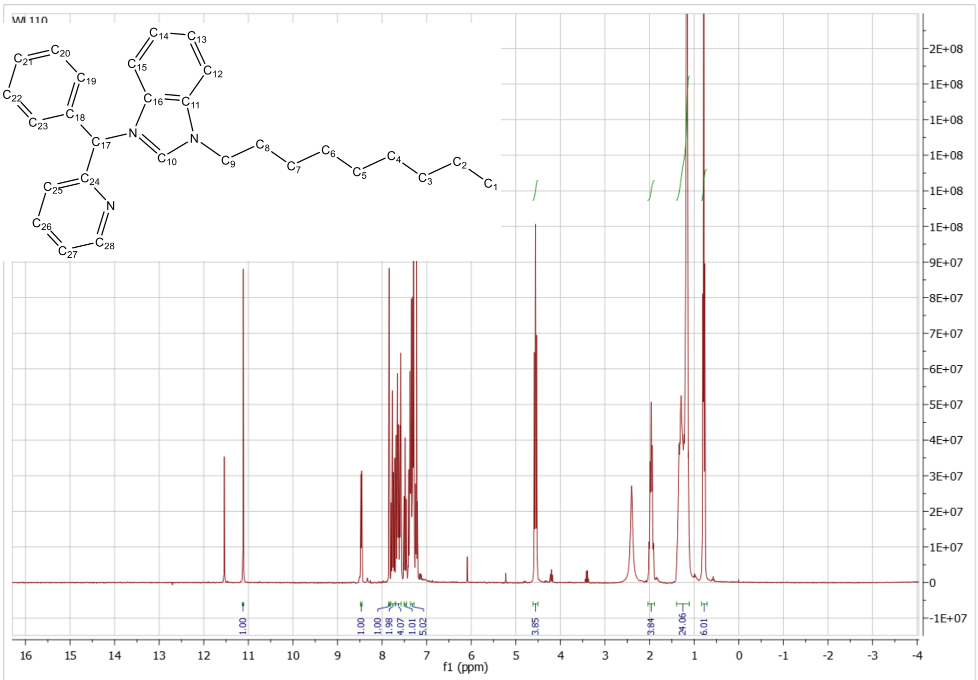

Figure A2.37. ^{1}H-NMR spectrum for compound **Bz-71g.**

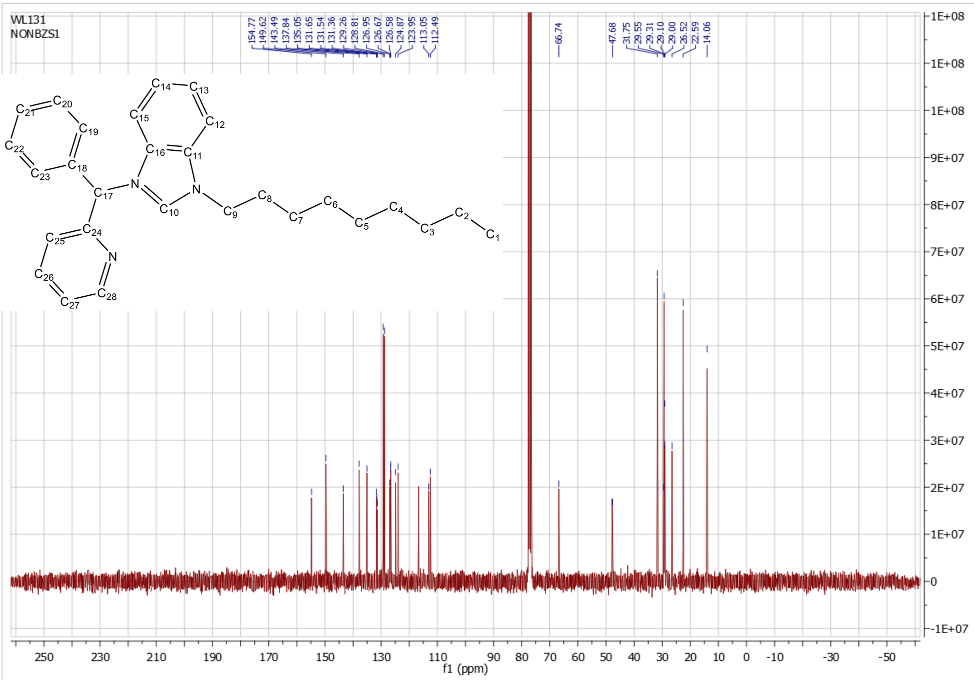

Figure A2.38. ^{13}C-NMR spectrum for compound **Bz-71g.**

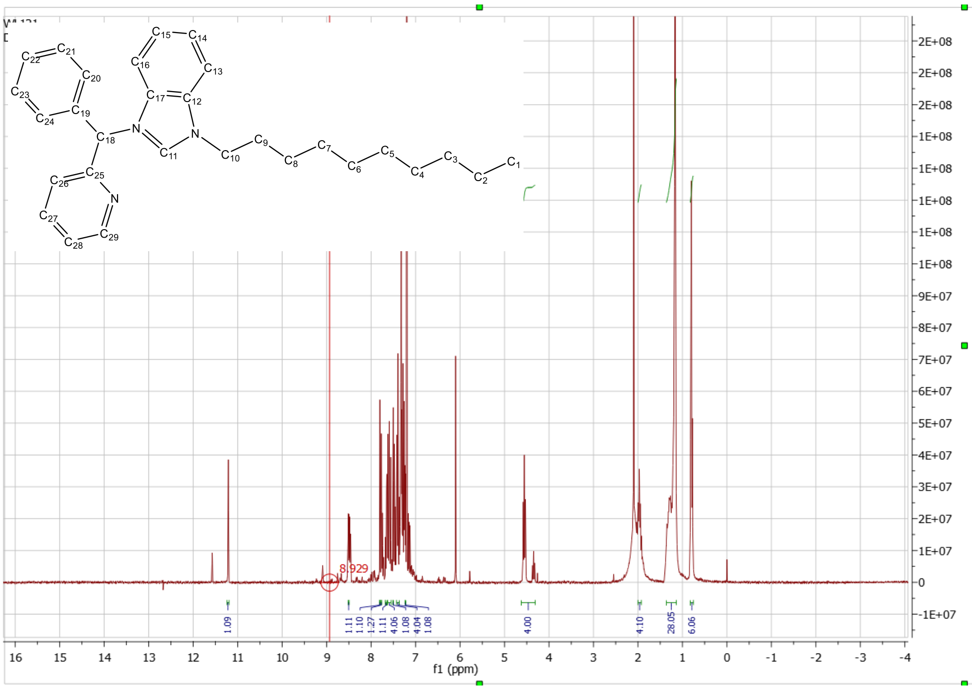

Figure A2.39. ^{1}H-NMR spectrum for compound **Bz-71h.**

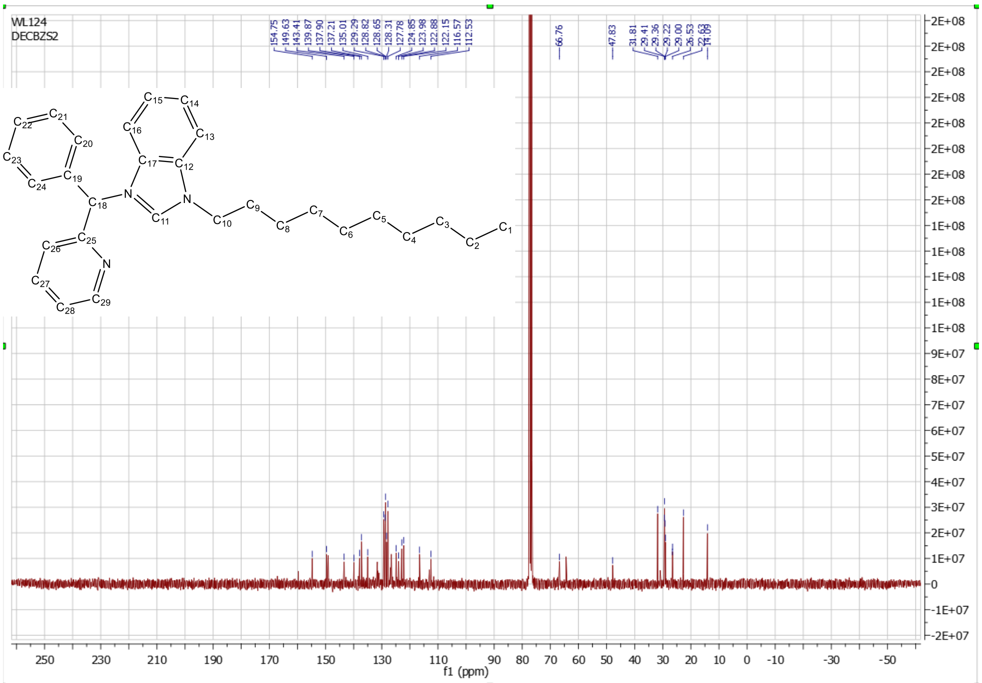

Figure A2.40. ^{13}C-NMR spectrum for compound **Bz-71h.**

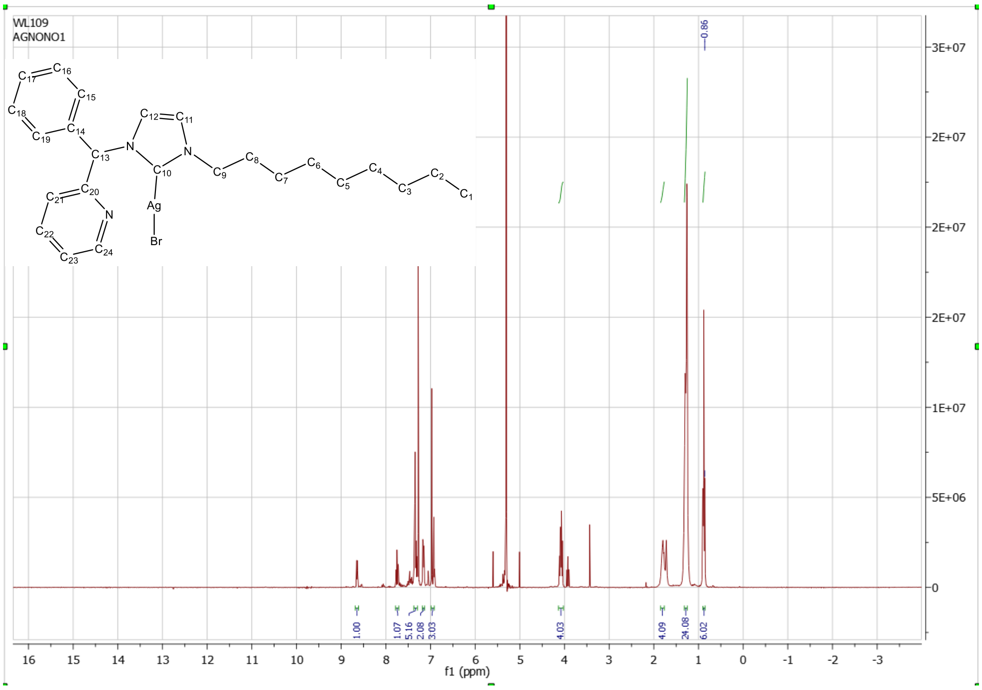

Figure A2.41. ^{1}H-NMR spectrum for compound **Ag-Im-77g-Br.**

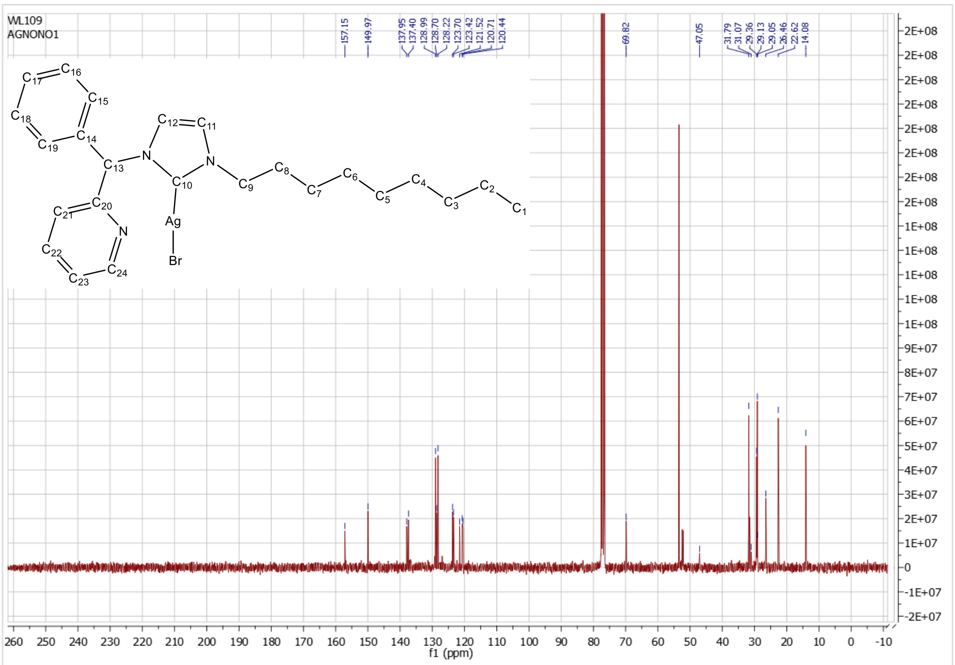

Figure A2.42. ^{13}C-NMR spectrum for compound **Ag-Im-77g-Br.**

APPENDIX 3: LCMS SPECTRAL DATA

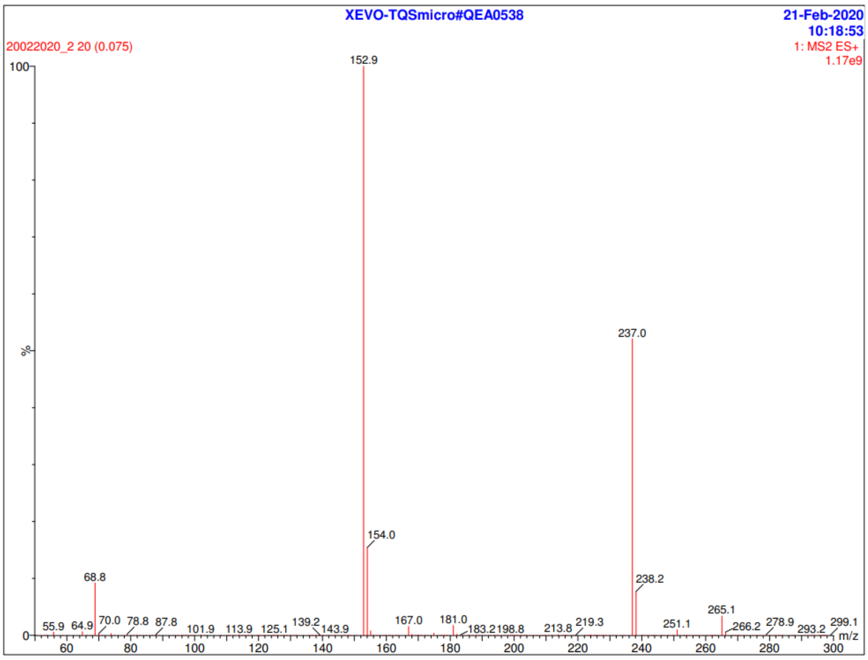

Figure A3.1. Mass spectrum for compound **Im-76d.**

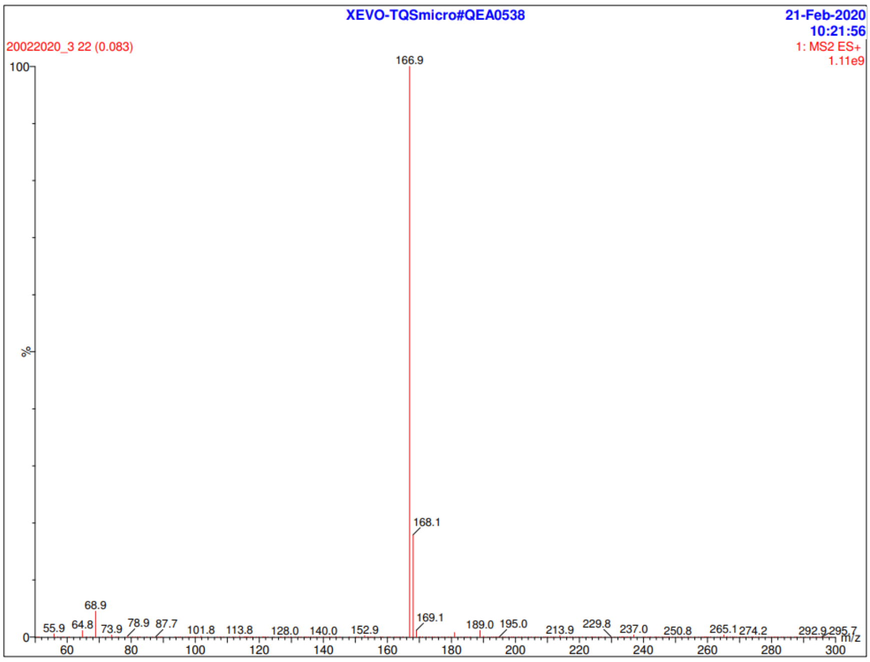

Figure A3.2. Mass spectrum for compound **Im-76e.**

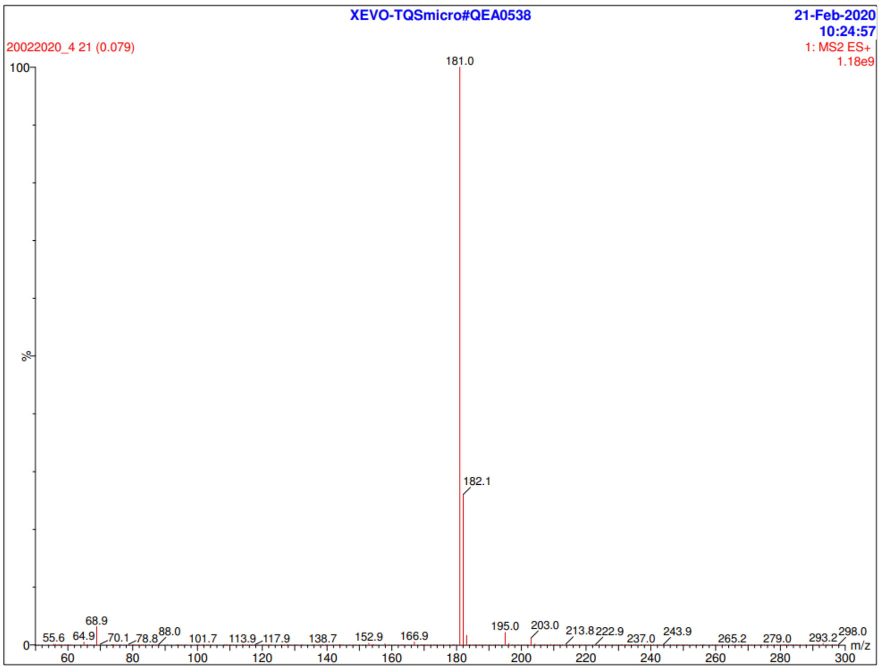

Figure A3.3. Mass spectrum for compound **Im-76f.**

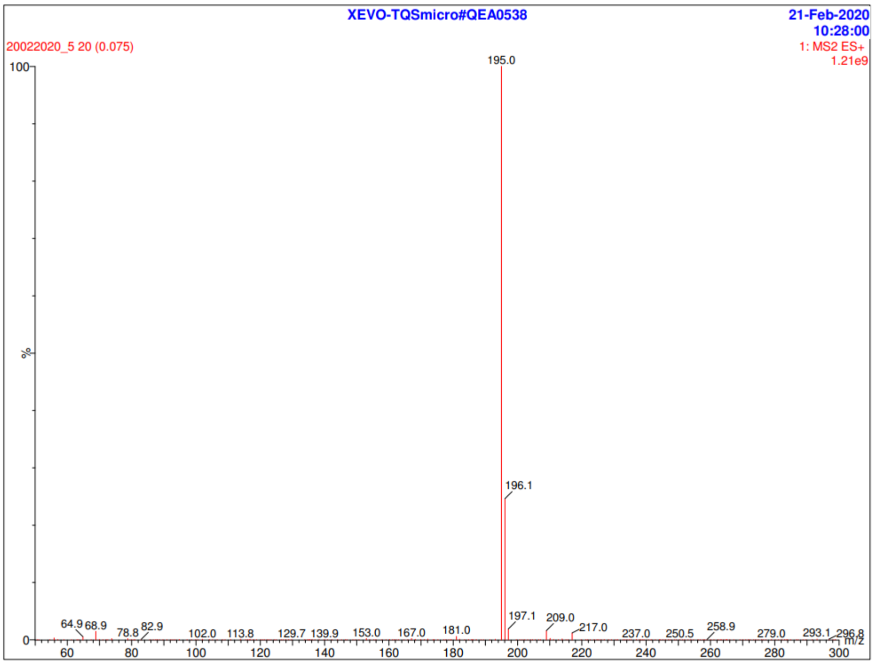

Figure A3.4. Mass spectrum for compound **Im-76g.**

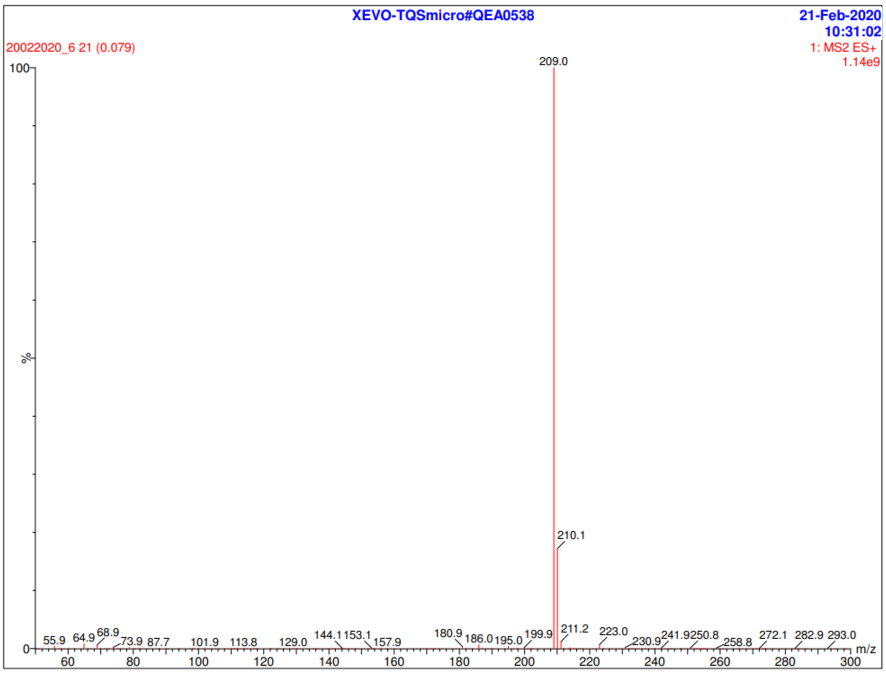

Figure A3.5. Mass spectrum for compound **Im-76h.**

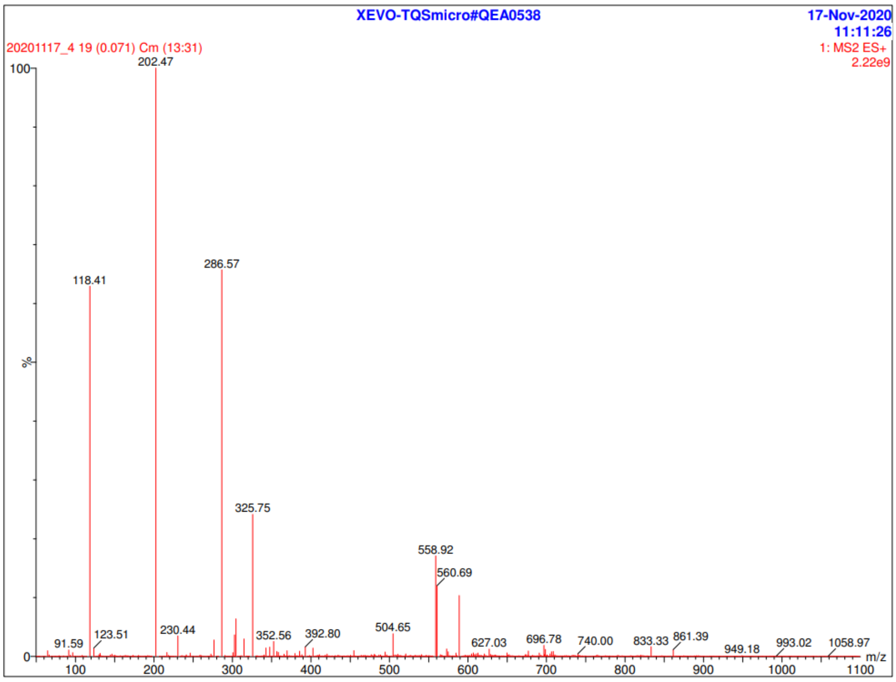

Figure A3.6. Mass spectrum for compound **Bz-76d.**

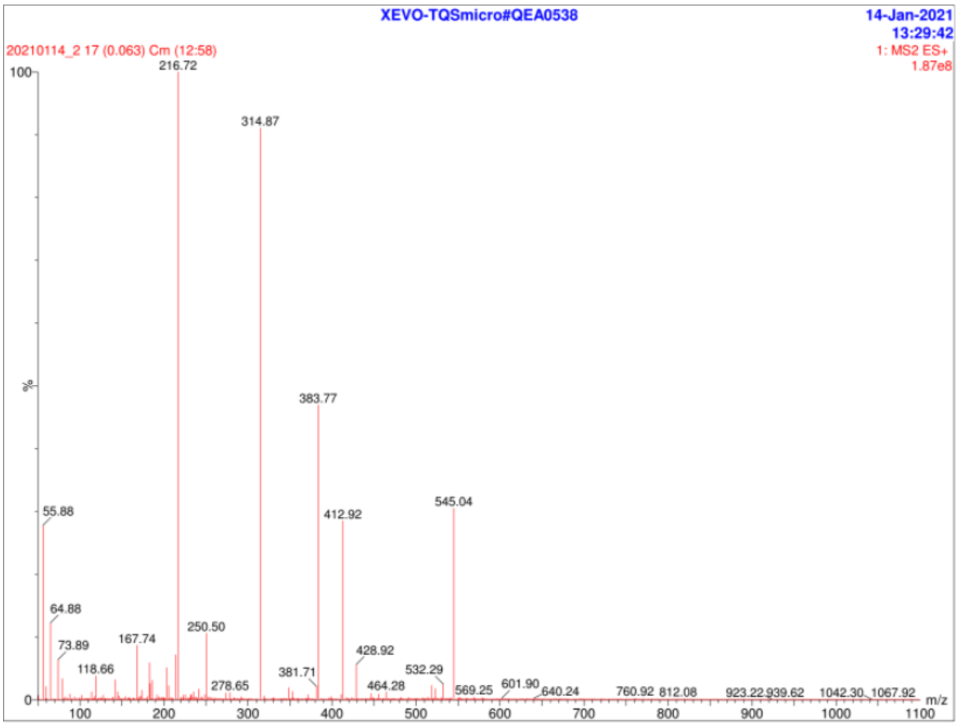

Figure A3.7. Mass spectrum for compound **Bz-76e.**

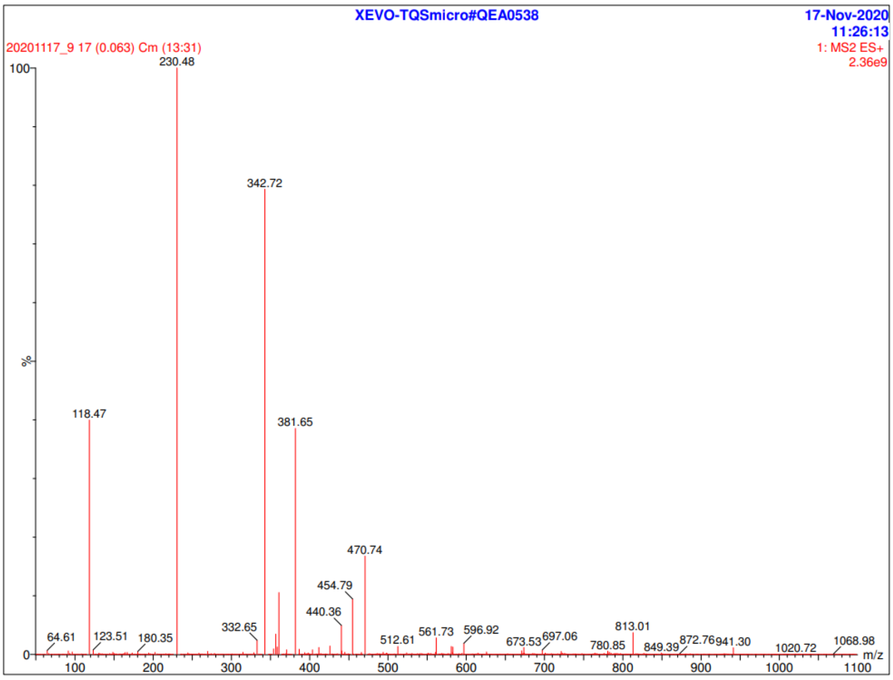

Figure A3.8. Mass spectrum for compound **Bz-76f.**

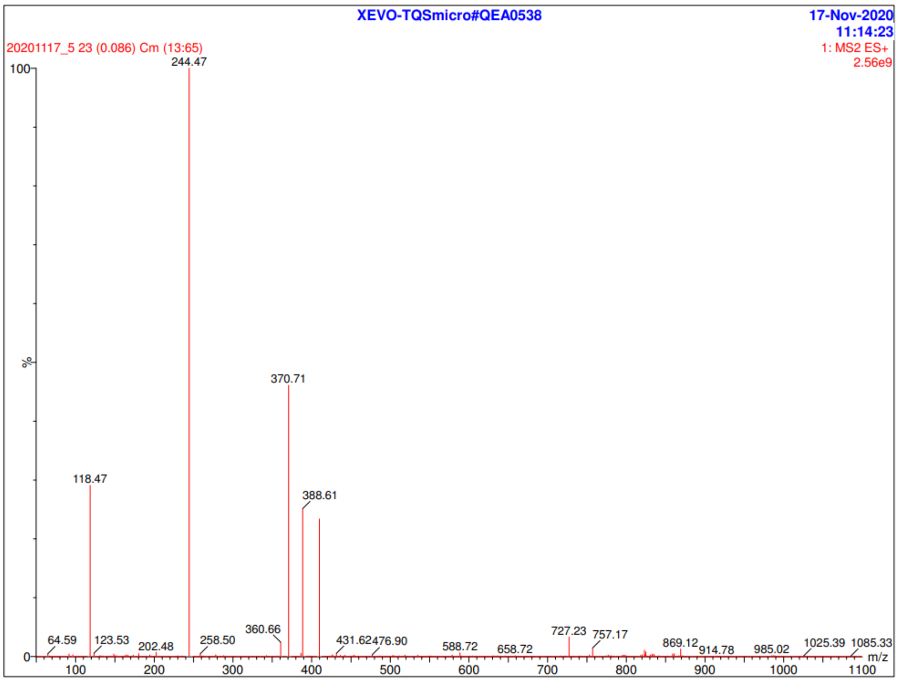

Figure A3.9. Mass spectrum for compound **Bz-76g.**

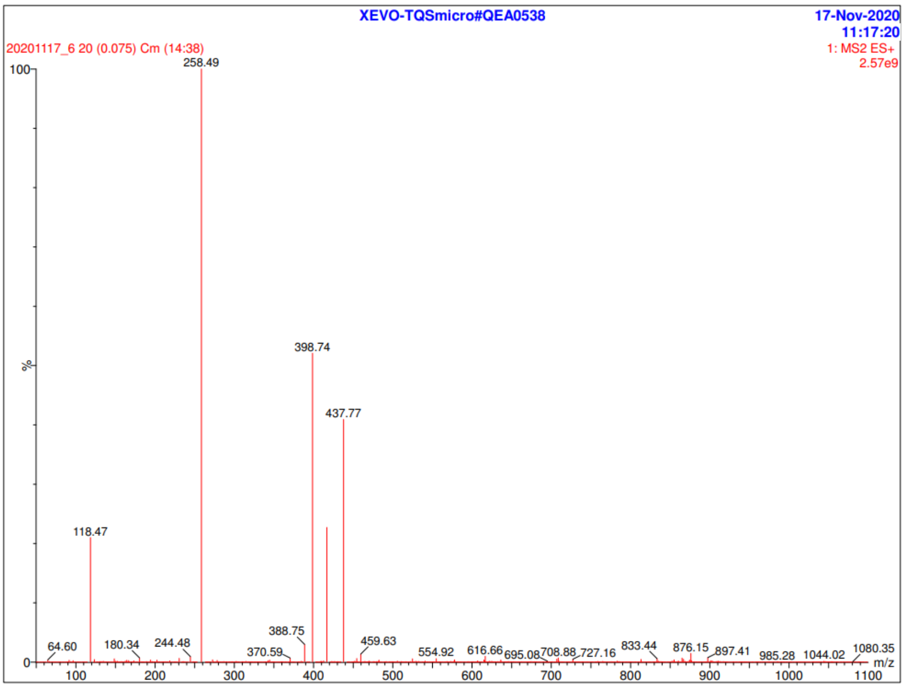

Figure A3.10. Mass spectrum for compound **Bz-76h.**

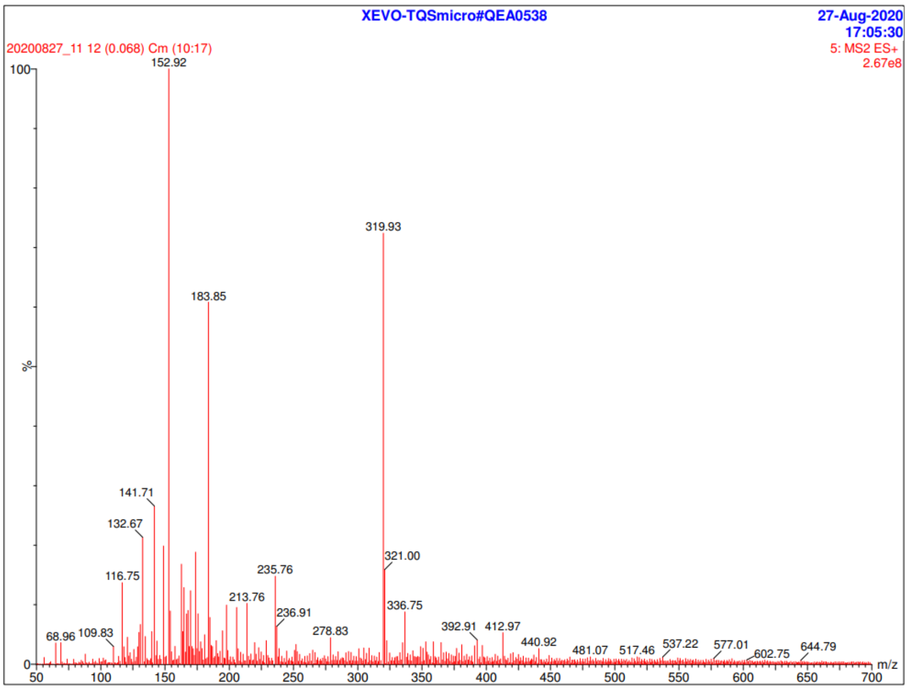

Figure A3.11. Mass spectrum for compound **Im-71d.**

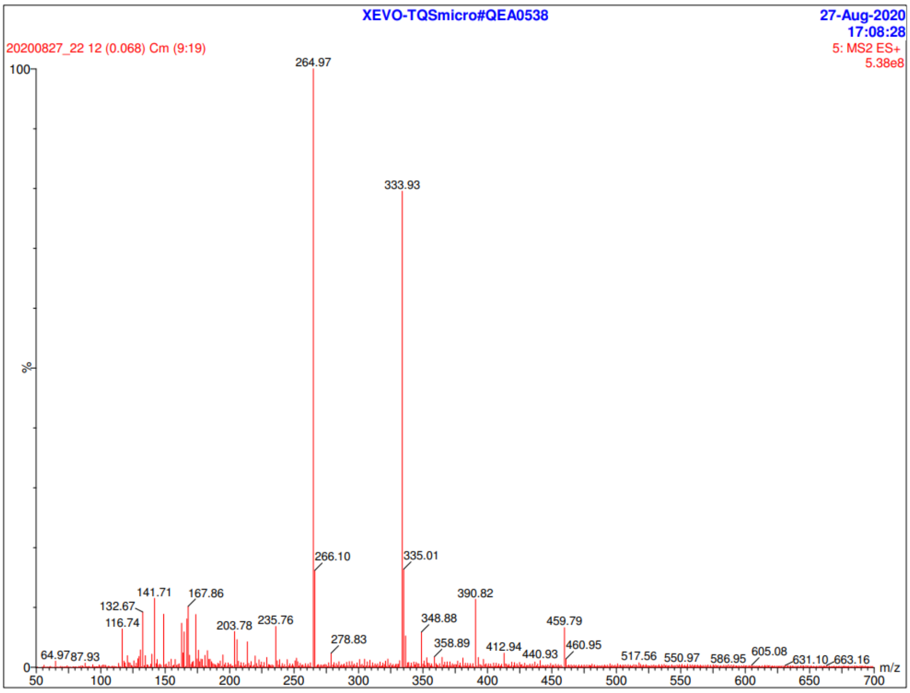

Figure A3.12. Mass spectrum for compound **Im-71e.**

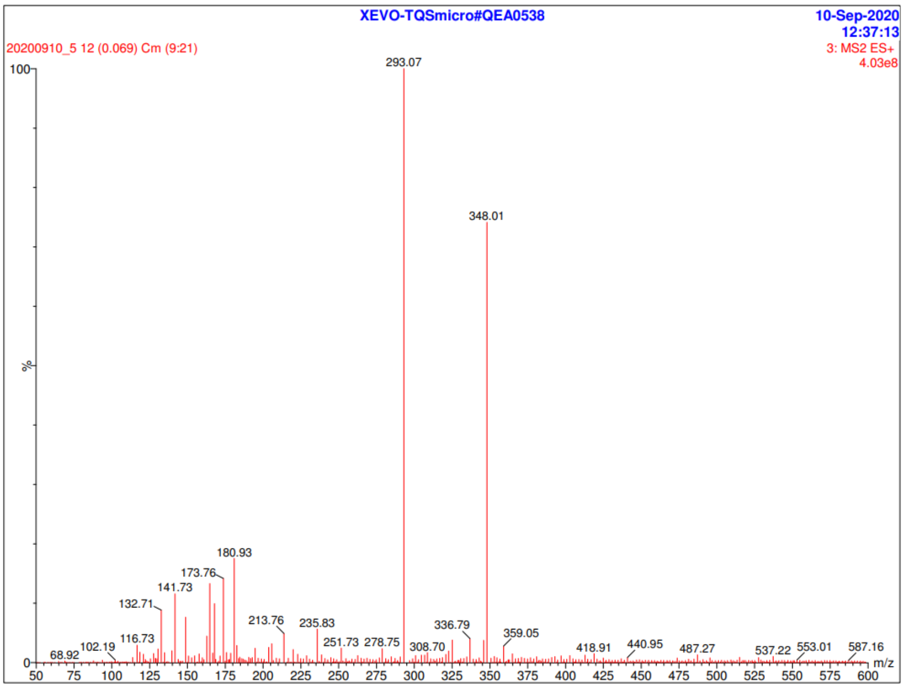

Figure A3.13. Mass spectrum for compound **Im-71f.**

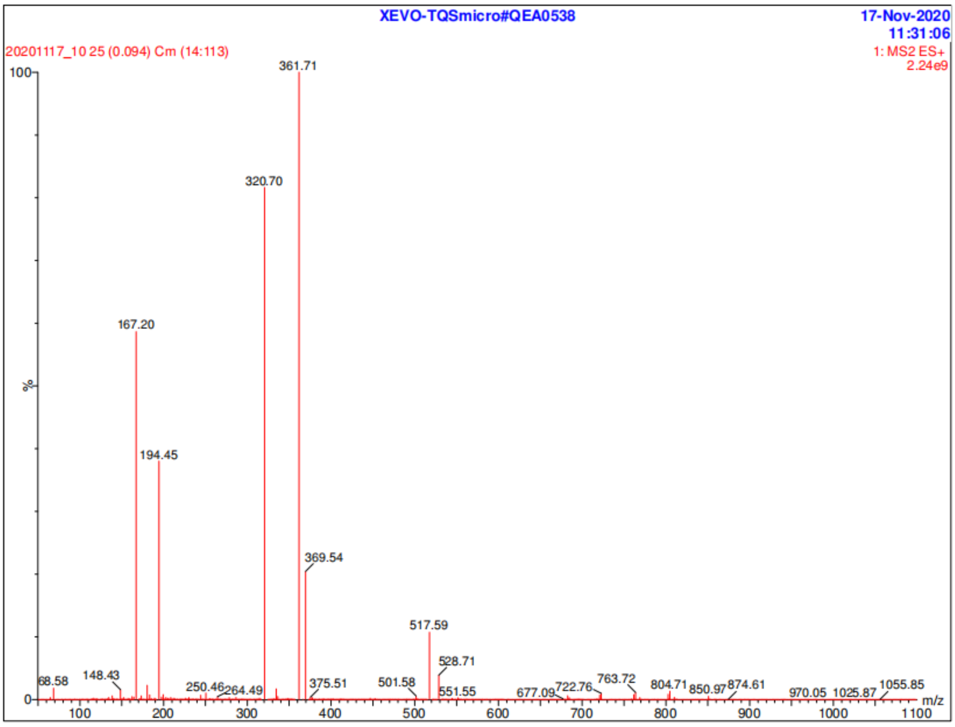

Figure A3.14. Mass spectrum for compound **Im-71g.**

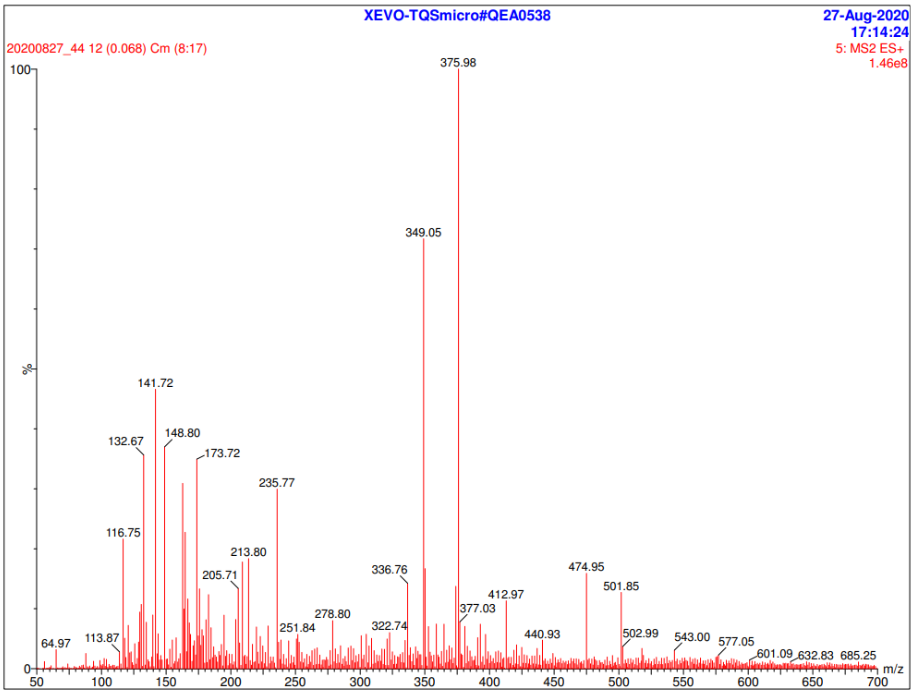

Figure A3.15. Mass spectrum for compound **Im-71h.**

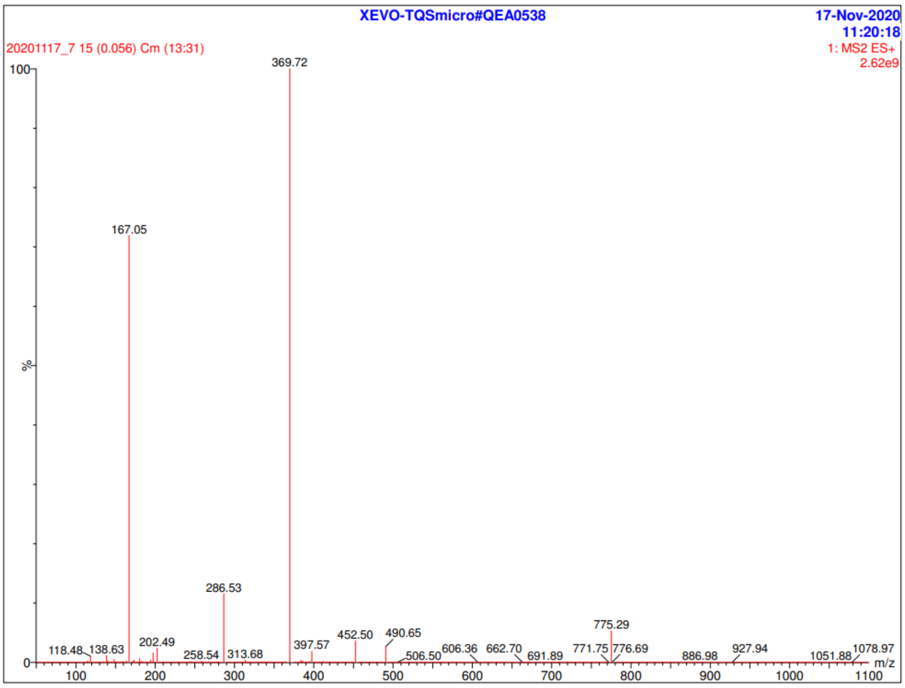

Figure A3.16. Mass spectrum for compound **Bz-71d.**

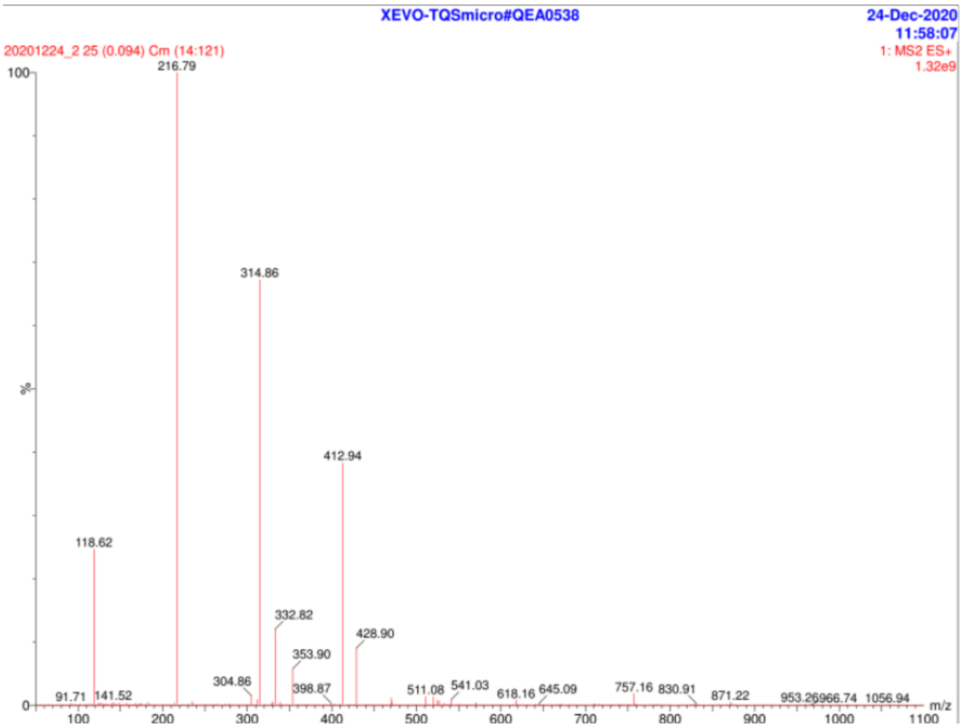

Figure A3.17. Mass spectrum for compound **Bz-71e.**

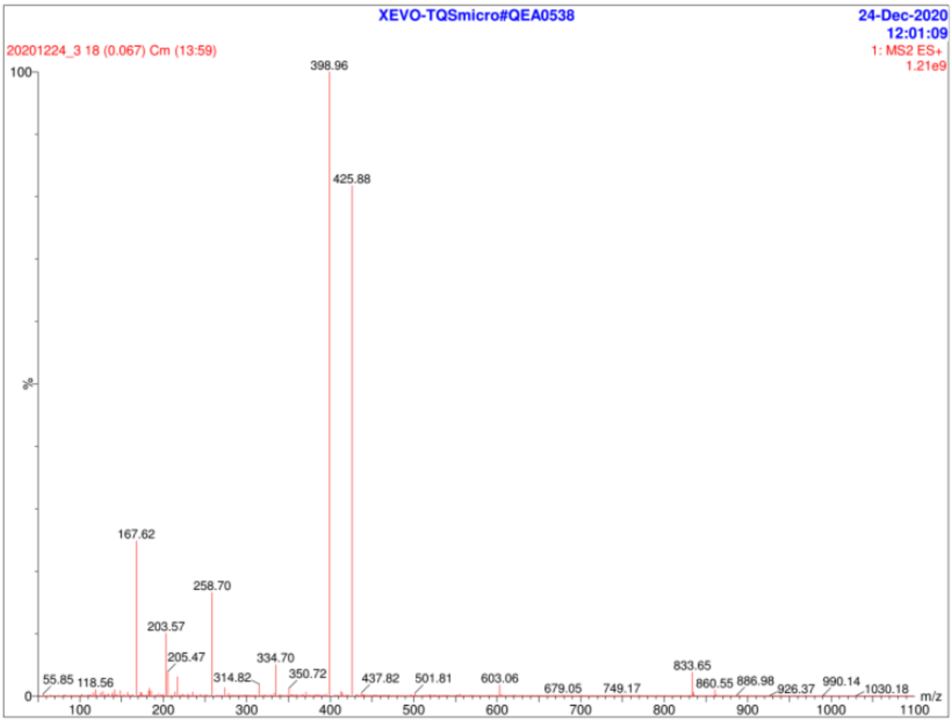

Figure A3.18. Mass spectrum for compound **Bz-71f.**

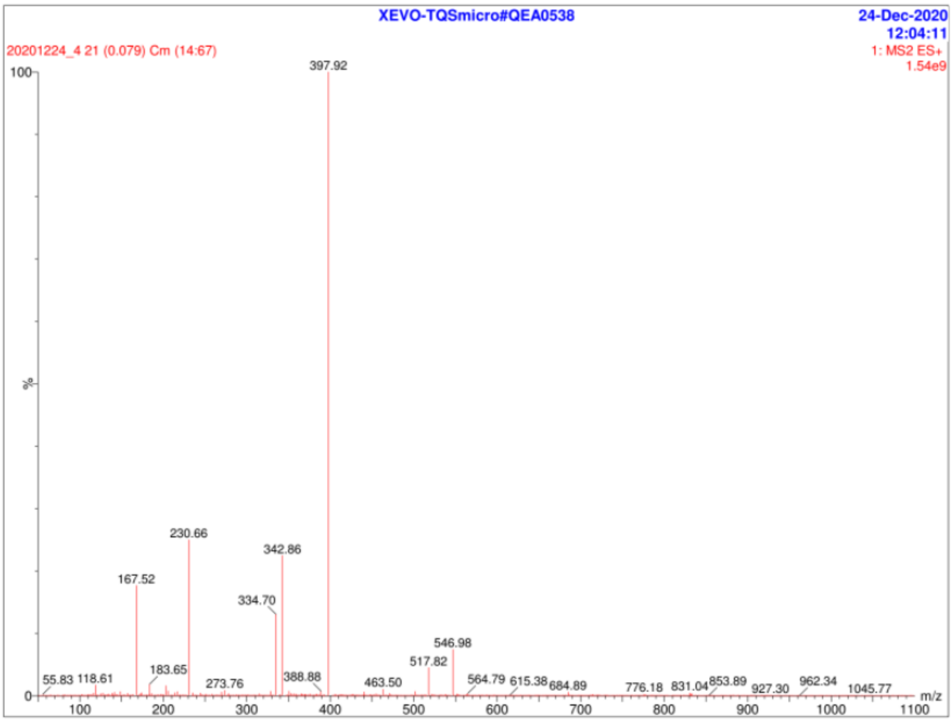

Figure A3.19. Mass spectrum for compound **Bz-71g.**

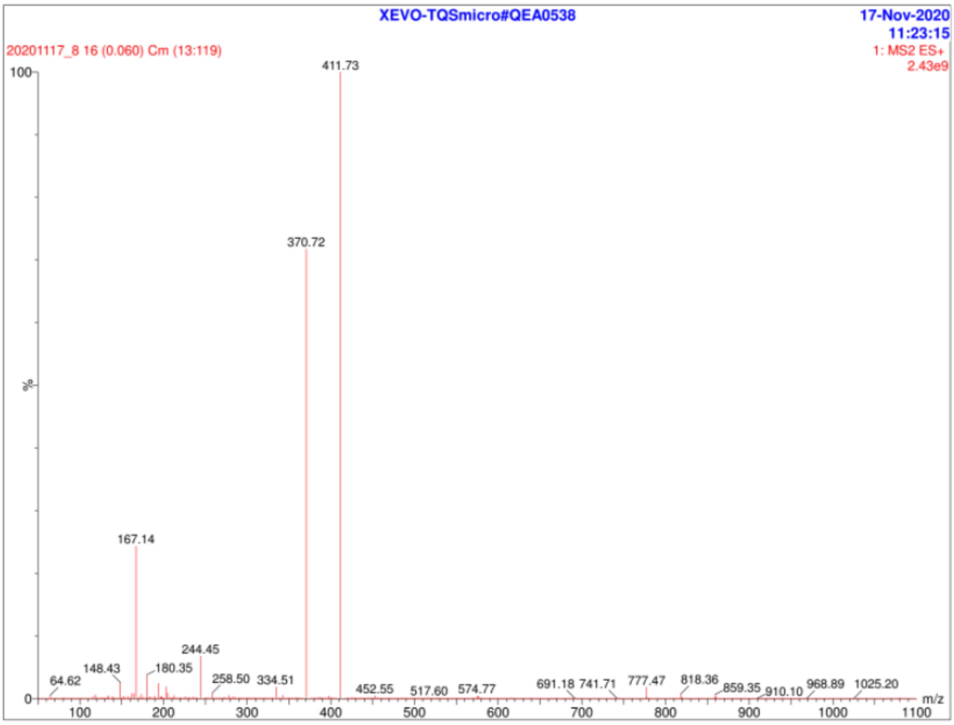

Figure A3.20. Mass spectrum for compound **Bz-71h.**

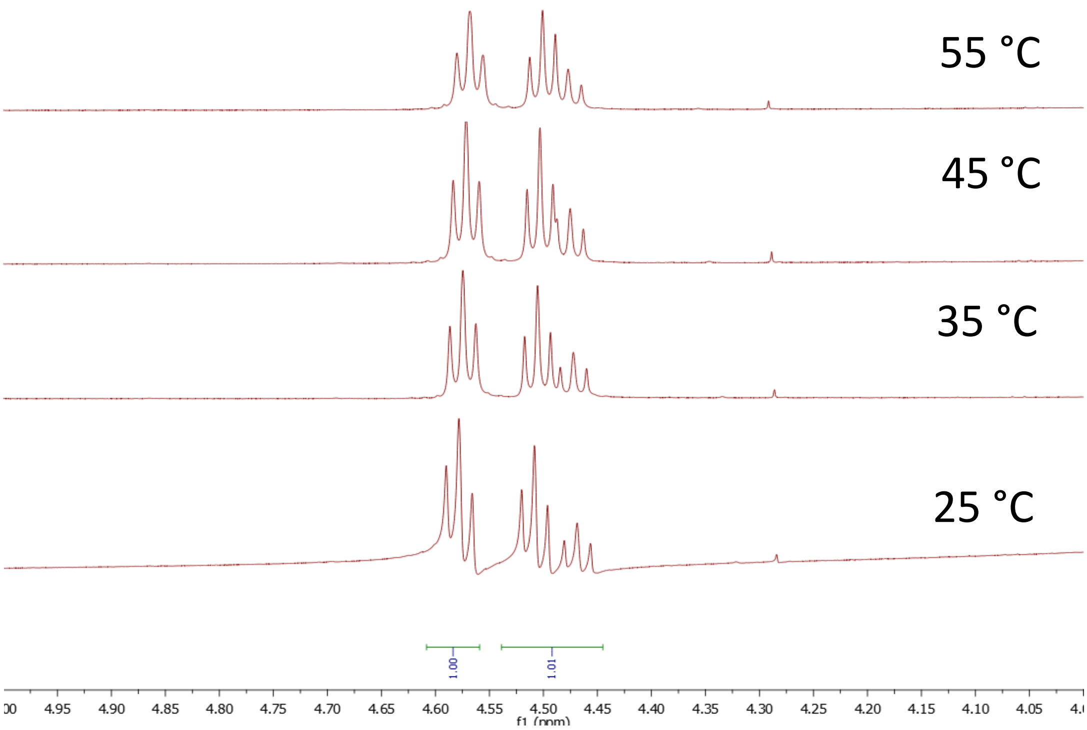

Figure A3.21. Selected region of VT-NMR of **Im-71g**.

APPENDIX 4: PLOTS OF MTT CELL VIABILITY ASSAY

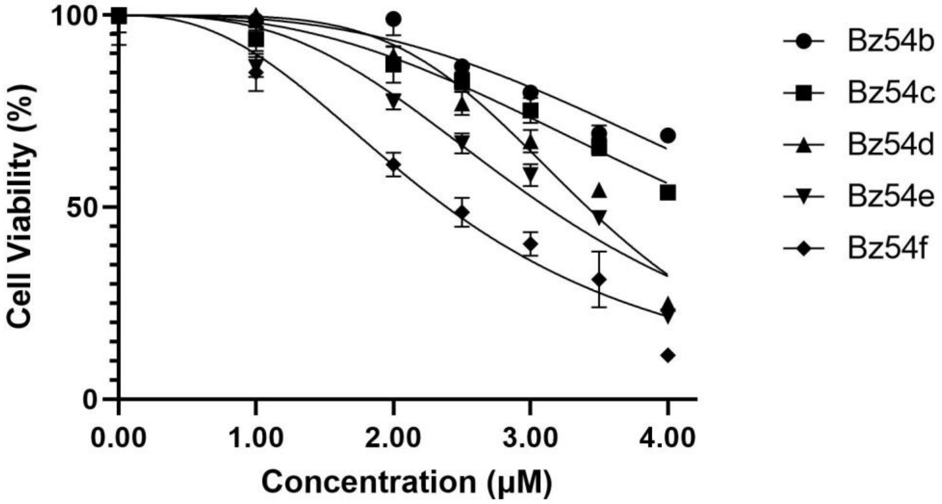

Figure A4.1: Cytotoxicity of **Bz-71d – h** against BEAS2B (human lung epithelial cells) after 24 hours of treatment. Cell viability was assessed using MTT cell viability assay at 570 nm (reference wavelength at 620 nm).

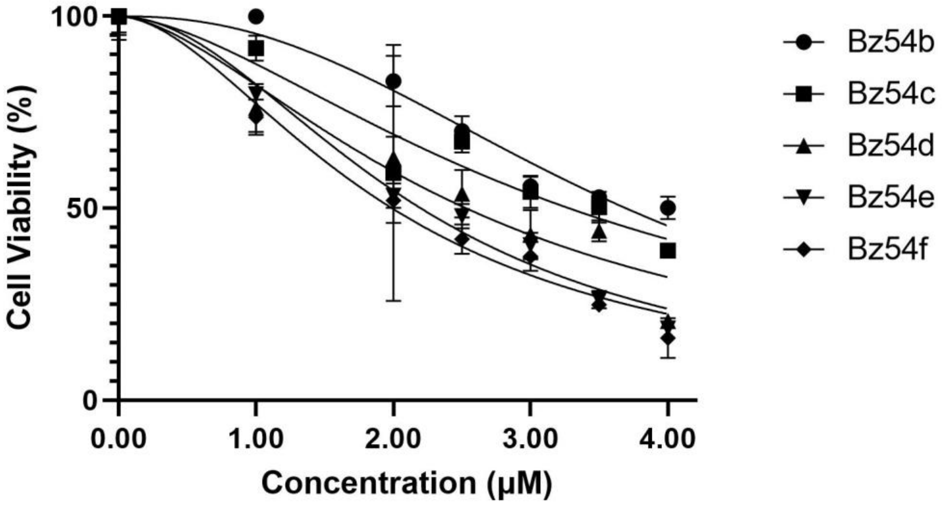

Figure A4.2: Cytotoxicity of **Bz-71d – h** against H103 (human oral squamous cancer cells) after 24 hours of treatment. Cell viability was assessed using MTT cell viability assay at 570 nm (reference wavelength at 620 nm).

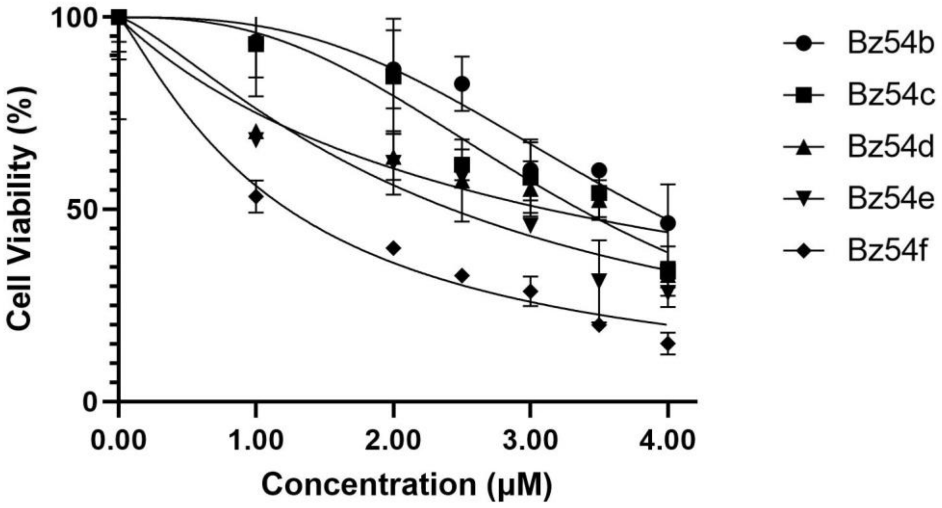

Figure A4.3: Cytotoxicity of **Bz-71d – h** against HCT116 (human colorectal cancer cells) after 24 hours of treatment. Cell viability was assessed using MTT cell viability assay at 570 nm (reference wavelength at 620 nm).

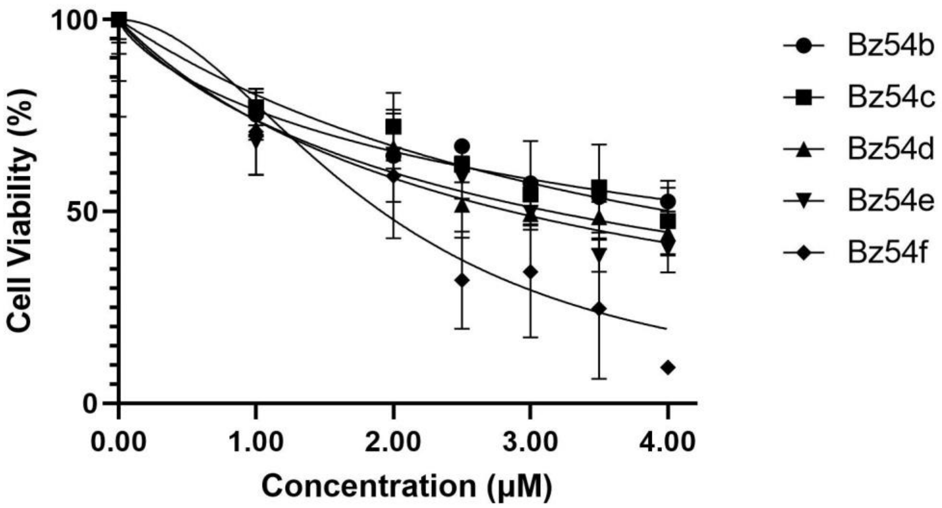

Figure A4.4: Cytotoxicity of **Bz-71d – h** against HT1080 (human skin cancer cells) after 24 hours of treatment. Cell viability was assessed using MTT cell viability assay at 570 nm (reference wavelength at 620 nm).

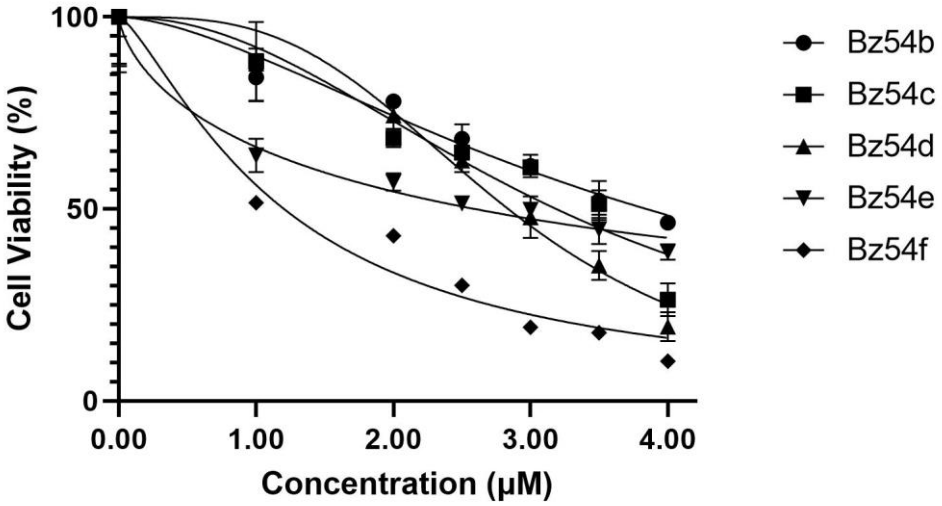

Figure A4.5: Cytotoxicity of **Bz-71d – h** against HaCaT (human skin cells) after 24 hours of treatment. Cell viability was assessed using MTT cell viability assay at 570 nm (reference wavelength at 620 nm).

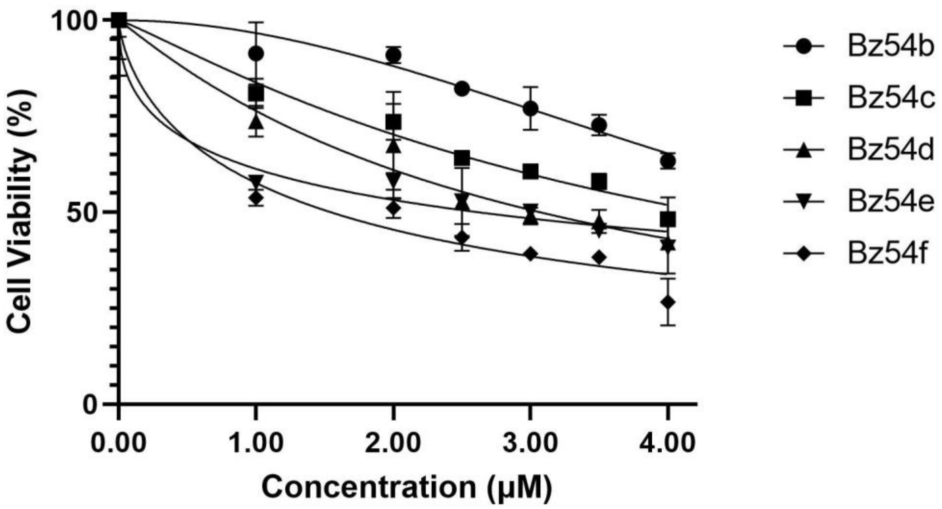

Figure A4.6: Cytotoxicity of **Bz-71d – h** against MCF7 (human breast cancer cells) after 24 hours of treatment. Cell viability was assessed using MTT cell viability assay at 570 nm (reference wavelength at 620 nm).

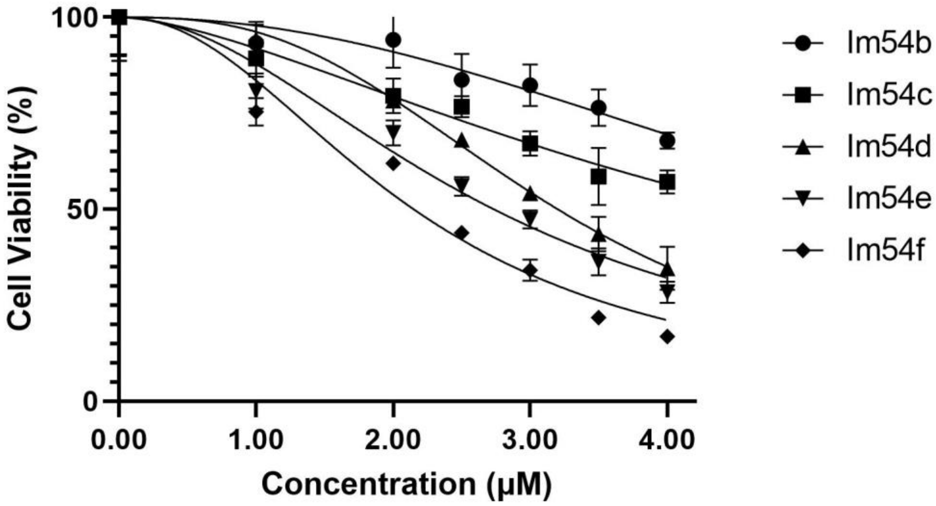

Figure A4.7: Cytotoxicity of **Im-71d – h** against BEAS2B (human lung epithelial cells) after 24 hours of treatment. Cell viability was assessed using MTT cell viability assay at 570 nm (reference wavelength at 620 nm).

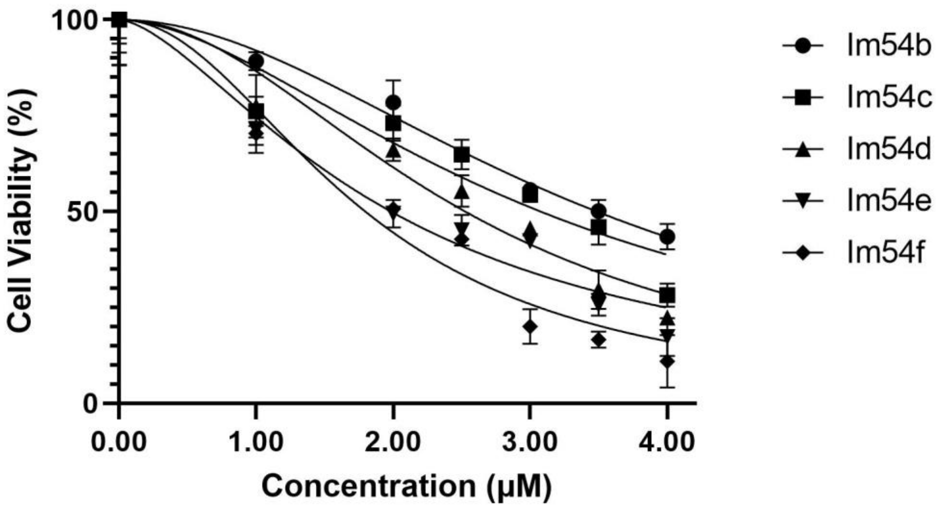

Figure A4.8: Cytotoxicity of **Im-71d – h** against H103 (human oral squamous cancer cells) after 24 hours of treatment. Cell viability was assessed using MTT cell viability assay at 570 nm (reference wavelength at 620 nm).

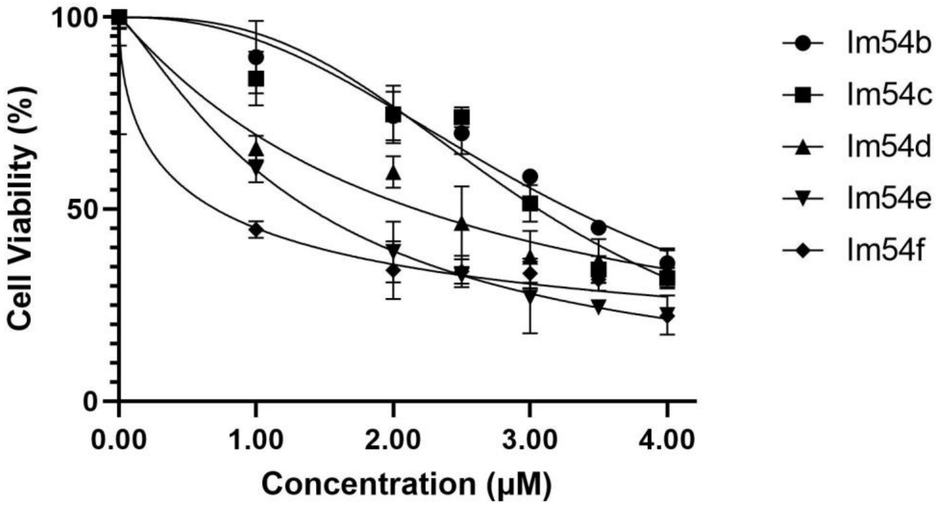

Figure A4.9: Cytotoxicity of **Im-71d – h** against HCT116 (human colorectal cancer cells) after 24 hours of treatment. Cell viability was assessed using MTT cell viability assay at 570 nm (reference wavelength at 620 nm).

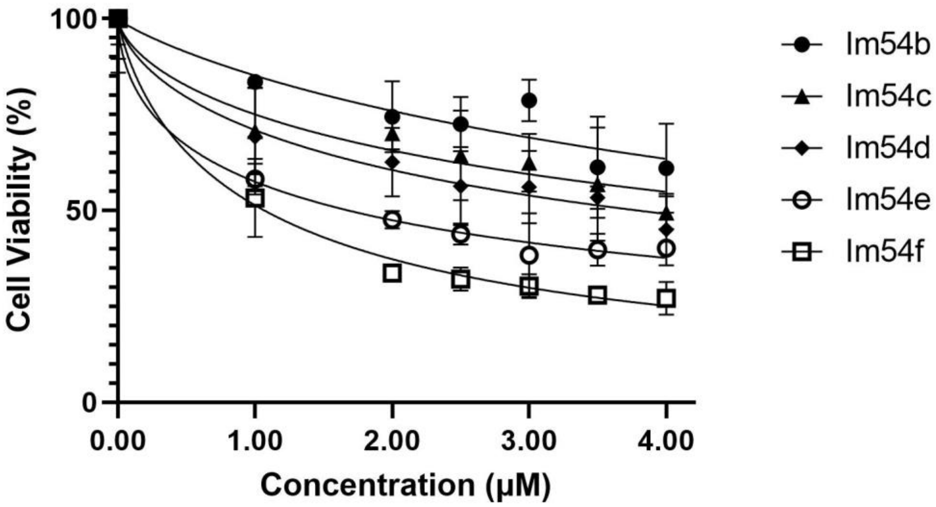

Figure A4.10: Cytotoxicity of **Im-71d – h** against HT1080 (human skin cancer cells) after 24 hours of treatment. Cell viability was assessed using MTT cell viability assay at 570 nm (reference wavelength at 620 nm).

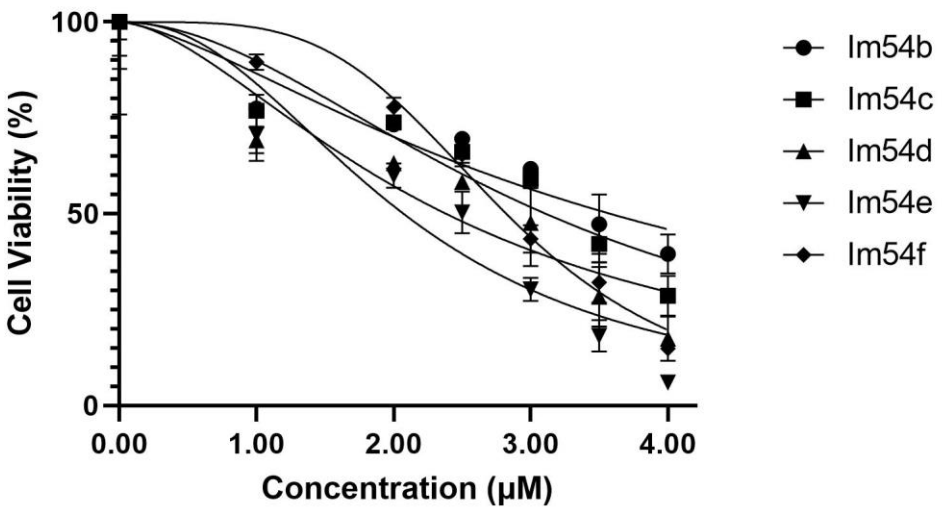

Figure A4.11: Cytotoxicity of **Im-71d – h** against HaCaT (human skin cells) after 24 hours of treatment. Cell viability was assessed using MTT cell viability assay at 570 nm (reference wavelength at 620 nm).

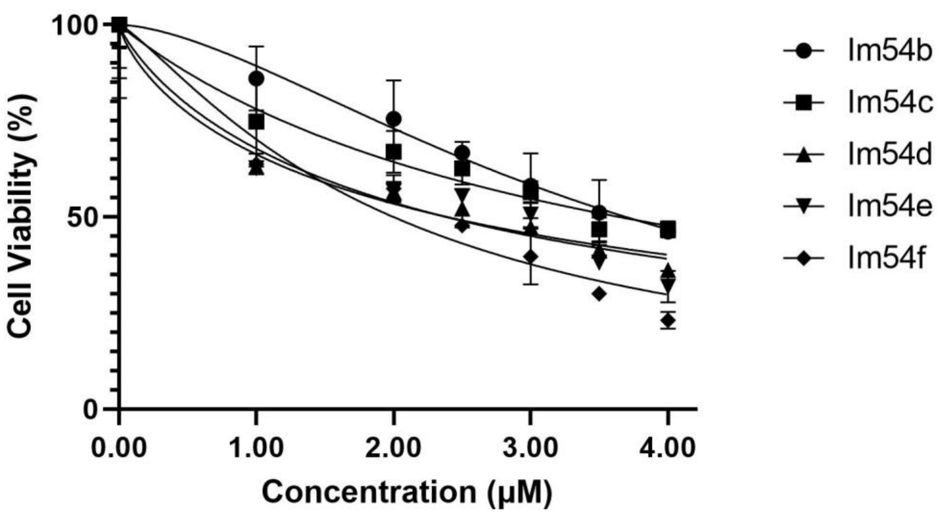

Figure A4.12: Cytotoxicity of **Im-71d – h** against MCF7 (human breast cancer cells) after 24 hours of treatment. Cell viability was assessed using MTT cell viability assay at 570 nm (reference wavelength at 620 nm).

APPENDIX 5: POSTER PRESENTATION #1 & #2

MONASH
SCIENCE

FACILE SYNTHESIS OF BIOACTIVE PYRIDINE-FUNCTIONALIZED IMIDAZOLIUM SALTS

Wee Li Mah[1], Keng Yoon Yeong[1], Sui Mae Lee[1], Yuen Lin Cheow[1]*

[1]*School of Science, Monash University Malaysia, Jalan Lagoon Selatan, Bandar Sunway, 47500 Subang Jaya, Selangor, Malaysia*

Corresponding e-mail : cheow.yuen.lin@monash.edu

INTRODUCTION

Imidazolium salts are derived from their parent imidazoles *via* alkylation of the two nitrogen atoms in the heterocycle, resulting in the cationic charge[1]. Imidazolium salts are often utilized as ionic liquids for wide range of applications including acting as a green solvent. During the recent decades, imidazolium salts were found useful in various biological applications, including antibacterial, antiproliferative, antioxidant and etc[2].

OBJECTIVES

⇒ To synthesize and characterize a series of pyridine-functionalized imidazolium salts.

⇒ To develop a energy-effective methodology (microwave irradiation) in synthesis of pyridine-functionalized imidazolium salts.

⇒ To evaluate the antiproliferative and antimicrobial activities of the synthesized imidazolium salts.

METHODOLOGY

Synthesis Pathway

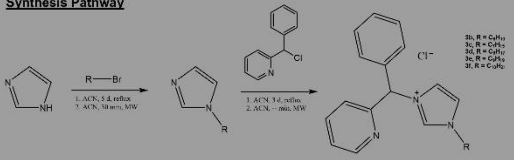

1 2b - f 3b - f

Evaluation of Antiproliferative Activities

The antiproliferative activities are tested against HCT-116 (Human colorectal carcinoma), H103 (Human tongue squamous carcinoma), MCF-7 (Human breast adenocarcinoma), HT1080 (Human fibrosarcoma) using cell cytotoxicity assay.

Evaluation of Antimicrobial Activities

The antimicrobial activities are tested against 8 Gram-positive and 4 Gram-negative bacterial strains, as well as 3 yeast strains using broth microdilution assay.

RESULTS & DISCUSSION

Synthesis Pathway

Table 1. Comparison of reaction yields between conventional heating and microwave irradiation for imidazole derivatives and their imidazolium salts.

Compound	Conventional heating		Microwave irradiation	
	Duration (h)	Yield (%)	Duration (h)	Yield (%)
2b	120	67.7	3	86.3
2c	120	56.4	3	88.0
2d	120	62.3	3	82.1
2e	120	47.7	3	83.1
2f	120	68.0	3	84.8
3b	48	53.6	1	71.1
3c	48	49.9	1	79.4
3d	48	50.2	1	83.7

**Yield refers to isolated yield.*
***Products are characterized with ^{1}H-NMR.*

Antiproliferative Activities

Table 2. Half maximal inhibitory concentration (IC_{50}) (µM) of synthesized imidazole derivatives and their imidazolium salts.

Compound	IC_{50} of compound tested (µM)		
	H103	HCT116	MCF7
Cisplatin	6.16 ± 0.04	10.78 ± 0.21	19.78 ± 0.21
3b	> 40	> 40	N/A
3c	> 40	24.6	N/A
3d	> 40	20.9	N/A

Antimicrobial Activities

Table 3. Minimum inhibitory concentration (MIC) (µg/mL) and minimum bactericidal concentration (MBC) (µg/mL) of synthesized imidazole derivatives and their imidazolium salts.

Compound	*B. cereus* ATCC 14579		MRSA ATCC 33591		*E. coli* ATCC 25922		*K. pneumoniae* ATCC 10031		*C. albicans* IMR	
	MIC	MBC	MIC	MBC	MIC	MBC	MIC	MBC	MIC	MBC
2b	1000.00	> 1000	1000.00	> 1000	500.00	> 1000	500.00	> 1000	> 1000	> 1000
2c	62.5	125	62.5	500.00	62.5	250.0	125	250.0	> 1000	> 1000
2d	62.5	125	31.3	250.0	31.3	125	62.5	125	> 1000	> 1000
2e	7.81	31.3	7.81	62.5	31.3	62.5	15.6	31.3	> 1000	> 1000
2f	125	250.0	500.00	> 1000	500.00	> 1000	500.00	> 1000	> 1000	> 1000
3b	250.0	500.00	500.00	1000.00	> 1000	> 1000	500.00	1000.00	> 1000	> 1000
3c	62.5	125	62.5	125	62.5	250.0	62.5	62.5	> 1000	> 1000
3d	31.3	125	31.3	125	15.6	62.5	15.6	31.3	> 1000	> 1000

Discussion

⇒ Use of microwave irradiation shortened the reaction time
- Enclosed system builds up pressure, raising the boiling point of solvent, thus allowing reaction to be carried out at higher temperature.

⇒ Increase in alkyl chain length at the *N*-wingtip enhanced the antimicrobial activities.
- Increase in alkyl chain length increases the hydrophobicity, thus allowing the compound to bind to target bacterium more easily.
- However, weakened activities were observed when C_n = 10. This is due to high hydrophobicity which hinders the diffusion efficiency of the compound.

⇒ No obvious trend was observed in antiproliferative activities.

CONCLUSION

⇒ Use of microwave irradiation shortened the time significantly (120 h to 3 h; 48 h to 1 h).

⇒ Compound 3b—d were found to be non-cytotoxic to H103, but cytotoxic activity at 20.9 µM against HCT116 was observed in compound 3d.

⇒ Compound 3b—d were found to be generally active against Gram-positive microorganism at as low as 31.3 µg/mL, Gram-negative microorganism at 15.6 µg/mL, and inactive against yeast strain.

⇒ As the alkyl chain length increased, antimicrobial activities were observed.

ACKNOWLEDGEMENT

The authors would like to express their gratitude to School of Science, Monash University Malaysia, and Tropical Medicine and Biology Multidisciplinary Platform, Monash University Malaysia for the financial support on this project.

REFERENCES

[1] Riduan, SN & Zhang, Y (2013) Imidazolium salts and their polymeric materials for biological applications, *Chemical Society Review*, vol. 42(23): 9055—9070.

[2] Ali, I, Lone, MN & Aboul-Enein, HY (2017) Imidazoles as potential anticancer agents, *MedChemComm*, vol. 8(9): 1742—1773.

Presenter Contact Info:
Wee Li Mah
wee.mah@monash.edu
+60 18 2334 607